BIOACTIVE NATURAL PRODUCTS FROM MICROBES: ISOLATION, CHARACTERIZATION, BIOSYNTHESIS AND STRUCTURE MODIFICATION

EDITED BY: Xiachang Wang, Khaled A. Shaaban, Guojun Wang, Javier Echeverria, Xuekui Xia and Yuanyuan Lu

PUBLISHED IN: Frontiers in Chemistry

frontiers Research Topics

frontiers

ISSN 1664-8714
ISBN 978-2-88974-907-2
DOI 10.3389/978-2-88974-907-2

About Frontiers

Frontiers is more than just an open-access publisher of scholarly articles: it is a pioneering approach to the world of academia, radically improving the way scholarly research is managed. The grand vision of Frontiers is a world where all people have an equal opportunity to seek, share and generate knowledge. Frontiers provides immediate and permanent online open access to all its publications, but this alone is not enough to realize our grand goals.

Frontiers Journal Series

The Frontiers Journal Series is a multi-tier and interdisciplinary set of open-access, online journals, promising a paradigm shift from the current review, selection and dissemination processes in academic publishing. All Frontiers journals are driven by researchers for researchers; therefore, they constitute a service to the scholarly community. At the same time, the Frontiers Journal Series operates on a revolutionary invention, the tiered publishing system, initially addressing specific communities of scholars, and gradually climbing up to broader public understanding, thus serving the interests of the lay society, too.

Dedication to Quality

Each Frontiers article is a landmark of the highest quality, thanks to genuinely collaborative interactions between authors and review editors, who include some of the world's best academicians. Research must be certified by peers before entering a stream of knowledge that may eventually reach the public - and shape society; therefore, Frontiers only applies the most rigorous and unbiased reviews.
Frontiers revolutionizes research publishing by freely delivering the most outstanding research, evaluated with no bias from both the academic and social point of view. By applying the most advanced information technologies, Frontiers is catapulting scholarly publishing into a new generation.

What are Frontiers Research Topics?

Frontiers Research Topics are very popular trademarks of the Frontiers Journals Series: they are collections of at least ten articles, all centered on a particular subject. With their unique mix of varied contributions from Original Research to Review Articles, Frontiers Research Topics unify the most influential researchers, the latest key findings and historical advances in a hot research area! Find out more on how to host your own Frontiers Research Topic or contribute to one as an author by contacting the Frontiers Editorial Office: frontiersin.org/about/contact

BIOACTIVE NATURAL PRODUCTS FROM MICROBES: ISOLATION, CHARACTERIZATION, BIOSYNTHESIS AND STRUCTURE MODIFICATION

Topic Editors:
Xiachang Wang, Nanjing University of Chinese Medicine, China
Khaled A. Shaaban, University of Kentucky, United States
Guojun Wang, Florida Atlantic University, United States
Javier Echeverria, University of Santiago, Chile
Xuekui Xia, Shandong Academy of Sciences, China
Yuanyuan Lu, China Pharmaceutical University, China

Citation: Wang, X., Shaaban, K. A., Wang, G., Echeverria, J., Xia, X., Lu, Y., eds. (2022). Bioactive Natural Products From Microbes: Isolation, Characterization, Biosynthesis and Structure Modification. Lausanne: Frontiers Media SA.
doi: 10.3389/978-2-88974-907-2

Table of Contents

frontiers in Chemistry

EDITORIAL
published: 22 March 2022
doi: 10.3389/fchem.2022.883652

Editorial: Bioactive Natural Products from Microbes: Isolation, Characterization, Biosynthesis and Structure Modification

Xiachang Wang[1], Yuanyuan Lu[2], Khaled A. Shaaban[3], Guojun Wang[4], Xuekui Xia[5] and Youjuan Zhu[1]*

[1]Jiangsu Key Laboratory for Functional Substances of Chinese Medicine, Nanjing University of Chinese Medicine, Nanjing, China, [2]State Key Laboratory of Natural Medicines, China Pharmaceutical University, Nanjing, China, [3]Center for Pharmaceutical Research and Innovation, College of Pharmacy, University of Kentucky, Lexington, KY, United States, [4]Harbor Branch Oceanographic Institute, Florida Atlantic University, Fort Pierce, FL, United States, [5]Key Biosensor Laboratory of Shandong Province, Biology Institute, Qilu University of Technology (Shandong Academy of Sciences), Jinan, China

Keywords: microbes, natural product, structure elucidation and modification, activity evaluation, biosynthesis

Editorial on the Research Topic

Bioactive Natural Products from Microbes: Isolation, Characterization, Biosynthesis and Structure Modification

OPEN ACCESS

Edited and reviewed by:
Michael Kassiou,
The University of Sydney, Australia

****Correspondence:***
Xiachang Wang
xiachangwang@njucm.edu.cn

Specialty section:
This article was submitted to Medicinal and Pharmaceutical Chemistry, a section of the journal Frontiers in Chemistry

Received: *25 February 2022*
Accepted: *08 March 2022*
Published: *22 March 2022*

Citation:
Wang X, Lu Y, Shaaban KA, Wang G, Xia X and Zhu Y (2022) Editorial: Bioactive Natural Products from Microbes: Isolation, Characterization, Biosynthesis and Structure Modification. Front. Chem. 10:883652. doi: 10.3389/fchem.2022.883652

Natural products have played an invaluable role in drug development, as about 24 percent of approved drugs belong to natural products or their derivative (Newman and Cragg, 2020). Compared with the limitation of medicinal resources such as plants and animals, microbes from soil, air, ocean and even endophytes, have now become a potential source for drug lead discovery, due to their abundant sources and characteristic biosynthetic pathways for novel bioactive compounds. The ability of all living organisms to biosynthesize endogenous, specialized small molecules is genetically encoded. The magnitude of biosynthetic gene clusters in microbial genome suggests that the secondary metabolite wealth of microbe is largely untapped. Mining algorithms and scalable expression platforms have greatly expanded access to the chemical repertoire of microbial secondary metabolites. This current Research Topic aims to discover bioactive natural products from microbes as drug leads, using new technologies such as metagenomics and gene mining to look for the breakthrough of new drug research and development. Overall, fourteen contributions were collected including one review and thirteen original articles, highlighting the importance of microbial natural products discovery for drug leads.

A review article by Yu et al. summarized the biological and chemical aspects of *Aspergillus niger* strains including their sources, BGCs, and secondary metabolites as well as biological properties and biosynthetic pathways. *A. niger* has become promising application products which possess a large number of cryptic biosynthetic gene clusters (BGCs) and produce various biomolecules as secondary metabolites with a broad spectrum of application fields including agriculture, food industry, and medicine. In the past 5 years, the number of new bioactive compounds from *A. niger* has been decreasing so that more efforts should be made to explore more sources for isolation of new *A. niger* strains and to awaken their silent BGCs to manufacture novel functional biomolecules using new strategies.

As one of the diseases with high mortality, cancer is one of the focuses of new drug research and development. Chen et al. discovered the fusarisetins E and F produced by a Mangrove endophytic fungus *Fusarium* sp. 2ST2 from the healthy leaves of *Kandelia candel* which showed significant

cytotoxicity against human A549 cell lines with IC_{50} values of 8.7 and 4.3 μM, respectively. At the same time, other new compounds including one new chromone fusarimone A, two new benzofurans fusarifurans A and B, three new isocoumarins fusarimarins A–C were isolated, which expanded the microbial secondary metabolite pool. Lu et al. also isolated novel secondary metabolite foeniculin K with cytotoxic activity from endophytic fungus *Diaporthe foeniculina*. Unfortunately, the other ten isolated analogues foeniculins I-J did not show cytotoxic activity. Their structures were established on the basis of ^{1}H and ^{13}C NMR spectra together with COSY, HSQC, HMBC, and NOESY experiments. Modern pharmacological research has revealed that *Dendrobium huoshanense* has anti-inflammatory, cytotoxic, hypoglycemic and antioxidant activity. Zhu et al. studied on an endophytic *Streptomyce*s sp. HS-3-L-1 isolated from the leaves of *Dendrobium huoshanense*, and isolated three unique polyketide dimers with the cytotoxicity against MV4-11 human leukemia cell. So far only two similar natural products, strepolyketides B and C (Jiang et al., 2020) were recently reported from a marine-derived *Streptomyces*. Kang et al. discovered one new *c*-butyrolactone derivative, diaportone A, one cyclopentenone derivative, diaportone B, and one monoterpene derivative, diaportone C, along with six known compounds from endophytic fungus *Diaporthe foeniculina* BZM-15. Two of these compounds displayed significant antiproliferative effects on three human cancer cell lines (SF-268, MCF-7, and HepG2).

With the widespread use of antibiotics in clinic, bacteria gradually developed drug resistance, and this is a serious threat to the health and safety of the world. Therefore, it is of great significance to discover novel antibiotics. An original article by Ding et al. focused on the polycyclic tetramate macrolactams (PTM), and revealed that biosynthetic gene clusters (BGCs) are widespread in both Gram-positive and Gram-negative bacteria. In this study, they investigated a sponge endosymbiont *Actinoalloteichus hymeniacidonis* harboring a potential PTM-BGC. Xanthobaccin A as well as two previously reported tetramates, equisetin and ikarugamycin, exhibited antibacterial activities against *Bacillus subtilis*. In addition, these three tetramates were confirmed as metallophores for the first time. They found that all three tetramates could reduce ferric into ferrous iron, which triggers the Fenton chemistry reaction, and their antimicrobial mechanism is possibly mediated through Fenton chemistry.

Endophytic bacteria is a valuable resource pool of microorganisms with wide distribution, diverse species and diverse biological functions, and is an important source of novel compounds. In this topic, Wang et al. reported that three new humulane-type sesquiterpenoids, penirolide A, penirolide B, and 10-acetyl-phomanoxide, together with three known compounds aurasperone A, pughiinin A, and cyclo (L-Leu-L-Phe) from the endophytic fungus *Penicillium* sp. derived from the leaves of *Carica papaya* L. And four compounds penirolide B, 10-acetyl-phomanoxide, pughiinin A, and cyclo (L-Leu-L-Phe) can significantly inhibit glucagon-induced hepatic glucose production, with EC_{50} values of 33.3, 36.1, 18.8, and 32.1 μM, respectively. In response to glucagon, cAMP is a second messenger to initiate glucagon signaling cascades in hepatic glucose production. The treatment of these compounds suppressed cAMP accumulation indicated that they inhibited hepatic glucose production by suppression glucagon-induced cAMP accumulation. Liu et al. reported six new phthalan derivatives cytorhizophins D-I as well as three known derivatives cytorhizophin C, pestacin and rhizophol B from endophytic fungus *Cytospora rhizophorae*. Among them, cytorhizophins D-E and F-G were two pairs of diastereoisomers, all of them featuring a 1-phenyl-1,3-dihydroisobenzofuran scaffold with a highly oxygenated O-linked isopentenyl unit, and cytorhizophins H-I represent the first examples of phthalide family with fascinating 6/6/6/5 tetracyclic ring system fusing as unprecedented furo [4,3,2-kl]xanthen-2 (10bH)-one skeleton. Cytorhizophins D-E and F-G showed significant DPPH radical scavenging activities with EC_{50} values ranging from 5.86 to 26. 80 μM, which are much better than that of the positive control ascorbic acid, they may be the promising lead compounds for the development of more effective antioxidants. Jia et al. focused on the mangrove-derived endophytes which are rich in bioactive secondary metabolites with a variety of biological activities. They isolated a fungus *Pseudofusicoccum* sp. J003 from mangrove species *Sonneratia apetala* Buch.-Ham. And then they identified a new sesquiterpenoid named acorenone C, two alkaloids, four phenolic compounds, and four steroid derivatives from this endophytic strain. Among them, acorenone C showed mild AChE inhibitory activity, with an inhibition rate of 23.34% at the concentration of 50 μM.

Wang et al. work reported that two new alkaloids tryptoquivaline Y and pseurotin I, together with eight known compounds, were isolated from *Aspergillus felis* FM324, and the fungus were purified from Hawaiian beach soil sample. One of the compounds showed weak antibacterial activity against *Staphylococcus aureus*, *methicillin resistant Staphylococcus aureus* and *Bacillus subtilis*. Two compounds inhibited NF-κB with IC_{50} values of 26.7 and 30.9 μM, respectively.

Wu et al. research selected the appropriate mutant *Aspergillus terreus* ASM-1 through the chemical mutagenesis of *A. terreus* ML-44 and resulted in the isolation of three new prenylated aspulvinones V–X, together with analogs, aspulvinone H, J-CR, and R. All the compounds were evaluated for α-glucosidase inhibitory effects with acarbose as positive control. The results showed that aspulvinones V and aspulvinone H exhibited potent α-glucosidase inhibitory activities with IC_{50} values of 2.2 and 4. 6 μM in mixed-type manners and aspulvinone H significantly suppressed the increases in postprandial blood glucose levels in the C57BL/6J mice. The results suggested that aspulvinones could be promising candidates for further pharmacologic research and the mechanism of the mutagenesis of the strain ASM-1 from strain ML-44 deserve further investigation which may make contribution to understanding the metabolic regulation of aspulvinones biosynthesis.

Tuberculosis (TB) is still a global disease threatening people's lives. Ilamycins are novel cyclopeptides with potent anti-TB activities, Li et al. focused on the preparation of ilamycin F, a major secondary metabolite isolated from the marine-derived mutant strain *Streptomyces atratus* SCSIO ZH16 ΔilaR which

were used as a scaffold to semi-synthesize eighteen new ilamycin derivatives (ilamycin NJL1–NJL18). Their study revealed that four of ilamycin NJLs have slightly stronger anti-TB activities against Mtb H37Rv (minimum inhibitory concentration, 1.6–1. 7 μM) compared with that of ilamycin F on day 14th, but obviously display more potent activities than ilamycin F on day third, which means that these derivatives have fast-onset effect. In addition, most ilamycin NJLs had low cytotoxicity except ilamycin NJL1. These findings will promote the further exploration of structure-activity relationships for ilamycins and the development of anti-TB drugs.

This special issue also covers some biosynthesis research. Deng et al. discovered three sulfur-containing granaticin congeners, mycothiogranaticins A, B and granaticin MA from a granaticin-producing strain of *Streptomyces vietnamensis* GIMV4.0001. Gene disruptions suggested that the biosynthesis of mycothiogranaticins is mycothioldependent, providing experimental evidence for the biological origin of sulfur in this category of sulfurcontaining polyketides. And mycothiol was found to be involved in positive regulation of the biosynthesis of granaticins by maintaining the cellular redox balance. This is the first report that mycothiol can not only be a building block of polyketides but also play a regulatory role in the polyketide biosynthesis. Based on previous research that P450 Astb can dually oxidize two methyl groups (C-19 and C-21) of preasperterpenoid A to asperterpenoid A with 3-carboxyl and 11-hydroxymethyl groups, Huang et al. confirmed the oxidation order of C-19 and C-21 catalyzed by AstB, by using the combination of the quantum chemistry calculations and the experiments of obtaining the potential intermediates and the HPLC-MS detection of the potential intermediates. In the end, they revealed the catalyzed order of AstB in asperterpenoid A biosynthesis and the relationship between the oxidation stations of C-19 and C-21 in asperterpenoids and their mPTPB inhibition.

In summary, the above works presented in this special research topic illustrate the diversity of microbial natural products and highlight the importance of developing new methods to impulse the discovery of new compounds. Microorganisms are still the treasure house of new drug development in the future.

AUTHOR CONTRIBUTIONS

All authors listed, have made substantial, direct and intellectual contribution to the work, and approved it for publication.

ACKNOWLEDGMENTS

The Editors would like to thank all authors that participated in this Research Topic in "New frontiers in the search of antimicrobials agents from natural products." Special acknowledgment is given to each reviewer (external or editorial board member), who has contributed and whose valuable support is fundamental to the success of the journal.

REFERENCE

Newman, D. J., and Cragg, G. M. (2020). Natural Products as Sources of New Drugs over the Nearly Four Decades from 01/1981 to 09/2019. *J. Nat. Prod.* 83, 770–803. doi:10.1021/acs.jnatprod.9b01285

Jiang, Y., Huang, Y., Chen, S., Ji, Y., Ding, W., and Ma, Z. (2020). Strepolyketides A-C, three novel SEK15-derived polyketides from Streptomyces sp. HN2A53. *Tetrahedron Lett.* 61, 151996. doi:10.1016/j.tetlet.2020.151996

Conflict of Interest: The authors declare that the research was conducted in the absence of any commercial or financial relationships that could be construed as a potential conflict of interest.

frontiers in Chemistry

REVIEW
published: 30 July 2021
doi: 10.3389/fchem.2021.701022

Aspergillus niger as a Secondary Metabolite Factory

Ronglu Yu[1], *Jia Liu*[1], *Yi Wang*[1], *Hong Wang*[1,2] *and Huawei Zhang*[1,2]*

[1]School of Pharmaceutical Sciences, Zhejiang University of Technology, Hangzhou, China, [2]Key Laboratory of Marine Fishery Resources Exploitment and Utilization of Zhejiang Province, Hangzhou, China

Aspergillus niger, one of the most common and important fungal species, is ubiquitous in various environments. *A. niger* isolates possess a large number of cryptic biosynthetic gene clusters (BGCs) and produce various biomolecules as secondary metabolites with a broad spectrum of application fields covering agriculture, food, and pharmaceutical industry. By extensive literature search, this review with a comprehensive summary on biological and chemical aspects of *A. niger* strains including their sources, BGCs, and secondary metabolites as well as biological properties and biosynthetic pathways is presented. Future perspectives on the discovery of more *A. niger*-derived functional biomolecules are also provided in this review.

Keywords: *Aspergillus niger*, secondary metabolite, bioactivity, biosynthesis, application

OPEN ACCESS

Edited by:
Yuanyuan Lu,
China Pharmaceutical University, China

Reviewed by:
Weaam Ebrahim,
Mansoura University, Egypt
Paul-Henri Ducrot,
INRA UMR1318 Institut Jean Pierre Bourgin, France

***Correspondence:**
Huawei Zhang
hwzhang@zjut.edu.cn

Specialty section:
This article was submitted to Organic Chemistry, a section of the journal Frontiers in Chemistry

Received: *30 April 2021*
Accepted: *28 May 2021*
Published: *30 July 2021*

Citation:
Yu R, Liu J, Wang Y, Wang H and Zhang H (2021) Aspergillus niger *as a Secondary Metabolite Factory. Front. Chem. 9:701022. doi: 10.3389/fchem.2021.701022*

INTRODUCTION

Aspergillus, one sizeable genus belonging to Aspergillaceae family, comprises as many as 492 species registered on the database of the National Center for Biotechnology Information (NCBI) to date. Its section *Nigri* is an important group of species, and the *A. niger* aggregate represents its most complicated taxonomic subgroup with eight morphologically indistinguishable taxa (Perrone et al., 2011). Owing to superior adaptability and survivability, *A. niger* is ubiquitous in nature, including in terrestrial soil (Xie et al., 2006), ocean (Li et al., 2016; Uchoa et al., 2017), the Arctic (Singh et al., 2011), and space. It also occupies a wide spectrum of habitats in plants and animals such as herb (Shreelalitha and Sridhar, 2015; Manganyi et al., 2018), shrub (Kaur et al., 2015; Liu et al., 2016), tree (Soltani and Moghaddam, 2014; Wang et al., 2019), lichen (Elissawy et al., 2019), shrimp (Liu et al., 2013; Fang et al., 2016), and marine sponge (Takano et al., 2001; Hiort et al., 2004). *A. niger* strain grows well in various media with different carbon sources, including glucose, bran, maltose, xylan, xylose, sorbitol, and lactose (Toghueo et al., 2018). However, its metabolism is remarkably affected by culture conditions, such as medium composition and fermentation mode.

The genome features of strain L14 are summarized in a polycyclic graph (**Figure 1**), which consists of in-paralog pair, GC skew, widely, SM biosynthetic gene cluster (BGC), ncRNA, repeat, strand coding sequence (CDS) annotation, and scaffold. There are some in-paralog pairs between different scaffolds, and SM BGCs and CDS distributed widely in genome. As shown in **Table 1**, genome sizes of WT *A. niger* strains range from 33.8 to 36.1 Mb. Their G + C% and gene numbers are closely similar, while the numbers of scaffolds are different owing to various sequencing and assembling manners. The antibiotics and Secondary Metabolite Analysis Shell (antiSMASH) results indicated that each WT *A. niger* strain harbors at least 20 cryptic SM BGCs, including PKS, NRPS, NRPS-like, and their hybrids (**Figure 2** and **Supplementary Table S1**) (Blin et al., 2019). These BGCs involving in indole and terpene biosynthesis are ubiquitous and have great potential to synthesize therapeutical agents and pesticides, such as AbT1, azanigerone A, fusarin, ferrichrome, nidulanin A, melanin, TAN-1612, yanuthone D, and aflavarin (**Supplementary Table S2**).

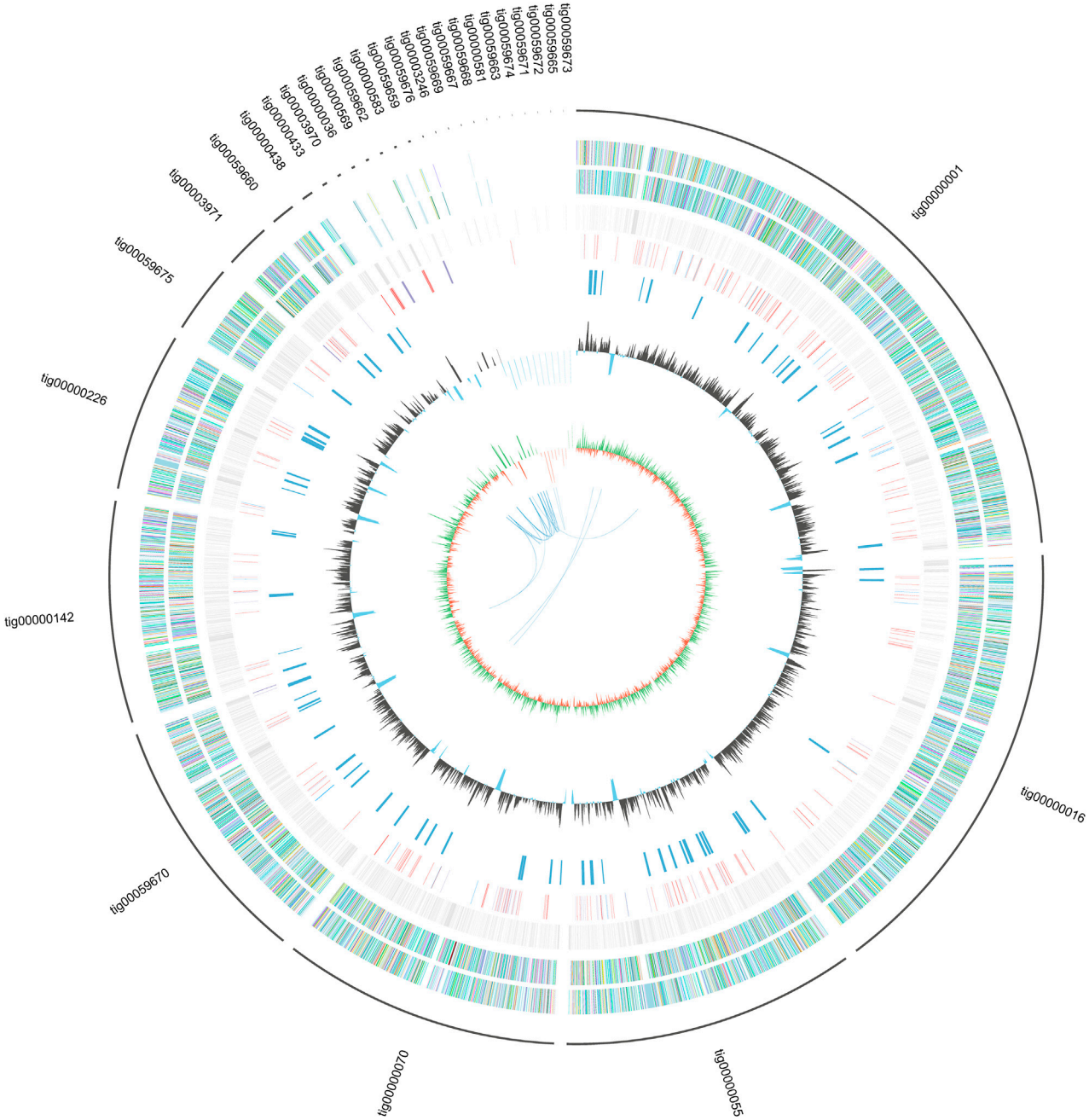

FIGURE 1 | General genome features of marine strain *Aspergillus niger* L14 (From the inside out: In-paralog pairs; GC skew, the green part represent positive value while the orange part represent negative value; G + C%; SMs gene clusters; ncRNA; repeat; minus strand coding sequence (CDS) annotation; plus strand CDS annotation; scaffolds).

It is a matter of controversy that some *A.* niger isolates are renowned for biosynthesis of valuable natural products of nutritional, agrochemical, and pharmaceutical interest, while others are reputed to cause the "black mold" disease (Hayden et al., 1994; Ozer and Koycu, 2006) and produce a plethora of mycotoxins (Sanchez et al., 2012). *A. niger* possesses a bulk warehouse of prolific genes, which involve in regulation of primary and secondary metabolisms (Pel et al., 2007). A genome-scale metabolic network for *A. niger* has been established on account of its high efficiency in rational metabolic design and systems biology studies, such as strain improvement and process optimization (Sun et al., 2007; Lu

TABLE 1 | General genomic features of 12 *Aspergillus niger* strains from NCBI database.

Strain	Genome size (Mb)	G + C%	Scaffold	Gene	tRNA	Protein-coding genes	Isolation source	Assembly ID
ATCC 1015	34.8	50.3	24	10947	–	10950	–	GCA_000230395.2
CBS 513.88	34.0	50.4	20	10828	263	14165	–	GCA_000002855.2
SH-2	34.6	50.3	349	–	–	–	Soil	GCA_000633045.1
ATCC 13496	35.7	49.5	133	12468	273	12194	–	GCA_003344705.1
An76	34.9	49.4	669	10373	–	10373	Soil	GCA_001515345.1
JSC-093350089	36.1	49.5	223	–	–	–	International space station environmental surface	GCA_001931795.1
H915-1	36.0	49.2	30	–	–	–	Soil	GCA_001741905.1
L2	36.4	49.2	30	–	–	–	Soil	GCA_001741915.1
A1	34.6	50.1	319	–	–	–	Soil	GCA_001741885.1
MOD1-FUNGI2	33.8	50.4	3199	–	–	–	Red seedless grapes	GCA_004634315.1
RAF 106	35.1	49.1	10	–	–	–	Pu-er tea	GCA_011316255.1
L14	36.1	49.3	30	11524	296	–	Marine sponge	JADEYF000000000

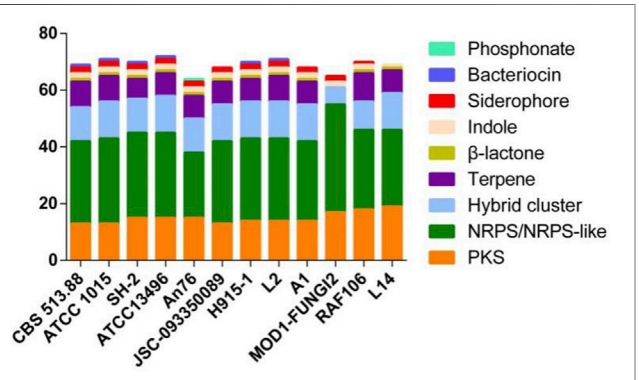

FIGURE 2 | Biosynthetic gene clusters of secondary metabolites of 12 *A. niger* strains.

et al., 2017). Numerous *A. niger* strains have been applied in many fields for a long time. For instance, citric acid as one of incredible organic acids in food industry had been produced on a large scale by *A. niger* 100 years ago (Cairns et al., 2018; Li et al., 2020). It is important that *A. niger* is one of the excellent producers of valuable proteases, which had been widely used as detergents and food ingredients and additives, such as acetylesterase, amylase, fucosidase, glucose oxidase, glucosidase, mannanase, phospholipase, phytase, prolyl endopeptidase, triacylglycerol lipase, trehalase, and xylanase. In addition, numerous chemical studies have indicated that *A. niger* is one of the rich sources of bioactive SMs, with great potential application in agriculture and medicine. Moreover, endoxylanase isozymes of *A. niger* have great potential transforming lignocellulose in pulp and paper industry as industrial bleaching aids (Duarte and Costaferreira, 1994). Furthermore, *A. niger* is also able to deal with the phenolic contaminants in waste water of fermentation broth from industry (Duarte and Costaferreira, 1994). Since genetic engineering is inefficient for fully exploiting in the filamentous fungi industry, a CRISPR (clustered regularly interspaced short palindromic repeats)–Cas9 system had been developed (Nødvig et al., 2015; Nødvig et al., 2018). Based on these genome-editing toolbox, gene inactivation and knockout, gene insertion, base editing, promoter replacement, and regulation of gene expression in *A. niger* have come true. In the future, more importance may be focused on traceless gene editing, multiple gene editing and fine regulation of gene expression in *A. niger*.

SECONDARY METABOLITES FROM *ASPERGILLUS NIGER*

By extensive search on the database of Dictionary of Natural Products (DNP), as many as 166 *A. niger*–derived secondary metabolites (**1**–**166**) were detected till 2020. On the basis of chemical structures, these chemicals are grouped into five types: pyranone, alkaloid, cyclopentapeptide, polyketide, and sterol and, respectively, introduced as follows. (More detailed information about these substances is provided in the Supplementary Materials (**Supplementary Table S3**).)

Pyranones

γ-Naphthylpyradone Monomers

Pyranone derivatives are the most isolated SMs from *A. niger*, including γ-naphthylpyradones (**1**–**31**), α-pyranones (**32**–**56**), and γ-pyranones (**57**–**60**). *A. niger*–derived naphthylpyradones are sorted into two classifications: monomers and dimers, with linear and angular naphtho-γ-pyrone. Fonsecin (**1**) is one of the most frequently isolated γ-naphthylpyradone produced by several *A. niger* strains from various sources, including terrestrial soil (Sakurai et al., 2002), marine (Leutou et al., 2016; Zhou et al., 2016), and plants (Bouras et al., 2005; Fernand et al., 2017; Akinfala et al., 2020). Biological tests suggested that compound 1 possesses dose-dependent inhibitory effect on the interleukin-4 (IL-4) signal transduction and stronger radical scavenging activity against 2,2-diphenyl-1-picrylhydrazyl (DPPH) than ascorbic acid (Sakurai et al., 2002; Leutou et al., 2016). Two analogs TMC-256A1 (**3**) and TMC-256C1 (**8**) also effectively inhibited the IL-4 driven luciferase (Sakurai et al., 2002). However, fonsecin B (**2**) and nigerasperone A (**4**) exhibited weak bioactivity against luciferase and DPPH

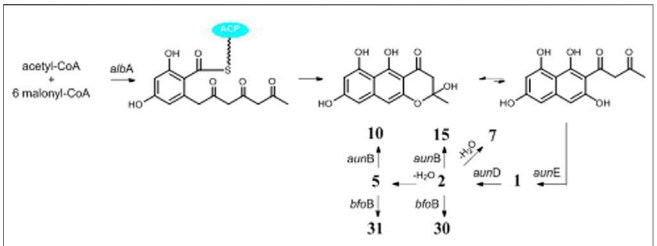

FIGURE 3 | Proposed biosynthetic pathway of γ-naphthylpyridones.

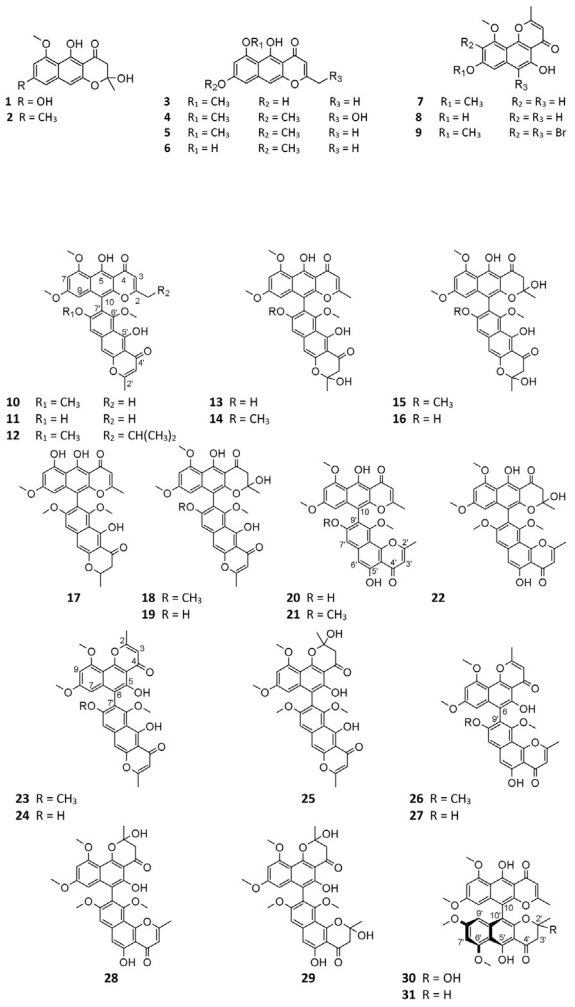

(Sakurai et al., 2002; Zhang et al., 2007b). One new cytotoxic and antimicrobial rubrofusarin B (**5**) was purified from strain IFB-E003 endophytic on *Cynodon dactylon* Linn. (Song et al., 2004). When cultivated in NaBr or $CaBr_2$-containing medium, one marine-derived strain MSA773 was found to secrete a new brominated derivative 6,9-dibromoflavasperone (**9**) with potent radical scavenging activity (Leutou et al., 2016).

γ-Naphthylpyradone Dimers

A. niger–derived dimeric naphthylpyradones (**10**–**31**) consist of two monomers with linear and/or angular structure(s). It is interesting that most of these bis-naphtho-γ-pyrones were produced by symbiotic *A. niger* strains. Chemical investigation of eight *A. niger* strains led to isolation of the same SM aurasperone A (**10**) (Tanaka et al., 1966; Tanaka et al., 1972; Akiyama et al., 2003; Zhang et al., 2007b; Fang et al., 2016; Li et al., 2016; Wang et al., 2018; Padhi et al., 2020), which possessed a broad spectrum of bioactivities including moderate cytotoxicity (Fang et al., 2016; Padhi et al., 2020), strong antimicrobial effect (Lu et al., 2014; Padhi et al., 2020), and xanthine oxidase (XO) inhibitory and anti-hyperuricosuric activity (Song et al., 2004). Aurasperone B (**15**) had potent radical scavenging activity against DPPH with an IC_{50} value of 0.01 μM (Leutou et al., 2016). Marine strain SCSIO Jcsw6F30 was a prolific producer of asperpyrone-type bis-naphtho-γ-pyrones (BNPs) **10**, **13**–**16**, **18**, **20**–**22**, **24**, and **27**, among which compounds **13**, **16**, and **20** exhibited remarkable inhibitory effects on COX-2 (Fang et al., 2016). In addition to nigerasperone A (**4**), two dimeric naphthylpyradones nigerasperones B (**29**) and C (**19**) were obtained from strain EN-13 and shown to exhibit a moderate radical scavenging effect on DPPH (Zhang et al., 2007b). Bioassay-guided fractionation of the crude extract of strain AKRN associated with *Entandrophragma congoënse* afforded a new antibacterial naphtho-γ-pyrone dimer 2-hydroxydihydronigerone (**30**) (Happi et al., 2015).

One possible pathway for biosynthesis of γ-naphthylpyradone derivatives had been first proposed by Obermaier and Muller (2019). As shown in **Figure 3**, one acetyl-CoA and six malonyl-CoA clusters were used as substrates for the biosynthesis of compounds **1**–**3** and 8 by successive catalytic reactions in a nonreducing PKS (nrPKS) system. Two of these monomers further dimerized at various carbon positions (C-6, C-7, C-9, or C-10) and resulted in the formation of dimers **16**, **21**, **27**, and **28**. Lately, one nrPKS gene *D8.t287* responsible for the biosynthesis of the initial precursor heptaketone was identified and characterized by target gene knockout experiment and UPLC-MS analysis (Hua et al., 2020). However, the role of the gene *AunB* or *BfoB* is not confirmed so far.

α-Pyranones

A. niger–derived α-pyranones contain 14 monocyclic compounds (**32**–**40**, **50**), 7 dicyclics (**41**–**47**, **51**), three tricyclics (**48**, **49**, and **56**), and four tetracyclics (**52**–**55**). Chemical analysis of an endophytic *A. niger* strain colonizing in liverwort *Heteroscyphus tener* (Steph.) Schiffn resulted in isolation of three new amide campyrones A–C (**38**–**40**) together with compounds **33** and **34** (Talontsi et al., 2013; Li et al., 2015). One possible biosynthetic pathway proposed by Reber and Burdge (2018) suggested that compounds **38**–**40** were, respectively, formed by one malonyl-CoA and three *N*-acetyl aliphatic amino acids including *L*-valine, *L*-leucine, and *L*-isoleucine (**Figure 4**), along with two congeners asnipyrones A (**42**) and B (**46**) and nigerapyrones A-H (**35**–**37**, **43**–**45**, **48**–**49**) were first discovered from a mangrove plant–derived strain MA-132 (Liu et al., 2011).

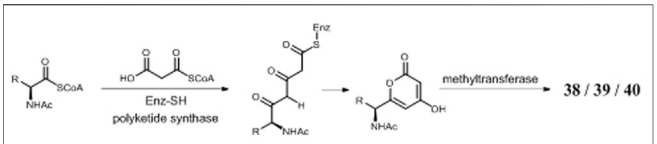

FIGURE 4 | Proposed biosynthetic pathway of campyrones.

Unfortunately, none of these compounds showed potent cytotoxic or antimicrobial activities. Nafuredin (**50**) and bicoumanigrin (**52**) were new α-pyranone analogs produced by marine sponge-derived *A. niger* strains; the former exhibited a powerful and selective inhibitory effect on NFRD (NADH-fumarate reductase) (Takano et al., 2001; Ui et al., 2001) and the latter 3,3′-bicoumarin had moderate cytotoxicity against leukemia and carcinoma cell lines (Hiort et al., 2004). Three 8,8′-bicoumarins, orlandin (**53**), kotanin (**54**), and 7-desmethyl-kotanin (**55**) were produced by a number of *A. niger* strains from various sources, and **53** showed potent inhibitory activity against wheat coleoptile growth at 1 mM but not toxic to day-old cockerels (Cutler et al., 1979; Ovenden et al., 2004; Sorensen et al., 2009; Jomori et al., 2020). Biosynthetically, one acetyl-CoA and four malonyl-CoAs comprised one coumarin through several successive reactions catalyzed by PKSs, followed by formation of compounds 52–55 through dimerization (**Figure 5**) (Huttel et al., 2003; Huttel and Muller, 2007; Girol et al., 2012). In this pathway, PKS gene *ktnS* was responsible for origination of dimeric coumarins **52–55**, gene *ktnB* encode O-methyltransferase, and gene *ktnC* encode CYP450 monooxygenase, manipulating the dimerization of **52–55**.

γ-Pyranones

To the best of our knowledge, only four γ-pyranone derivatives (**57–60**) had been detected in SM of *A. niger*. Among these substances, kojic acid (**57**) is the most common product with weak antimicrobial property (Liu et al., 2011; Happi et al., 2015; Padhi et al., 2020). In addition to carbonarone A (**59**) and tensidol B (**60**), one new benzyl γ-pyranone nigerpyrone (**58**) was discovered from a mutant strain FGSC A1279 ΔgcnE and was found to have potent and selective activity against *Candida parapsilosis* (Wang et al., 2018; Padhi et al., 2020).

Alkaloids

Pyrroles

Pyranonigrin derivatives (**61–69**) are a family characterized by pyrano [2,3-b] pyrrole skeleton, and their biosynthesis are

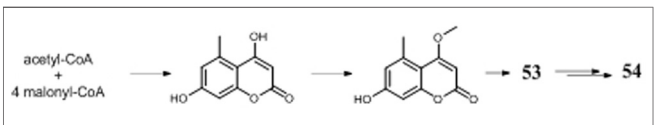

FIGURE 5 | Proposed biosynthetic pathway of orlandin (**53**) and kotanin (**54**).

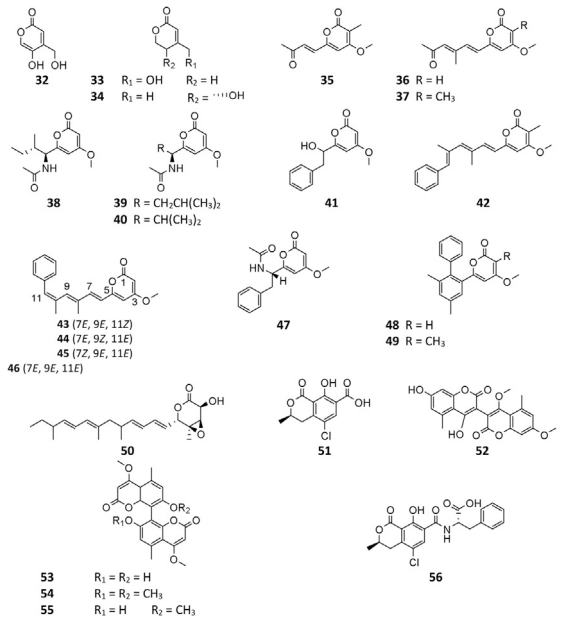

manipulated by the *pyn* gene cluster in *A. niger* (Riko et al., 2014; Yamamoto et al., 2015). Chemical investigation of one marine sponge–derived strain afforded four pyranonigrins B-D (**61**, **62**, **64**) and Ab (**63**), which 63 showed a strong inhibitory effect on the growth of neonate larvae of the plant pest insect *Spodoptera littoralis* (Hiort et al., 2004). Pyranonigrins A (**65**), S (**66**), and E (**67**) were important agents with potent radical scavenging activity toward DPPH and superoxide (Miyake et al., 2007; Riko et al., 2014). One possible biosynthetic pathway of pyranonigrin E (**67**) had been first proposed by Yamamoto et al. (2015) and coworker in 2015, in which the start units contained one acetyl-CoA, six malonyl-CoAs, and one *L*-Ser (**Figure 6**), under the action of gene *pynA* (PKS-NRPS hybrid synthase), *pynI* (encode thioesterase), *pynC* (encode methyltransferase), *pynG* (encode flavin-dependent oxidase), *pynD* (encode CYP450), and *pynH* (encode aspartyl protease). After non-enzymatic reaction, two pyranonigrin E (**67**) units could be dimerized to form pyranonigrin F (**69**). One soil-derived *A. niger* strain was found to produce a new dichlorinated pyrrole pyoluteorin (**70**), which obviously induced cell cycle arrest and apoptosis in human triple-negative breast cancer cells MDA-MB-231 (Ding et al., 2020). Two benzyl furopyrrols tensidols A (**71**) and B (**72**) from strain

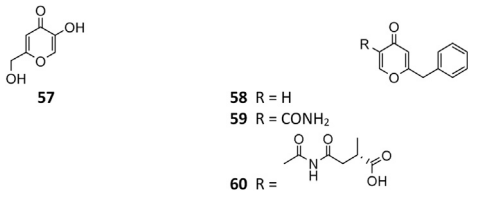

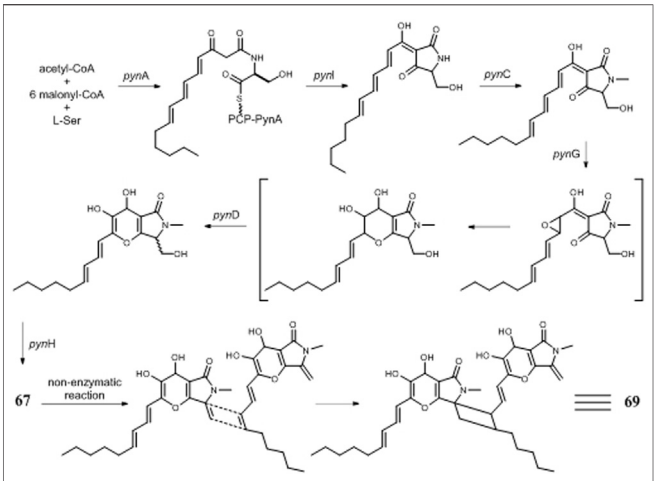

FIGURE 6 | Proposed biosynthetic pathway of pyranonigrin E (**67**) and pyranonigrin F (**69**).

FKI-2342 were potentiators of antifungal miconazole activity (Fukuda et al., 2006) and lately corrected as compounds **59** and **60** (Henrikson et al., 2011).

Pyridones

A. niger–derived pyridone derivatives (**73**–**82**) have one benzyl group and possess antimicrobial and cytotoxic properties (chatr 4). Two new α-pyridones aspernigrins A (**73**) and B_b (**74**) were isolated from one *A. niger* strain of marine sponge *Axinella damicornis* and showed moderate cytotoxicity and a potent neuroprotective effect, respectively, (Hiort et al., 2004). When cultivated in fermentation medium containing suberoylanilide hydroxamic acid (SAHA) and *p*-fluoro SAHA, strain ATCC 1015 was discovered to produce three antifungal γ-pyridones, nygerones A (**78**), B (**75**), and *p*-fluoro nygerone B (**77**) (Henrikson et al., 2009; Henrikson et al., 2011). In addition to three γ-naphthylpyradones (**1**, **3**, and **5**) and one cyclic peptide (**111**), three 2-benzyl-γ-pyridones aspernigrins B-D (**80**–**82**) were obtained from the marine strain SCSIO Jcsw6F30, and **81** was found to have potent inhibitory activity toward HIV-1 SF162-infected TZM-bl cells (Zhou et al., 2016).

Other Alkaloids

Three fatty amines fumonisins B_2 (**83**), B_1 (**84**), and B_4 (**85**) from stains FGSC A1279 and IBT 28144 were carcinogenic (Nielsen et al., 2009; Sorensen et al., 2009; Li et al., 2019). The *aza* gene cluster in strain ATC C1015 was found be responsible for biosynthesis of azanigerone D (**86**) (Zabala et al., 2012). In addition to pyoluteorin (**70**), phenazine-1-carboxylic acid (**87**) was produced by the soil *A. niger* strain (Ding et al., 2020). Two new piperazines nigragillin (**88**) and nigerazine B (**89**) were purified from strain ATCC 11414, and their biosynthesis were regulated by the naphthopyrone precursor BGC *alb* gene cluster (Chiang et al., 2011). Endophytic strain IFB-E003–derived aspernigerin (**90**) displayed a potent effect on the tumor cell lines nasopharyngeal epidermoid KB, cervical carcinoma Hela, and colorectal carcinoma SW1116 (Shen et al., 2006).

Amides

Till the end of 2020, only six amides (**91**–**96**) had been isolated and characterized from *A. niger* strains. Fractionation of crude extract of marine strain BRF-074A afforded one furan ester derivative (**91**), one cerebroside chrysogeside D (**93**), and two spiro amides pseurotins A (**95**) and D (**96**), among which 91 exerted a cytotoxic effect on HCT-116 cell line (Uchoa et al., 2017). When cultivated on wheat bran, strains CFR-W-105 and MTCC-5166 were discovered to produce nigerloxin (**92**) with free radical DPPH scavenging activity and inhibitory effect on lipoxygenase-I (LOX-1) and rat lens aldose reductase (RLAR) (Rao et al., 2002; Chakradhar et al., 2009). Ergosterimide (**94**) was a new natural Diels–Alder adduct of ergosteroid and maleimide produced by the strain EN-13 from marine alga (Zhang et al., 2007a).

Cyclopeptides

All peptides of *A. niger* are cyclic and consist of ten dipeptides (**97**–**106**), eight pentapeptides (**107**–**114**), and three bis(dipeptide)s (**115**–**117**). In addition to α-pyranones **32**–**34**, **38**, and **40**, four diketopiperazines (**97**, **99**, **115**, and **116**) were isolated from an endophytic strain of liverwort *Heteroscyphus tener* (Steph.). Schiffn, and compounds **115** and **116** showed weak activity against the human ovarian carcinoma cancer cell line A2780 (Li et al., 2015). However, **115** exhibited significant selective cytotoxicity to human leukemia murine colon 38 and human colon H116 and CX1 cell lines (Varoglu et al., 1997; Varoglu and Crews, 2000). One strain BRF-074A from Northeast Brazilian coast was a prolific producer of cyclopeptides (**101**–**107**, **114**) (Uchoa et al., 2017). Phytochemcial analysis of an uncoded marine strain afforded a new diketopiperazine dimer (**117**) and nine monomers (**98**–**106**) (Ovenden et al., 2004; Zhang et al., 2010; Uchoa et al., 2017). Compounds **98** and **99** had been reported to regulate plant growth (Kimura et al., 1996; Kimura et al., 2005), and **101** had selectively potential cytotoxicity (Graz et al., 2000). Eight malformin analogs (**107**–**114**) were a group of SMs containing structural skeleton of cyclo-*D*-cysteinyl-*D*-cysteinyl-*L*-amino acid-*D*-amino acid-*L*-amino acid (Kim et al., 1993). Malformin A (**107**) demonstrated antibacterial (Suda and Curtis, 1966; Liu et al., 2013) and

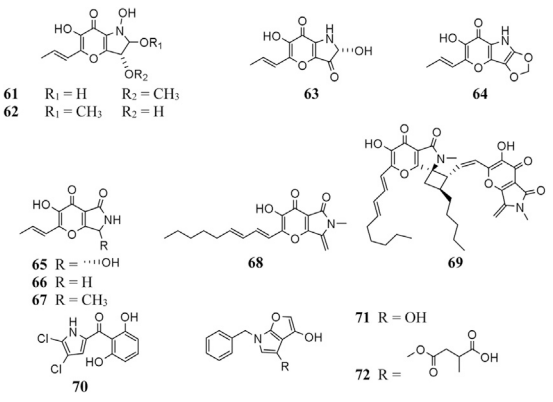

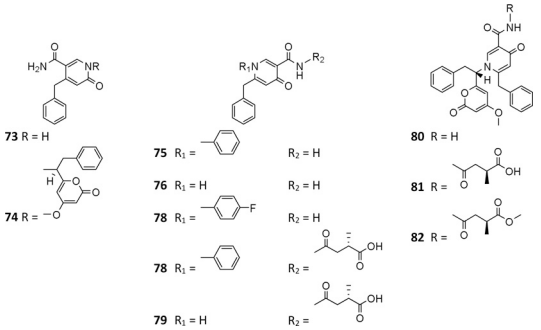

anticancer activities (Wang et al., 2015), while malformin C (**114**) exhibited a broad spectrum of biological properties including anti-HIV-1 (Zhou et al., 2016), cytotoxic (Jomori et al., 2020), anticancer (Wang et al., 2015), and antibacterial (Suda and Curtis, 1966; Liu et al., 2013).

Polyketides

Polyketides (**118**–**155**) are the largest group of SMs produced by *A. niger*. Citric acid (**118**) and itaconic acid (**119**) have been large-scale products in food and pharmaceutical industry for decades (Andersen et al., 2011; Li et al., 2012). Some other valuable chemicals with low molecular weight are also produced by *A. niger*, such as 2-phenylethanol (**128**) (Etschmann et al., 2015), *p*-hydroxyphenylacetic acid (**129**) (Happi et al., 2015), gallic acid (**130**) (Saeed et al., 2020), benzoic acid derivative (**131**) (Zabala et al., 2012), and asperyellone (**147**) (Jefferson, 1967; Chidananda et al., 2008). In comparison with **119**, the biological activity of hexylitaconic acid (**120**) dramatically attenuated (Varoglu et al., 1997; Varoglu and Crews, 2000). By overexpression of transcriptional regulator pBARAGA-CaaR of BGC *caa* in glucose minimal medium, strain ATC C1015 successfully produced three acyltetronic acid derivatives carlosic acid (**123**), carlosic acid methyl ester (**124**), and agglomerin F (**125**) (Yang et al., 2014). Chemical analysis of two strains KB1001 and F97S11 afforded fifteen meroterpenoid derivatives (**132**–**146**), in which biosynthesis was deduced to be manipulated by the *yan* gene cluster in strain KB1001 (**Figure 7**) (Bugni et al., 2000; Holm et al., 2014). Furthermore, *yan* gene cluster consisted of gene *yanA* [encode 6-methylsalicylic acid synthase (6-MSAS)] together with eight additional genes *yanB* (encode decarboxylase), *yanC* (encode CYP450), *yanD* (encode dehydrogenase), *yanE* (unknown), *yanF* (encode oxidase), *yanI*

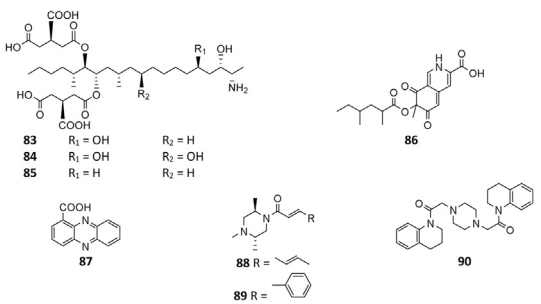

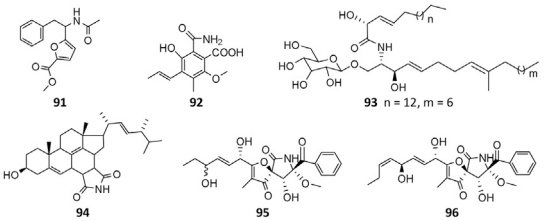

(encode O-mevalon tiransferase), *yanH* (encode CYP450), and *yanG* (encode prenyl transferase).

Asperyellone (**147**) was the common product of strains NRRL-3 and CFTRI 1105 (Jefferson, 1967; Chidananda et al., 2008) and exhibited inhibitory effect on lipoxygenase and human platelet aggregation (Rao et al., 2002), UVB protection (Santhakumaran et al., 2019), and antifungal activity (Ayer et al., 1996). In addition

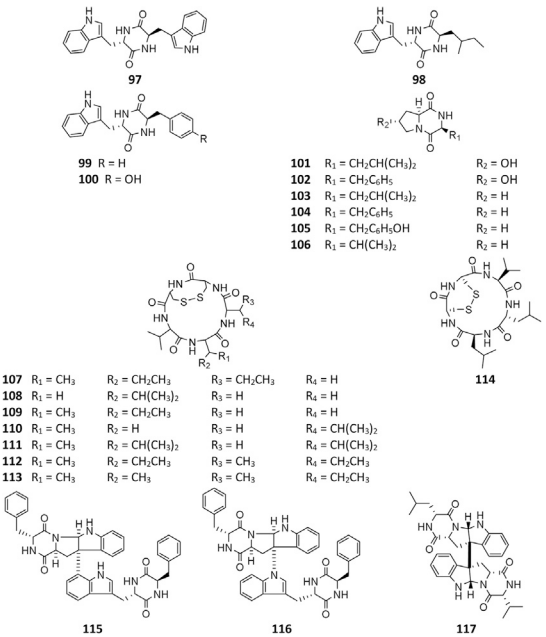

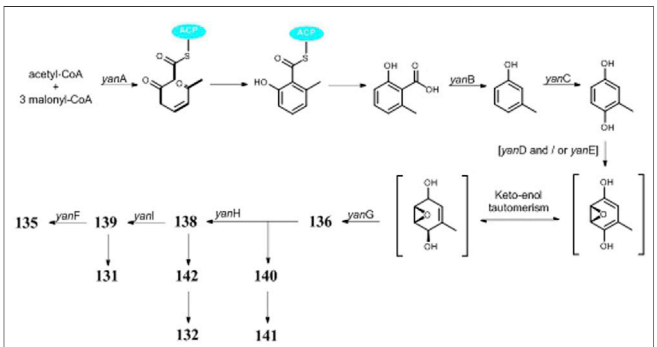

FIGURE 7 | Proposed biosynthetic pathway of yanuthones.

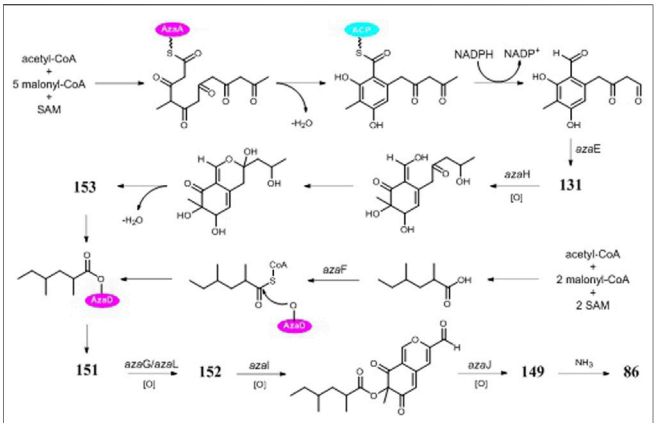

FIGURE 8 | Proposed biosynthetic pathway of pyranoquinones in strain ATCC 1015.

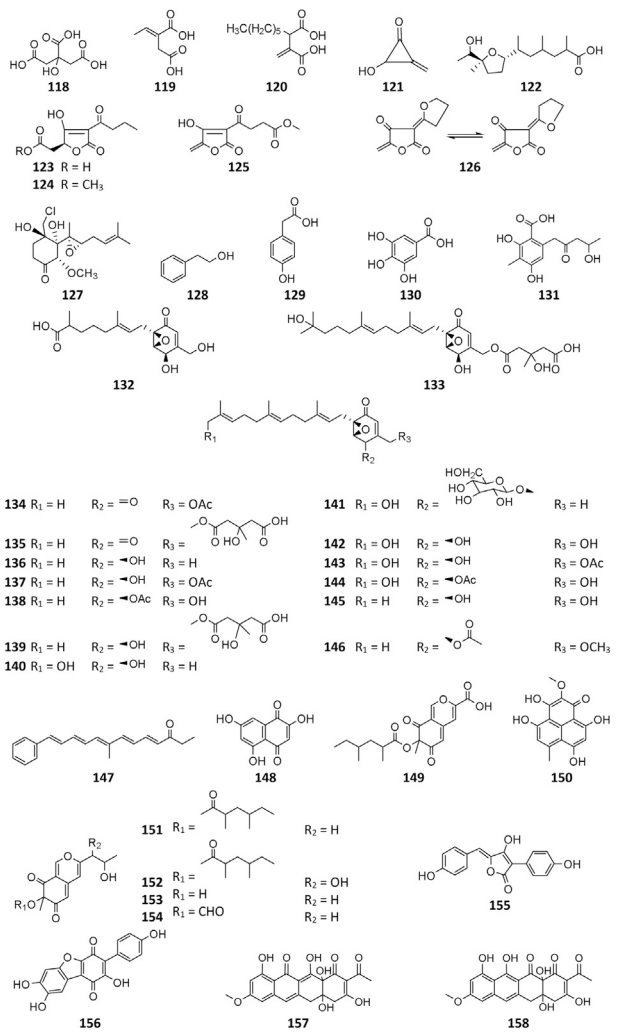

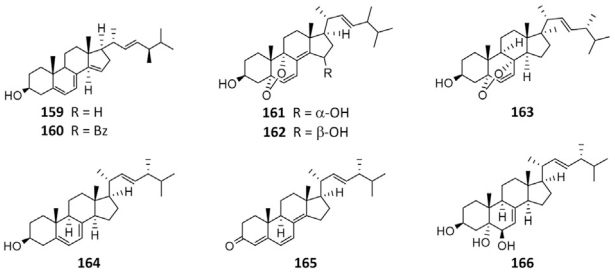

to γ-pyridone (**86**), five highly oxygenated pyranoquinones (**86, 149, and 151–154**) were detected in SMs of strain T1 by activation of the *aza* gene cluster (Zabala et al., 2012) (**Figure 8**). In biosynthesis of pyranoquinones, genes *azaE* (encode ketoreductase), *azaF* (encode acyl:CoA ligase), *azaG* (encode FAD-dependent oxygenase), *azaH* (encode salicylate monooxygenase), *azaI* (encode CYP450), *azaJ* (encode dehydrogenase), and *azaL* (encode FAD-dependent oxygenase) play important roles. Funalenone (**150**), one phenalene derivative, was obtained from strain ATCC 11414 whether the *alb*A gene was auxotrophic or not (Chiang et al., 2011). Meanwhile, funalenone (**150**) was also found in *A. niger* mutant Δ*gcn*E (strain FGSC A1279 lacking epigenetic regulator*gcn*E) (Wang et al., 2018). Two tetracycline analogs BMS-192548 (**157**) and TAN-1612 (**158**) were, respectively, obtained from strains WB2346 and ATC C1015 and shown to be acyclic binding inhibitors of neuropeptide Y receptors (Kodukula et al., 1995; Shu et al., 1995; Li et al., 2011).

Sterols

As the by-product of manufacture of citric acid, 14-dehydroergosterol (**159**) and its benzoate (**160**) were the first steroids isolated from *A. niger* (Barton and Bruun, 1951) and possessed anti-inflammatory and cytotoxic properties (Ano et al., 2017). Strain MA-132–derived nigerasterols A (**161**) and B (**162**) had potent antiproliferative activity against human promyelocytic leukemia (HL60) and human lung carcinoma (A549), with IC_{50} values of 0.11 and 0.43 μM, respectively, (Liu et al., 2013). In addition to ergosterimide (**94**), four steroid derivatives (**163–166**) were discovered from the endophytic strain EN-13 associated with marine brown alga (Zhang et al., 2007a).

CONCLUSION AND FUTURE PROSPECTS

A. niger strains are ubiquitous in nature and occupy a wide spectrum of habitats in animal and plant environments, and they are economically important both as harmful or beneficial microorganisms. Numerous chemical studies suggest that *A. niger* is one of the prolific sources of functional biomolecules, including organic acids, vitamins, pesticides, valuable proteases, and therapeutic agents, which have potential

application in various fields including agriculture, food industry, and medicine. However, the number of new bioactive compounds from *A. niger* has been decreasing for the past 5 years. This deteriorating trend will result in a negative impact on discovery and development of new *A. niger*–derived valuable substances, such as new drug leads. Therefore, more efforts should be made to explore more sources for isolation of new *A. niger* strains and to awaken their silent BGCs to manufacture novel functional biomolecules using new strategies, such as one strain many compounds (OSMAC) approach (Hemphill et al., 2017; Pan et al., 2019) and genetic mining combined with metabolic engineering (Zhang et al., 2019; Li et al., 2020; Wei et al., 2021). Moreover, functional genomics should allow for an in-depth understanding of the underlying biosynthetic logic of *A. niger*–derived SMs (He et al., 2018). In order to accelerate development of valuable products from *A. niger*, construction and breeding of robust strains as well as optimization of their cultivation and fermentation processes should be intensively conducted at various levels (Zou et al., 2015; Xu et al., 2019).

AUTHOR CONTRIBUTIONS

RY made a draft of this review; JL and YW searched and collected all references; HW helped in critical assessing this manuscript; and HZ conceived and revised this review.

FUNDING

Financial supports from the National Key R&D Program of China (2018YFC0311004), the National Natural Science Foundation of China (41776139) and the Fundamental Research Fund for the Provincial Universities of Zhejiang (RF-C2019002) were greatly appreciated.

SUPPLEMENTARY MATERIAL

The Supplementary Material for this article can be found online at: https://www.frontiersin.org/articles/10.3389/fchem.2021.701022/full#supplementary-material

REFERENCES

Akinfala, T. O., Houbraken, J., Sulyok, M., Adedeji, A. R., Odebode, A. C., Krska, R., et al. (2020). Moulds and Their Secondary Metabolites Associated with the Fermentation and Storage of Two cocoa Bean Hybrids in Nigeria. *Int. J. Food Microbiol.* 316, 108490. doi:10.1016/j.ijfoodmicro.2019.108490

Akiyama, K., Teraguchi, S., Hamasaki, Y., Mori, M., Tatsumi, K., Ohnishi, K., et al. (2003). New Dimeric Naphthopyrones from *Aspergillus niger*. *J. Nat. Prod.* 66 (1), 136–139. doi:10.1021/np020174p

Andersen, M. R., Salazar, M. P., Schaap, P. J., van de Vondervoort, P. J. I., Culley, D., Thykaer, J., et al. (2011). Comparative Genomics of Citric-Acid-Producing Aspergillus niger ATCC 1015 versus Enzyme-Producing CBS 513.88. *Genome Res.* 21 (6), 885–897. doi:10.1101/gr.112169.110

Ano, Y., Ikado, K., Shindo, K., Koizumi, H., and Fujiwara, D. (2017). Identification of 14-dehydroergosterol as a Novel Anti-inflammatory Compound Inducing Tolerogenic Dendritic Cells. *Sci. Rep.* 7. doi:10.1038/s41598-017-14446-1

Ayer, W. A., Muir, D. J., and Chakravarty, P. (1996). Phenolic and Other Metabolites of *Phellinus Pini*, a Fungus Pathogenic to pine. *Phytochemistry* 42 (5), 1321–1324. doi:10.1016/0031-9422(96)00125-2

Barton, D. H. R., and Bruun, T. (1951). 607. A New Sterol from a Strain of *Aspergillus niger*. *J. Chem. Soc.*, 2728. doi:10.1039/jr9510002728

Blin, K., Shaw, S., Steinke, K., Villebro, R., Ziemert, N., Lee, S. Y., et al. (2019). antiSMASH 5.0: Updates to the Secondary Metabolite Genome Mining Pipeline. *Nucleic Acids Res.* 47 (W1), W81–W87. doi:10.1093/nar/gkz310

Bouras, N., Mathieu, F., Coppel, Y., and Lebrihi, A. (2005). Aurasperone F - a New Member of the Naphtho-Gamma-Pyrone Class Isolated from a Cultured Microfungus,Aspergillus nigerC-433. *Nat. Product. Res.* 19 (7), 653–659. doi:10.1080/14786410412331286955

Bugni, T. S., Abbanat, D., Bernan, V. S., Maiese, W. M., Greenstein, M., Van Wagoner, R. M., et al. (2000). Yanuthones: Novel Metabolites from a Marine Isolate ofAspergillusniger. *J. Org. Chem.* 65 (21), 7195–7200. doi:10.1021/jo0006831

Cairns, T. C., Nai, C., and Meyer, V. (2018). How a Fungus Shapes Biotechnology: 100 Years of *Aspergillus niger* Research. *Fungal Biol. Biotechnol.* 5, 13. doi:10.1186/s40694-018-0054-5

Chakradhar, D., Javeed, S., and Sattur, A. P. (2009). Studies on the Production of Nigerloxin Using Agro-Industrial Residues by Solid-State Fermentation. *J. Ind. Microbiol. Biotechnol.* 36 (9), 1179–1187. doi:10.1007/s10295-009-0599-7

Chiang, Y.-M., Meyer, K. M., Praseuth, M., Baker, S. E., Bruno, K. S., and Wang, C. C. C. (2011). Characterization of a Polyketide Synthase in Aspergillus niger Whose Product Is a Precursor for Both Dihydroxynaphthalene (DHN) Melanin and Naphtho-γ-Pyrone. *Fungal Genet. Biol.* 48 (4), 430–437. doi:10.1016/j.fgb.2010.12.001

Chidananda, C., Kumar, C. M., and Sattur, A. P. (2008). Strain Improvement of *Aspergillus niger* for the Enhanced Production of Asperenone. *Indian J. Microbiol.* 48 (2), 274–278. doi:10.1007/s12088-008-0026-1

Cutler, H. G., Crumley, F. G., Cox, R. H., Hernandez, O., Cole, R. J., and Dorner, J. W. (1979). Orlandin: a Nontoxic Fungal Metabolite with Plant Growth Inhibiting Properties. *J. Agric. Food Chem.* 27 (3), 592–595. doi:10.1021/jf60223a043

Ding, T., Yang, L.-J., Zhang, W.-D., and Shen, Y.-H. (2020). Pyoluteorin Induces Cell Cycle Arrest and Apoptosis in Human Triple-Negative Breast Cancer Cells MDA-MB-231. *J. Pharm. Pharmacol.* 72 (7), 969–978. doi:10.1111/jphp.13262

Duarte, J. C., and Costaferreira, M. (1994). *Aspergilli* and Lignocellulosics - Enzymology and Biotechnological Applications. *FEMS Microbiol. Rev.* 13 (2-3), 377–386. doi:10.1111/j.1574-6976.1994.tb00038.x

Elissawy, A. M., Ebada, S. S., Ashour, M. L., El-Neketi, M., Ebrahim, W., and Singab, A. B. (2019). New Secondary Metabolites from the Mangrove-Derived Fungus *Aspergillus Sp*. AV-2. *Phytochemistry Lett.* 29, 1–5. doi:10.1016/j.phytol.2018.10.014

Etschmann, M. M. W., Huth, I., Walisko, R., Schuster, J., Krull, R., Holtmann, D., et al. (2014). Improving 2-phenylethanol and 6-Pentyl-α-Pyrone Production with Fungi by Microparticle-Enhanced Cultivation (MPEC). *Yeast* 32 (1), a–n. doi:10.1002/yea.3022

Fang, W., Lin, X., Wang, J., Liu, Y., Tao, H., and Zhou, X. (2016). Asperpyrone-Type Bis-Naphtho-γ-Pyrones with COX-2-Inhibitory Activities from Marine-Derived Fungus Aspergillus niger. *Molecules* 21 (7), 941. doi:10.3390/molecules21070941

Fernand, M. G., Roullier, C., Guitton, Y., Lalande, J., Lacoste, S., Dupont, J., et al. (2017). Fungi Isolated from Madagascar Shrimps - Investigation of the *Aspergillus niger* Metabolism by Combined LC-MS and NMR Metabolomics Studies. *Aquaculture* 479, 750–758. doi:10.1016/j.aquaculture.2017.07.015

Fukuda, T., Hasegawa, Y., Hagimori, K., Yamaguchi, Y., Masuma, R., Tomoda, H., et al. (2006). Tensidols, New Potentiators of Antifungal Miconazole Activity, Produced by *Aspergillus niger* FKI-2342. *J. Antibiot.* 59 (8), 480–485. doi:10.1038/ja.2006.67

Girol, C. G., Fisch, K. M., Heinekamp, T., Guenther, S., Huettel, W., Piel, J., et al. (2012). Regio- and Stereoselective Oxidative Phenol Coupling in *Aspergillus niger*. *Angew. Chemie-International Edition* 51 (39), 9788–9791. doi:10.1002/anie.201203603

Graz, C. J. M., Grant, G. D., Brauns, S. C., Hunt, A., Jamie, H., and Milne, P. J. (2010). Cyclic Dipeptides in the Induction of Maturation for Cancer Therapy. *J. Pharm. Pharmacol.* 52 (1), 75–82. doi:10.1211/0022357001773535

Happi, G. M., Kouam, S. F., Talontsi, F. M., Nkenfou, C. N., Longo, F., Zühlke, S., et al. (2015). A New Dimeric Naphtho-γ-Pyrone from an Endophytic Fungus Aspergillus niger AKRN Associated with the Roots of Entandrophragma Congoënse Collected in Cameroon. *Z. Naturforschung Section B-a J. Chem. Sci.* 70 (9), 625–630. doi:10.1515/znb-2015-0036

Hayden, N. J., Maude, R. B., and Proctor, F. J. (1994). Studies on the Biology of Black Mould (Aspergillus niger) on Temperate and Tropical Onions. 1. A Comparison of Sources of the Disease in Temperate and Tropical Field Crops. *Plant Pathol.* 43 (3), 562–569. doi:10.1111/j.1365-3059.1994.tb01591.x

He, Y., Wang, B., Chen, W., Cox, R. J., He, J., and Chen, F. (2018). Recent Advances in Reconstructing Microbial Secondary Metabolites Biosynthesis in *Aspergillus Spp*. *Biotechnol. Adv.* 36 (3), 739–783. doi:10.1016/j.biotechadv.2018.02.001

Hemphill, C. F. P., Sureechatchaiyan, P., Kassack, M. U., Orfali, R. S., Lin, W., Daletos, G., et al. (2017). OSMAC Approach Leads to New Fusarielin Metabolites from *Fusarium Tricinctum*. *J. Antibiot.* 70 (6), 726–732. doi:10.1038/ja.2017.21

Henrikson, J. C., Ellis, T. K., King, J. B., and Cichewicz, R. H. (2011). Reappraising the Structures and Distribution of Metabolites from Black *Aspergilli* Containing Uncommon 2-Benzyl-4h-Pyran-4-One and 2-Benzylpyridin-4(1h)-One Systems. *J. Nat. Prod.* 74 (9), 1959–1964. doi:10.1021/np200454z

Henrikson, J. C., Hoover, A. R., Joyner, P. M., and Cichewicz, R. H. (2009). A Chemical Epigenetics Approach for Engineering the in Situbiosynthesis of a Cryptic Natural Product from Aspergillus niger. *Org. Biomol. Chem.* 7 (3), 435–438. doi:10.1039/b819208a

Hiort, J., Maksimenka, K., Reichert, M., Perović-Ottstadt, S., Lin, W. H., Wray, V., et al. (2004). New Natural Products from the Sponge-Derived FungusAspergillus niger. *J. Nat. Prod.* 67 (9), 1532–1543. doi:10.1021/np030551d

Holm, D. K., Petersen, L. M., Klitgaard, A., Knudsen, P. B., Jarczynska, Z. D., Nielsen, K. F., et al. (2014). Molecular and Chemical Characterization of the Biosynthesis of the 6-MSA-Derived Meroterpenoid Yanuthone D in *Aspergillus niger*. *Chem. Biol.* 21 (4), 519–529. doi:10.1016/j.chembiol.2014.01.013

Hua, Y., Pan, R., Bai, X., Wei, B., Chen, J., Wang, H., et al. (2020). Aromatic Polyketides from a Symbiotic Strain *Aspergillus fumigatus* D and Characterization of Their Biosynthetic Gene *D8.T287*. *Mar. Drugs* 18 (6), 324. doi:10.3390/md18060324

Hüttel, W., and Müller, M. (2007). Regio- and Stereoselective Intermolecular Oxidative Phenol Coupling in Kotanin Biosynthesis byAspergillus Niger. *Chembiochem* 8 (5), 521–529. doi:10.1002/cbic.200600434

Huttel, W., Nieger, M., and Muller, M. (2003). A Short and Efficient Total Synthesis of the Naturally Occurring Coumarins Siderin, Kotanin, Isokotanin A and Desertorin C. *Synthesis-Stuttgart* (12), 1803–1808. doi:10.1055/s-2003-41027

Jefferson, W. E., Jr. (1967). The Isolation and Characterization of Asperenone, a New Phenylpolyene from Aspergillus niger*. *Biochemistry* 6 (11), 3479–3484. doi:10.1021/bi00863a019

Jomori, T., Hara, Y., Sasaoka, M., Harada, K., Setiawan, A., Hirata, K., et al. (2020). *Mycobacterium Smegmatis* Alters the Production of Secondary Metabolites by marine-derived *Aspergillus niger*. *J. Nat. Med.* 74 (1), 76–82. doi:10.1007/s11418-019-01345-0

Kaur, T., Singh, B., Kaur, A., and Kaur, S. (2015). Endophyte-mediated Interactions between Cauliflower, the Herbivore Spodoptera Litura, and the Ectoparasitoid Bracon Hebetor. *Oecologia* 179 (2), 487–494. doi:10.1007/s00442-015-3358-7

Kim, K.-W., Sugawara, F., Yoshida, S., Murofushi, N., Takahashi, N., and Curtis, R. W. (1993). Structure of Malformin B, a Phytotoxic Metabolite Produced byAspergillus niger. *Biosci. Biotechnol. Biochem.* 57 (5), 787–791. doi:10.1271/bbb.57.787

Kimura, Y., Sawada, A., Kuramata, M., Kusano, M., Fujioka, S., Kawano, T., et al. (2005). Brevicompanine C, Cyclo-(*d*-Ile-*L*-Trp), and Cyclo-(d-Leu-L-Trp), Plant Growth Regulators from *Penicillium* Brevi-Compactum. *J. Nat. Prod.* 68 (2), 237–239. doi:10.1021/np040178p

Kimura, Y., Tani, K., Kojima, A., Sotoma, G., Okada, K., and Shimada, A. (1996). Cyclo-(L-tryptophyl-L-phenylalanyl), a Plant Growth Regulator Produced by the Fungus *Penicillium Sp*. *Phytochemistry* 41 (3), 665–669. doi:10.1016/0031-9422(95)00693-1

Kodukula, K., Arcuri, M., Cutrone, J. Q., Hugill, R. M., Lowe, S. E., Pirnik, D. M., et al. (1995). BMS-192548, a Tetracyclic Binding Inhibitor of Neuropeptide Y Receptors, from *Aspergillus niger* WB2346. I. Taxonomy, Fermentation, Isolation and Biological Activity. *J. Antibiot.* 48 (10), 1055–1059. doi:10.7164/antibiotics.48.1055

Leutou, A. S., Yun, K., and Son, B. W. (2016). Induced Production of 6,9-dibromoflavasperone, a New Radical Scavenging Naphthopyranone in the marine-mudflat-derived Fungus *Aspergillus niger*. *Arch. Pharm. Res.* 39 (6), 806–810. doi:10.1007/s12272-016-0764-2

Li, A., Pfelzer, N., Zuijderwijk, R., and Punt, P. (2012). Enhanced Itaconic Acid Production in *Aspergillus niger* Using Genetic Modification and Medium Optimization. *BMC Biotechnol.* 12. doi:10.1186/1472-6750-12-57

Li, C., Zhou, J., Du, G., Chen, J., Takahashi, S., and Liu, S. (2020). Developing *Aspergillus niger* as a Cell Factory for Food Enzyme Production. *Biotechnol. Adv.* 44, 107630. doi:10.1016/j.biotechadv.2020.107630

Li, D.-H., Han, T., Guan, L.-P., Bai, J., Zhao, N., Li, Z.-L., et al. (2016). New Naphthopyrones from marine-derived Fungus *Aspergillus* niger 2HL-M-8 and Their *In Vitro* Antiproliferative Activity. *Nat. Product. Res.* 30 (10), 1116–1122. doi:10.1080/14786419.2015.1043553

Li, M., Yu, R., Bai, X., Wang, H., and Zhang, H. (2020). Fusarium: a Treasure Trove of Bioactive Secondary Metabolites. *Nat. Prod. Rep.* 37, 1568–1588. doi:10.1039/d0np00038h

Li, X.-B., Li, Y.-L., Zhou, J.-C., Yuan, H.-Q., Wang, X.-N., and Lou, H.-X. (2015). A New Diketopiperazine Heterodimer from an Endophytic Fungus Aspergillus niger. *J. Asian Nat. Prod. Res.* 17 (2), 182–187. doi:10.1080/10286020.2014.959939

Li, X., Pan, L., Wang, B., and Pan, L. (2019). The Histone Deacetylases *HosA* and *HdaA* Affect the Phenotype and Transcriptomic and Metabolic Profiles of *Aspergillus niger*. *Toxins* 11 (9), 520. doi:10.3390/toxins11090520

Li, Y., Chooi, Y.-H., Sheng, Y., Valentine, J. S., and Tang, Y. (2011). Comparative Characterization of Fungal Anthracenone and Naphthacenedione Biosynthetic Pathways Reveals an α-Hydroxylation-Dependent Claisen-like Cyclization Catalyzed by a Dimanganese Thioesterase. *J. Am. Chem. Soc.* 133 (39), 15773–15785. doi:10.1021/ja206906d

Liu, D., Li, X.-M., Li, C.-S., and Wang, B.-G. (2013). Nigerasterols A and B, Antiproliferative Sterols from the Mangrove-Derived Endophytic FungusAspergillus nigerMA-132. *Hca* 96 (6), 1055–1061. doi:10.1002/hlca.201200332

Liu, D., Li, X.-M., Meng, L., Li, C.-S., Gao, S.-S., Shang, Z., et al. (2011). Nigerapyrones A-H, α-Pyrone Derivatives from the Marine Mangrove-Derived Endophytic FungusAspergillus nigerMA-132. *J. Nat. Prod.* 74 (8), 1787–1791. doi:10.1021/np200381u

Liu, Y., Nan, L., Liu, J., Yan, H., Zhang, D., and Han, X. (2016). Isolation and Identification of Resveratrol-Producing Endophytes from Wine Grape *Cabernet Sauvignon*. *Springerplus* 5. doi:10.1186/s40064-016-2571-0

Lu, H., Cao, W., Ouyang, L., Xia, J., Huang, M., Chu, J., et al. (2017). Comprehensive Reconstruction and In Silico Analysis ofAspergillus Nigergenome-Scale Metabolic Network Model that Accounts for 1210 ORFs. *Biotechnol. Bioeng.* 114 (3), 685–695. doi:10.1002/bit.26195

Lu, S., Tian, J., Sun, W., Meng, J., Wang, X., Fu, X., et al. (2014). Bis-naphtho-γ-pyrones from Fungi and Their Bioactivities. *Molecules* 19 (6), 7169–7188. doi:10.3390/molecules19067169

Manganyi, M. C., Regnier, T., Kumar, A., Bezuidenhout, C. C., and Ateba, C. N. (2018). Biodiversity and Antibacterial Screening of Endophytic Fungi Isolated from *Pelargonium Sidoides*. *South Afr. J. Bot.* 116, 192–199. doi:10.1016/j.sajb.2018.03.016

Miyake, Y., Ito, C., Itoigawa, M., and Osawa, T. (2007). Isolation of the Antioxidant Pyranonigrin-A from rice Mold Starters Used in the Manufacturing Process of Fermented Foods. *Biosci. Biotechnol. Biochem.* 71 (10), 2515–2521. doi:10.1271/bbb.70310

Nielsen, K. F., Mogensen, J. M., Johansen, M., Larsen, T. O., and Frisvad, J. C. (2009). Review of Secondary Metabolites and Mycotoxins from the *Aspergillus niger* Group. *Anal. Bioanal. Chem.* 395 (5), 1225–1242. doi:10.1007/s00216-009-3081-5

Nødvig, C. S., Hoof, J. B., Kogle, M. E., Jarczynska, Z. D., Lehmbeck, J., Klitgaard, D. K., et al. (2018). Efficient Oligo Nucleotide Mediated CRISPR-Cas9 Gene Editing in Aspergilli. *Fungal Genet. Biol.* 115, 78–89. doi:10.1016/j.fgb.2018.01.004

Nødvig, C. S., Nielsen, J. B., Kogle, M. E., and Mortensen, U. H. (2015). A CRISPR-Cas9 System for Genetic Engineering of Filamentous Fungi. *PLoS One* 10 (7), e0133085. doi:10.1371/journal.pone.0133085

Obermaier, S., and Müller, M. (2019). Biaryl-Forming Enzymes from Aspergilli Exhibit Substrate-dependent Stereoselectivity. *Biochemistry* 58 (22), 2589–2593. doi:10.1021/acs.biochem.9b00291

Ovenden, S. P. B., Sberna, G., Tait, R. M., Wildman, H. G., Patel, R., Li, B., et al. (2004). A Diketopiperazine Dimer from a Marine-Derived Isolate ofAspergillusniger. *J. Nat. Prod.* 67 (12), 2093–2095. doi:10.1021/np0497494

Özer, N., and Köycü, N. D. (2006). The Ability of Plant Compost Leachates to Control Black Mold (*Aspergillus niger*) and to Induce the Accumulation of Antifungal Compounds in Onion Following Seed Treatment. *Biocontrol* 51 (2), 229–243. doi:10.1007/s10526-005-1035-1

Padhi, S., Masi, M., Panda, S. K., Luyten, W., Cimmino, A., Tayung, K., et al. (2020). Antimicrobial Secondary Metabolites of an Endolichenic *Aspergillus niger* Isolated from Lichen Thallus of *Parmotrema Ravum*. *Nat. Product. Res.* 34 (18), 2573–2580. doi:10.1080/14786419.2018.1544982

Pan, R., Bai, X., Chen, J., Zhang, H., and Wang, H. (2019). Exploring Structural Diversity of Microbe Secondary Metabolites Using OSMAC Strategy: a Literature Review. *Front. Microbiol.* 10. doi:10.3389/fmicb.2019.00294

Pel, H. J., de Winde, J. H., Archer, D. B., Dyer, P. S., Hofmann, G., Schaap, P. J., et al. (2007). Genome Sequencing and Analysis of the Versatile Cell Factory *Aspergillus niger* CBS 513.88. *Nat. Biotechnol.* 25 (2), 221–231. doi:10.1038/nbt1282

Perrone, G., Stea, G., Epifani, F., Varga, J., Frisvad, J. C., and Samson, R. A. (2011). *Aspergillus niger* Contains the Cryptic Phylogenetic Species A. Awamori. *Fungal Biol.* 115 (11), 1138–1150. doi:10.1016/j.funbio.2011.07.008

Rao, K. C. S., Divakar, S., Babu, K. N., Rao, A. G. A., Karanth, N. G., and Sattur, A. P. (2002). Nigerloxin, a Novel Inhibitor of Aldose Reductase and Lipoxygenase with Free Radical Scavenging Activity from *Aspergillus niger* CFR-W-105. *J. Antibiot.* 55 (9), 789–793. doi:10.7164/antibiotics.55.789

Reber, K. P., and Burdge, H. E. (2018). Total Synthesis of Pyrophen and Campyrones A-C. *J. Nat. Prod.* 81 (2), 292–297. doi:10.1021/acs.jnatprod.7b00720

Riko, R., Nakamura, H., and Shindo, K. (2014). Studies on Pyranonigrins-Isolation of Pyranonigrin E and Biosynthetic Studies on Pyranonigrin A. *J. Antibiot.* 67 (2), 179–181. doi:10.1038/ja.2013.91

Saeed, S., Aslam, S., Mehmood, T., Naseer, R., Nawaz, S., Mujahid, H., et al. (2020). Production of Gallic Acid under Solid-State Fermentation by Utilizing Waste from Food Processing Industries. *Waste Biomass Valor.* 12 (1), 155–163. doi:10.1007/s12649-020-00980-z

Sakurai, M., Kohno, J., Yamamoto, K., Okuda, T., Nishio, M., Kawano, K., et al. (2002). TMC-256A1 and C1, New Inhibitors of IL-4 Signal Transduction Produced by *Aspergillus niger* Var niger TC 1629. *J. Antibiot.* 55 (8), 685–692. doi:10.7164/antibiotics.55.685

Sanchez, J. F., Somoza, A. D., Keller, N. P., and Wang, C. C. C. (2012). Advances in *Aspergillus* Secondary Metabolite Research in the post-genomic Era. *Nat. Prod. Rep.* 29 (3), 351–371. doi:10.1039/c2np00084a

Santhakumaran, I., Kesavan, S. S., and Arumugam, G. (2019). Asperyellone Pretreatment Protects HaCaT Cells from UVB Irradiation Induced Oxidative Damages: Assessment under *In Vitro* and *In Vivo* Conditions and at Molecular Level. *J. Cel Biochem* 120 (6), 10715–10725. doi:10.1002/jcb.28363

Shen, L., Ye, Y.-H., Wang, X.-T., Zhu, H.-L., Xu, C., Song, Y.-C., et al. (2006). Structure and Total Synthesis of Aspernigerin: A Novel Cytotoxic Endophyte Metabolite. *Chem. Eur. J.* 12 (16), 4393–4396. doi:10.1002/chem.200501423

Shreelalitha, S. J., and Sridhar, K. R. (2015). Endophytic Fungi of Wild Legume *Sesbania Bispinosa* in Coastal Sand Dunes and Mangroves of the Southwest Coast of India. *J. For. Res.* 26 (4), 1003–1011. doi:10.1007/s11676-015-0103-3

Shu, Y.-Z., Cutrone, J. Q., Klohr, S. E., and Huang, S. (1995). BMS-192548, a Tetracyclic Binding Inhibitor of Neuropeptide Y Receptors, from Aspergillus niger WB2346. II. Physico-Chemical Properties and Structural Characterization. *J. Antibiot.* 48 (10), 1060–1065. doi:10.7164/antibiotics.48.1060

Singh, S. M., Yadav, L. S., Singh, S. K., Singh, P., Singh, P. N., and Ravindra, R. (2011). Phosphate Solubilizing Ability of Two Arctic *Aspergillus niger* Strains. *Polar Res.* 30. doi:10.3402/polar.v30i0.7283

Soltani, J., and Moghaddam, M. S. H. (2014). Diverse and Bioactive Endophytic *Aspergilli* Inhabit Cupressaceae Plant Family. *Arch. Microbiol.* 196 (9), 635–644. doi:10.1007/s00203-014-0997-8

Song, Y. C., Li, H., Ye, Y. H., Shan, C. Y., Yang, Y. M., and Tan, R. X. (2004). Endophytic Naphthopyrone Metabolites Are Co-inhibitors of Xanthine Oxidase, SW1116 Cell and Some Microbial Growths. *FEMS Microbiol. Lett.* 241 (1), 67–72. doi:10.1016/j.femsle.2004.10.005

Sørensen, L. M., Lametsch, R., Andersen, M. R., Nielsen, P. V., and Frisvad, J. C. (2009). Proteome Analysis of Aspergillus niger: Lactate Added in Starch-Containing Medium Can Increase Production of the Mycotoxin Fumonisin B2 by Modifying Acetyl-CoA Metabolism. *BMC Microbiol.* 9, 255. doi:10.1186/1471-2180-9-255

Suda, S., and Curtis, R. W. (1966). Antibiotic Properties of Malformin. *Appl. Microbiol.* 14 (3), 475–476. doi:10.1128/aem.14.3.475-476.1966

Sun, J., Lu, X., Rinas, U., and Zeng, A. (2007). Metabolic Peculiarities of *Aspergillus niger* Disclosed by Comparative Metabolic Genomics. *Genome Biol.* 8 (9), R182. doi:10.1186/gb-2007-8-9-r182

Takano, D., Nagamitsu, T., Ui, H., Shiomi, K., Yamaguchi, Y., Masuma, R., et al. (2001). Absolute Configuration of Nafuredin, a New Specific NADH-Fumarate Reductase Inhibitor. *Tetrahedron Lett.* 42 (16), 3017–3020. doi:10.1016/s0040-4039(01)00355-0

Talontsi, F. M., Tatong, M. D. K., Dittrich, B., Douanla-Meli, C., and Laatsch, H. (2013). Structures and Absolute Configuration of Three Alpha-Pyrones from an Endophytic Fungus *Aspergillus niger*. *Tetrahedron* 69 (34), 7147–7151. doi:10.1016/j.tet.2013.05.098

Tanaka, H., Pie-Lang, W., and Namiki, M. (1972). Structure of Aurasperone C. *Agric. Biol. Chem.* 36 (13), 2511–2517. doi:10.1080/00021369.1972.10860562

Tanaka, H., Wang, P.-L., Yamada Late, O., and Tamura, T. (1966). Yellow Pigments ofAspergillus nigerandAsp. Awamori. *Agric. Biol. Chem.* 30 (2), 107–113. doi:10.1080/00021369.1966.10858561

Toghueo, R. M. K., Sahal, D., Zabalgogeazcoa, Í., Baker, B., and Boyom, F. F. (2018). Conditioned media and Organic Elicitors Underpin the Production of Potent Antiplasmodial Metabolites by Endophytic Fungi from *Cameroonian* Medicinal Plants. *Parasitol. Res.* 117 (8), 2473–2485. doi:10.1007/s00436-018-5936-1

Uchoa, P. K. S., Pimenta, A. T. A., Braz-Filho, R., de Oliveira, M. d. C. F., Saraiva, N. N., Rodrigues, B. S. F., et al. (2017). New Cytotoxic Furan from the marine Sediment-Derived Fungi *Aspergillus niger*. *Nat. Product. Res.* 31 (22), 2599–2603. doi:10.1080/14786419.2017.1283499

Ui, H., Shiomi, K., Yamaguchi, Y., Masuma, R., Nagamitsu, T., Takano, D., et al. (2001). Nafuredin, a Novel Inhibitor of NADH-Fumarate Reductase, Produced by *Aspergillus niger* FT-0554. *J. Antibiot.* 54 (3), 234–238. doi:10.7164/antibiotics.54.234

Varoglu, M., Corbett, T. H., Valeriote, F. A., and Crews, P. (1997). Asperazine, a Selective Cytotoxic Alkaloid from a Sponge-Derived Culture ofAspergillus niger. *J. Org. Chem.* 62 (21), 7078–7079. doi:10.1021/jo970568z

Varoglu, M., and Crews, P. (2000). Biosynthetically Diverse Compounds from a Saltwater Culture of Sponge-DerivedAspergillus niger. *J. Nat. Prod.* 63 (1), 41–43. doi:10.1021/np9902892

Wang, B., Li, X., Yu, D., Chen, X., Tabudravu, J., Deng, H., et al. (2018). Deletion of the Epigenetic Regulator *GcnE* in *Aspergillus niger* FGSC A1279 Activates the Production of Multiple Polyketide Metabolites. *Microbiol. Res.* 217, 101–107. doi:10.1016/j.micres.2018.10.004

Wang, J., Jiang, Z., Lam, W., Gullen, E. A., Yu, Z., Wei, Y., et al. (2015). Study of Malformin C, a Fungal Source Cyclic Pentapeptide, as an Anti-cancer Drug. *PLoS One* 10 (11), e0140069. doi:10.1371/journal.pone.0140069

Wang, L.-X., Ren, L.-L., Liu, X.-B., Shi, J., Wang, J.-Z., and Luo, Y.-Q. (2019). Effects of Endophytic Fungi in Mongolian pine on the Selection Behavior of Woodwasp (*Sirex noctilio*) and the Growth of its Fungal Symbiont. *Pest Manag. Sci.* 75 (2), 492–505. doi:10.1002/ps.5146

Wei, Q., Bai, J., Yan, D., Bao, X., Li, W., Liu, B., et al. (2021). Genome Mining Combined Metabolic Shunting and OSMAC Strategy of an Endophytic Fungus Leads to the Production of Diverse Natural Products. *Acta Pharmaceutica Sinica B* 11 (2), 572–587. doi:10.1016/j.apsb.2020.07.020

Xie, H., Zhuang, X., Bai, Z., Qi, H., and Zhang, H. (2006). Isolation of Levoglucosan-Assimilating Microorganisms from Soil and an Investigation of Their Levoglucosan Kinases. *World J. Microbiol. Biotechnol.* 22 (9), 887–892. doi:10.1007/s11274-006-9133-5

Xu, Y., Shan, L., Zhou, Y., Xie, Z., Ball, A. S., Cao, W., et al. (2019). Development of a Cre-loxP-Based Genetic System in *Aspergillus niger* ATCC1015 and its Application to Construction of Efficient Organic Acid-Producing Cell Factories. *Appl. Microbiol. Biotechnol.* 103 (19), 8105–8114. doi:10.1007/s00253-019-10054-3

Yamamoto, T., Tsunematsu, Y., Noguchi, H., Hotta, K., and Watanabe, K. (2015). Elucidation of Pyranonigrin Biosynthetic Pathway Reveals a Mode of Tetramic Acid, Fused γ-Pyrone, and Exo-Methylene Formation. *Org. Lett.* 17 (20), 4992–4995. doi:10.1021/acs.orglett.5b02435

Yang, X.-L., Awakawa, T., Wakimoto, T., and Abe, I. (2014). Three Acyltetronic Acid Derivatives: Noncanonical Cryptic Polyketides fromAspergillus nigerIdentified by Genome Mining. *Chembiochem* 15 (11), 1578–1583. doi:10.1002/cbic.201402172

Zabala, A. O., Xu, W., Chooi, Y.-H., and Tang, Y. (2012). Characterization of a Silent Azaphilone Gene Cluster from *Aspergillus niger* ATCC 1015 Reveals a Hydroxylation-Mediated Pyran-Ring Formation. *Chem. Biol.* 19 (8), 1049–1059. doi:10.1016/j.chembiol.2012.07.004

Zhang, Y., Li, X.-M., Feng, Y., and Wang, B.-G. (2010). Phenethyl-α-pyrone Derivatives and Cyclodipeptides from a marine Algous Endophytic Fungus Aspergillus niger EN-13. *Nat. Product. Res.* 24 (11), 1036–1043. doi:10.1080/14786410902940875

Zhang, Y., Li, X.-M., Proksch, P., and Wang, B.-G. (2007a). Ergosterimide, a New Natural Diels-Alder Adduct of a Steroid and Maleimide in the Fungus *Aspergillus niger*. *Steroids* 72 (9-10), 723–727. doi:10.1016/j.steroids.2007.05.009

Zhang, Y., Li, X.-M., and Wang, B.-G. (2007b). Nigerasperones A~C, New Monomeric and Dimeric Naphtho-γ-Pyrones from a Marine Alga-Derived Endophytic Fungus Aspergillus niger EN-13. *J. Antibiot.* 60 (3), 204–210. doi:10.1038/ja.2007.24

Zhang, Y., Zhang, X., Yu, Q., Yuan, Z., and Chen, X. (2019). Mutant Breeding of Furfural Tolerant *Aspergillus terreus* for Itaconic Acid Production. *j biobased mat bioenergy* 13 (6), 799–805. doi:10.1166/jbmb.2019.1909

Zhou, X., Fang, W., Tan, S., Lin, X., Xun, T., Yang, B., et al. (2016). Aspernigrins with Anti-HIV-1 Activities from the marine-derived Fungus *Aspergillus niger* SCSIO Jcsw6F30. *Bioorg. Med. Chem. Lett.* 26 (2), 361–365. doi:10.1016/j.bmcl.2015.12.005

Zou, S.-P., Zhong, W., Xia, C.-J., Gu, Y.-N., Niu, K., Zheng, Y.-G., et al. (2015). Mutagenesis Breeding of High Echinocandin B Producing Strain and Further Titer Improvement with Culture Medium Optimization. *Bioproc. Biosyst Eng* 38 (10), 1845–1854. doi:10.1007/s00449-015-1425-4

Conflict of Interest: The authors declare that the research was conducted in the absence of any commercial or financial relationships that could be construed as a potential conflict of interest.

Publisher's Note: All claims expressed in this article are solely those of the authors and do not necessarily represent those of their affiliated organizations, or those of the publisher, the editors and the reviewers. Any product that may be evaluated in this article, or claim that may be made by its manufacturer, is not guaranteed or endorsed by the publisher.

frontiers in Chemistry

ORIGINAL RESEARCH
published: 09 August 2021
doi: 10.3389/fchem.2021.724617

New Alkaloids From a Hawaiian Fungal Strain *Aspergillus felis* FM324

Cong Wang[1,2], *Ariel M. Sarotti*[3], *KH Ahammad Uz Zaman*[1], *Xiaohua Wu*[1] *and Shugeng Cao*[1]*

[1]*Department of Pharmaceutical Sciences, Daniel K. Inouye College of Pharmacy, University of Hawai'i at Hilo, Hilo, HI, United States,* [2]*Key Laboratory of Chemistry and Engineering of Forest Products, State Ethnic Affairs Commission, Guangxi Key Laboratory of Chemistry and Engineering of Forest Products, Guangxi Collaborative Innovation Center for Chemistry and Engineering of Forest Products, School of Chemistry and Chemical Engineering, Guangxi University for Nationalities, Nanning, China,* [3]*Facultad de Ciencias Bioquímicas y Farmacéuticas, Instituto de Química Rosario (CONICET), Universidad Nacional de Rosario, Rosario, Argentina*

Two new alkaloids tryptoquivaline Y (1) and pseurotin I (2), together with eight known compounds (3–10), were purified from a fungal strain *Aspergillus felis* FM324, which was isolated from a Hawaiian beach soil sample. The absolute configuration and physicochemical data of tryptoquivaline Z (3) were reported for the first time here in this paper. Compound 1 is an uncommon tryptoquivaline analog containing a 3-*O*-isobutanoyl group. The structures of the new compounds 1–2 and known compound 3 were elucidated through HRESIMS, NMR spectroscopy and ECD analysis. All the compounds were evaluated for their antiproliferative, antibacterial and NF-κB inhibitory activities. Compound 4 showed weak antibacterial activity against *Staphylococcus aureus*, methicillin resistant *Staphylococcus aureus* and *Bacillus subtilis* with the same MIC value of 59.2 μM. Compounds **3** and **2** inhibited NF-κB with IC_{50} values of 26.7 and 30.9 μM, respectively.

Keywords: *Aspergillus felis*, trichocomaceae, alkaloids, antiproliferative, antibacterial, NF-κB inhibitory activities

OPEN ACCESS

Edited by:
Guojun Wang,
Florida Atlantic University,
United States

Reviewed by:
Mohamed Saleh Abdelfattah,
Helwan University, Egypt
Sabrin R. M. Ibrahim,
Batterjee Medical College, Saudi Arabia

***Correspondence:**
Shugeng Cao
scao@hawaii.edu

Specialty section:
This article was submitted to Organic Chemistry, a section of the journal Frontiers in Chemistry

Received: *16 June 2021*
Accepted: *28 July 2021*
Published: *09 August 2021*

Citation:
Wang C, Sarotti AM, Zaman KHAU, Wu X and Cao S (2021) New Alkaloids From a Hawaiian Fungal Strain Aspergillus felis *FM324. Front. Chem. 9:724617. doi: 10.3389/fchem.2021.724617*

INTRODUCTION

Marine fungi remain one of the few underexplored resources of natural products (Overy et al., 2019), and they have become the main source of new compounds from marine microorganisms due to their complex genetic background (Zhao et al., 2016). Most of the reported marine fungal secondary metabolites showed certain biological properties including antibacterial (Wang et al., 2021) and anticancer (Deshmukh et al., 2017) activities. *Aspergillus* is a huge and diverse fungal genus (Ibrahim and Asfour, 2018), ubiquitously found in soil, terrestrial plants, animals and marine. Totally, there are about 380 species in the genus *Aspergillus*. As a dominant and the most studied fungal genus in endophytes, more than 350 new fungal metabolites were isolated from *Aspergillus* during 2015–2019 (Vadlapudi et al., 2017). Marine *Aspergillus* sp. produced plenty of secondary metabolites including polyketides, sterols, fatty acids, peptides, alkaloids, terpenoids and miscellaneous compounds, which exhibited different pharmacological activities such as antimicrobial, cytotoxicity, anti-inflammatory and antioxidant activity (Ibrahim et al., 2017a; Ibrahim et al., 2017b; Elkhayat, et al., 2016; Mohamed, et al., 2020). In the past few years, our research group has studied the secondary metabolites of some marine fungi including different *Aspergillus* species from Hawaii. These secondary metabolites had different types of structures and exhibited various biological activities (Li et al., 2015; Fei-Zhang et al., 2016; Li et al., 2016; Huang et al., 2017; Li et al., 2018; Li et al., 2019; Wang et al., 2019; Zaman et al., 2020a; Wang et al., 2020; Zaman et al., 2021). In our continuing search for bioactive molecules from Hawaiian fungi, we studied an extract of *Aspergillus felis* FM324, which led to the separation and

identification of ten compounds (1–10). Here, we report two new molecules (1–2) along with eight known secondary metabolites (3–10). Compounds 1–10 were evaluated for their NF-κB inhibitory property and anti-proliferative activity against A2780 as well as their antibacterial potential against both Gram-positive and Gram-negative bacteria.

MATERIALS AND METHODS

General Experimental Procedures

Optical rotations, CD, UV and FT-IR spectra were measured with a Rudolph Research analytical AutoPol automatic polarimeter (Rudolph Research Analytical, NJ, United States), JASCO J-815 CD (Jasco Corporation, Japan), Shimadzu UV spectrophotometer UV-1800 and Thermo Scientific Nicolet iS10 IR spectrometer (Thermo Fisher Scientific, WI, United States), respectively. The structure characterizations of all the compounds were based on 1D NMR (^{1}H, ^{13}C) and 2D NMR (COSY, HSQC, HMBC, 1D-NOE and ROESY) data, recorded on a Bruker AM-400 spectrometer (Bruker BioSpin AG, Switzerland). An Agilent 6,530 Accurate-Mass Q-TOF LC-MS spectrometer (Agilent Technologies, Germany) was used to record high-resolution mass spectra. Preparative RP-HPLC was carried out on an Ultimate 3000 chromatographic system (Agilent Technologies, Germany) with a Phenomenex preparative column (Phenyl-hexyl, 5 μ, 100 × 21.2 mm) and semipreparative RP-HPLC on an Ultimate 3000 chromatographic system (Agilent Technologies, Germany) with a Phenomenex semipreparative column (C_{18}, 5 μ, 250 × 10 mm), connected to a Dionex Ultimate 3000 DAD detector (Agilent Technologies, Germany) (detected at 210, 254, 320, and 365 nm) and a Dionex Ultimate 3000 automated fraction collector. All solvents were HPLC grade. Diaion HP-20 (Alfa Aesar, Japan) was used to run the open-column chromatography.

Strain Isolation and Fermentation

The strain FM324 was isolated from a sample collected at a beach at Kona, the Big Island, Hawaii. The strain was deposited in an −80°C freezer at Daniel K. Inouye College of Pharmacy, University of Hawaii at Hilo, HI, United States. The strain was grown on PDA plates at 28°C for 3 days, then it was cut into small pieces and inoculated into an autoclaved liquid PDB medium (20 L) for fermentation at 24°C for 30 days.

Molecular Identification of the Fungal Strain M324

DNA extraction: DNA was extracted according to the literature (Liu et al., 2000), with slight modifications. Mycelium was added to 500 μl of lysis buffer (400 mM Tris-HCl [pH 8.0], 60 mM EDTA, 150 mM NaCl, 1% sodium dodecyl sulfate) and incubated at 85°C for 20 min. After adding 150 μl of 3 M sodium acetate (pH 5.2), the tube was vortexed briefly and centrifuged (12,500rpm) for 1 min. The supernatant was transferred to another tube and centrifuged again. After transferring the supernatant to a new tube, an equal volume of isopropanol was added and mixed by inversion. The tube was centrifuged for 2 min and the supernatant was discarded. The DNA pellet was washed twice with 300 μl of 70% ethanol. The DNA was air dried at room temperature for 45 min, then dissolved in 100 μL of 10 mM Tris-HCl (pH 8.0). Sequencing of ITS region: The ITS region was amplified with the ITS1 and ITS4 primers. The PCR reaction included 1X High Fidelity PCR Buffer (Invitrogen), 2 mM MgSO4, 0.2 mM dNTP mix, 4% DMSO, 0.2 μM of each primer, 1 U Platinum Taq DNA Polymerase High Fidelity (Invitrogen), and 10 ng of genomic DNA. The PCR cycling conditions were 95°C for 3 min, followed by 35 cycles of 95°C for 30 s, 50°C for 30 s and 72°C for 1 min, and a final extension of 72°C for 5 min. The PCR product was purified using Mag-Bind Total Pure NGS beads (Omega Bio-tek), then sequenced using a 3730xl DNA Analyzer (Applied Biosystems). The sequence was compared to the NCBI nucleotide collection (limited to sequences from type material) using the Basic Local Alignment Search Tool (BLAST), and was deposited in GenBank under the accession no. MZ227547.

Extraction and Isolation

After filtration of the fermentation broth, the mycelia of FM324 were extracted three times with acetone. Acetone was removed by evaporation in vacuum. After combining the aqueous mycelia extraction and supernatant solution, it was subjected to HP-20 column eluted with MeOH-H_2O into four fractions (30, 50, 90 and 100% MeOH). Fraction 3 (3.21 g) was separated by using prep-HPLC (Phenyl-Hexyl, 100 × 21.20 mm, 5 μm; 8 ml/min) eluted with 40–100% MeOH-H_2O in 20 min to yield 26 sub-fractions (SFr3–1~26). SFr 3–11 (180 mg) was purified by semi-preparative HPLC (38% MeCN/H_2O, v/v, 1.0% formic acid, 3.0 ml/min) over a C18 column to afford compound **1** (1.6 mg, t_R 32.2 min). SFr 3–14 (152.7 mg) was purified by semi-preparative HPLC (20% MeCN/H_2O, v/v, 1.0% formic acid, 3.0 ml/min) over a C18 column to afford compounds **2** (1.2 mg, t_R 35.3 min) and **7** (2.2 mg, t_R 21.4 min). SFr 3–9 (720 mg) was purified by semi-preparative HP2LC (30% MeCN/H_2O, v/v, 1.0% formic acid, 3.0 ml/min) over a C18 column to afford compounds **3** (2.7 mg, t_R 27.6 min) and **5** (1.6 mg, t_R 8.3 min). SFr 3–20 (100.1 mg) was purified by semi-preparative HPLC (60% MeCN/H_2O, v/v, 1.0% formic acid, 3.0 ml/min) over a C18 column to afford compound **4** (1.1 mg, t_R 16.5 min). SFr 3–17 (6.3 mg) afford compound **6** (6.3 mg). SFr 3–12 (201.8 mg) was purified by semi-preparative HPLC (30% MeCN/H_2O, v/v, 1.0% formic acid, 3.0 ml/min) over a C18 column to afford compounds **8** (12.6 mg, t_R 19.8 min), **9** (5.2 mg, t_R 23.9 min) and **10** (1.0 mg, t_R 26.3 min).

Tryptoquivaline Y (**1**): White amorphous powder; $[\alpha]_D^{25}$ +135 (*c* 0.10, MeOH); UV (MeOH) λ_{max} (log ε) 212 (4.42), 302 (3.47) nm; CD (0.10 mM, MeOH) λ_{max} (Δε) 224 (−29.85), 250 (+21.67), 288 (+16.88) nm; IR (KBr) ν_{max} 3,335, 2,921, 2,847, 1,651, 1,613, 1,519, 1,418, 1,375, 1,344, 1,271, 1,235, 1,083, 1,050, 1,033, 748.4 cm^{-1}; ^{1}H and ^{13}C NMR data (see **Table 1**); HRESIMS *m/z*521.2042 $[M + H]^+$ (calcd for $C_{27}H_{29}N_4O_7$, 521.2031).

Pseurotin I (**2**): White amorphous powder; $[\alpha]_D^{25}$ −5.6 (*c* 0.50, MeOH); UV (MeOH) λ_{max} (log ε) 204 (4.03), 252 (3.81), 280 (3.57) nm; CD (0.11 mM, MeOH) λ_{max} (Δε) 210 (+18.00), 232

TABLE 1 | ^{1}H (400 MHz) and ^{13}C (100 MHz) NMR data of compounds 1–3 in DMSO-d_6.

No	1		2		3	
	δ_C	δ_H (*J* in Hz)	δ_C	δ_H (*J* in Hz)	δ_C	δ_H (*J* in Hz)
2	85.1, CH	5.08 (s)	187.0, C	-	84.7, CH	4.88 (s)
3	84.1, C	-	111.6, C	-	77.3, C	
4	139.8, C	-	196.8, C	-	138.2, C	
5	123.8, CH	7.36 (d, 6.5)	92.5, C	-	124.8, CH	7.38 (d, 7.8)
6	124.7, CH	7.09 (m)	166.6, C	-	124.7, CH	7.11 (dd, 7.8, 6.6)
7	130.0, CH	7.35 (overlap)	-	-	129.5, CH	7.11 (dd, 7.8, 6.6)
7-NH	-	-	-	9.95 (s)	-	-
8	114.9, CH	7.35 (overlap)	91.2, C	-	114.7, CH	7.42 (d, 7.8)
9	133.6, C	-	75.0, CH	4.40 (brs)	137.1, C	-
10	170.1, C		71.9, CH	4.33 (d, 5.8)	170.7, C	-
11	58.0, CH	5.29 (brs)	68.3, CH	4.45 (ddd, 5.8, 7.8, 11.0)	58.6, CH	5.22 (brs)
12	38.2, CH_2	2.81 (d, 14.4)	129.9, CH	5.42 (overlap)	38.0, CH_2	2.74 (d, 15.6)
		3.15 (dd,14.4, 7.7)				2.81 (dd,15.6, 7.0)
13	173.1, C	-	132.0, CH	5.44 (overlap)	172.3, C	-
14	69.4, C	-	29.3, CH_2	2.02 (m); 1.97 (m)	69.6, C	-
15		-	22.2, CH_2	1.31 (m); 1.28 (m)	-	-
16		-	13.6, CH_3	0.82 (t, 7.3)	-	-
17	160.2, C	-	5.7, CH_3	1.63 (s)	159.9, C	-
18	121.6, C	-	196.4, C	-	121.8, C	-
19	126.1, CH	8.19 (d, 7.0)	133.4, C	-	126.1, CH	8.18 (d, 8.0)
20	127.1, CH	7.59 (t, 7.0)	130.3, CH	8.25 (overlap)	127.0, CH	7.59 (t, 8.0, 7.3)
21	134.6, CH	7.88 (t, 8.0)	128.4, CH	7.53 (t, 8.0)	134.5, CH	7.87 (d, 8.2, 7.3)
22	127.1, CH	7.75 (d, 8.0)	133.9, CH	7.67 (t, 7.4)	127.1, CH	7.73 (d, 8.2)
23	147.8, C	-	128.4, CH	7.53 (t, 8.0)	147.9, C	-
24	-	-	130.3, CH	8.25 (overlap)	-	-
25	148.6, CH	8.57 (s)	-	-	149.2, CH	8.52 (s)
26	18.2, CH_3	1.34 (s)	-	-	16.5, CH_3	1.30 (s)
27	22.5, CH_3	1.13 (s)	-	-	22.7, CH_3	1.28 (s)
28	174.0, C	-	-	-	-	-
29	33.0, CH	2.16 (s)	-	-	-	-
30	18.1, CH_3	0.76 (d, 6.4)	-	-	-	-
31	18.6, CH_3	0.52 (d, 7.0)	-	-	-	-
8-OMe	-	-	51.7, CH_3	3.24 (s)	-	-
9-OH	-	-	-	6.31 (s)	-	-

(−4.70), 250 (+5.58), 278 (−32.22), 314 (+8.18) nm; IR (KBr) ν_{max} 3,370, 2,958, 2,929, 2,850, 1,723, 1,703, 1,627, 1,449, 1,263, 1,104 cm^{-1}; ^{1}H and ^{13}C NMR data (see **Table 1**);HRESIMS *m/z* 468.1623 [M + Na]$^{+}$ (calcd for $C_{23}H_{27}NNaO_8$, 468.1629).

Tryptoquivaline Z (**3**): White amorphous powder; $[\alpha]_D^{25}$ +135 (*c* 0.10, MeOH); UV (MeOH) λ_{max} (log ε) 208 (4.33), 296 (3.28) nm; CD (0.11 mM, MeOH) λ_{max} ($\Delta\varepsilon$) 222 (−11.10), 244 (−2.27), 258 (−4.95), 302 (+1.30) nm; IR (KBr) ν_{max} 3,359, 2,932, 1712, 1,661, 1,611, 1,483, 1,465, 1,403, 1,293, 1,271, 1,172, 1,122, 1,019, 904, 758, 701 cm^{-1}; ^{1}H and ^{13}C NMR data (see **Table 1**); HRESIMS *m/z* 451.1622 [M + H]$^{+}$ (calcd for $C_{23}H_{23}N_4O_6$, 451.1612).

Computational Details

All the quantum mechanical calculations were performed using Gaussian 09 (Frisch et al., 2009). Systematic conformational searches were done for each compound in the gas phase using the MMFF force field, implemented in Spartan 14 (Spartan'14), and the results were validated using Macromodel (MacroModel, 2018) (MMFF force field, mixed torsional/low-mode sampling protocol) using an energy cutoff of 10 kcal/mol. The choice for the 10 kcal/mol of cutoff was set as a balance between reducing the overall CPU calculation time and minimizing the possibility of losing further contributing conformers. The numbers of unique conformations found within these boundaries were 92 for **1**, 73 for *11epi*-**1**, and 290 for **2**. All conformers were kept for full geometry optimization at the RHF/3-21G level in gas phase. All structures within 5 kcal/mol from the corresponding global minima were reoptimized at the B3LYP/6-31G* level in gas phase. Frequency calculations were done at the same level to determine the nature of the stationary points found. The ECD calculations were carried out using the B3LYP/6-31G* optimized geometries. The excitation energies (nm) and rotatory strength (*R*) in dipole velocity (R_{vel}) of the first forty singlet excitations were calculated using TDDFT implemented in Gaussian 09 at the PBE0/def2-SVP and B3LYP/6-31G* levels from all significantly populated conformers, which were averaged using Boltzmann weighting. The Boltzmann amplitudes obtained by refining the Gibbs free energies of all compounds at the SMD/M06-2X/6-31G* level using methanol as solvent. The calculated rotatory strength were simulated into the ECD curve as the sum of Gaussians with 0.3 eV width at

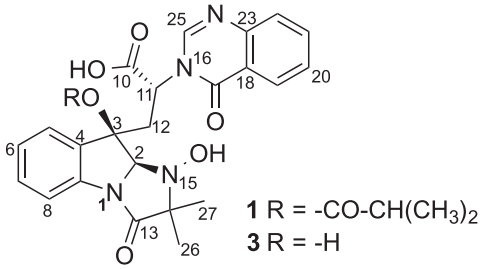

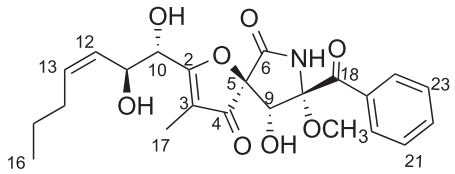

FIGURE 1 | Chemical structures of compounds 1–3.

half-heights (σ), which were UV-corrected and scaled (Pescitelli and Bruhn., 2016).

Antibacterial Assays

Antibacterial assay was conducted by the previously described method (Cheng et al., 2013). DMSO (5%) was used as negative controls whereas chloramphenicol was used as a positive control, which was active against *S. aureus, methicillin resistant S. aureus, Bacillus subtilis* and *E. coli* with MIC values ranging from 2.5 μg/ml to 12.5 μg/ml. The maximum concentration of the used compounds was 160 μg/ml. All experiments were repeatedly performed in triplicate.

Anti-Proliferative Assays

The viability of A2780 human ovarian cancer cells was determined using the CyQuant assay according to the manufacturer's instructions (Life Technologies, CA, United States). Briefly, cells were cultured in 96-well plates at 5×10^3 cells per well for 24 h and subsequently treated with compounds (50 μM) for 72 h and analyzed. Relative viability of the treated cells was normalized to the DMSO-treated control cells (Cao et al., 2007; Cao et al., 2010; Hou et al., 2008. Cisplatin was used as a positive control, which had an IC_{50} value of 0.36 μM. All experiments were performed in triplicate.

NF-κB Assay

We employed human embryonic kidney cells 293, Panomic for monitoring changes occurring along the NF-κB pathway (Li et al., 2017). Stable constructed cells were seeded into 96-well plates at 20×10^3 cells per well. Cells were maintained in Dulbecco's modified Eagle's medium (DMEM) (Invitrogen Co.), supplemented with 10% FBS, 100 units/mL penicillin, 100 μg/ml streptomycin, and 2 mM L-glutamine. After 48 h incubation, the medium was replaced and the cells were treated with various concentrations of test substances. TNF-α (human, recombinant, *E. coli*, Calbiochem) was used as an activator at a concentration of 2 ng/ml (0.14 nM). The plate was incubated for 6 h. Spent medium was discarded, and the cells were washed once with PBS. Cells were lysed using 50 μL (for 96-well plate) of reporter lysis buffer from Promega by incubating for 5 min on a shaker, and stored at −80°C. The luciferase assay was performed using the Luc assay system from Promega. The gene product, luciferase enzyme, reacts with luciferase substrate, emitting light, which was detected using a luminometer (LUMIstar Galaxy BMG). Data for

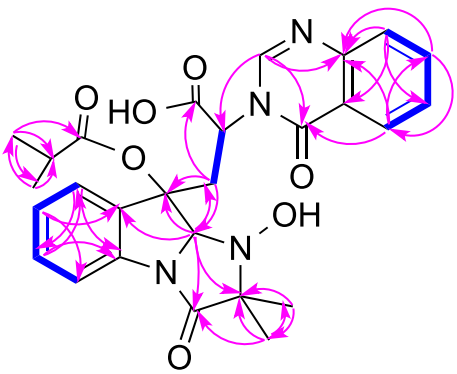

FIGURE 2 | Key COSY (bolds, blue), HMBC (arrows, pink) and ROESY (double arrows, pink) correlations of **1**.

NF-κB inhibition are expressed as IC_{50} values (i.e., concentration required to inhibit TNF-induced NF-κB activity by 50%). The known NF-κB inhibitor TPCK was used as a positive control.

RESULTS AND DISCUSSION

Identification of Compounds

Compound **1** (**Figure 1**) was obtained as a white amorphous powder and its molecular formula was determined as $C_{27}H_{28}N_4O_7$ by HRESIMS, indicating sixteen degrees of unsaturation. The ^{13}C NMR and HSQC spectra of **one** demonstrated the presence of nineteen carbons including four methyl (4× CH_3), nine sp^2 methines (9× =CH), four sp^2 non-protonated carbons (4× = C), four carbonyls (4× -CO), and one methylenes (1×-CH_2), three sp^3 methines (3× -CH), one nitrogenated nonprotonated sp^3 carbon (1× -C), and one oxygenated nonprotonated sp^3 carbon (1× -C) (**Table 1**). The COSY spectrum of **1** indicated the presence of three spin systems including one CH-CH_2 and two CH = CH-CH = CH (**Figure 2**). The HMBC spectrum of **1** showed long-range ^1H–^{13}C correlations from H-5 (δ_H 7.36) to C-7 (δ_C 130.0) and C-9 (δ_C 133.6), from H-6 (δ_H 7.09) to C-4 (δ_C 139.8) and C-8 (δ_C 114.9), from H-7 (δ_H 7.35) to C-5 (δ_C 123.8) and C-9, from H-27 (δ_H 1.13) to C-14 (δ_C 69.4) and C-26 (δ_C 18.2), from H-26 (δ_H 1.34) to C-13 (δ_C 173.1) and C-14, and from H-2 (δ_H 5.08) to C-3 (δ_C 84.1), C-4, C-13, and C-14 (**Figure 2**), which confirmed the

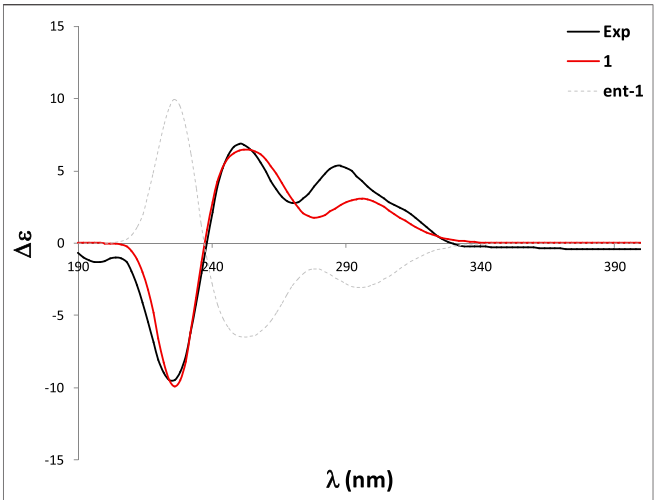

FIGURE 3 | Experimental and calculated ECD spectra of **1**.

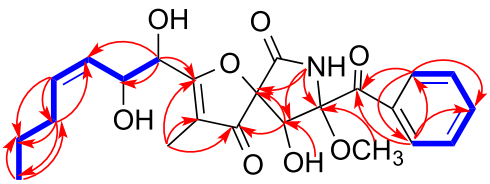

FIGURE 4 | Key COSY (bolds, blue), HMBC (arrows, red) correlations of **2**.

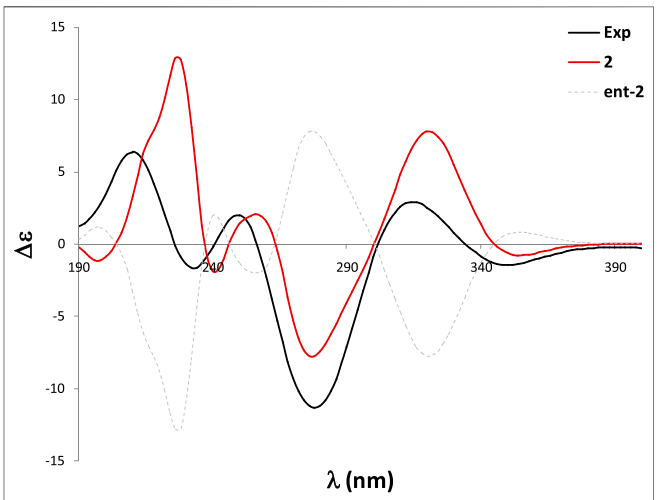

FIGURE 5 | Experimental and calculated ECD spectra of **2**.

presence of an indole imidazole moiety, 2,2-dimethyl-1,2,9,9a-tetrahydro-3*H*-imidazo [1,2-*a*]indol-3-one. In the HMBC spectrum of **1**, H-22 (δ_H 7.75) correlated to C-20 (δ_C 127.1) and C-18 (δ_C 121.6), H-21 (δ_H 7.88) to C-19 (δ_C 126.1) and C-23 (δ_C 147.8), H-19 (δ_H 8.19) to C-21 (δ_C 134.6) and C-17 (δ_C 160.2), H-25 (δ_H 8.57) to C-17 and C-23, and H-25 to C-17 and C-22 (δ_C 127.1), which confirmed the presence of a quinazolin-4(3*H*)-one moiety. The HMBC correlations from H-12 (δ_H 2.81, 3.15) to C-2 (δ_C 85.1), C-3 and C-10 (δ_C 170.1), and H-25 and C-11 indicated that the indole imidazole and quinazolin-4(3*H*)-one moieties were connected through the $^{12}CH_2$-^{11}CH spin system with a carboxylic acid group at 11-position.The HMBC spectrum of **1** also showed long-range ^1H–^{13}C correlations from H-31 (δ_H 0.52) to C-29 (δ_C 33.0) and C-30 (δ_C 18.1), H-30 (δ_H 0.76) to C-28 (δ_C 174.0), C-29 and C-31 (δ_C 18.6), indicating the presence of an isobutyric acid group in compound **1**. On the basis of the NOESY correlations from H-30 to H-25 (δ_H 8.57) and H-31 to H-5, the isobutyric acid group must be located at 3-position (**Figure 2**). Finally, the hydroxyl group was assigned at 15-position because this was the only available position. Hence, the planar structure of **one** was determined as shown, and it was named tryptoquivaline Y. The ROESY spectrum of compound **1** exhibited correlations between H-2 (δ_H 5.08) and H-12 (δ_H 2.81), indicating that H-2 and H-12 were on the same side of the molecule.

In order to determine the absolute configuration of **1**, a CD spectrum was collected, which was very similar to that of tryptovaline K (Zhou et al., 2012), indicating that both compounds should have the same absolute configuration. To confirm the absolute configuration of **1**, TDDFT ECD calculations were carried out. The experimental ECD of **1** showed a strong negative Cotton effect (CE) at 224 nm, and two positive CEs at 250 and 288 nm. The MMFF conformational analysis of **1** yielded 92 conformations within the 10 kcal/mol window, which were further subsequently reoptimized at the RHF/3-21G and B3LYP/6-31G* levels. The Gibbs free energies of the most stable conformations found were further refined at the SMD/M06-2X/6-31G* level of theory, using methanol as solvent. The ECD calculations were performed at the PBE0/def2SVP//B3LYP/6-31G* level, and were Boltzmann-averaged using the Gibbs free energies calculated in the previous step. The same computational work was carried out with *11epi*-**1** in order to define the relative configuration at C-11 as well. As shown in **Figure 3**, the calculated ECD of **1** showed an excellent agreement with the experimental data, allowing to assign the structure of **1** as shown. On the other hand, the calculated spectrum of *11epi*-**1** did not reflect good match with the experimental data (**Supplementary Figures S22, 23**), hence reinforcing our relative and absolute configurational assignment.

Pseurotin F (**2**) was obtained as white amorphous powder and has a molecular formula of $C_{23}H_{27}NO_8$ derived from the HRESIMS peak at *m/z* 468.1623 $[M + Na]^+$. The COSY spectrum of **2** exhibited the presence of two spin system, CH_3-CH_2-CH_2-CH = CH-CH(OH)-CH(OH)- and a mono-substituted benzene ring (**Figure 4**). HMBC correlations from H-17 (δ_H 1.63) to C2 (δ_C 187.0), and C-4 (δ_C 196.8), H-9 (δ_H 4.40) to C-4 and C-5 (δ_C 92.5), 9-OH (δ_H 6.31) to C-9 (δ_C 75.0), 8-OMe (δ_H 3.24) to C-8 (δ_C 91.2), and NH-7 (δ_H 9.95) to C-5, C-8, and C-9 indicated the presence of 1-oxa-7-azaspiro [4.4]non-2-ene-4,6-dione core. An HMBC correlation from H-10

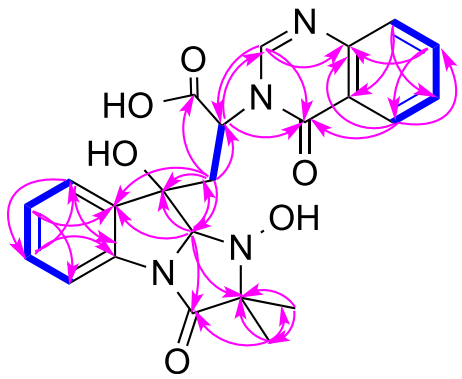

FIGURE 6 | Key COSY (bolds, blue), HMBC (arrows, pink) correlations of **3**.

(δ_H 4.33) to C-2 confirmed the connectivity of the spin system CH_3-CH_2-CH_2-CH = CH-CH(OH)-CH(OH)- to the 1-oxa-7-azaspiro [4.4]non-2-ene-4,6-dione core. The mono-substituted benzene ring must be connected to the 1-oxa-7-azaspiro [4.4] non-2-ene-4,6-dione core through a ketone (C=O). Moreover, the NMR data of compound **2** (**Table 1**) were very similar to those of compound **8**. The main NMR difference between **2** and **8** was attributable to one more methylene group in the chain of compound **2**. No ROESY correlation between H-9 (δ_H 4.40, s) and 8-OMe (δ_H 3.24, s) was observed. In fact, no other ROESY correlations were clear except for those in the two spin systems. On the other hand, the ^{13}C NMR data of compound **2** and compound **8** were almost the same, indicating both **2** and compound **8** should have the same configuration. Interestingly, compounds **2** and **8** had completely the same ECD pattern (**Figure 5** and **Supplementary Figure S14**). Hence, it was confirmed that both compounds **2** and **8** should have the same configuration, and compound **2** was named pseurotin I.

To confirm the absolute configuration of **2**, we performed the ECD calculations. Starting with the 290 conformations found at the MMFF level, the geometries were subsequently reoptimized at the RHF/3-21G and B3LYP/6-31G* levels. The TDDFT calculations were carried at the B3LYP/6-31G* level (which in this case yielded better performance than the PBE0/def2SVP level) and were Boltzmann-averaged using the Gibbs free energies refined at the SMD/M06-2X/6-31G* level with methanol as solvent. The calculated ECD spectrum of **two** was in good agreement with the experimental ECD curve, which thus allowed an unambiguous configurational assignment (**Figure 5**).

Tryptoquivaline Z (**3**) was obtained as white amorphous powder and has a molecular formula of $C_{23}H_{22}N_4O_6$ derived from the HRESIMS peak at *m/z* 451.1622 $[M + H]^+$. The NMR data of compound **3** (**Table 1**) were very similar to those of compound **1**. The main NMR difference between **3** and **1** was that compound **1** had one extra isobutyric acid group (**Figures 1**, **6**). Compound **3** had a similar CD spectrum to that of **1**, so it was deducted that both should have the same configuration. The planar structure of compound **3** was recorded in SciFinder with an ACS registration number of 1214809–50-3 (Zheng et al., 2018), but no physio-chemical properties including NMR data were reported in the published patent (Zheng et al., 2018). The ROESY spectrum of compound **3** showed correlations between H-2 (δ_H 4.88, s) and H-26 (δ_H 1.30, s), H-12 (δ_H 2.74, d) (**Supplementary Figures S21**), which were very similar to those of compound **1**. Further, compounds **3** and **1** had the similar ECD patterns, indicating that both compounds **3** and **1** should have the same configuration. Hence, the structure including the absolute configuration of compound **3** was determined as shown, and it was given a trivial name tryptoquivaline Z.

Seven other compounds, β-cyclopiazonic acid (**4**) (Wang et al., 2016), *cyclo*-(L-Pro-L-Phe) (**5**) (Li et al., 2008), tryptoquivaline L (**6**) (Buttachon et al., 2012), Bisdethiobis (methylthio) gliotoxin (**7**) (Afiyatullov et al., 2005), pseurotin A (**8**), pseurotin A_1 (**9**) and pseurotin A_2 (**10**) (Wang et al., 2011) were also isolated from *Aspergillus felis* FM324. The structures of these known compounds (**4**–**10**) were determined based on comparisons of NMR and HRESIMS data with previously reported data.

Biological Activity

Except for compound **4**, the other nine compounds belong to three different classes of natural products, tryptoquivalines (**1**, **3**, and **6**), pseurotins (**2** and **8**–**10**) and diketopepirazines (**5** and **7**). These classes of compounds were reported to demonstrate anti-proliferative and antibacterial activities. Hence, we tested compounds **1**–**10** for their activities against A2780 cancer cell line, *S. aureus,* methicillin resistant *S. aureus, Bacillus subtilis* and *E. coli*. Besides, their anti-inflammatory activity against NF-κB was also evaluated. Compound **4** showed antibacterial activity against *S. aureus*, methicillin resistant *S. aureus* and *Bacillus subtilis* with the same MIC value of 59.2 μM. None of the compounds (**1**–**10**) exhibited any anti-proliferative activity against A2780, while compounds **3** and **2** inhibited NF-κB with IC_{50} values of 26.7 and 30.9 μM, respectively. In the absence of a cytotoxic response, inhibition of NF-κB activity suggests the potential of cancer chemoprevention.

CONCLUSION

Aspergillus species are well known for producing tryptoquivaline and pseurotin types of compounds. Our research group previously reported two new tryptoquivaline from *Aspergillus terreus* (Zaman K. A. U. et al., 2020). Pseurotins, with 1-oxa-7-azaspiro [4.4]non-2-ene-4,6-dione core, were also isolated from another *Aspergillus species* (Wang et al., 2011). In our current research, one new tryptoquivaline (**1**) and one new pseurotin (**2**) together with eight known compounds (**3**–**10**) were isolated from a Hawaiian fungal strain *Aspergillus felis* FM324. The absolute configuration and physicochemical properties of compound **3** were also described for the first time. Compound **4** showed weak antibacterial activity against Gram-positive bacteria, and compounds **2** and **3** mildly inhibited NF-κB.

DATA AVAILABILITY STATEMENT

The datasets presented in this study can be found in online repositories. The names of the repository/repositories and accession number(s) can be found below: GenBank under the accession no. MZ227547.

AUTHOR CONTRIBUTIONS

CW conducted the chemical experiments, and prepared the manuscript. KAUZ did the antibacterial assay. XW performed the antiproliferative and NF-κB assays. AMS carried out the ECD calculations. SC initiated the project, oversaw the research, and revised the manuscript. All authors approved the submission of the manuscript for publication.

FUNDING

This research was supported by Specific research project of Guangxi for research bases and talents (AD20297036), Guangxi Natural Science Foundation under Grant (2019GXNSFBA185002), start-up funding from University of Hawaii Cancer Center (UHCC) and Daniel K. Inouye College of Pharmacy (DKICP), Seed grants from the University of Hawaii at Hilo (UH Hilo), and Hawaii Community Foundation (15ADVC-74420, 17CON-86295, and 20CON-102163) (to SC). Funding for this work was also supported by Hawaii IDeA Network for Biomedical Research Excellence III and IV (INBRE-III and INBRE-IV) project (NIGMS Grant 5P20GM103466).

ACKNOWLEDGMENTS

We would also like to express our gratitude to Justin Reinicke for his help with HRMS, NMR, optical rotation and ECD data collection.

SUPPLEMENTARY MATERIAL

The Supplementary Material for this article can be found online at: https://www.frontiersin.org/articles/10.3389/fchem.2021.724617/full#supplementary-material

REFERENCES

Afiyatullov, S. S., Kalinovskii, A. I., Pivkin, M. V., Dmitrenok, P. S., and Kuznetsova, T. A. (2005). Alkaloids from the marine Isolate of the Fungus *Aspergillus fumigatus*. *Chem. Nat. Compd.* 41, 236–238. doi:10.1007/s10600-005-0122-y

Buttachon, S., Chandrapatya, A., Manoch, L., Silva, A., Gales, L., Bruyère, C., et al. (2012). Sartorymensin, a New Indole Alkaloid, and New Analogues of Tryptoquivaline and Fiscalins Produced by *Neosartorya Siamensis* (KUFC 6349). *Tetrahedron* 68, 3253–3262. doi:10.1016/j.tet.2012.02.024

Cao, S., Brodie, P. J., Callmander, M., Randrianaivo, R., Rakotobe, E., Rasamison, V. E., et al. (2010). Saponins and a Lignan Derivative of *Terminalia Tropophylla* from the Madagascar Dry Forest. *Phytochemistry* 71, 95–99. doi:10.1016/j.phytochem.2009.09.027

Cao, S., Norris, A., Wisse, J. H., Miller, J. S., Evans, R., and Kingston, D. G. I. (2007). Ipomoeassin F, a New Cytotoxic Macrocyclic Glycoresin from the Leaves of *Ipomoea squamosafrom* the Suriname Rainforest. *Nat. Product. Res.* 21, 872–876. doi:10.1080/14786410600929576

Cheng, B., Cao, S., Vasquez, V., Annamalai, T., Tamayo-Castillo, G., Clardy, J., et al. (2013). Identification of Anziaic Acid, a Lichen Depside from *Hypotrachyna* sp., as a New Topoisomerase Poison Inhibitor. *PLoS One* 8, e60770, 2013 . e60770. doi:10.1371/journal.pone.0060770

Deshmukh, S. K., Prakash, V., and Ranjan, N. (2017). Marine Fungi: a Source of Potential Anticancer Compounds. *Front. Microbiol.* 8, 2536. doi:10.3389/fmicb.2017.02536

Elkhayat, E. S., Ibrahim, S. R. M., Mohamed, G. A., and Ross, S. A. (2016). Terrenolide S, a New Antileishmanial Butenolide from the Endophytic fungus *Aspergillus terreus*. *Nat. Product. Res.* 30, 814–820. doi:10.1080/14786419.2015.1072711

Fei-Zhang, D. J., Li, C., and Cao, S. (2016). Hawaii Natural Compounds Are Promising to Reduce Ovarian Cancer Deaths. *Cancer Biol. Ther.* 17, 709–712. doi:10.1080/15384047.2016.1178428

Frisch, M. J., Trucks, G. W., Schlegel, H. B., Scuseria, G. E., Robb, M. A., Cheeseman, J. R., et al. (2009). *Gaussian 09*. Wallingford, CT: Gaussian, Inc.

Hou, Y., Cao, S., Brodie, P., Miller, J. S., Birkinshaw, C., Ratovoson, F., et al. (2008). Antiproliferative Cassane Diterpenoids of *Cordyla Madagascariensis* sp. *Madagascariensis* from the Madagascar Rainforest. *J. Nat. Prod.* 71, 150–152. doi:10.1021/np070437l

Huang, P., Li, C., Sarotti, A. M., Turkson, J., and Cao, S. (2017). Sphaerialactonam, a γ-lactam-isochromanone from the Hawaiian Endophytic Fungus *Paraphaeosphaeria* Sp. FT462. *Tetrahedron Lett.* 58, 1330–1333. doi:10.1016/j.tetlet.2017.02.052

Ibrahim, S. R. M., and Asfour, H. Z. (2018). Bioactive γ-butyrolactones from Endophytic Fungus *Aspergillus versicolor*. *Int. J. Pharmacol.* 14, 437–443. doi:10.3923/ijp.2018.437.443

Ibrahim, S. R. M., Mohamed, G. A., and Khedr, A. I. M. (2017a). γ-Butyrolactones from *Aspergillus* Species: Structures, Biosynthesis, and Biological Activities. *Nat. Product. Commun.* 12, 791–800. doi:10.1177/1934578X1701200526

Ibrahim, S. R. M., Mohamed, G. A., and Ross, S. A. (2017b). Aspernolides L and M, New Butyrolactones from the Endophytic Fungus *Aspergillus versicolor*. *Z. Naturforsch. C.* 72, 155–160. doi:10.1515/znc-2016-0138

Li, C.-S., Ding, Y., Yang, B.-J., Miklossy, G., Yin, H.-Q., Walker, L. A., et al. (2015). A New Metabolite with a Unique 4-Pyranone–γ-Lactam-1,4-Thiazine Moiety from a Hawaiian-Plant Associated Fungus. *Org. Lett.* 17, 3556–3559. doi:10.1021/acs.orglett.5b01650

Li, C.-S., Ren, G., Yang, B.-J., Miklossy, G., Turkson, J., Fei, P., et al. (2016). Meroterpenoids with Antiproliferative Activity from a Hawaiian-Plant Associated Fungus *Peyronellaea coffeae-arabicae* FT238. *Org. Lett.* 18, 2335–2338. doi:10.1021/acs.orglett.6b00685

Li, C.-S., Sarotti, A. M., Huang, P., Dang, U. T., Hurdle, J. G., Kondratyuk, T. P., et al. (2017). NF-κB Inhibitors, Unique γ-pyranol-γ-lactams with Sulfide and Sulfoxide Moieties from Hawaiian Plant Lycopodiella Cernua Derived Fungus *Paraphaeosphaeria neglecta* FT462. *Sci. Rep.* 7, 10424. doi:10.1038/s41598-017-10537-1

Li, C., Hu, Z., Liu, Q., Wu, X., and Cao, S. (2018). Two New Tricycloalternarenes from Hawaiian Endophytic Fungus *Didymella* Sp. FT433. *Tetrahedron Lett.* 59, 3381–3383. doi:10.1016/j.tetlet.2018.07.061

Li, C., Sarotti, A. M., Wu, X., Yang, B., Turkson, J., Chen, Y., et al. (2019). An Unusual Benzoisoquinoline-9-One Derivative and Other Related Compounds with Antiproliferative Activity from Hawaiian Endophytic Fungus *Peyronellaea* Sp. FT431. *Molecules* 24, 196. doi:10.3390/molecules24010196

Li, Z., Peng, C., Shen, Y., Miao, X., Zhang, H., and Lin, H. (2008). L,L-Diketopiperazines from *Alcaligenes Faecalis* A72 Associated with south china Sea Sponge *Stelletta Tenuis*. *Biochem. Syst. Ecol.* 36, 230–234. doi:10.1016/j.bse.2007.08.007

Liu, D., Coloe, S., Baird, R., and Pedersen, J. (2000). Rapid Mini-Preparation of Fungal DNA for PCR. *J. Clin. Microbiol.* 38, 471. doi:10.1128/JCM.38.1.471-471.2000

MacroModel (2018). *Schrodinger Release 2018-3*. New York: Schrodinger LLC.

Mohamed, G. A., Ibrahim, S. R. M., and Asfour, H. Z. (2020). Antimicrobial Metabolites from the Endophytic Fungus *Aspergillus versicolor*. *Phytochemistry Lett.* 35, 152–155. doi:10.1016/j.phytol.2019.12.003

Overy, D., Rämä, T., Oosterhuis, R., Walker, A., and Pang, K.-L. (2019). The Neglected Marine Fungi, Sensu Stricto, and Their Isolation for Natural Products' Discovery. *Mar. Drugs* 17, 42. doi:10.3390/md17010042

Pescitelli, G., and Bruhn, T. (2016). Good Computational Practice in the Assignment of Absolute Configurations by TDDFT Calculations of ECD Spectra. *Chirality* 28, 466–474. Spartan'14; Wavefunction: Irvine, CA. doi:10.1002/chir.22600

Vadlapudi, V., Borah, N., Yellusani, K. R., Gade, S., Reddy, P., Rajamanikyam, M., et al. (2017). Aspergillus Secondary Metabolite Database, a Resource to Understand the Secondary Metabolome of *Aspergillus* Genus. *Sci. Rep.* 7, 1–10. doi:10.1038/s41598-017-07436-w

Wang, C., Tang, S., and Cao, S. (2021). Antimicrobial Compounds from marine Fungi. *Phytochem. Rev.* 20, 85–117. doi:10.1007/s11101-020-09705-5

Wang, F.-Z., Li, D.-H., Zhu, T.-J., Zhang, M., and Gu, Q.-Q. (2011). Pseurotin A1 and A2, Two New 1-oxa-7-azaspiro[4.4]non-2-Ene-4,6-Diones from the Holothurian-Derived Fungus *Aspergillus fumigatus* WFZ-25. *Can. J. Chem.* 89, 72–76. doi:10.1139/V10-157

Wang, F., Hu, Z., Li, C., Wu, X., and Cao, S. (2019). Circumdatin M, a New Benzodiazepine Alkaloid with a Unique Pyrimidone-4-Pyrone Moiety from a Hawaiian marine Fungus *Aspergillus* sp. FM242. *Tetrahedron Lett.* 60, 1724–1726. doi:10.1016/j.tetlet.2019.05.061

Wang, F., Sarotti, A. M., Jiang, G., Huguet-Tapia, J. C., Zheng, S.-L., Wu, X., et al. (2020). Waikikiamides A-C: Complex Diketopiperazine Dimer and Diketopiperazine-Polyketide Hybrids from a Hawaiian Marine Fungal Strain *Aspergillus* sp. FM242. *Org. Lett.* 22, 4408–4412. doi:10.1021/acs.orglett.0c01411

Wang, L.-N., Di, W.-J., Zhang, Z.-M., Zhao, L.-l., Zhang, T., Deng, Y.-R., et al. (2016). Small-molecule Inhibitors of the Tuberculosis Target, Phenylalanyl-tRNA Synthetase from *Penicillium griseofulvum* CPCC-400528. *Cogent Chem.* 2, 1181536. doi:10.1080/23312009.2016.1181536

Zaman, K. A. U., Hu, Z., Wu, X., and Cao, S. (2020a). Tryptoquivalines W and X, Two New Compounds from a Hawaiian Fungal Strain and Their Biological Activities. *Tetrahedron Lett.* 61, 151730. doi:10.1016/j.tetlet.2020.151730

Zaman, K. A. U., Hu, Z., Wu, X., Hou, S., Saito, J., Kondratyuk, T. P., et al. (2020b). NF-κB Inhibitory and Antibacterial Helvolic and Fumagillin Derivatives from *Aspergillus terreus*. *J. Nat. Prod.* 83, 730–737. doi:10.1021/acs.jnatprod.9b01190

Zaman, K. A. U., Park, J. H., DeVine, L., Hu, Z., Wu, X., Kim, H. S., et al. (2021). Secondary Metabolites from the Leather Coral-Derived Fungal Strain *Xylaria* Sp. FM1005 and Their Glycoprotein IIb/IIIa Inhibitory Activity. *J. Nat. Prod.* 84, 466–473. doi:10.1021/acs.jnatprod.0c01330

Zhao, C., Liu, H., and Zhu, W. (2016). [New Natural Products from the marine-derived *Aspergillus* Fungi-A Review]. *Wei Sheng Wu Xue Bao* 56, 331–362. doi:10.13343/j.cnki.wsxb.20150478

Zheng, N., Li, M., Li, S., Zhang, Y., Li, H., and Wang, J. (2018). *Screening Methods of* Staphylococcus auresus *Inhibitors*. Beijing: Faming Zhuanlin Shenqing. CN 107904279 A 20180413.

Zhou, Y., Debbab, A., Mándi, A., Wray, V., Schulz, B., Müller, W. E. G., et al. (2012). Alkaloids from the Sponge-Associated Fungus *Aspergillus* sp *Eur. J. Org. Chem.* 2013, 894–906. doi:10.1002/ejoc.20120122

Conflict of Interest: The authors declare that the research was conducted in the absence of any commercial or financial relationships that could be construed as a potential conflict of interest.

Publisher's Note: All claims expressed in this article are solely those of the authors and do not necessarily represent those of their affiliated organizations, or those of the publisher, the editors and the reviewers. Any product that may be evaluated in this article, or claim that may be made by its manufacturer, is not guaranteed or endorsed by the publisher.

frontiers in Chemistry

ORIGINAL RESEARCH
published: 17 August 2021
doi: 10.3389/fchem.2021.736070

Aspulvinones Suppress Postprandial Hyperglycemia as Potent α-Glucosidase Inhibitors From *Aspergillus terreus* ASM-1

Changjing Wu[1,2,3†], Xiang Cui[1†], Luzhen Sun[1], Jiajia Lu[1], Feng Li[1], Minghui Song[1], Yunxia Zhang[1], Xinqi Hao[2], Congkui Tian[3], Maoping Song[2]* and Xiaomeng Liu[1,4]**

[1]College of Life Sciences and Agronomy, Zhoukou Normal University, Zhoukou, China, [2]College of Chemistry and Molecular Engineering, Zhengzhou University, Zhengzhou, China, [3]Wuling Mountain Institute of Natural Medicine, Hubei Minzu University, Enshi, China, [4]College of Public Health, Xinxiang Medical University, Xinxiang, China

OPEN ACCESS

Edited by:
Yuanyuan Lu,
China Pharmaceutical University, China

Reviewed by:
Yi Wang,
Zhejiang University, China
Reshma Rani,
Amity University, India
Jianhua Shao,
Yangzhou University, China

***Correspondence:**
Xiaomeng Liu
lxmxm_99@126.com
Maoping Song
mpsong@zzu.edu.cn
Congkui Tian
pkutianck@163.com

[†]These authors have contributed equally to this work

Specialty section:
This article was submitted to Medicinal and Pharmaceutical Chemistry, a section of the journal Frontiers in Chemistry

Received: 04 July 2021
Accepted: 04 August 2021
Published: 17 August 2021

Citation:
Wu C, Cui X, Sun L, Lu J, Li F, Song M, Zhang Y, Hao X, Tian C, Song M and Liu X (2021) Aspulvinones Suppress Postprandial Hyperglycemia as Potent α-Glucosidase Inhibitors From Aspergillus terreus ASM-1. Front. Chem. 9:736070. doi: 10.3389/fchem.2021.736070

Chemical investigation of *Aspergillus terreus* ASM-1 fermentation resulted in the isolation of three new prenylated aspulvinones V–X (**1**–**3**), together with the previously reported analogs, aspulvinone H (**4**), J-CR (**5**), and R (**6**). Their structures were elucidated by various spectroscopic methods including HRESIMS and NMR, and the absolute configurations of **2** and **3** were determined by ECD comparison. Compounds **1**–**6** were evaluated for α-glucosidase inhibitory effects with acarbose as positive control. As a result, compounds **1** and **4** exhibited potent α-glucosidase inhibitory activities with IC_{50} values of 2.2 and 4.6 μM in mixed-type manners. The thermodynamic constants recognized the interaction between inhibitors and α-glucosidase was hydrophobic force-driven spontaneous exothermic reaction. The CD spectra also indicate that the compounds **1** and **4** changed the enzyme conformation. Furthermore, compound **4** significantly suppressed the increases in postprandial blood glucose levels in the C57BL/6J mice.

Keywords: *Aspergillus terreus*, secondary metabolites, aspulvinone, structure elucidation, α-glucosidase inhibitory effect

INTRODUCTION

Diabetes mellitus is chronic metabolic disease with worldwide concerns, which causes a major challenge for the health system (Kharroubi and Darwish, 2015). The high prevalence of diabetes has focalized much efforts for novel therapeutic alternatives (Ghosh et al., 2016). Nowadays, alleviating postprandial hyperglycemia is one of the first-line therapeutical strategies for the treatment of diabetes and its complications (Taylor et al., 2021). α-Glucosidase inhibitors (AGIs), such as acarbose, miglitol, and voglibose, are usually employed for controlling postprandial blood glucose levels by delaying the intestinal digestion of carbohydrates (Hossain et al., 2020). However, utilization of clinical AGIs often have some shortcomings such as side-effects including abdominal discomfort and flatulence, limited efficacy, failure in metabolism adjustment (Calcutt et al., 2009). Therefore, much effort has been focused on searching for natural AGIs with better safety and efficacy from natural sources in the past decade (Deng et al., 2015; Zhang et al., 2020).

Aspergillus terreus ML-44 is marine-derived fungi previously isolated from the fresh gut of pacific oyster. Our former study reported five terretonins isolated from ML-44 fermentation, including a new one, which showed weak anti-inflammatory activity (Wu et al., 2019). In order to exploit the

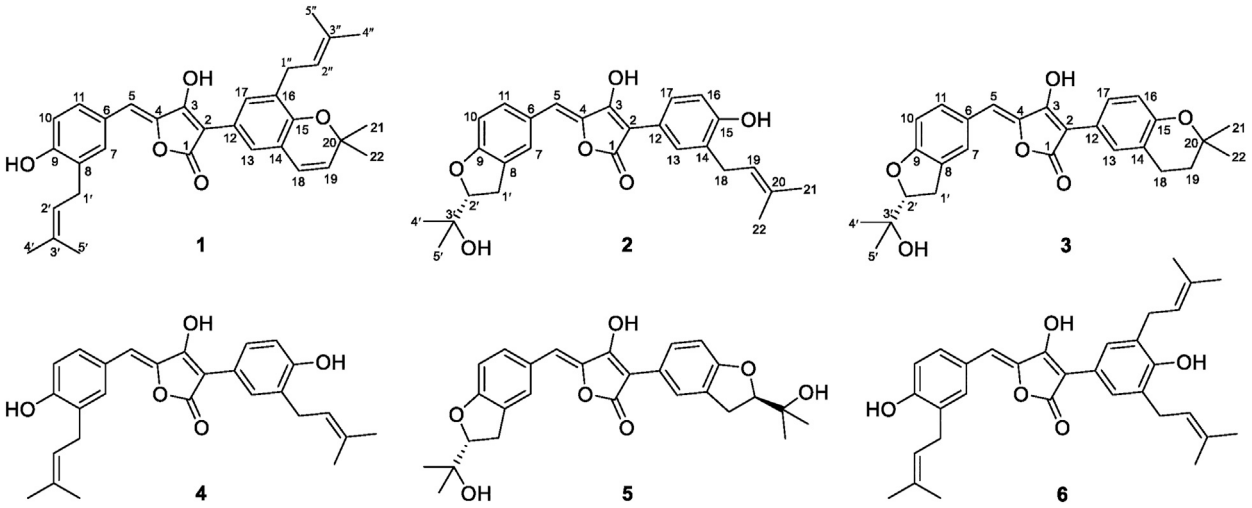

FIGURE 1 | Chemical structures of Compounds **1**–**6**.

potential of strain ML-44 in the medical field, the diethyl sulfate (DES) mutagenesis strategy (Fang et al., 2014) was applied to strain ML-44 in this study, mutant strain ASM-1 was screened out with different phenotypic morphology of colonies. HPLC-DAD-UV analysis of the mutant fermentations comparing to parent strain exhibited a series of metabolites with unique ultraviolet absorption were observed in the mutant ASM-1. Subsequent HPLC-guided chemical investigation of ASM-1 fermentation resulted in the isolation of six aspulvinone derivatives (**1**–**6**), including three new ones (**1**–**3**) (**Figure 1**). Aspulvinones and the analogs have been reported with various biological activities, such as inhibiting antibacterial (Machado et al., 2021), luciferase (Cruz et al., 2011), anti-influenza A viral (Gao et al., 2013), anticancer (Sun et al., 2019), anti-DPPH radicals (Zhang et al., 2015), as well as α-glucosidase inhibitory activity (Dewi et al., 2014; Wang et al., 2016; Zhang et al., 2016). However, there has been no systematic report on the mechanism for inhibition of α-glucosidase, structure–activity relationships, and hpyerglycemic effect *in vivo* by natural aspulvinones. In this study, the α-glucosidase inhibitory activities of compounds **1**–**6** were evaluated *in vitro*, in silico, and *in vivo*. Herein, we report the isolation, structure elucidation, and the α-glucosidase inhibitory activities of the isolated aspulvinones.

MATERIAL AND METHODS

General Experimental Procedures

Sephadex™ LH-20 (GE Healthcare, Uppsala, Sweden), and YMC*GEL® ODS-A-HG (12 nm S-50 μm, YMC Co., Ltd., Kyoto, Japan) were used for column chromatography. The MPLC was performed on a QuikSep chromatographic system (H&E, Beijing, China), and a Gemini C18 column (21.2 × 250 mm, column temperature: 26°C) was used for separation and purification. Optical rotations were measured on a JASCO P-2000 digital polarimeter (JASCO, Tokyo, Japan). UV spectra were recorded on a PerkinElmer Lambda 25 spectrophotometer. Electronic Circular Dichroism (ECD) data were taken on a Chirascan circular dichroism spectrometer (Applied Photophysics, Surrey, United Kingdom). HR-ESI-MS was measured on Agilent 6520 Q-TOP mass spectrometer (Agilent, CA, United States), and all 1D and 2D NMR spectra were obtained on a Bruker-500 (500 MHz ^{1}H and 125 MHz ^{13}C-NMR) NMR spectrometer. A SynergyHTX micro plate reader (BioTek, VT, United States) was used to read optical density (OD). The intrinsic fluorescence spectra (280–500 nm) were measured using Perkin Elmer LS55 fluorescence spectrophotometer (United Kingdom).

Chemical Mutagenesis of *A. terreus* ML-44 and Mutant Selection

The DES mutagenesis procedure was referred to the method that we previously reported (Fang et al., 2014), and with proper modifications: DES was dissolved in DMSO to obtain a 20% (v/v) solution, which was further mixed with spore suspension of *A. terreus* ML-44 in a ratio of 1:9 (v/v). The mixture was treated with assistance of ultrasonic wave (40 KHz) at room temperature. Each 80 μl portion of the treated spore suspensions was sampled and spread on PDA plates at 1 and 2 h of treatment followed by incubation at 28°C for 5–7 days. Mutants from the test groups were obtained by selection of colonies with different colonial morphology, and the genetic stability were verified by passing three generations.

The initial ML-44 strain and mutants were activated by incubation at 28°C for 3–5 days, and further inoculated into 100 ml of liquid medium (glucose 2%, maltose 1%, mannitol 2%, glutamic acid 1%, peptone 0.5%, and yeast extract 0.3% in distilled water) in an Erlenmeyer (250 ml) and fermented at 28°C on a rotary shaker at 200 rpm for 12 days. Each 100 ml of the fermentation broth was extracted with equal volumes of EtOAc

with assistance of ultrasonic wave (40 KHz) for 30 min. The EtOAc extractions were concentrated in vacuo at 37°C, followed by re-dissolved in 1.0 ml methanol which were used for further chemical analysis. HPLC-PDAD-UV analysis was performed using an analytical Kromasil C18 column (5 μm, 100 Å, 4.6 × 250 mm; Akzo Nobel) on an Agilent 1100 HPLC system equipped with photo-diode array detector (G1316A). After filtered with 0.45 μm membrane, the extraction solution in methanol (1.0 ml) was injected (10 μl) into the column and eluted with a MeOH-H_2O linear gradient (20%→100% MeOH in 30 min followed by 5 min with isocratic 100% MeOH) mobile phase (flow rate 1 ml/min). The acquired PDAD data were processed with Agilent OpenLAB software.

Chemical Investigation to Mutant ASM-1

The mutant ASM-1 was inoculated into ten Erlenmeyer (500 ml) each containing 200 ml of sterile liquid medium and cultured at 28°C for 48 h on a rotary shaker at 200 rpm providing a seed culture (2 L). The seed culture was inoculated into a fermentation cylinder containing the same sterile liquid medium (70 L), and was cultured at 28°C for 12 days, with sterile compressed air passes from the bottom of the cylinder keeping a positive pressure of 0.15 MPa. The whole broth (65 L) was filtered to separate into the filtrate and the mycelial cake. The filtrate (60 L) was subjected to an AB-8 macroporous resin column (column volume, CV 2.4 L), eluted by water and 95% ethanol successively. The water elute (3 CVs) was discarded, and the 95% ethanol elute (3 CVs) was gathered. The mycelial cake was extracted two times with 95% ethanol (5 L) assisted by ultra-sonication for 2 h, followed by filtration giving the ethanol extract. All the ethanol solutions were combined and concentrated to a water suspension, which was further extracted with EtOAc to afford a total of 60.5 g of EtOAc extract.

The EtOAc extract (60.5 g) of the mutant ASM-1 was subjected to silica gel column chromatography by stepwise elution with b. p. 60–90°C petroleum ether (P)- dichloromethane (D)-methanol (M) to obtain 9 fractions. HPLC analysis showed that the newly produced metabolites were contained in Fr-4 (1.9 g, eluted by D), Fr-5 (5 g, eluted by DM 98:2), and Fr-7 (2.3 g, eluted by DM 90:10) (**Supplementary Figure S3**). Subsequent repeated preparative reverse phase HPLC separation led to the purification of compounds. Fr-4 was subjected to reduced pressure ODS column chromatography (cc) to give subfraction Fr-4–8 (0.3 g, eluted by 90%M), which was further separated by HPLC (Methanol-H_2O (0.1%HCl) 90: 10, 10 ml/min) to afford **1** (25 mg, t_R = 36.0 min) and **6** (2.1 mg, t_R = 24.5 min); Fr-5–4 (1.6 g, eluted by 80%M), the subfraction of Fr-5 by ODS cc, afforded **3** (12 mg, t_R = 64.0 min) and **4** (218 mg, t_R = 67.5 min) with preparative HPLC separation (Methanol-H_2O (0.1%HCl) 65:35, 10 ml/min); Fr-7 was separated by ODS cc to give subfraction Fr-7–9 (0.6 g, eluted by 80%M), which provided **2** (28 mg, t_R = 28.4 min) and **5** (16 mg, t_R = 18.6 min) after preparative HPLC separation (Methanol-H_2O (0.1%HCl) 77:23, 10 ml/min).

Aspulvinone V (**1**): yellow solid (MeOH), UV (MeOH) λmax (log ε): 203 (4.36), 239 (4.11), 380 (4.23). Positive HR-ESI-MS: *m/z* measured 499.2480 $[M + H]^+$, calcd for $C_{32}H_{35}O_5$ $[M + H]^+$ 499.2484. ^1H NMR and ^{13}C NMR spectroscopic data, see **Table 1**.

Aspulvinone W (**2**): yellow solid (MeOH) $[\alpha]_D^{24}$−32.8 (c 0.23, MeOH). UV (MeOH) λmax (log ε): 203 (4.35), 243 (3.98), 374 (4.15). Positive HR-ESI-MS: *m/z* measured 449.1963 $[M + H]^+$, calcd for $C_{27}H_{29}O_6$ $[M + H]^+$ 449.1964. ^1H NMR and ^{13}C NMR spectroscopic data, see **Table 1**.

Aspulvinone X (**3**): yellow solid (MeOH) $[\alpha]_D^{24}$−27.9 (c 0.26, MeOH). UV (MeOH) λmax (log ε): 203 (4.35), 242 (3.98), 376 (4.16). Positive HR-ESI-MS: m/z measured 449.1958 $[M + H]^+$, calcd for $C_{27}H_{29}O_6$ $[M + H]^+$ 449.1964. ^1H NMR and ^{13}C NMR spectroscopic data, see **Table 1**.

α-Glucosidase Inhibitory Assay

α-Glucosidase (EC:3.2.1.20, MAL12) from *Saccharomyces cerevisiae* was dissolved in 0.1 mol/L PBS solutions with a pH of 6.8, and diluted to be a 1.0 U/ml solution. The substrate p-nitrophenyl-β-D-glucopyranoside (pNPG) was dissolved in PBS to be a 1 mM solution. Acarbose and the compounds were dissolved in mehanol and further diluted to a series of concentrations from 0.1 μmol/L to 10 mmol/L. *In vitro* α-glucosidase inhibitory assay was performed according to a method described previously with some modification (Dan et al., 2019). Briefly, 20 μl of 1.0 U/ml enzyme solution and 10 μl of acarbose or compound solution, was mixed with 50 μl PBS solution in 96-well plate, and the mixed solution was incubated at 37°C for 10 min 20 μl of 1 mmol/L pNPG was subsequently added and further incubated at 37°C for 15 min, after which 100 μl of 1 M Na_2CO_3 solution was added to terminate the reaction. The absorbance of p-nitrophenol was monitored at 405 nm. All samples were analysed in triplicate, and acarbose was used as positive control. The negative control was performed by adding PBS instead of α-glucosidase, the blank was prepared by adding solvent without tested compounds. The inhibition rate was calculated as **Eq. 1**:

$$IR\% = [(Ac - As)/Ac] \times 100\% \quad (1)$$

where Ac represents the absorbance of control without sample solution, and As denotes the absorbance of sample.

Enzymatic Kinetics of α-Glucosidase

pNPG with a concentration range of 100–4,000 μM and α-glucosidase were incubated with different concentrations of inhibitor for 10 min, respectively. 20 μl of 1.0 U/ml enzyme solutions were first mixed with 10 μl of different concentrations of inhibitors, then 50 μl PBS solutions were added, and the mixed solutions were incubated at 37°C for 10 min. Subsequently, 20 μl of pNPG solutions (1.25, 2.5, 5, 10 and 20 mM) were added, and the mixed solutions were further incubated at 37°C for 25 min, the absorbance of reaction solution was measured at 405 nm every 3 min. The kinetic parameters, Michaelis–Menten (K_m) and maximum velocity (V_{max}), were found using Lineweaver–Burk plots to check the mode of α-glucosidase inhibition for compounds **1** and **4**. The dissociation constants between inhibitor and enzyme (K_i) were calculated from Dixon plots. Two inhibition constants, K_I or K_{IS},

TABLE 1 | 500 MHz ^{1}H and 125 MHz^{13}C NMR data of compounds **1**–**3**, **5** in CD_3OD.[a]

No	1		2		3		5	
	δ_C	δ_H (J in Hz)	δ_C	δ_H (J in Hz)	δ_C	δ_H (J in Hz)	δ_C	δ_H (J in Hz)
1	171.2 s	—	171.3 s	—	171.2 s	—	171.1 s	—
2	102.2 s	—	102.7 s	—	102.4 s	—	102.6 s	—
3	163.5 s	—	163.1 s	—	163.3 s	—	163.3 s	—
4	141.5 s	—	141.8 s	—	141.8 s	—	141.8 s	—
5	109.5 d	6.37, s	108.9 d	6.36, s	109.1 d	6.38, s	109.1 d	6.39, s
6	125.8 s	—	127.1 s	—	127.0 s	—	127.1 s	—
7	133.4 d	7.50, brs	128.0 d	7.67, brs	128.1 d	7.68, brs	128.0 d	7.70, brs
8	129.8 s	—	129.7 s	—	129.7 s	—	129.8 s	—
9	157.6 s	—	162.2 s	—	162.2 s	—	162.2 s	—
10	116.1 d	6.79, d (8.6)	110.3 d	6.75, d (8.3)	110.3 d	6.76, d (8.4)	110.3 d	6.77, d (8.4)
11	130.8 d	7.49, brd (8.6)	132.5 d	7.46, brd (8.3)	132.5 d	7.46, brd (8.4)	132.5 d	7.47, brd (8.4)
12	123.2 s	—	122.2 s	—	122.0 s	—	123.2 s	—
13	124.8 d	7.41, d (2.1)	124.8 d	7.65, d (2.3)	130.1 d	7.61, d (2.1)	125.5 d	7.72, brs
14	122.2 s	—	129.1 s	—	122.5 s	—	128.6 s	—
15	151.1 s	—	155.7 s	—	154.7 s	—	160.7 s	—
16	130.0 s	—	115.5 d	6.78, d (8.3)	117.9 d	6.72, d (8.4)	109.7 d	6.77, d (8.4)
17	130.2 d	7.55, d (2.1)	127.6 d	7.56, dd (8.3, 2.3)	128.0 d	7.59, dd (8.4, 2.1)	129.0 d	7.64, brd (8.4)
18	123.7 d	6.36, d (9.7)	29.3 t	3.31, overlapped	23.4 t	2.81, t (6.8)	31.5 t	3.16–3.28, m
19	131.8 d	5.68, d (9.7)	123.9 d	5.35, brt (7.3)	33.8 t	1.82, t (6.8)	90.7 s	4.65, t-like (8.8)
20	77.4 s	—	133.0 s	—	75.5 s	—	72.5 s	—
21	28.2 q	1.40, s	26.0 q	1.75, brs	27.13 q	1.32, s	25.4 q	1.22, s
22	28.2 q	1.40, s	17.9 q	1.74, brs	27.11 q	1.32, s	25.18 q	1.26, s
1′	29.2 t	3.30, d (7.4)	31.2 t	3.20, dd (16.0, 8.5) 3.15, dd (16.0, 9.6)	31.2 t	3.21, dd (16.0, 8.4) 3.16, dd (16.0, 9.4)	31.2 t	3.16–3.28, m
2′	123.6 d	5.33, brt (7.4)	91.1 d	4.59, dd (9.6, 8.5)	91.1 d	4.61, dd (9.4, 8.4)	91.2 d	4.63, t-like (8.8)
3′	133.5 s	—	72.4 s	—	72.4 s	—	72.4 s	—
4′	26.0 q	1.76, brs	25.4 q	1.21, s	25.4 q	1.22, s	25.4 q	1.22, s
5′	17.9 q	1.74, brs	25.2 q	1.26, s	25.2 q	1.26, s	25.20 q	1.26, s
1″	29.3 t	3.26, d (7.4)	—	—	—	—		
2″	124.0 d	5.28, brt (7.4)	—	—	—	—	—	—
3″	132.7 s	—	—	—	—	—	—	—
4″	26.0 q	1.72, brs	—	—	—	—	—	—
5″	18.0 q	1.75, brs	—	—	—	—	—	—

[a]*Chemical shift values were recorded using the solvent signal (CD_3OD: δ_H 3.31, δ_C 49.00) as references.*

for inhibitor binding with either free or enzyme-substrate complex, were calculated from secondary plots of the slopes of the straight lines (V_{max}/K_m) or vertical intercept ($1/V_{max}$) verse the concentration of inhibitors, respectively (Jenis et al., 2019).

Fluorescence Quenching Analysis

α-Glucosidase (1 μM) was mixed with different concentrations of inhibitors (0–15 μM) at 20, 31, and 37°C, respectively, and the fluorescence spectra of mixed solutions were determined after equilibration for 5 min at an excitation wavelength of 250 nm. Both the excitation and emission slits were set at 10 nm. The quenching rate constant (K_q), binding constant (K_a), the number of the binding sites (n), and thermodynamic parameters enthalpy change (ΔH) and entropy change (ΔS) were calculated according to the Stern-Volmer **Eq. 2** and the van't Hoff **Eqs 3**–**5**, which were listed as follows (Xu et al., 2019):

$$F_0/F = 1 + K_{sv}[Q] = 1 + K_q\tau_0[Q] \quad (2)$$

$$\log((F_0 - F)/F) = \log K_a + n\log Q \quad (3)$$

$$\ln K_a = (-1/T(\Delta H/R)) + \Delta S/R \quad (4)$$

$$\Delta G = \Delta H - T\Delta S \quad (5)$$

Where F_0 and F represent the fluorescence intensities in the absence or presence of inhibitor, [Q] denote the concentration of inhibitor, τ_0 is the constant of the lifetime of fluorophore (10^{-8} s) and R is the gas constant of 8.31 J/(mol × K).

Circular Dichroism Spectroscopy

The CD measurements were performed in a wavelength range of 190–250 nm at a speed of 60 nm/min. All measurements were carried out at 20°C using 1.0 mm path length quartz cuvette and sodium phosphate buffer (pH 6.8) was considered as a blank. The concentration of α-glucosidase was 1.25 μM, whereas the molar ratios of inhibitors (25 and 50 μM) to α-glucosidase were 20:1 and 40:1. All the results were expressed as ellipticity in mill degrees.

Molecular Docking

Autodock Vina software was used in docking calculations to investigate the modes of glucosidase inhibition for individual aspulvinones. The 3D structures of aspulvinones were generated and then energetically minimized with MM_2 force field to a minimum Root Mean Square (RMS) gradient of 0.005 using Chem3D Ultra 2017 (Version 17.0.0.206). The crystal structure of *Saccharomyces cerevisiae* isomaltase (PDB ID: 3A4A; Resolution

1.6 Å) was retrieved from protein Data Bank (www.rcsb.org/pdb/), and was prepared by removing the water molecules and original inhibitors. The ligand and protein pdb files were prepared and grid box formation was accomplished using AutoDock Tools. AutoGrid was used in order to prepare the grid map using a grid box. The dimension of the grid size was set to 50 × 50 × 50, and the grid box center was designated in coordinates x = 21.285, y = −0.64, and z = 18.475. Nine output poses were generated and evaluated by their calculated free energy of binding. The best pose of each ligand was determined by its Affinity score (kcal/mol), which was visualized by Discovery Studio Visualizer v21.1.0. 20298 (Accelrys, San Diego, United States) to analyze the interactions between the target enzyme and the inhibitor.

Oral Disaccharide Tolerance Test

Female C57BL/6J mice, 6 weeks old, weighting 16–20 g, were obtained from the Skbex Biotechenology Company Limited (Henan, China). The animals were housed in Experimental Animal Center of Zhoukou Normal University under 12 h light-dark cycle at controlled temperature (22 ± 1°C), and provided with a standard pellet diet and water ad libitum. The mice were adapted to diet and general conditions of vivarium for 1 week before the experiment. After an 16 h fasting, the mice were divided into three groups randomly (eight mice each group). Sucrose or maltose, as well as the inhibitors (compound **4** and acarbose), was dissolved in 0.5% sodium carboxymethyl cellulose (CMC–Na) solution. Compound **4** was tested at dose of 25 mg/kg, whereas acarbose was evaluated at dose of 50 mg/kg of body weight (BW). Mice were fasted 16 h and then intragastrically (i.g.) administrated the inhibitors, 15 min later, 2 g/kg BW of sucrose or 2 g/kg BW of maltose solution was given i.g. to the animals. Blood samples were taken from the tail vein at 0, 30, 60, and 120 min after sucrose or maltose loading, and blood glucose was measured with Accu-Chek Active glucometer (Roche, Germany). Area under the curve (AUC) over 0–120 min was calculated by the trapezoidal method. All animals were cared under the frame of the China Council on Animal Care and all procedures were approved by the Health Sciences Animal Welfare Committee of Zhoukou Normal University.

RESULTS AND DISCUSSION

Isolation and Structure Determination of Aspulvinones

The mutant ASM-1 was obtained with different colonial morphologies with the parent strain ML-44 (**Supplementary Figure S1**), through treatment of ML-44 spores with 2% (v/v) DES under ultrasonic assistance for 1 h, and its EtOAc extract HPLC profile showed a series of chromatographic peaks of newly produced secondary metabolites with unique UV absorption spectra comparing to the wild strain ML-44 (**Supplementary Figure S2**). This mutant was deposited at the China General Microbiological Culture Collection Center under the accession number CGMCC No. 22417. In order to clarify the newly produced secondary metabolites, large scale fermentation of mutant ASM-1 and HPLC-guided separation were performed (**Supplementary Figure S3**). The EtOAc extract of the mutant ASM-1 was separated by silica gel column chromatography and repeated preparative reverse phase HPLC separation under HPLC-PDAD-UV monitoring, resulted in the isolation of aspulvinones **1**–**6**. Compound **4** was determined to be aspulvinone H by comparison its MS and NMR data with that of literature (Nagia et al., 2012). Compound **6** was identified as aspulvinone R, which was recently isolated from a marine sponge-associated fungus *A. flavipes* KUFA1152 as the first example of triprenylated aspulvinones (Machado et al., 2021).

Compound **1** was obtained as yellow solid. The molecular formula was determined to be $C_{32}H_{34}O_5$ on the basis of a HRESIMS peak at m/z 499.2480 $[M + H]^+$ (calcd. 499.2484), indicating 16 degrees of unsaturation. The illustration of ^{13}C NMR, DEPT, and HSQC spectra came up with 32 resonances, which were indicative of one ketone carbonyl, twelve sp^2 and one sp^3 quaternary carbons, ten sp^2 methine, two sp^3 methylene, six methyl groups in **1**. The remaining unsaturation was thus attributed to four rings. The ^1H NMR spectroscopic data of **1** (**Table 1**) showed a series of protons signals, and were affiliated to relevant carbons via HSQC analysis. The detailed 1D (**Table 1**) and 2D (**Figure 2**) NMR analyses of **1** indicated the same pulvinone nucleus as **4** and **6**. The ^1H NMR signals δ6.36 (d, J = 9.7 Hz, H-18) and δ5.68 (d, J = 9.7 Hz, H-19) indicated that one of the prenyl occurred cyclization, which was verified by the HMBC correlations between the above two protons with related carbons (**Figure 2**). In addition, there were two linear prenyl groups (C-1′ to C-5′, and C-1″ to C-5″) in the molecular of **1** according the NMR data analysis. Thus, compound **1** should also be a triprenylated pulvinone. Subsequently, the HMBC correlations between H-18 to C-13 and C-15, H-1″ to C-17 and H-2″ to C-16, H-19 to C-14, H-13 and H-17 to C-2, indicated that a 1,3,4,5-tetrasubstituted benzene ring bound to the γ-butenolide core directly at C-2. Thus, the another one prenylated benzene ring linked to the core via C-5, which was also confirmed by relative HMBC signals. At this stage, the planar structure has been constructed as **1**. The relatively small chemical shifts of C-2 (δ_C 102.2) and C-5 (δ_C 109.5) established the Z geometry of the $\Delta_{4,5}$-double bond (Campbell et al., 1985), which was the same as that of compound **6**. Since **1** has never been reported previously, it was named as aspulvinone V in the order of the names for this series of prenylated pulvinones from *A. terreus*.

Compound **2** was obtained as yellow solid. Its molecular formula was established as $C_{27}H_{28}O_6$ on the basis of a HRESIMS peak at *m/z* 449.1963 $[M + H]^+$ (calcd. 449.1964), which indicated 14 degrees of unsaturation and 16 amu more than compound **4** ($C_{27}H_{28}O_5$). The ^1H and ^{13}C NMR data (**Table 1**) indicated that the structure of **2** is very similar to compound **4**. The most significant differences in the NMR data exist in the high-field shift effect of the signal at C-1′ (δ_H 3.20, 3.15, δ_C 31.2), and the presence of a O-substituted sp^3 methine instead of a sp^2 methine at C-2′ (δ_H 4.59, δ_C 91.1), a O-substituted sp^3 quaternary carbon instead of a sp^2 one at C-3′ (δ_C 72.4). These data indicated that compound **2** bears a dihydrofuran ring fused to the benzene ring, as opposed to the linear prenyl present in

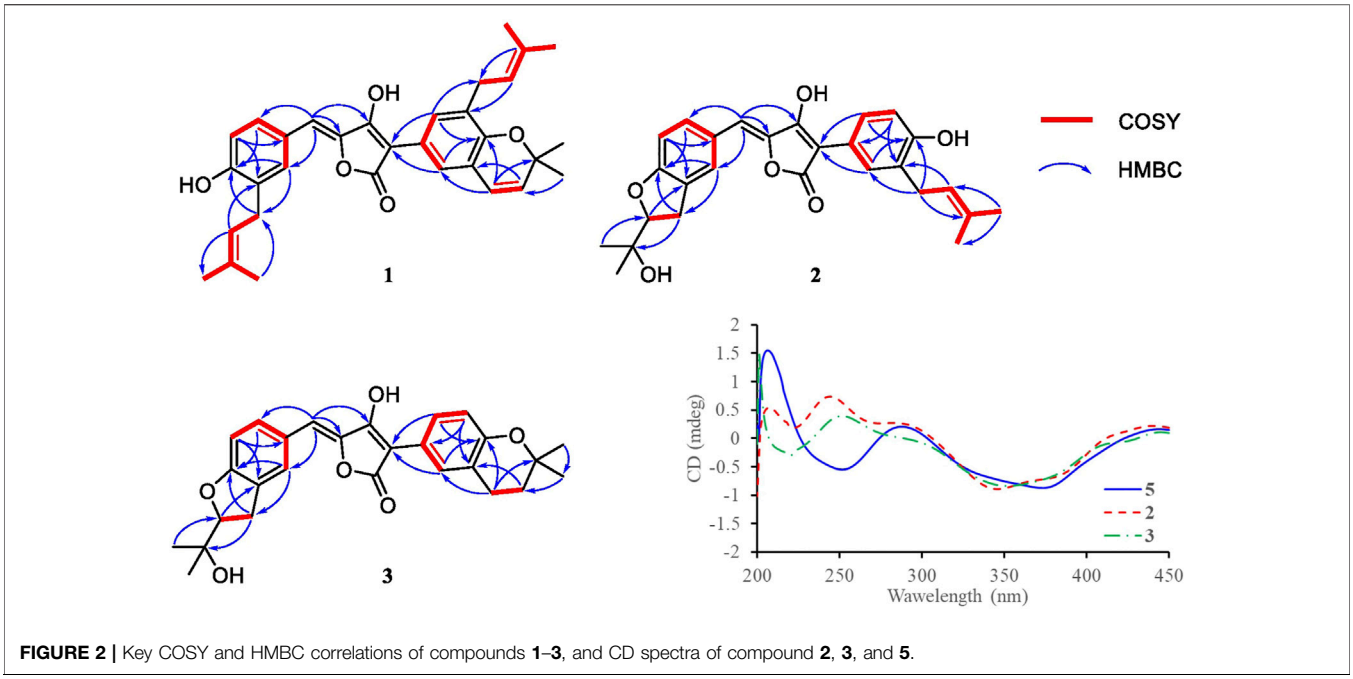

FIGURE 2 | Key COSY and HMBC correlations of compounds **1**–**3**, and CD spectra of compound **2**, **3**, and **5**.

compound **4**. This structure was further supported by COSY, HSQC, and HMBC spectra. COSY correlations between H_2-1′ and H-2′, as well supported the presence of one dihydrofuran ring systems. HMBC correlation from H_2-1′ to C-8 and C-9, H-10 to C-8, H-7, and H-11 to C-9 confirmed the presence of a dihydrofuran fused to one of the benzene rings. Furthermore, HMBC signals of H-5 to C-7 and C-11 indicated the dihydrofuran fused benzene ring was linked to C-5.

Compound **3** was isolated as yellow solid with the same molecular formula as **2** base on HRESIMS peak at *m/z* 449.1958 $[M + H]^+$ (calcd. 449.1964). The ^1H and ^{13}C NMR data of **3** (**Table 1**) were similar to those of **2** except for the high-field shift effect of the signal at C-18 (δ_H 2.81, δ_C 23.4), the presence of a sp^3 methylene instead of a sp^2 methine at C-19 (δ_H 1.82, δ_C 33.8), and a O-substituted sp^3 quaternary carbon instead of a sp^2 one at C-20 (δ_C 75.5). These data indicated that compound **3** bears a tetrahydropyran ring fused to the benzene ring, instead of the linear prenyl present in compound **2**. The location of furan ring and pyran ring were confirmed through HMBC analysis (**Figure 2**). In addition, both **2** and **3** have the Z geometry for the $\Delta_{4,5}$-double bond according to ^{13}C NMR data. The transisomer of compound **3** (*trans*-**3**) has been reported previously, which was determined the absolute configuration as *R* by the ECD calculations (Sun et al., 2018). The CD spectra of **2** and **3** was tested, and the negative cotton effect at 350 nm and general spectrum shapes were both consistent with *trans*-**3** (**Figure 2**), indicating the *R* configuration at C-2′ for compounds **2** and **3**.

By illustration of 1D and 2D NMR data, compound **5** was deduced to have the same structure with aspulvinone J-CR, whereas there exists considerable discrepancy between our ^{13}C NMR data and that of the literature (Cruz et al., 2011), especially for C2–C5 and C12. Taking consideration of the relatively strong acidity of 4-OH (predicted pK_a value of 4.50 ± 1.00 calculated by Advanced Chemistry Development (ACD/Labs) Software V11.02), it is presumed that pulvinone derivatives may be dissociative in relative high pH solutions, which would cause changes in NMR and UV spectral characteristics. Based on this assumption, **5** sodium was prepared by adding $NaHCO_3$ aqueous solution to **5** methanol solution in molar ratio 1:1. The ^{13}C NMR data of **5** sodium exhibited significant difference with **5** (**Figure 3A**), while it is identical with the literature data. Therefore, the NMR data for aspulvinone J-CR and other analogs in the literature should be for their sodium. In addition, the UV spectra of the **5** and its sodium represented different maximum absorption peaks both in number and intensity (**Figure 3B**), **5** has one absorption peak at 376 nm, while **5** sodium exhibited two absorption peaks at 327 and 376 nm, and the latter with a relatively low absorbance exists as a shoulder peak of the former.

α-Glucosidase Inhibitory Activities

All compounds **1**–**6** showed potent inhibitions towards α-glucosidase with IC_{50}s ranging from 2.2 to 44.3 μM (**Table 2**). It was reported that the transisomer of compound **3** inhibited α-glucosidase with IC_{50} of 24.8 μM (Sun et al., 2018). The inhibitory potencies varied with the modification of benzene rings. In term of diprenylated aspulvinones, compound **4** (IC_{50} 4.6 μM) is appropriate ten times more potent than **2**, **3** and its transisomer, and **5**, indicating that the linear prenyl is significant to the α-glucosidase inhibitory activity, while the configuration of Δ4,5-double bond has little influence. However, Aspulvinone E (IC_{50} 2.70 μM) was reported with higher inhibitory activity than its transisomer, isoaspulvinone E (IC_{50} 8.92 μM), and the Δ4,5-double bond stereochemistry significantly affected the inhibition activity to α-glucosidase for non-prenylated pulvinones (Dewi

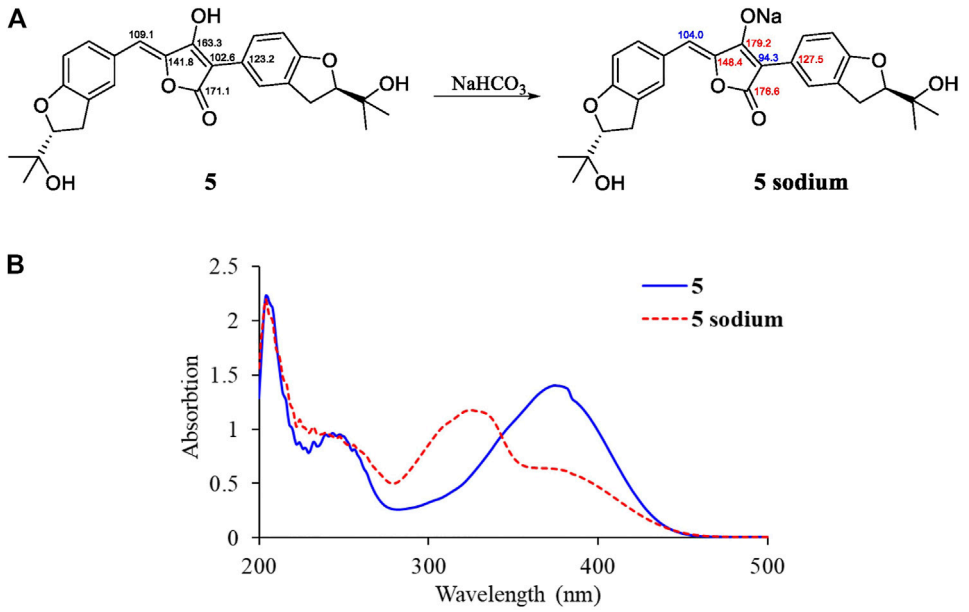

FIGURE 3 | Spectral comparisons between **5** and **5** sodium. **(A)** ^{13}C-NMR data differences; **(B)** UV spectra of **5** and **5** sodium.

TABLE 2 | α-Glucosidase inhibitory activity of aspulvinones **1**–**6**.

Compounds	IC50 (μM)[a]	K_i (μM)[b]	K_I (μM)	K_{IS} (μM)	Inhibition mode
1	2.2 ± 0.4	6.60	3.15	8.23	mixed-type
2	32.0 ± 5.8	NT[c]	NT	NT	NT
3	38.6 ± 5.2	NT	NT	NT	NT
4	4.6 ± 1.3	6.58	4.70	6.62	mixed-type
5	44.3 ± 8.9	NT	NT	NT	NT
6	10.8 ± 2.3	NT	NT	NT	NT
Acarbose[d]	17.2 ± 1.8	NT	NT	NT	NT

[a]*Sample concentration which led to 50% enzyme activity loss.*
[b]*Ki is the inhibition constant.*
[c]*NT is not tested.*
[d]*Acarbose is used as a positive control.*

et al., 2014). Therefore, we presumed that non-prenylated and prenylated pulvinones had different binding modes with α-glucosidase. On the other hand, both of compound **1** (IC_{50} 2.2 μM) and **4** were more potent than **6** (IC_{50} 10.8 μM). It was speculated that the fork-like structure of two linear prenyl groups has steric hindrance effect hampering the binding of **6** with enzyme.

Compounds **1** and **4**, the most potent inhibitors, were selected for enzyme kinetic studies to elucidate the inhibition mode. In the Lineweaver–Burk double-reciprocal plots, as shown in **Figure 4**, the plots of 1/V versus 1/[S] give a group of straight lines with different slopes that intersect at the second quadrant for both of **1** and **4**, suggesting that both of them are mixed-type inhibitors (Dan et al., 2019). Therefore, both compounds could bind to free enzyme (EI), and interfere with the formation of the α-glucosidase-pNPG (ES) intermediate through forming an α-glucosidase-pNPG-inhibitor (ESI) complex (Wikul et al., 2012; Wu et al., 2014). The inhibition constant for the inhibitor binding with free enzyme (K_I) was determined by a plot of the slope (K_m/V_m) versus the inhibitor concentration, and the inhibition constant for the inhibitor binding with enzyme–substrate complex (K_{IS}) was obtained from the vertical intercept ($1/V_m$) versus the inhibitor concentration (**Supplementary Figure S5**) (Sheng et al., 2018). The results are shown in **Table 2**: the K_I values of both **1** and **4** are smaller than their K_{IS} values, which suggest that them have higher affinity with the free enzyme than with the enzyme-substrate complex.

Fluorescence Quenching Mechanism and Binding Characterizations

Subsequently, the interaction between the inhibitors and α-glucosidase was investigated by fluorescence spectroscopy and circular dichroism (CD) spectroscopy. As shown in

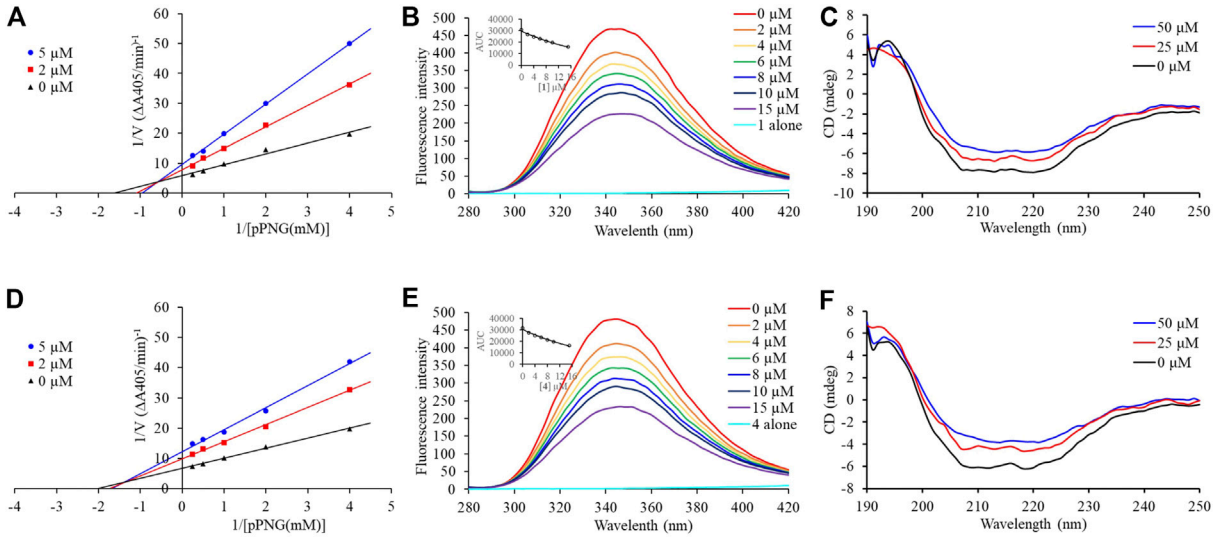

FIGURE 4 | Inhibition mechanism of **1** and **4** against α-glucosidase. Lineweaver–Burk plot of **1 (A)** and **4 (D)**. Fluorescence spectra of α-glucosidase with **1 (B)** and **4 (E)**. CD spectra of α-glucosidase with **1 (C)** and **4 (F)**.

TABLE 3 | Quenching constants (Ksv), binding constants (Ka), number of binding sites (*n*), and thermodynamic parameters for the α-glucosidase-inhibitor system.

Inhibitor	T (°C)	K_{sv} (× 10^4 L/mol)/K_q (× 10^{12} L/mol/s)	K_a (× 10^4 L/mol)	n	ΔG (kJ/mol)	ΔH (kJ/mol)	ΔS (J/mol/K)
1	20	5.35	11.0	1.04	−14.8	31.2	148.2
	31	7.87	30.6	1.12	−13.9		
	37	5.81	56.0	1.23	−12.3		
4	20	5.69	2.9	0.92	−14.0	60.4	240.1
	31	5.53	7.9	1.04	−12.5		
	37	6.02	23.2	1.13	−9.9		

Figure 4, with the increased concentrations of **1** and **4**, the intrinsic fluorescence intensity of α-glucosidase decreased gradually, indicating that the inhibitors interacted with α-glucosidase and then quenched its intrinsic fluorescence. Comparing to the maximum scattering collision quenching constant of the biomacromolecule (2×10^{10} L/mol/s), the quenching rate constants (K_q) were much larger, demonstrating that the fluorescence quenching process was static quenching predominantly (**Table 3**). The number of binding sites (n) were all close to one at the three incubation temperatures, indicating that both **1** and **4** interact with α-glucosidase at only one binding site. The binding constants (K_a) at the three temperatures were in the order of 10^5 and 10^4 L/mol for **1** and **4**, respectively, indicating that there were high binding affinities existed in the complex of α-glucosidase with the both compounds, especially as for **1**. In addition, the thermodynamic parameters (ΔS, ΔH and ΔG) were calculated, showing that ΔH and ΔS were positive, while ΔG was negative (**Table 3**). The binding process could be defined to be thermodynamically favorable and spontaneous, which was driven mainly by a hydrophobic force (Ross and Subramanian, 1981). In the CD spectroscopy analysis, after the addition of 25 and 50 mM of **1** or **4**, the absorption of the two negative peaks at 209 and 222 nm decreased, which demonstrated a loss of the α-helix structure (**Figure 4**) (Xu et al., 2019). In addition, with an increase in molar ratios of inhibitors to α-glucosidase (from 20:1 to 40:1), the loss of the α-helix structure increased, associating with the decreased α-glucosidase activity. The transformation from the α-helix to other conformations in the presence of inhibitors indicated a partial unfolding of the α-glucosidase structure, causing alterations of the secondary structure of α-glucosidase, and thereby some hydrogen bonding networks might be destroyed. These alterations may prevent the binding of the substrate to α-glucosidase or hamper the formation of an active center, eventually resulted in the dysfunction of the enzyme (Xu et al., 2019).

Molecular Docking

Since there is no crystal structure for the commercially available Saccharomyces cerevisiae α-glucosidase for preparing the protein for docking, the constructed homology models based on the isomaltases or itself were often used to perform the molecular docking (Xu et al., 2019; Khosravi et al., 2020). In this

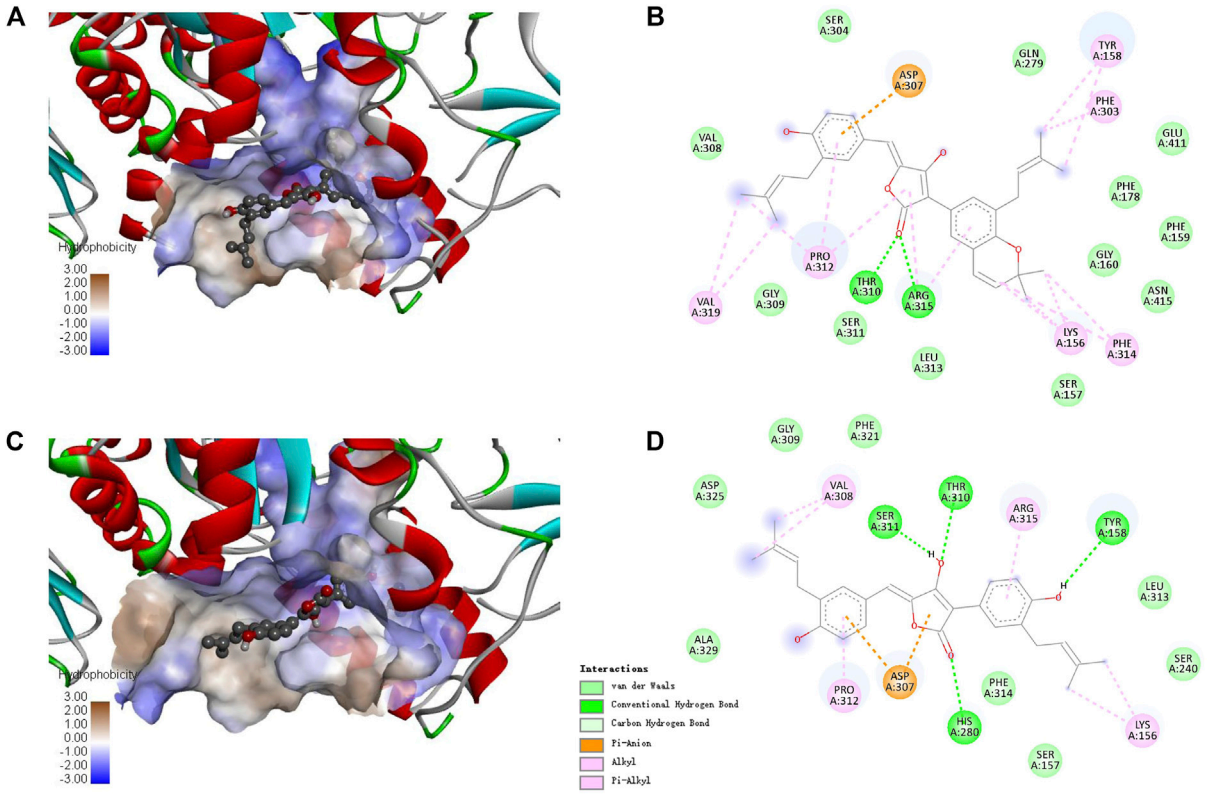

FIGURE 5 | Docking binding model of inhibitors with *Saccharomyces cerevisiae* isomaltase (3A4A). Predicted dock conformation of the isomaltase to inhibitors **1 (A)** and **4 (C)**; 2D interaction diagrams between 3A4A and inhibitors **1 (B)** and **4 (D)**.

study, the crystal structure of isomaltase from *Saccharomyces cerevisiae* (PDB ID: 3A4A; Resolution 1.6 Å) was adopted for silico docking of to confirm the interaction. Compounds **1** and **4** exhibits a strong binding affinity with the protein by the low binding energy of −10.9 and −9.6 kcal/mol, respectively. As shown in **Figure 5**, both compounds could bond at the gate of the hydrophobic pocket, and partially inserted into the binding pocket. In this bonding mode, the ligands could hamper the substrate loading into the catalytic pocket in EI complex formation, or cause structural modification of α-glucosidase leading to the dysfunction in ESI complex formation (Kim et al., 2005). According to the molecular docking results, the binding pocket involves the amino acid residues Asp307, Pro312, Tyr158, Thr310, Arg315, and Lys156 for the both inhibitors, and additional Phe303, Phe314 and Val319 for **1**, whereas additional Val308, Ser311, and His280 for **4**. There were the hydrogen bond interactions between the carbonyl group of **1** with Thr310 and Arg315 (the distance: 2.26 and 2.62 Å), and the rest interactions were all hydrophobic effect including alkyl, Pi-alkyl and Pi-anion (**Figure 5C**). In comparison, there are relatively more hydrogen bonds and less hydrophobic interaction for **4** (**Figure 5D**), indicating the different binding force compositions between the two inhibitors.

Effect of Compound 4 on Postprandial Hyperglycemia *in vivo*

The intestinal α-glucosidase inhibitory activity *in vivo* was evaluated by oral sucrose and oral maltose tolerance tests in female C57BL/6J mice. Acarbose (50 mg/kg BW) was used as a positive control, and compound **4** was chosen for its potent inhibitory activity and high yield. In the oral sucrose tolerance test (**Figure 6A**), after oral administration of sucrose (2 g/kg of BW), the blood glucose level rapidly increased from 5.00 ± 0.07 mM to a maximum of 14.24 ± 0.45 mM in 30 min, and then recovered to the pretreatment level at 120 min. In the treatment group, **4** significantly suppressed the blood glucose rise at 30 and 60 min comparing to that of the negative control group, and led to 13.2% decrease of the AUC at a dose of 25 mg/kg BW comparable to that of acarbose (11.8% decrease) at dose of 50 mg/kg BW (**Figure 6B**). Similarly, in the sucrose tolerance test, compound **4** treatment resulted in a significant decrease in the postprandial blood glucose peak versus the negative control group (**Figure 6C**) and he AUC for postprandial plasma glucose was reduced by 19.7% in 2 h after **4** administration, which was more potent than acarbose (16.2%) (**Figure 6D**). These results strongly confirmed that **4** could alleviate the postprandial hyperglycemia through inhibiting intestinal α-glucosidase. Therefore, natural

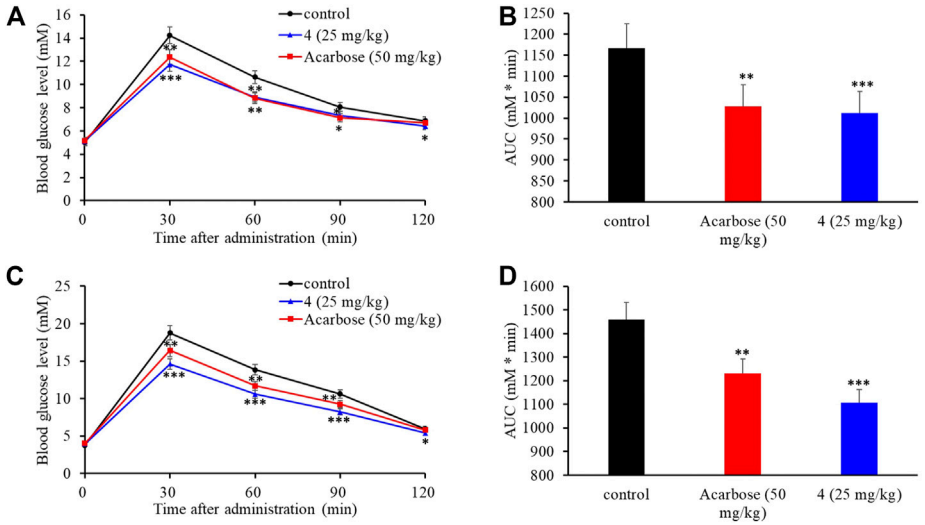

FIGURE 6 | Effects of acarbose and **4** on postprandial blood glucose levels in female C57BL/6J mice. **(A)** Blood glucose concentrations after oral administration of **4** and sucrose. **(B)** Area under the curve (AUC) after oral administration of **4** and sucrose for 2 h. **(C)** Blood glucose concentrations after an oral administration of **4** and maltose. **(D)** Area under the curve (AUC) after oral administration of **4** and maltose for 2 h. Each value represents the mean standard deviation ($n = 8$). Asterisks indicate a significant difference (*$p < 0.05$, **$p < 0.01$, and ***$p < 0.001$) compared with the control group.

aspulvinones can be regarded as potential candidate for hpyerglycemic agents.

CONCLUSION

In summary, we conducted the DES mutagenesis on the marine-derived *A. terreus* ML-44, and a mutant strain ASM-1 was obtained by morphological and HPLC analyses. Six aspulvinone secondary metabolites were isolated from the ASM-1 culture, including three new ones. Their structures including the absolute configurations were elucidated by various spectroscopic methods and ECD comparison. All compounds were evaluated for α-glucosidase inhibitory activity with acarbose as positive control. Among them, compounds **1** and **4** exhibited potent α-glucosidase inhibitory activities with IC_{50} values of 2.2 and 4.6 μM in mixed-type manners. The thermodynamic and molecular docking studies recognized the interaction between inhibitors and α-glucosidase was spontaneous exothermic reaction driven mainly by hydrophobic forces. Furthermore, **4** significantly suppressed the increases in postprandial blood glucose levels in the C57BL/6J mice more potently than acarbose at a smaller dosage. The results suggested that aspulvinones could be promising candidates for further pharmacologic research. In addition, the mechanism of the mutagenesis of the strain ASM-1 from strain ML-44 deserve further investigation through genome and transcriptome analyses, which may make contribution to understanding the metabolic regulation of aspulvinones biosynthesis.

DATA AVAILABILITY STATEMENT

The original contributions presented in the study are included in the article/**Supplementary Material**, further inquiries can be directed to the corresponding authors.

ETHICS STATEMENT

The animal study was reviewed and approved by the Health Sciences Animal Welfare Committee of Zhoukou Normal University.

AUTHOR CONTRIBUTIONS

CW and XC performed isolation, structure determination and bioassays of the compounds and wrote the manuscript. LS and JL performed the mutation and fermentation of the fungus, extraction of the culture broths and isolation of the compounds. FL, MS, and YZ. performed the bioassays. XH carried out spectroscopic tests. CT illustrated the inhibitory activity data and revised the manuscript. MS and XL designed the study and revised the manuscript. All authors have read and agreed to the published version of the manuscript.

FUNDING

This research was funded by the National Natural Science Foundation of China (No. 81803425), China Postdoctoral Science Foundation (No. 2019M662552).

ACKNOWLEDGMENTS

We thank Jinwei Ren from Institute of Microbiology, Chinese Academy of Sciences, for his professional technological support on NMR and HRESIMS tests.

SUPPLEMENTARY MATERIAL

The Supplementary Material for this article can be found online at: https://www.frontiersin.org/articles/10.3389/fchem.2021.736070/full#supplementary-material

REFERENCES

Calcutt, N. A., Cooper, M. E., Kern, T. S., and Schmidt, A. M. (2009). Therapies for Hyperglycaemia-Induced Diabetic Complications: from Animal Models to Clinical Trials. *Nat. Rev. Drug Discov.* 8, 417–430. doi:10.1038/nrd2476

Campbell, A. C., Maidment, M. S., Pick, J. H., and Stevenson, D. F. M. (1985). Synthesis of (E)- and (Z)-pulvinones. *J. Chem. Soc. Perkin Trans. 1* 1, 1567–1576. doi:10.1039/P19850001567

Cruz, P. G., Auld, D. S., Schultz, P. J., Lovell, S., Battaile, K. P., MacArthur, R., et al. (2011). Titration-based Screening for Evaluation of Natural Product Extracts: Identification of an Aspulvinone Family of Luciferase Inhibitors. *Chem. Biol.* 18, 1442–1452. doi:10.1016/j.chembiol.2011.08.011

Dan, W.-J., Zhang, Q., Zhang, F., Wang, W.-W., and Gao, J.-M. (2019). Benzonate Derivatives of Acetophenone as Potent α-glucosidase Inhibitors: Synthesis, Structure-Activity Relationship and Mechanism. *J. Enzyme Inhib. Med. Chem.* 34, 937–945. doi:10.1080/14756366.2019.1604519

Deng, Y.-T., Lin-Shiau, S.-Y., Shyur, L.-F., and Lin, J.-K. (2015). Pu-erh tea Polysaccharides Decrease Blood Sugar by Inhibition of α-glucosidase Activity *In Vitro* and in Mice. *Food Funct.* 6, 1539–1546. doi:10.1039/c4fo01025f

Dewi, R. T., Tachibana, S., Fajriah, S., and Hanafi, M. (2014). α-Glucosidase Inhibitor Compounds from Aspergillus terreus RCC1 and Their Antioxidant Activity. *Med. Chem. Res.* 24, 737–743. doi:10.1007/s00044-014-1164-0

Fang, S.-M., Wu, C.-J., Li, C.-W., and Cui, C.-B. (2014). A Practical Strategy to Discover New Antitumor Compounds by Activating Silent Metabolite Production in Fungi by Diethyl Sulphate Mutagenesis. *Mar. Drugs* 12, 1788–1814. doi:10.3390/md12041788

Gao, H., Guo, W., Wang, Q., Zhang, L., Zhu, M., Zhu, T., et al. (2013). Aspulvinones from a Mangrove Rhizosphere Soil-Derived Fungus *Aspergillus terreus* Gwq-48 with Anti-influenza A Viral (H1N1) Activity. *Bioorg. Med. Chem. Lett.* 23, 1776–1778. doi:10.1016/j.bmcl.2013.01.051

Ghosh, A. K., Reddy, B. S., Yen, Y.-C., Cárdenas, E. L., Rao, K. V., Downs, D., et al. (2016). Design of Potent and Highly Selective Inhibitors for Human β-secretase 2 (Memapsin 1), a Target for Type 2 Diabetes. *Chem. Sci.* 7, 3117–3122. doi:10.1039/c5sc03718b

Hossain, U., Das, A. K., Ghosh, S., and Sil, P. C. (2020). An Overview on the Role of Bioactive α-glucosidase Inhibitors in Ameliorating Diabetic Complications. *Food Chem. Toxicol.* 145, 111738. doi:10.1016/j.fct.2020.111738

Jenis, J., Baiseitova, A., Yoon, S. H., Park, C., Kim, J. Y., Li, Z. P., et al. (2019). Competitive α-glucosidase Inhibitors, Dihydrobenzoxanthones, from the Barks of Artocarpus Elasticus. *J. Enzyme Inhib. Med. Chem.* 34, 1623–1632. doi:10.1080/14756366.2019.1660653

Kharroubi, A. T., and Darwish, H. M. (2015). Diabetes Mellitus: the Epidemic of the century. *Wjd* 6, 850–867. doi:10.4239/wjd.v6.i6.850

Khosravi, A., Vaezi, G., Hojati, V., and Abdi, K. (2020). Study on the Interaction of Triaryl-Dihydro-1,2,4-Oxadiazoles with α-glucosidase. *DARU J. Pharm. Sci.* 28, 109–117. doi:10.1007/s40199-019-00322-y

Kim, Y.-M., Jeong, Y.-K., Wang, M.-H., Lee, W.-Y., and Rhee, H.-I. (2005). Inhibitory Effect of pine Extract on α-glucosidase Activity and Postprandial Hyperglycemia. *Nutrition* 21, 756–761. doi:10.1016/j.nut.2004.10.014

Machado, F. P., Kumla, D., PereiraSousa, J. A. E., Sousa, E., Dethoup, T., Freitas-Silva, J., et al. (2021). Prenylated Phenylbutyrolactones from Cultures of a marine Sponge-Associated Fungus *Aspergillus flavipes* KUFA1152. *Phytochemistry* 185, 112709. doi:10.1016/j.phytochem.2021.112709

Nagia, M. M., El-Metwally, M., Shaaban, M., El-Zalabani, S. M., and Hanna, A. G. (2012). Four Butyrolactones and Diverse Bioactive Secondary Metabolites from Terrestrial *Aspergillus flavipes* MM2: Isolation and Structure Determination. *Org. Med. Chem. Lett.* 2, 9. doi:10.1186/2191-2858-2-9

Ross, P. D., and Subramanian, S. (1981). Thermodynamics of Protein Association Reactions: Forces Contributing to Stability. *Biochemistry* 20, 3096–3102. doi:10.1021/bi00514a017

Sheng, Z., Ge, S., Xu, X., Zhang, Y., Wu, P., Zhang, K., et al. (2018). Correction: Design, Synthesis and Evaluation of Cinnamic Acid Ester Derivatives as Mushroom Tyrosinase Inhibitors. *Med. Chem. Commun.* 9, 897. doi:10.1039/C8MD00099A10.1039/c8md90024h

Sun, K., Zhu, G., Hao, J., Wang, Y., and Zhu, W. (2018). Chemical-epigenetic Method to Enhance the Chemodiversity of the marine Algicolous Fungus, *Aspergillus terreus* OUCMDZ-2739. *Tetrahedron* 74, 83–87. doi:10.1016/j.tet.2017.11.039

Sun, W., Luan, S., Qi, C., Tong, Q., Yan, S., Li, H., et al. (2019). Aspulvinone O, a Natural Inhibitor of GOT1 Suppresses Pancreatic Ductal Adenocarcinoma Cells Growth by Interfering Glutamine Metabolism. *Cell Commun Signal* 17, 111. doi:10.1186/s12964-019-0425-4

Taylor, S. I., Yazdi, Z. S., and Beitelshees, A. L. (2021). Pharmacological Treatment of Hyperglycemia in Type 2 Diabetes. *J. Clin. Invest.* 131, e142243. doi:10.1172/JCI142243

Wang, C., Guo, L., Hao, J., Wang, L., and Zhu, W. (2016). α-Glucosidase Inhibitors from the Marine-Derived Fungus Aspergillus flavipes HN4-13. *J. Nat. Prod.* 79, 2977–2981. doi:10.1021/acs.jnatprod.6b00766

Wikul, A., Damsud, T., Kataoka, K., and Phuwapraisirisan, P. (2012). (+)-Pinoresinol Is a Putative Hypoglycemic Agent in Defatted Sesame (Sesamum indicum) Seeds Though Inhibiting α-glucosidase. *Bioorg. Med. Chem. Lett.* 22, 5215–5217. doi:10.1016/j.bmcl.2012.06.068

Wu, C.-J., Cui, X., Xiong, B., Yang, M.-S., Zhang, Y.-X., and Liu, X.-M. (2019). Terretonin D1, a New Meroterpenoid from marine-derived *Aspergillus terreus* ML-44. *Nat. Product. Res.* 33, 2262–2265. doi:10.1080/14786419.2018.1493583

Wu, P.-P., Zhang, K., Lu, Y.-J., He, P., and Zhao, S.-Q. (2014). *In Vitro* and *In Vivo* Evaluation of the Antidiabetic Activity of Ursolic Acid Derivatives. *Eur. J. Med. Chem.* 80, 502–508. doi:10.1016/j.ejmech.2014.04.073

Xu, Y., Xie, L., Xie, J., Liu, Y., and Chen, W. (2019). Pelargonidin-3-O-rutinoside as a Novel α-glucosidase Inhibitor for Improving Postprandial Hyperglycemia. *Chem. Commun.* 55, 39–42. doi:10.1039/c8cc07985d

Zhang, L.-H., Feng, B.-M., Zhao, Y.-Q., Sun, Y., Liu, B., Liu, F., et al. (2016). Polyketide Butenolide, Diphenyl Ether, and Benzophenone Derivatives from the Fungus Aspergillus flavipes PJ03-11. *Bioorg. Med. Chem. Lett.* 26, 346–350. doi:10.1016/j.bmcl.2015.12.009

Zhang, P., Li, X.-M., Wang, J.-N., Li, X., and Wang, B.-G. (2015). New Butenolide Derivatives from the marine-derived Fungus *Paecilomyces variotii* with DPPH Radical Scavenging Activity. *Phytochemistry Lett.* 11, 85–88. doi:10.1016/j.phytol.2014.11.014

Zhang, X., Li, G., Wu, D., Yu, Y., Hu, N., Wang, H., et al. (2020). Emerging Strategies for the Activity Assay and Inhibitor Screening of Alpha-Glucosidase. *Food Funct.* 11, 66–82. doi:10.1039/c9fo01590f

Conflict of Interest: The authors declare that the research was conducted in the absence of any commercial or financial relationships that could be construed as a potential conflict of interest.

Publisher's Note: All claims expressed in this article are solely those of the authors and do not necessarily represent those of their affiliated organizations, or those of the publisher, the editors and the reviewers. Any product that may be evaluated in this article, or claim that may be made by its manufacturer, is not guaranteed or endorsed by the publisher.

frontiers in Chemistry

ORIGINAL RESEARCH
published: 01 September 2021
doi: 10.3389/fchem.2021.738307

Cyclohexanone and Phenolic Acid Derivatives from Endophytic Fungus *Diaporthe foeniculina*

Xiuxiang Lu[1,2], *Yanjiang Zhang*[1,2], *Wenge Zhang*[1,2], *Huan Wang*[1,3], *Jun Zhang*[3], *Sasa Wang*[4]* *and Haibo Tan*[1,3]*

[1]*Key Laboratory of Plant Resources Conservation and Sustainable Utilization, Guangdong Provincial Key Laboratory of Applied Botany, South China Botanical Garden, Chinese Academy of Sciences, Guangzhou, China,* [2]*University of Chinese Academy of Sciences, Beijing, China,* [3]*National Engineering Research Center of Navel Orange, Gannan Normal University, Ganzhou, China,* [4]*Key Laboratory of Chemistry and Engineering of Forest Products, Guangxi University for Nationalities, Nanning, China*

Chemical investigation of an endophytic fungus *Diaporthe foeniculina* SCBG-15, led to the isolation of eight new cyclohexanone derivatives, foeniculins A–H (1–8) and three new phenolic acid derivatives, foeniculins I–K (9–11). Their structures were extensively established on the basis of ^{1}H and ^{13}C NMR spectra together with COSY, HSQC, HMBC, and NOESY experiments. The absolute configurations were confirmed by quantum chemical ECD calculations and single-crystal X-ray diffractions. Moreover, the *in vitro* cytotoxic and antibacterial activities of isolated compounds 1–11 were also evaluated.

Keywords: *Diaporthe foeniculina*, *Leptospermum brachyandrum*, foeniculins A-K, cytotoxic activity, antibacterial activity

OPEN ACCESS

Edited by:
Xuekui Xia,
Shandong Academy of Sciences, China

Reviewed by:
Hongbo Huang,
South China Sea Institute of Oceanology (CAS), China
Sang Hee Shim,
Seoul National University, South Korea

***Correspondence:**
Sasa Wang
wgsasa@163.com
Haibo Tan
tanhaibo@scbg.ac.cn

Specialty section:
This article was submitted to Organic Chemistry, a section of the journal Frontiers in Chemistry

Received: *09 July 2021*
Accepted: *03 August 2021*
Published: *01 September 2021*

Citation:
Lu X, Zhang Y, Zhang W, Wang H, Zhang J, Wang S and Tan H (2021) Cyclohexanone and Phenolic Acid Derivatives from Endophytic Fungus Diaporthe foeniculina. *Front. Chem. 9:738307. doi: 10.3389/fchem.2021.738307*

INTRODUCTION

Leptospermum brachyandrum belongs to the genus *Leptospermum*, it is an important member in the plant family Myrtaceae (Beardsell et al., 1993; Brophy et al., 1999). It mainly occurred in Australia and had been introduced into China a few decades ago. Nowadays, this plant is widely planted in the southern of China due to its ornamental and medicinal properties. Our previous phytochemical works proved that the chemical constitutes of *L. brachyandrum* were ploymethylated meroterpenoid and phloroglucinol derivatives (Zou et al., 2018). In recent years, our group focused on bioactive meaningful natural products from the plants and endophytic fungi towards the pharmaceutical drug discovery (Liu et al., 2016a; Liu et al., 2016b; Liu et al., 2016c; Xiang et al., 2017; Liu et al., 2018). As a part of our ongoing research effort to discover biologically active and structurally unique natural products (Liu et al., 2016d; Liu et al., 2016e; Li et al., 2017), the *Diaporthe foeniculinaan* SCBG-15, an endophytic strain derived from *L. brachyandrum*, which displayed a variety of secondary metabolisms with potentially structural diversity during the HPLC and TLC analyses, was selected as the target for the further chemical investigation.

In the latest years, plenty of new privileged natural compounds with highly structural diversities were isolated from the genus *Diaporthe*, and which exhibited significant biological activities (Zhu et al., 2010; Zang et al., 2012; Li et al., 2015; Mandavid et al., 2015; Cui et al., 2017; Cui et al., 2018; Luo et al., 2018; Gao et al., 2020). In this study, an extensively chemical constituent research on EtOAc extract of the fungus SCBG-15 using sequential column chromatography over silica gel, RP-C_{18} silica, and Sephadex LH-20 along with preparative and semipreparative HPLC resulted in the discovery of eight new cyclohexanone derivatives, foeniculins A–H (1–8), and three phenolic acid derivatives, foeniculins I–K (9–11). All of the novel compounds 1–11 possessed polymethylated

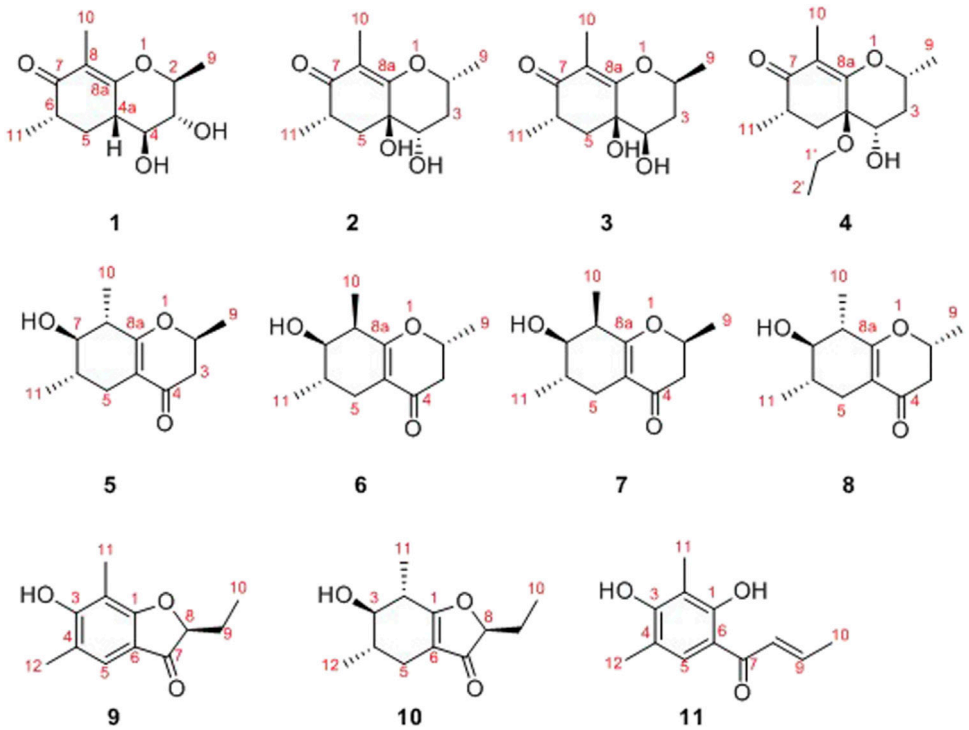

FIGURE1 | Structures of compounds 1–11.

skeleton (**Figure 1**). Herein, the details of isolation, structural elucidation by NMR spectral interpretation, single-crystal X-ray diffraction, and biological evaluation of these isolates are described.

MATERIALS AND METHODS

General Experimental Procedures

Optical rotations were recorded using an Anton Paar MCP-500 spectropolarimeter (Anton Paar, Graz, Austria). UV spectra were obtained by a Shimadzu UV-2600 spectrophotometer (Shimadzu, Kyoto, Japan). ECD spectra were measured with an Applied Photophysis Chirascan. IR data were measured on a Shimadzu IR Affinity-1 spectrometer (Shimadzu, Kyoto, Japan). 1D and ^{2}D NMR spectra were collected on a Bruker Avance-500 spectrometer with TMS as an internal standard (Bruker, Fällanden, Switzerland). HRESIMS spectra were acquired with a Thermo MAT95XP high resolution mass spectrometer (Thermo Fisher Scientific, Bremen, Germany). Silica gel (200–300 mesh, Qingdao Marine Chemical Inc. Qingdao, China) was used for column chromatography. TLC analysis was carried out on silica gel plate (Merck KGaA, Darmstadt, Germany). A Hitachi Primaide [Hitachi Instruments (Dalian) Co., Ltd.] equipped with a diode array detector (DAD) using a semi-preparative YMC ODS C_{18} column (20 × 250 mm, 5 μm) was used for semi-preparative HPLC separation. All solvents were analytical grade (Guangzhou Chemical Regents Company, Ltd. Guangzhou, China).

Fungal Material

The endophytic fungal strain *D. foeniculina* SCBG-15 was isolated from the plant of *L. brachyandrum*, which was collected at South China Botanical Garden (SCBG), Chinese Academy of Sciences, China, in September 2016. The strain was identified by sequence analysis of rDNA ITS (internal transcribed spacer) region. The sequence of the ITS region of the *D. foeniculina* has been submitted to GenBank (Accession No. MN788609). The strain is preserved at the Laboratory of Natural Product Medicinal Chemistry, SCBG.

Extraction and Isolation

The fungus *D. foeniculina* was fermented on an autoclaved rice solid medium (15 × 3 L Erlenmeyer flasks, each containing 300 g of grains and 360 ml of distilled water) for 30 days at 28°C. After cultivation, the mycelia and rice solid medium were extracted with EtOAc for three times, and the crude extract (50 g) was obtained. The crude extract was subjected to silica gel using gradient elution with petroleum ether-EtOAc as eluent (v/v, 100:1→50:50) and CH_2Cl_2-MeOH (v/v, 5:1→2:1). Then, they were combined by TLC analysis to afford six main fractions (Fr.1-Fr.6).

Fr.5 (7.22 g) was applied to column chromatography over RP-C_{18} silica gel, eluting with MeOH-H_2O (v/v, 2:5→1:0) to give six subfractions (Fr.5-1 to Fr.5-6). Fr.5-2 (1.94 g) was separated by Sephadex LH-20 column chromatography and eluted with $CHCl_3$-MeOH (v/v, 1:1) to afford six subfractions (Fr.5-2-1 to Fr.5-2-6). Fr.5-2-2 (1.23 g) was isolated by column chromatography on silica gel and eluted with *n*-hexane-EtOAc gradient (v/v, 4:1→1:5) to obtain six subfractions (Fr.5-2-2-1 to

TABLE 1 | ^{1}H (500 MHz) NMR data for compounds 1–4 (δ in ppm, J in Hz).

No	1[a]	2[a]	3[a]	4[b]
2	3.73, m	4.62, m	4.42, ddd (2.8, 6.3, 12.4)	4.60, qd (6.3, 11.6)
3α	3.29, m	1.60, dd (2.9, 14.3)	1.77, dd (6.3, 14.0)	1.65, m
3β		2.54, ddd (5.5, 7.5, 14.3)	2.34, ddd (2.2, 12.4, 14.0)	2.48, ddd, (5.2, 7.5, 14.3)
4	3.26, m	3.78, dd (2.9, 7.5)	3.66, dd (2.2, 3.5)	4.07, dd (2.8, 7.5)
	2.55, m			
5α	2.44, m	1.78, dd (4.6, 13.6)	1.72, dd (4.8, 13.0)	2.19, m
5β	1.34, m	2.25, dd (6.8, 13.6)	2.21, t 13.0	
6	2.27, m	2.79, ddd (4.6, 6.8, 13.6)	2.75, ddd (4.8, 6.8, 13.0)	2.61, m
9	1.48, d (6.2)	1.38, d (6.3)	1.38, d (6.3)	1.35, d (6.3)
10	1.68, s	1.65, s	1.66, s	1.65, s
11	1.16, d (6.2)	1.12, d (6.3)	1.13, d (6.3)	1.09, d (6.3)
1′				3.60, m
2′				1.16, t (7.0)

[a]*Recorded in CD_3OD.*
[b]*Recorded in CD_3COCD_3.*

Fr.5-2-2-6). Fr.5-2-2-5 (127.4 mg) was further purified by the semi-preparative HPLC system with CH_3CN-H_2O (10:90) as eluent to afford compounds 1 (3.0 mg, t_R = 35.0 min), 2 (4.4 mg, t_R = 15.7 min), and 3 (2.0 mg, t_R = 21.6 min). Fr.5-2-1 (311.4 mg) was isolated by column chromatography on silica gel and eluted with *n*-hexane-EtOAc gradient (v/v, 5:1→1:5) to get three subfractions (Fr.5-2-1-1 to Fr.5-2-1-3). Fr.5-2-1-1 (208.8 mg) was subjected to semi-preparative HPLC with CH_3CN-H_2O (v/v, 50:50) to give seven subfractions (Fr.5-2-1-1-1 to Fr.5-2-1-1-7). Fr.5-2-1-1-6 (28.3 mg) was purified by semi-preparative HPLC and washed with CH_3CN-H_2O (v/v, 35:65) to afford compound 4 (3.0 mg, t_R = 20.5 min). Fr.5-2-1-1-1 (23.1 mg) was purified by semi-preparative HPLC equipped with a chiral column and washed with isopropanol-hexane (30:70) to afford compounds 5 (1.0 mg, t_R = 19.8 min), 6 (1.0 mg, t_R = 18.5 min), 7 (0.8 mg, t_R = 22.8 min), and 8 (1.3 mg, t_R = 28.0 min). Fr.5-2-1-1-2 (40.2 mg) was purified by semi-preparative HPLC and washed with MeOH-H_2O (v/v, 75: 25) to afford compound 10 (3.0 mg, t_R = 20.5 min).

Fr.4 (2.26 g) was isolated by column chromatography on silica gel and eluted with *n*-hexane-EtOAc gradient (v/v, 30:1→1:1) to get four subfractions (Fr.4-1 to Fr.4-4). Fr.4-2 (197.1 mg) was separated by Sephadex LH-20 column chromatography and eluted with $CHCl_3$-MeOH (v/v, 1:1) to afford four subfractions (Fr.4-2-1 to Fr.4-2-4). Fr.4-2-4 (13.8 mg) was further purified by the semi-preparative HPLC system and eluted with MeOH-H_2O (70:30) to give compound 9 (3.2 mg, t_R = 19.4 min).

Fr.6 (19.0 g) was separated into four subfractions (Fr.6-1 to Fr.6-4) on ODS column chromatography with MeOH-H_2O (v/v, 3:10→4:1). Fr.6-1 (2.79 g) was loaded onto Sephadex LH-20 column chromatography and eluted with $CHCl_3$-MeOH (v/v, 1:1) to give four subfractions (Fr.6-1-1 to Fr.6-1-4). Fr.6-1-2 (643.0 mg) was isolated by column chromatography on silica gel and eluted with CH_2Cl_2-MeOH (v/v, 50:1→1:5) to get seven subfractions (Fr.6-1-2-1 to Fr.6-1-2-7). Fr.6-1-2-4 (311.0 mg) was separated by semi-preparative HPLC with CH_3CN-H_2O (v/v, 10:90) and then repeatedly purified by semi-preparative HPLC with CH_3CN-H_2O (v/v, 2: 98) to afford compound 11 (5.4 mg, t_R = 8.7 min).

TABLE 2 | ^{13}C (125 MHz) NMR data for compounds 1–4 (δ_C in ppm).

No	1[a]	2[a]	3[a]	4[b]
1				
2	79.1, CH	71.1, CH	71.9, CH	69.8, CH
3	76.3, CH	39.0, CH_2	35.5, CH_2	38.2, CH
4	76.0, CH	70.6, CH	71.0, CH	66.9, CH
4a	43.8, C	70.5, C	69.0, C	75.1, C
5	33.1, CH_2	40.9, CH_2	40.3, CH_2	34.4, CH_2
6	41.5, CH	36.2, CH	37.6, CH	35.9, CH
7	204.1, C	203.6, C	204.0, C	198.9, C
8	115.9, C	115.2, C	118.0, C	115.2, C
8a	171.0, C	170.1, C	170.8, C	165.5, C
9	18.8, CH_3	22.6, CH_3	22.8, CH_3	21.9, CH_3
10	8.2, CH_3	7.9, CH_3	8.2, CH_3	7.3, CH_3
11	15.8, CH_3	15.7, CH_3	15.6, CH_3	15.1, CH_3
1′				59.3, CH_2
2′				15.4, CH_3

[a]*Recorded in CD_3OD.*
[b]*Recorded in CD_3COCD_3.*

Foeniculin A (1): colorless needle crystals $(\alpha)_D^{20}$–12.4 (*c* 0.1, MeOH); UV (MeOH): λ_{max} (log ε): 259 (2.77), 202 (2.41) nm; IR (KBr): 3,381, 2,996, 2,905, 2,837, 1,616, 1,559, 1,456, 1,385, 1,308, 1,229, 1,206, 1,098, 1,024, 695, 758, 733, 667, 596, 556 cm^{-1}; HRESIMS: *m/z* 227.1274 $(M + H)^+$ (calcd for $C_{12}H_{19}O_4$, 227.1278). ^{1}H (500 MHz) and ^{13}C (125 MHz) NMR data, see **Tables 1** and **2**.

Foeniculin B (2): colorless needle crystals; m. p. 120–121°C (α) $^{20}_{D}$ + 8.2 (*c* 0.1, MeOH); UV (MeOH): λ_{max} (log ε): 267 (3.28) nm; IR (KBr): 3,370, 2,976, 2,932, 2,884, 1,717, 1,614, 1,381, 1,337, 1,242, 1,217, 1,146, 1,105, 1,026, 978, 874, 773, 739, 689, 667, 596 cm^{-1}; HRESIMS: *m/z* 227.1275 $(M + H)^+$ (calcd for $C_{12}H_{19}O_4$, 227.1278). ^{1}H (500 MHz) and ^{13}C (125 MHz) NMR data, see **Tables 1** and **2**.

Foeniculin C (3): white solid $(\alpha)_D^{20}$–33.4 (*c* 0.1, MeOH); UV (MeOH): λ_{max} (log ε): 263 (3.10) nm; IR (KBr): 3,377, 2,974, 2,926, 1,616, 1,456, 1,386, 1,333, 1,289, 1,252, 1,209, 1,141, 1,103, 1,068, 1,011, 976, 914, 883, 760, 692 cm^{-1}; HRESIMS: *m/z* 227.1276 $(M + H)^+$ (calcd for $C_{12}H_{19}O_4$,

TABLE 3 | ^{1}H NMR (500 MHz) data for compounds 5–8 in CD_3OD (δ in ppm, J in Hz).[a]

No	5	6	7	8
2	4.48, m	4.45, m	4.50, m	4.43, m
3	2.44, ddd (4.9, 8.4, 9.3)	2.43, m	2.43, m	2.41, m
5α	2.55, dd (4.9, 15.9)	2.43, m	2.49, dd (5.1, 15.7)	2.26, m
5β	1.65, dd (2.5, 11.4, 15.9)	1.73, m	1.80, m	1.95, m
6	1.52, ddd (6.1, 11.1, 17.2)	1.81, m	1.86, m	1.86, m
7	2.98, dd (8.9, 10.2)	3.48, dd (5.5, 9.7)	3.55, dd (5.1, 8.5)	3.57, m
8	2.33, ddd (4.9, 8.4, 9.3)	2.60, m	2.57, m	2.41, m
9	1.42, d (6.3)	1.42, d (6.3)	1.41, d (6.3)	1.42, d (6.3)
10	1.26, d (7.0)	1.17, d (7.2)	1.18, d (7.2)	1.19, d (7.4)
11	1.08, d (6.4)	1.03, d (6.4)	1.01, d (6.5)	1.05, d (6.8)

TABLE 4 | ^{13}C (125 MHz) NMR data for compounds 5–8 in CD_3OD (δ in ppm).

No	5	6	7	8
1				
2	75.2, CH	75.1, CH	74.8, CH	76.5, CH
3	42.2, CH_2	41.9, CH_2	42.1, CH_2	43.7, CH_2
4	194.0, C	193.4, C	193.8, C	195.4, C
4a	109.2, C	109.8, C	108.7, C	111.1, C
5	27.4, CH_2	27.0, CH_2	26.2, CH_2	25.3, CH_2
6	29.3, CH	35.2, CH	30.0, CH	29.6, CH
7	73.1, CH	78.0, CH	73.0, CH	75.6, CH
8	38.4, CH	42.2, CH	37.7, CH	42.7, CH
8a	174.2, C	173.0, C	173.9, C	175.2, C
9	19.3, CH_3	19.0, CH_3	19.1, CH_3	20.8, CH_3
10	16.5, CH_3	13.7, CH_3	11.3, CH_3	17.2, CH_3
11	11.2, CH_3	16.6, CH_3	16.3, CH_3	17.4, CH_3

227.1278). ^{1}H (500 MHz) and ^{13}C (125 MHz) NMR data, see **Tables 1** and **2**.

Foeniculin D (4): white solid $(\alpha)_D^{20}$ + 11.6 (*c* 0.05, MeOH); UV (MeOH): λ_{max} (log ε): 269 (2.54) nm; IR (KBr): 3,329, 2,947, 2,835, 1,651, 1,456, 1,410, 1,115, 1,017, 667, 608, 546 cm^{-1}; HRESIMS: *m/z* 255.1598 (M + H)$^+$ (calcd for $C_{14}H_{23}O_4$, 255.1591). ^{1}H (500 MHz) and ^{13}C (125 MHz) NMR data, see **Tables 1** and **2**.

Foeniculin E (5): colorless needle crystals $(\alpha)_D^{20}$–11.6 (*c* 0.03, MeOH); UV (MeOH): λ_{max} (log ε): 275 (2.98) nm; IR (KBr): 3,356, 1,653, 1,616, 667, 600, 552 cm^{-1}; HRESIMS: *m/z* 211.1329 (M + H)$^+$ (calcd for $C_{12}H_{19}O_3$, 211.1329). ^{1}H (500 MHz) and ^{13}C (125 MHz) NMR data, see **Tables 3** and **4**.

Foeniculin F (6): white solid $(\alpha)_D^{20}$ + 12.0 (*c* 0.05, MeOH); UV (MeOH); λ_{max} (log ε): 268 (3.34), 202 (2.23) nm; HRESIMS: *m/z* 233.1146 (M + Na)$^+$ (calcd for $C_{12}H_{18}NaO_3$, 233.1148). ^{1}H (500 MHz) and ^{13}C (125 MHz) NMR data, see **Tables 3** and **4**.

Foeniculin G (7): white solid $(\alpha)_D^{20}$–13.7 (*c* 0.05, MeOH); UV (MeOH): λ_{max} (log ε): 275 (3.08) nm; IR (KBr): 3,337, 1,636, 669, 600, 554 cm^{-1}; HRESIMS: *m/z* 211.1339 (M + H)$^+$ (calcd for $C_{12}H_{19}O_3$, 211.1329). ^{1}H (500 MHz) and ^{13}C (125 MHz) NMR data, see **Tables 3** and **4**.

Foeniculin H (8): white solid $(\alpha)_D^{20}$ + 10.8 (*c* 0.1, MeOH); UV (MeOH): λ_{max} (log ε): 274 (3.23) nm; IR (KBr): 3,360, 1,636, 667, 600, 557 cm^{-1}; HRESIMS: *m/z* 211.1339 (M + H)$^+$ (calcd for $C_{12}H_{19}O_3$, 211.1329). ^{1}H (500 MHz) and ^{13}C (125 MHz) NMR data, see **Tables 3** and **4**.

Foeniculin I (9): colorless needle crystals; m. p. 108–109°C; UV (MeOH): λ_{max} (log ε): 328 (3.02), 279 (3.33), 217 (3.47) nm; IR (KBr): 3,379, 2,976, 2,922, 2,851, 1,676, 1,608, 1,458, 1,329, 1,292, 1,220, 1,151, 1,092, 1,024, 947, 768 cm^{-1}; HRESIMS: *m/z* 207.1013 (M + H)$^+$ (calcd for $C_{12}H_{15}O_3$, 207.1016). ^{1}H (500 MHz) and ^{13}C (125 MHz) NMR data, see **Table 5**.

Foeniculin J (10): colorless oil $(\alpha)_D^{20}$–11.4 (*c* 0.05, MeOH); UV (MeOH): λ_{max} (log ε): 270 (2.80) nm; IR (KBr): 3,312, 2,976, 2,930, 2,899, 1,717, 1,668, 1,607, 1,456, 1,400, 1,344, 1,271, 1,246, 1,180, 1,130, 1,032, 945, 856, 764, 669 cm^{-1}; HRESIMS: *m/z* 211.1333 (M + H)$^+$ (calcd for $C_{12}H_{19}O_3$, 211.1329). ^{1}H (500 MHz) and ^{13}C (125 MHz) NMR data, see **Table 5**.

Foeniculin K (11): green needle crystals; UV (MeOH): λ_{max} (log ε): 305 (3.00) nm; IR (KBr): 3,358, 2,974, 2,920, 1,649, 1,626, 1,560, 1,479, 1,445, 1,362, 1,305, 1,290, 1,169, 1,113, 1,028, 953, 829 cm^{-1}; HRESIMS: *m/z* 207.1025 (M + H)$^+$ (calcd for $C_{12}H_{15}O_3$, 207.1016). ^{1}H (500 MHz) and ^{13}C (125 MHz) NMR data, see **Table 5**.

X-Ray Crystallographic Analysis

The single-crystal X-ray diffraction data were collected at 100 K for 1, 2, 5, and 9 on Agilent Xcalibur Nova single-crystal diffractometer using CuKα radiation. Crystallographic data for 1, 2, 5, and 9 reported in this paper have been deposited in the Cambridge Crystallographic Data Centre. (Deposition number: CCDC 2008519 for 1, 2008520 for 2, 2047671 for 5, and 2047672 for 9). Copies of these data can be obtained free of charge *via* www.ccdc.cam.au.ck/conts/retrieving.html.)

Cytotoxicity Assay

The *in vitro* cytotoxic activities of compounds 1–11 were assayed against three human tumor cell lines SF-268, MCF-7, HePG-2, and normal cell line LX-2 with adriamycin as positive control. Assays were performed by the SRB method (Mosmann, 1983).

Antimicrobial Assay

Compounds 1–11 were evaluated the antimicrobial activity against *Staphylococcus aureus* (CMCC 26003) and *Escherichia coli* (ATCC 8739). Assays were performed by the published microdilution method for the estimation of minimum inhibitory concentration (MIC) values (Li et al., 2017). Vancomycin was used as positive control.

TABLE 5 | ^{1}H (500 MHz) and^{13}C (125 MHz) NMR data (δ in ppm, J in Hz) of 9–11.

No	9[c]		10[a]		11[a]	
	δ_H (J in Hz)	δ_C	δ_H (J in Hz)	δ_C	δ_H (J in Hz)	δ_C
1		172.0, C		189.4, C		164.0, C
2		106.8, C	2.70, m	38.6, CH		112.4, C
3		160.5, C	3.73, br s	76.0, CH		162.5, C
4		118.7, C	2.02, m	29.9, CH		117.5, C
5	7.29, s	122.4, CH	2.28, m; 2.02, m	21.6, CH_2	7.53, s	130.6, CH
6		113.7, C		111.1, C		113.7, C
7		200.6, C		203.1, C		194.1, C
8	4.50, dd (4.5, 7.1)	87.0, CH	4.42, dd (4.5, 6.8)	86.9, CH	7.14, d (15.6)	127.4, CH
9	2.05, m; 1.80, m	24.8, CH_2	2.02, m; 1.75, m	24.4, CH_2	7.08, dq (15.6, 5.5)	145.1, CH
10	1.00, t (7.4)	8.9, CH_3	0.96, t (7.4)	8.5, CH_3	2.00, d (5.5)	18.8, CH_3
11	2.19, s	7.3, CH_3	1.30, d (7.3)	15.8, CH_3	1.07, s	8.3, CH_3
12	2.23, s	15.8, CH_3	1.10, d (6.7)	16.2, CH_3	2.18, s	16.6, CH_3

[a]*Recorded in CD_3OD.*
[b]*Recorded in CD_3COCD_3.*
[c]*Recorded in $CDCl_3$.*

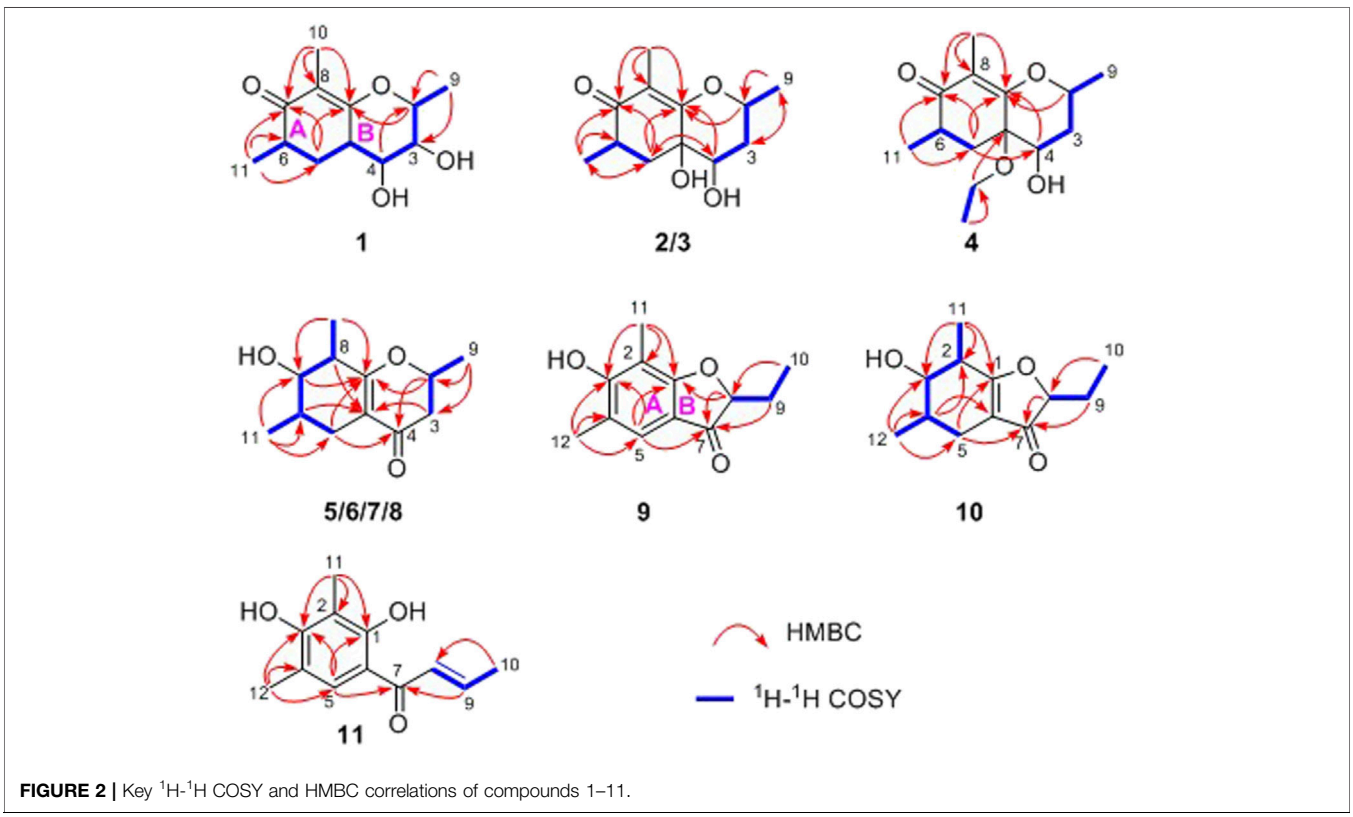

FIGURE 2 | Key ^{1}H-^{1}H COSY and HMBC correlations of compounds 1–11.

RESULTS AND DISCUSSION

Compound 1 was isolated as needle crystals. Its molecular formula of $C_{12}H_{18}O_4$ was established on the basis of (+)-HRESIMS m/z 227.1274 $(M + H)^+$ (calcd for $C_{12}H_{19}O_4$, 227.1278), implying four degrees of hydrogen deficiency. The IR spectrum of 1 logically revealed the presence of carbonyl and free hydroxyl functional groups through the characteristic resonance absorptions at 1,616 and 3,381 cm^{-1}, respectively. The ^{1}H NMR data (**Table 1**) of 1 exhibited a series of typical proton signals, which were responsive for three oxygenated methines [δ_H 3.73 (1H, m, H-2), 3.29 (1H, m, H-3), 3.26 (1H, m, H-4)] and three methyl moieties [δ_H 1.48 (3H, d, J = 6.2 Hz, H-9), 1.68 (3H, s, H-11), 1.16 (3H, d, J = 6.3 Hz, H-10)]. The ^{13}C NMR data (**Table 2**) combined with HSQC spectrum of 1 resolved 12 carbon resonances attributable to three methyls, one methylene, four methines, and four quaternary carbons including one carbonyl functionality (δ_C 204.1).

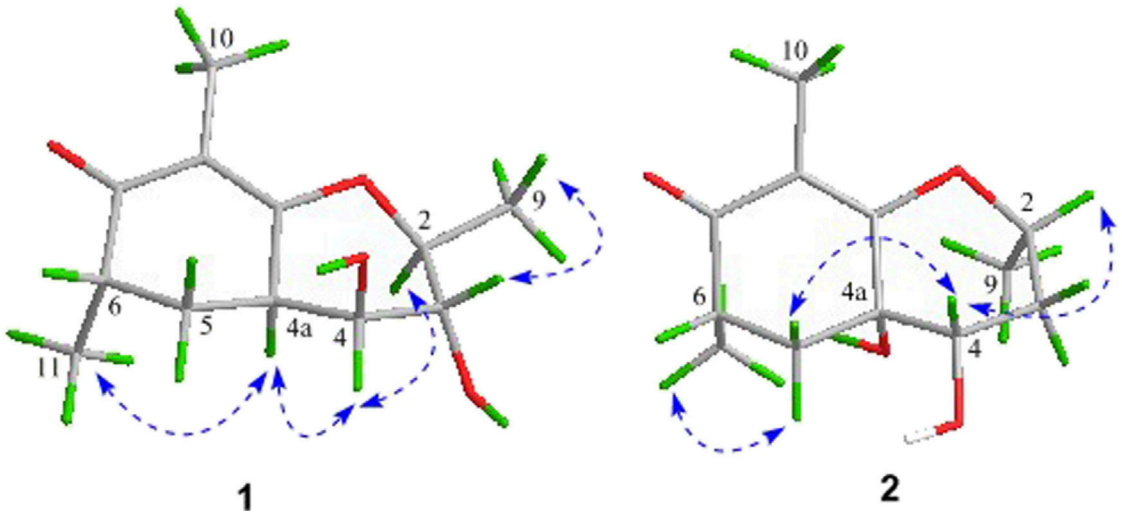

FIGURE 3 | Key NOESY correlations of compounds 1 and 2.

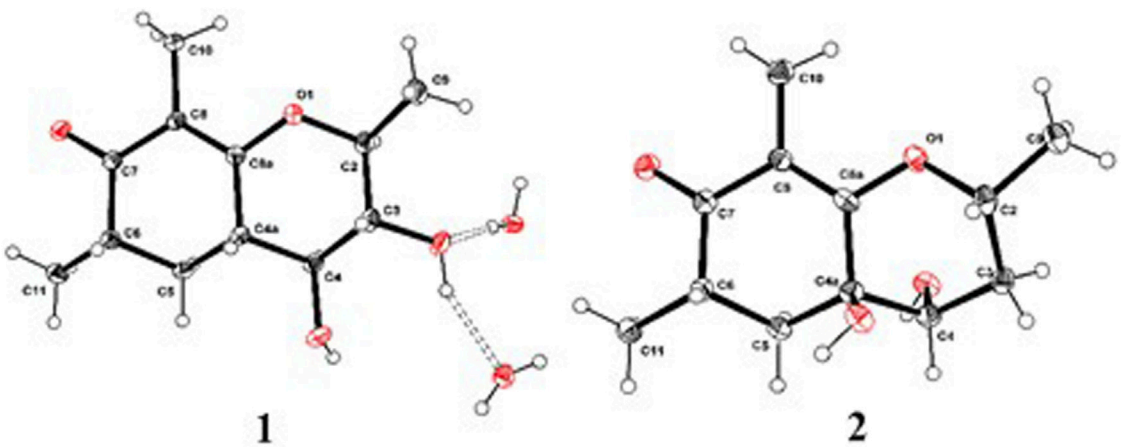

FIGURE 4 | ORTEP drawings of the X-ray structures for compounds 1 and 2.

In the ^{1}H-^{1}H COSY spectrum (**Figure 2**), the cross peaks of H_3-11/H-6/H_2-5 suggested the presence of fragment a (C-11/C-6/C-5). The HMBC correlations from H_3-10 to C-5 (δ_C 33.1), C-6 (δ_C 41.5), and C-7 (δ_C 204.1), H-11 to C-7, C-8 (δ_C 115.9), and C-8a (δ_C 171.0), H_2-5 to C-7 and C-8a coupled with the fragment a were significantly suggested the existence of a cyclohexanone ring (ring A) with a carbonyl group located at C-7 position as well as two methyls attached at C-6 and C-8 positions, respectively. In addition, the obvious HMBC correlations from H-2 to C-4 (δ_C 76.0) and C-8a, H-9 to C-2 (δ_C 79.1) and C-3 (δ_C 76.3) together with the ^{1}H-^{1}H COSY spin system b (C-4a/C-4/C-3/C-2/C-9) confirmed the presence of the pyran ring B. Therefore, the planar structure of 1 was established as shown in **Figure 1**.

As shown in **Figure 3**, key NOE correlations of H-2/H-4, H-4/H-4a, H-4a/H_3-11 confirmed these protons were co-facial, and assigned as α-oriented. Then, the NOE correlation between H-5 and H_3-9 indicated that the methyl group at C-9 was β-oriented (**Figure 3**). Therefore, the relative configuration of 1 was established. The absolute configuration of 1 was finally determined by the single-crystal X-ray diffraction experiment (**Figure 4**), and it provided the perfect evidence for the absolute configuration of 1 with a Flack parameter of 0.02 (5). Moreover, this conclusion was also verified by the ECD calculations (**Figure 5**). Therefore, the structure elucidation of compound 1 was completely finished, and its absolute structure was deduced to be 2*S*,3*R*,4*S*,4a*S*,6*S* and trivially named as foeniculin A.

Compound 2 was obtained as needle crystals. Its molecular formula was established as $C_{12}H_{18}O_4$ on the basis of the protonated molecule peak at *m/z* 227.1275 $(M + H)^+$ in its HRESIMS spectrum, requiring four degrees of unsaturation. The 1D NMR data (**Tables 1** and **2**) of 2 were almost in accordance with those of 1, except for the lack of a hydroxyl group at C-3 position in 2,

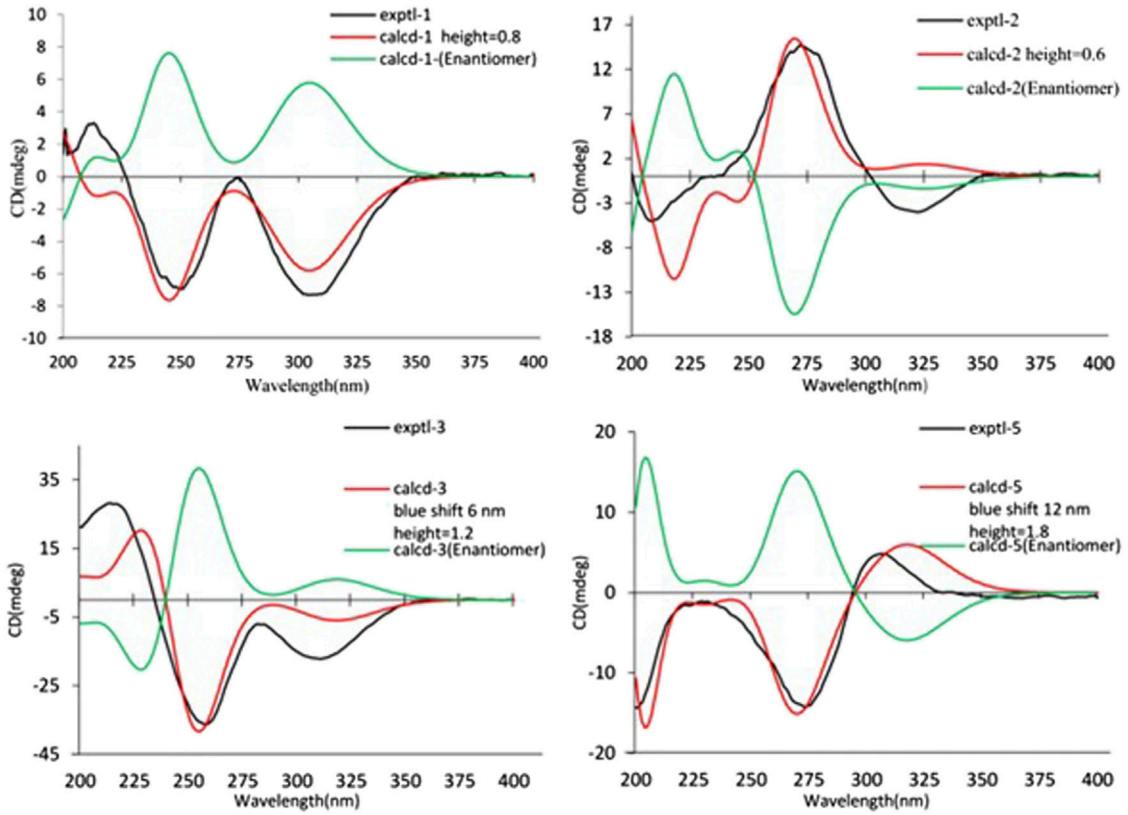

FIGURE 5 | Experimental and calculated ECD spectra of 1–3, 5.

which could be further strengthened by the ^{1}H-^{1}H COSY cross peaks of H-2/H-3/H-4 as well as the predominant HMBC correlations from H_3-9 to C-2 and C-3 as well as carbon shit of C-3 (δ_C 39.0).

The relative configuration of 2 was established by the NOESY experiment. The obvious NOESY cross-peak of H_3-11 with H-5α indicated that these protons should be co-facial, and they were tentatively assigned as α-oriented. Moreover, H-5β exhibited a conclusive NOESY correlation with H-4, which further correlated with H-2, thus strongly suggesting that they should be located as β-oriented (**Figure 3**). Notably, the relative configuration of the hydroxyl group at C-4 was not determined because of the lack of critical hydroxyl proton signal. Fortunately, the absolute configuration of 2 was successfully determined to be 2*R*,4*S*,4a*R*,6*S* by the analysis of X-ray diffraction data using CuKα radiation (**Figure 4**) and ECD calculation (**Figure 5**). Therefore, the configuration of 2 was conclusively assigned as shown in **Figure 1** and given the trivial name foeniculin B.

Compound 3 was also obtained as a white amorphous powder with the same molecular formula $C_{12}H_{18}O_4$ as that of 2. The ^{1}H NMR data of 3 (**Table 1**) were closely related to those of 2, only slight differences could be distinguished between the chemical shifts of H-2 (δ_H 4.62 for 2; δ_H 4.42 for 3), H-3 (δ_H 2.54 and 1.60 for 2; δ_H 2.34 and 1.77 for 3), and H-4 (δ_H 3.78 for 2; δ_H 3.66 for 3). Comparing the ^{13}C NMR spectra of 2 and 3, the signals attributed to the methylene C-3 (δ_C 39.0 for 2, δ_C 35.5 for 3) and quaternary carbon C-8 (δ_C 115.2 for 2, δ_C 118.0 for 3) indicated that they should be a pair of diastereoisomers, which showed a little structural difference on the ring B. Interestingly, the partial relative configuration of 3 was determined by NOESY experiment (**Figure 6**). The NOESY correlations from H-3β to H-2 and H-4 assigned these protons as cofacial, thus, the related methyl and hydroxyl functionalities were suggestively established to be α-oriented on the ring B. However, the relative configuration of 4a-OH was failed to be determined for the lack of any valuable correlation in the NOESY spectrum. Then, the ECD calculations were employed to establish the absolute configurations of the two diastereoisomers. By fitting the experimental and calculated ECD curves, the 2*S*,4*R*,4a*R*,6*S*-configuration was elucidated for 3 (**Figure 5**).

Compound 4 was isolated as white solid. Its molecular formula of $C_{14}H_{22}O_4$ was established on the basis of HRESIMS *m*/*z* 255.1598 $(M + H)^+$ (calcd for $C_{14}H_{23}O_4$, 255.1591), implying four degrees of hydrogen deficiency. After a careful inspection of the NMR spectra of 4 with those of 2, it could be readily disclosed that they showed very close similarity in most NMR profiles. The major difference between them was the hydroxyl group at C-4a in 2 replaced by a hydroxyethyl one in 4, which could be substantiated by its chemical shifts [δ_H 3.60 (2H, m), δ_C (59.3); δ_H 1.16 (3H, t, J = 7.0 Hz), δ_C (15.4)] in conjunct with the HMBC correlation from H_2-1′ to C-4a and the ^{1}H-^{1}H COSY fragment H_2-1'/H_3-2'. Interestingly, compound 4 showed an ECD spectrum almost consistent with that of 2 (see **Supplementary Material**), which strongly illustrated that 4 should also share the similar absolute configuration by the

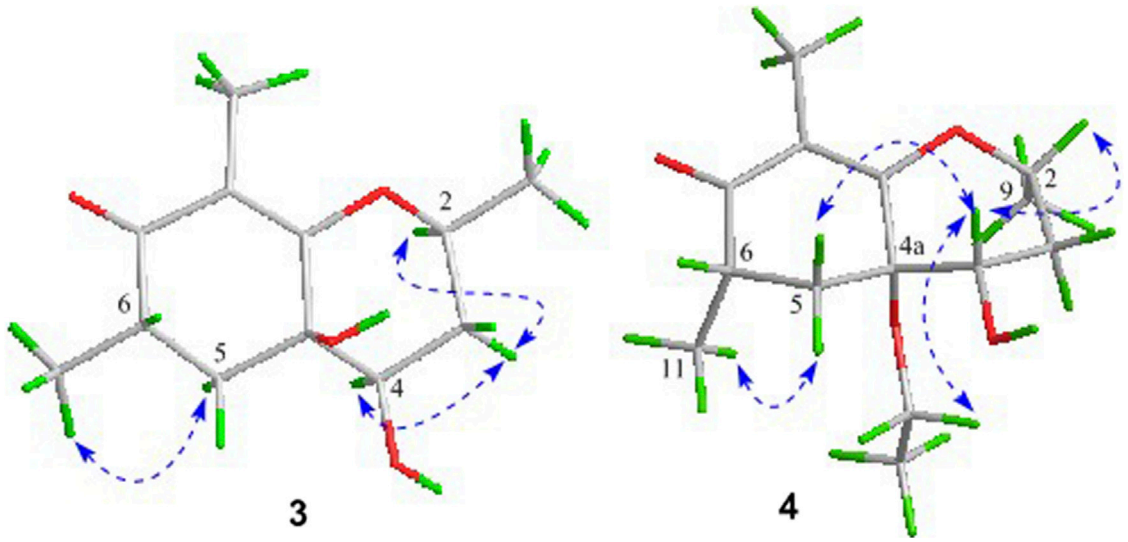

FIGURE 6 | Key NOESY correlations of compounds 3 and 4.

consideration of the same biogenesis. Therefore, the structure of 4 was elucidated as shown in **Figure 1** and named as foeniculin D.

Compound 5 was obtained as colorless needle-like crystals. The HRESIMS of compound 5 showed a positive molecular ion peak at *m/z* 211.1329, corresponding to a molecular formula of $C_{12}H_{18}O_3$. The ^{1}H NMR (**Table 3**) data of 5 exhibited a series of characteristic proton signals, which were responsive for two oxygenated methines [δ_H 4.48 (1H, m, H-2), 2.98 (1H, m, H-7)] and three methyl groups [δ_H 1.42 (3H, d, J = 6.3 Hz, H-9), 1.26 (3H, d, J = 7.0 Hz, H-10), 1.08 (3H, d, J = 6.4 Hz, H-11)]. The ^{13}C NMR spectrum combined with HSQC data of 5 resolved 12 carbon resonances, and they were attributable to three methyls, two methylenes, four methines, and three quaternary carbons including a carbonyl group (δ_C 193.4).

In the ^{1}H-^{1}H COSY spectrum (**Figure 2**), the cross peaks of H_3-10/H-8/H-7/H-6/H_3-11 and H_2-3/H-2/H_3-9 suggested the presence of two independent fragments, a (C-11/C-6/C-7/C-8/C-10) and b (C-2/C-3/C-9). Based on the fragment a, the HMBC correlations from H-8 to C-6, C-7, and C-4a, H_3-11 to C-5, C-6, and C-7, H_3-10 to C-7, C-8, and C-8a suggested the existence of a cyclohexene ring A, which possessed a hydroxyl group located at C-7 and two methyls attached at C-6 and C-8, respectively. Furthermore, the obvious HMBC correlations from H-2 to C-4, H-9 to C-2 and C-3, H-3 to C-4a as well as the ^{1}H-^{1}H COSY fragment b confirmed the presence of the pyran ring B. The NOESY correlations from H-7 to H-5α, H_3-10, and H_3-11 assigned these protons as β-orientation (**Figure 7**). A single crystal of 5 was obtained in MeOH for X-ray diffraction analysis with Flack parameter of 0.04 (9), which suggested the absolute configuration of 5 to be 2*S*,6*S*,7*R*,8*S* shown in **Figure 8**. Thus, compound 5 was defined as (2*S*,6*S*,7*R*,8*S*)-7-hydroxy-2,6,8-trimethyl-2,3,5,6,7,8-hexahydro-4*H*-chromen-4-one and given the trivial name foeniculin E.

The HRESIMS data *m/z* 233.1146 [(M + Na)$^+$, calcd $C_{12}H_{18}NaO_3$ 233.1148] of 6, 211.1339 (M + H)$^+$ (calcd for $C_{12}H_{19}O_3$, 211.1334) of 7, and *m/z* 211.1339 (M + H)$^+$ (calcd for $C_{12}H_{19}O_3$, 211.1334) of 8 indicated that compounds 7 and 8 should share the same molecular formula with $C_{12}H_{18}O_3$ as that of 6. Careful comparison of the ^{1}H and ^{13}C NMR spectra of 6–8 (**Tables 3** and **4**) with those of foeniculin E (5) revealed that they shared the same planar structure. Moreover, the ^{2}D NMR correlations of them (**Figure 2**) further strengthened this conclusion. Therefore, the aforementioned information suggested that the novel compounds 6–8 should be a series of closely related diastereoisomers of 5.

The relative configuration of 6 was determined by NOESY experiments. In the NOESY spectrum, the obvious NOESY correlations of H-2/H_3-10, H-6/H_3-10, and H-7/H_3-11 indicated the α-orientation of H_3-11 as well as β-orientation of H-2, H-6, H_3-10 and 7-OH. Furthermore, the ECD calculation results showed that the absolute configuration of 6 was 2*R*,6*S*,7*R*,8*R* (**Figure 9**). Therefore, the structure of 6 was established as shown in **Figure 1** and given the trivial name foeniculin F.

Compound 7 shared the same planar structure as those of 5 and 6. In its NOESY spectrum, the key NOESY correlations between H-6/H_3-10 and H-7/H_3-11 were readily discovered, which thus successfully established the relative configuration of B ring. However, the lack of the critical NOESY correlations from the protons of A ring to those of B ring made the determination of the absolute configuration of 7 bleak. In order to solve this intractable problem, the ECD calculation method was then performed. Finally, the close comparison of the experimental and calculated ECD curves (**Figure 9**) revealed the absolute configuration of 7 as 2*S*,6*S*,7*R*,8*R*. Collectively, compound 7 was finally permitted to assign as (2*S*,6*S*,7*R*,8*R*)-7-hydroxy-2,6,8-trimethyl-2,3,5,6,7,8-hexahydro-4H-chromen-4-one and given the trivial name foeniculin G.

Compound 8 also shared very close similarity in the NMR data to those of 6. These subtle differences indicated that the methyl group at C-6 adopted an α-orientation and the hydroxyl group at C-7 should be β-orientation. This deduction was consistent with the analysis of the ECD calculations (**Figure 9**). Thus, the

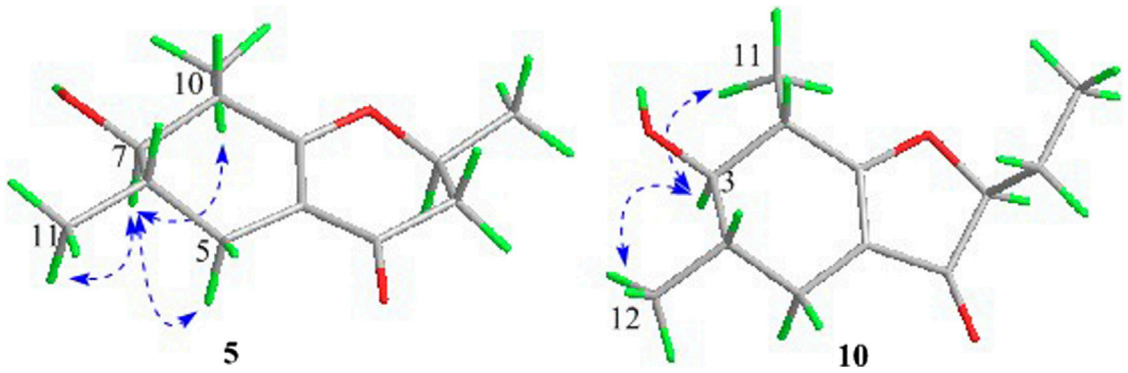

FIGURE 7 | Key NOESY correlations of compounds 5 and 10.

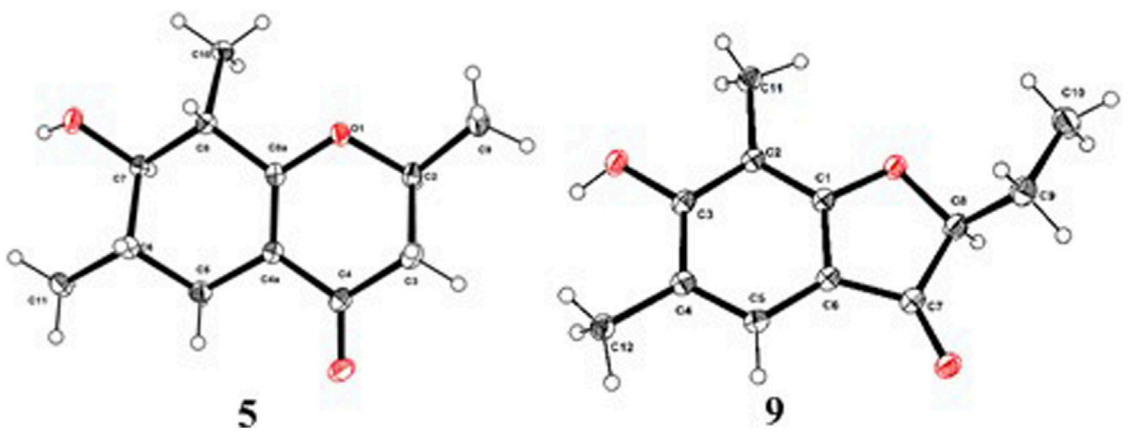

FIGURE 8 | ORTEP drawings of the X-ray structures for compounds 5 and 9.

absolute structure of compound 8 was determined to be (2*R*,6*S*,7*R*,8*S*)-7-hydroxy-2,6,8-trimethyl-2,3,5,6,7,8-hexahydro-4H-chromen-4-one and given the trivial name foeniculin H.

Compound 9 was isolated as colorless needle crystals, and the molecular formula of $C_{12}H_{14}O_3$ was deduced from the HRESIMS peak at *m*/*z* 207.1013 $(M + H)^+$ (calcd for $C_{12}H_{15}O_3$, 207.1021), which clearly suggested the presence of six indices of unsaturation. ^{1}H NMR data of 9 (**Table 5**) revealed three methyl groups including two benzyl protons (δ_H 2.19 and 2.23, each s), an oxymethine (δ_H 4.50, dd, J = 4.5, 7.1 Hz), a methylene (δ_H 1.80, m), and an olefinic methine (δ_H 7.29, s). The ^{13}C NMR data (**Table 5**) and the HSQC spectra revealed the presence of 12 carbons, which included six olefinic carbons (δ_C 106.8, 113.7, 118.7, 122.4, 160.5, and 172.0), a ketocarbonyl (δ_C 200.6), three methyls (δ_C 7.3, 8.9, 15.8), and one oxymethine (δ_C 87.0). The ^{1}H-^{1}H COSY revealed one spin-spin system (C-8/C-9/C-10). The HMBC correlations of H-5 to C-1, C-3, C-7, and C-12, H_3-12 to C-3, C-4, and C-5, as well as H_3-11 to C-1, C-2, and C-3 established a 3-hydroxy-2,4-dimethylph-2-en-1-one core scaffold for ring A (**Figure 1**). The HMBC correlations of H-8 to C-1 and C-7 together with H-5 to C-7 established the 5-membered ring B, which fused with ring A at C-1 and C-6 with an ethyl group at C-8. Thus, the planar structure of 9 was successfully established. The 8*S* absolute configuration of 9 was assigned by the X-ray diffraction (**Figure 8**). Finally, the absolute structure of compound 9 was determined to be (*S*)-8-ethyl-3-hydroxy-2,4-dimethylbenzofuran-3(2H)-one and given the trivial name foeniculin I.

Compound 10 was isolated as a white oil. The molecular formula was established as $C_{12}H_{18}O_3$ from the $(M + H)^+$ ion at *m*/*z* 211.1333 in HRESIMS data (calcd for $C_{12}H_{19}O_3$, 211.1329). The molecular unsaturation together with the ^{1}H and ^{13}C NMR data (**Table 5**) suggested that 10 was a hydrogenated derivative of 9 with the aid of the HSQC spectrum. The planar structure of 10 was determined unambiguously by ^{2}D NMR analyses (^{1}H-^{1}H COSY, HSQC, and HMBC). The partially relative configuration of 10 was established by analyses of NOESY correlations. The key NOESY correlations between H-3/H_3-11 and H-3/H_3-12 strongly suggested that these two methys should be in the same orientation (**Figure 7**). With its potential biogenesis from the biosynthetic precursor 9, the absolute configuration of C-8 in 10 was rationally deduced to be *S* configuration, which thus resulted the structure of 10 to be 2*R*,3*S*,4*S*,8*S* or 2*S*,3*R*,4*R*,8*S*. Therefore, the calculated ECD methodology was conducted to reveal the possible structure

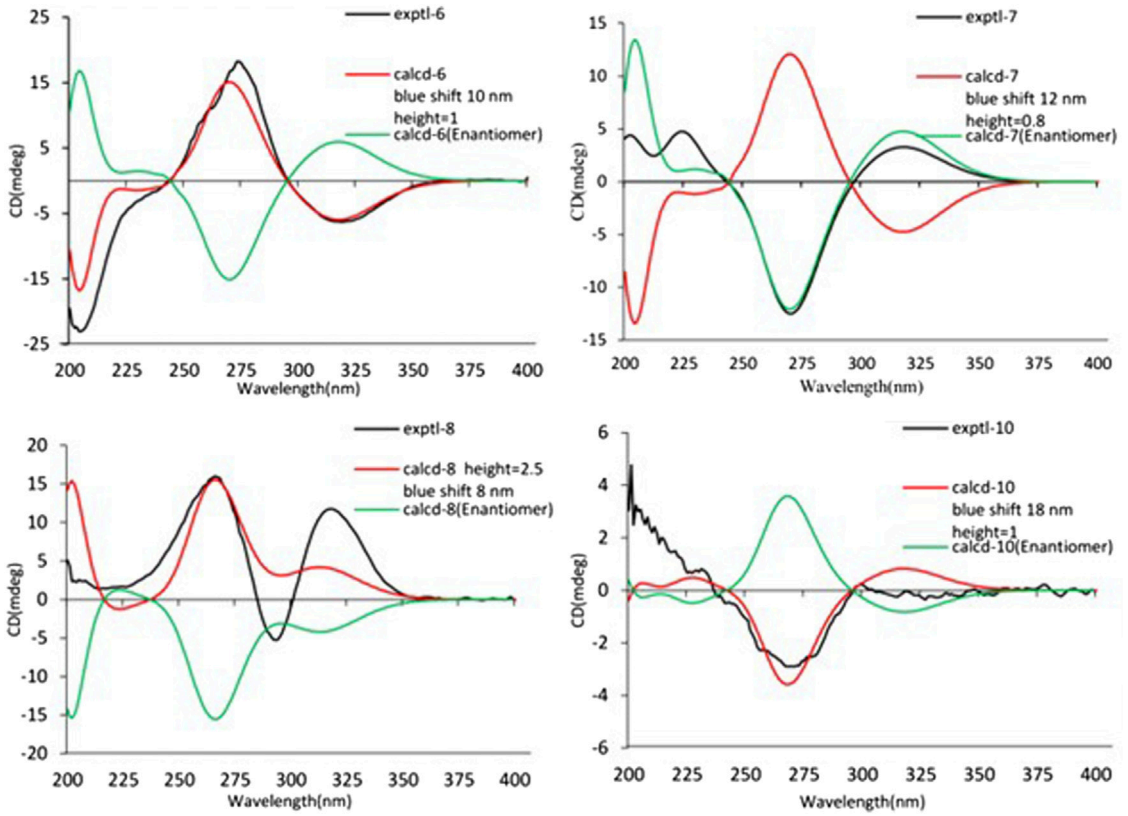

FIGURE 9 | Experimental and calculated ECD spectra of 6–8 and 10.

of 10. Fortunately, the calculated ECD spectrum of (2*S*,3*R*,4*S*,8*S*)-10 showed a negative Cotton effect at 270 nm, which well matched with that of the experimental result (**Figure 9**), allowing the absolute configuration of 10 as 2*S*,3*R*,4*S*,8*S*. Thus, the structure of compound 10 was finally determined and given the trivial name foeniculin J.

According to HRESIMS data, foeniculin K (11) was found to have a molecular formula of $C_{12}H_{14}O_3$, which was the same as that of 9. Analyses of the 1D and 2D NMR of 9 and 11 revealed that compound 11 also possessed a penta-substituted benzene ring A, which was similar to that in compound 9. The main difference between them located in the ring B. In which, compound 11 shared an *α,β*-unsaturated crotonoyl moiety substituted at the C-6 position. This conclusion could be further verified by the ^{1}H-^{1}H COSY fragment C-8/C-9/C-10 and HMBC correlations from H-5 to C-7. At last, the structure of 11 was determined as shown in **Figure 1**.

The isolated compounds 1–11 were tested *in vitro* cytotoxic activity against the tumor cell lines SF-268, MCF-7, HePG-2, and normal cell line LX-2. As a result, compound 11 exhibited mild cytotoxicity against the tumor cell line with IC_{50} values of 27.73, 42.54, and 25.12 μM. Compounds 1–10 were inactive to the tested tumor cell lines even at a concentration of 100 μM. The antimicrobial activity of compounds 1–11 was also evaluated against the bacteria *Escherichia coli* and *S. aureus*. However, all of them were found to be devoid of significant activity.

CONCLUSION

A phytochemical investigation on the *Diaporthe foeniculina* SCBG-15 resulted in the isolation and structural elucidation of eleven new compounds foeniculins. The structures including absolute configurations were determined by extensive physicochemical and spectroscopic analysis, as well as ECD calculation and X-ray diffraction crystallography. All the novel compounds 1–11 possessed polymethylated skeleton. Compound 11 exhibited cytotoxic activity against the tumor cell lines SF-268, MCF-7, HePG-2 with IC_{50} values of 27.73, 42.54, 25.12 μM, which might serve as a promising antitumor lead compound for the drug discovery.

DATA AVAILABILITY STATEMENT

All datasets generated for this study are included in the article/ **Supplementary Material**.

AUTHOR CONTRIBUTIONS

XL, YZ, WZ, HW, SW, and HT performed the experiments. XL was responsible for the isolation of compounds. YZ performed ECD calculation. XL and HT identified the structures. WZ tested cytotoxic activity of the compounds. XL and HT interpreted the

data and wrote the paper. YZ, WZ, HW, SW, and HT revised the manuscript. HT and SW conceived and designed the experiments. All authors read and approved the final manuscript.

FUNDING

We thank the National Natural Science Foundation of China (No. 81773602), Natural Science Foundation of Guangdong Province (2019A1515011694), Guangdong Special Support Program (2017TQ04R599), Guangxi Natural Science Foundation (2018GXNSFBA050015), and Youth Innovation Promotion Association of CAS (2020342).

SUPPLEMENTARY MATERIAL

The Supplementary Material for this article can be found online at: https://www.frontiersin.org/articles/10.3389/fchem.2021.738307/full#supplementary-material

REFERENCES

Beardsell, D., Obrien, S., Williams, E., Knox, R., and Calder, D. (1993). Reproductive Biology of Australian Myrtaceae. *Aust. J. Bot.* 41 (5), 511–526. doi:10.1071/BT9930511

Brophy, J. J., Goldsack, R. J., Bean, A. R., Forster, P. I., and Lepschi, B. J. (1999). Leaf Essential Oils of the genus *Leptospermum* (Myrtaceae) in Eastern Australia, Part 4.Leptospermum Deanei and Allies. *Flavour Fragr. J.* 14, 92–97. doi:10.1002/(sici)1099-1026(199903/04)14:2<92::aid-ffj787>3.0.co;2-d

Cui, H., Lin, Y., Luo, M., Lu, Y., Huang, X., and She, Z. (2017). Diaporisoindoles A-C: Three Isoprenylisoindole Alkaloid Derivatives from the Mangrove Endophytic Fungus *Diaporthe* sp. SYSU-HQ3. *Org. Lett.* 19, 5621–5624. doi:10.1021/acs.orglett.7b02748

Cui, H., Liu, Y., Li, J., Huang, X., Yan, T., Cao, W., et al. (2018). Diaporindenes A-D: Four Unusual 2,3-Dihydro-1H-Indene Analogues with Anti-inflammatory Activities from the Mangrove Endophytic Fungus *Diaporthe* sp. SYSU-HQ3. *J. Org. Chem.* 83, 11804–11813. doi:10.1021/acs.joc.8b01738

Gao, Y.-Q., Du, S.-T., Xiao, J., Wang, D.-C., Han, W.-B., Zhang, Q., et al. (2020). Isolation and Characterization of Antifungal Metabolites from the *Melia Azedarach*-associated Fungus *Diaporthe eucalyptorum*. *J. Agric. Food Chem.* 68, 2418–2425. doi:10.1021/acs.jafc.9b07825

Li, C., Liu, H., Zhao, L., Zhang, W., Qiu, S., Yang, X., et al. (2017). Antibacterial Neolignans from the Leaves of *Melaleuca bracteata*. *Fitoterapia* 120, 171–176. doi:10.1016/j.fitote.2017.06.015

Li, G., Kusari, S., Kusari, P., Kayser, O., and Spiteller, M. (2015). Endophytic *Diaporthe* sp. LG23 Produces a Potent Antibacterial Tetracyclic Triterpenoid. *J. Nat. Prod.* 78, 2128–2132. doi:10.1021/acs.jnatprod.5b00170

Liu, H.-X., Chen, K., Liu, Y., Li, C., Wu, J.-W., Xu, Z.-F., et al. (2016d). Callviminols A-E, New Terpenoid-Conjugated Phloroglucinols from the Leaves of *Callistemon viminalis*. *Fitoterapia* 115, 142–147. doi:10.1016/j.fitote.2016.10.007

Liu, H.-X., Chen, K., Tang, G.-H., Yuan, Y.-F., Tan, H.-B., and Qiu, S.-X. (2016c). Isolation and Biomimetic Total Synthesis of Tomentodiones A-B, Terpenoid-Conjugated Phloroglucinols from the Leaves of *Rhodomyrtus tomentosa*. *RSC Adv.* 6, 48231–48236. doi:10.1039/C6RA08776K

Liu, H.-X., Chen, K., Yuan, Y., Xu, Z.-F., Tan, H.-B., and Qiu, S.-X. (2016a). Rhodomentones A and B, Novel Meroterpenoids with Unique NMR Characteristics from *Rhodomyrtus tomentosa*. *Org. Biomol. Chem.* 14, 7354–7360. doi:10.1039/c6ob01215a

Liu, H.-X., Chen, Y.-C., Liu, Y., Zhang, W.-M., Wu, J.-W., Tan, H.-B., et al. (2016e). Acylphloroglucinols from the Leaves of *Callistemon viminalis*. *Fitoterapia* 114, 40–44. doi:10.1016/j.fitote.2016.08.010

Liu, H.-X., Tan, H.-B., Li, S.-N., Chen, Y.-C., Li, H.-H., Qiu, S.-X., et al. (2018). Two New 12-membered Macrolides from the Endophytic Fungal Strain *Cladosprium colocasiae* A801 of *Callistemon viminalis*. *J. Asian Nat. Prod. Res.* 21, 696–701. doi:10.1080/10286020.2018.1471067

Liu, H.-X., Zhang, W.-M., Xu, Z.-F., Chen, Y.-C., Tan, H.-B., and Qiu, S.-X. (2016b). Isolation, Synthesis, and Biological Activity of Tomentosenol A from the Leaves of *Rhodomyrtus tomentosa*. *RSC Adv.* 6, 25882–25886. doi:10.1039/c6ra01594h

Luo, X., Lin, X., Tao, H., Wang, J., Li, J., Yang, B., et al. (2018). Isochromophilones A-F, Cytotoxic Chloroazaphilones from the Marine Mangrove Endophytic Fungus *Diaporthe* sp. SCSIO 41011. *J. Nat. Prod.* 81, 934–941. doi:10.1021/acs.jnatprod.7b01053

Mandavid, H., Rodrigues, A. M. S., Espindola, L. S., Eparvier, V., and Stien, D. (2015). Secondary Metabolites Isolated from the Amazonian Endophytic Fungus *Diaporthe* sp. SNB-GSS10. *J. Nat. Prod.* 78, 1735–1739. doi:10.1021/np501029s

Mosmann, T. (1983). Rapid Colorimetric Assay for Cellular Growth and Survival: Application to Proliferation and Cytotoxicity Assays. *J. Immunol. Methods* 65, 55–63. doi:10.1016/0022-1759(83)90303-4

Xiang, Y.-Q., Liu, H.-X., Zhao, L.-Y., Xu, Z.-F., Tan, H.-B., and Qiu, S.-X. (2017). Callistemenonone A, a Novel Dearomatic Dibenzofuran-type Acylphloroglucinol with Antimicrobial Activity from *Callistemon viminalis*. *Sci. Rep.* 7, 2363. doi:10.1038/s41598-017-02441-5

Zang, L. Y., Wei, W., Guo, Y., Wang, T., Jiao, R. H., Ng, S. W., et al. (2012). Sesquiterpenoids from the Mangrove-Derived Endophytic Fungus *Diaporthe* sp. *J. Nat. Prod.* 75, 1744–1749. doi:10.1021/np3004112

Zhu, Y., Zhang, L.-X., Zhao, Y., and Huang, G.-D. (2010). Unusual Sesquiterpene Lactones with a New Carbon Skeleton and New Acetylenes from *Ajania przewalskii*. *Food Chem.* 118, 228–238. doi:10.1016/j.foodchem.2009.04.112

Zou, Z.-X., Tan, G.-S., Huang, Q., Sun, H.-H., Huo, L.-Q., Zhong, W.-Q., et al. (2018). Brachyanins A-C, Pinene-Derived Meroterpenoids and Phloroglucinol Derivative from *Leptospermum brachyandrum*. *Fitoterapia* 130, 184–189. doi:10.1016/j.fitote.2018.08.026

Conflict of Interest: The authors declare that the research was conducted in the absence of any commercial or financial relationships that could be construed as a potential conflict of interest.

Publisher's Note: All claims expressed in this article are solely those of the authors and do not necessarily represent those of their affiliated organizations, or those of the publisher, the editors and the reviewers. Any product that may be evaluated in this article, or claim that may be made by its manufacturer, is not guaranteed or endorsed by the publisher.

frontiers in Chemistry

ORIGINAL RESEARCH
published: 29 October 2021
doi: 10.3389/fchem.2021.774555

Semi-Synthesis of Marine-Derived Ilamycin F Derivatives and Their Antitubercular Activities

*Jun Li[1,2], Zhiyong Liu[3], Mingye Hong[4], Changli Sun[1,2], Tianyu Zhang[3], Hua Zhang[4], Jianhua Ju[1,2,5] and Junying Ma[1,2,5]**

[1]CAS Key Laboratory of Tropical Marine Bio-Resources and Ecology, Guangdong Key Laboratory of Marine Materia Medica, RNAM Center for Marine Microbiology, South China Sea Institute of Oceanology, Chinese Academy of Sciences, Guangzhou, China, [2]Southern Marine Science and Engineering Guangdong Laboratory (Guangzhou), Guangzhou, China, [3]Tuberculosis Research Laboratory, State Key Laboratory of Respiratory Disease, Guangdong-Hong Kong-Macao Joint Laboratory of Respiratory Infectious Diseases, Guangzhou Institutes of Biomedicine and Health, Chinese Academy of Sciences, Guangzhou, China, [4]Guangdong Provincial Key Laboratory of Medical Molecular Diagnostics, Institute of Laboratory Medicine, Guangdong Medical University, Dongguan, China, [5]College of Oceanology, University of Chinese Academy of Sciences, Qingdao, China

Tuberculosis (TB) is still a global disease threatening people's lives. With the emergence of multi-drug-resistant *Mycobacterium tuberculosis* the prevention and control of tuberculosis faces new challenges, and the burden of tuberculosis treatment is increasing among the world. Ilamycins are novel cyclopeptides with potent anti-TB activities, which have a unique target protein against *M. tuberculosis* and drug-resistant strains. Herein, ilamycin F, a major secondary metabolite isolated from the marine-derived mutant strain *Streptomyces atratus* SCSIO ZH16 Δ*ilaR*, is used as a scaffold to semi-synthesize eighteen new ilamycin derivatives (ilamycin NJL1–NJL18, **1**–**18**). Our study reveals that four of ilamycin NJLs (**1, 6, 8**, and **10**) have slightly stronger anti-TB activities against *Mtb* H37Rv (minimum inhibitory concentration, 1.6–1.7 μM) compared with that of ilamycin F on day 14th, but obviously display more potent activities than ilamycin F on day 3rd, indicating anti-TB activities of these derivatives with fast-onset effect. In addition, cytotoxic assays show most ilamycin NJLs with low cytotoxicity except ilamycin NJL1 (**1**). These findings will promote the further exploration of structure-activity relationships for ilamycins and the development of anti-TB drugs.

Keywords: streptomycetes, cyclopeptide, antitubercular activity, ilamycin, semi-synthesis, derivatization

OPEN ACCESS

Edited by:
Yuanyuan Lu,
China Pharmaceutical University, China

Reviewed by:
Scott Gary Franzblau,
University of Illinois at Chicago, United States
Rama P. Tripathi,
Csir-Central Drug Research Institute, Uttar Pradesh, India

****Correspondence:***
Junying Ma
majunying@scsio.ac.cn

Specialty section:
This article was submitted to Medicinal and Pharmaceutical Chemistry, a section of the journal Frontiers in Chemistry

Received: *12 September 2021*
Accepted: *27 September 2021*
Published: *29 October 2021*

Citation:
Li J, Liu Z, Hong M, Sun C, Zhang T, Zhang H, Ju J and Ma J (2021) Semi-Synthesis of Marine-Derived Ilamycin F Derivatives and Their Antitubercular Activities. Front. Chem. 9:774555. doi: 10.3389/fchem.2021.774555

INTRODUCTION

Tuberculosis (TB) is an infectious disease caused by the pathogen *Mycobacterium tuberculosis* (*Mtb*), which is the leading cause of death from a single infectious agent. Globally, it is estimated that 10 million new cases and 1.2 million deaths occurred in 2019 due to TB infections (World Health Organization, 2020). With the appearance of drug-resistant strains, multidrug resistance (MRD) TB and extensive drug resistance (XDR) TB have resulted in a major challenge to the prevention and treatment of TB in the world, especially in developing countries (Saravanan et al., 2018). Standard treatment of TB is a long course, including a 2-months induction phase and a 4-months consolidation phase, thus it is important that drugs with fast-onset action can contribute to shorten treatment in clinical trials (Horsburgh et al., 2015). Hence, there is an urgent demand for development of novel anti-TB drugs with unique targets and fast-onset action.

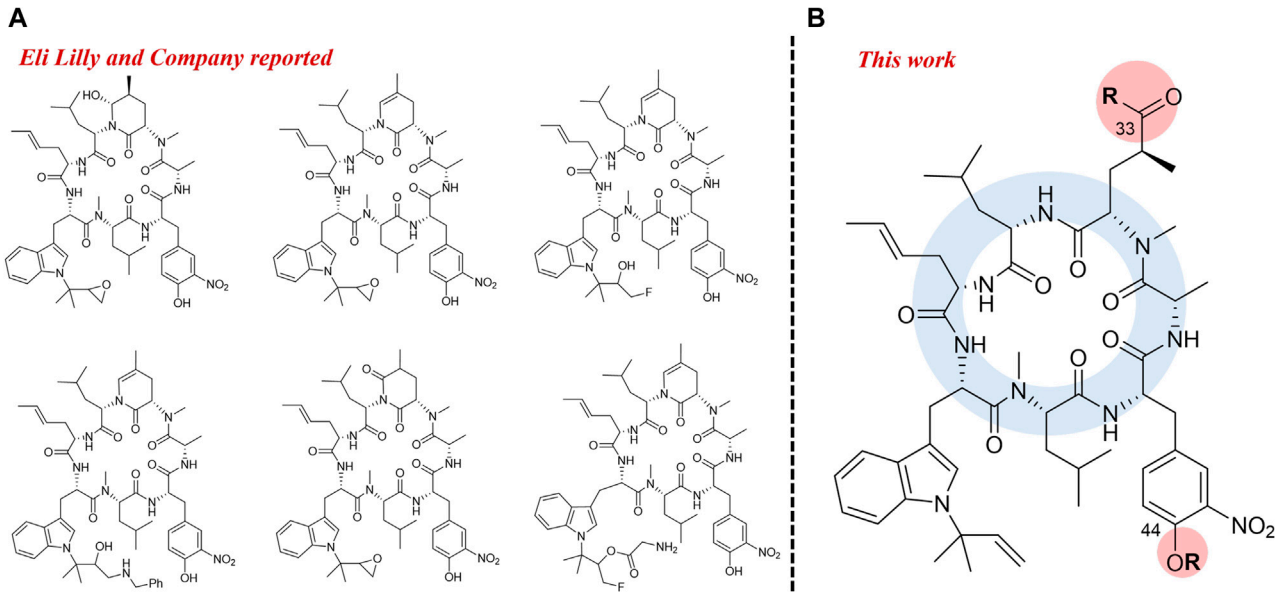

FIGURE 1 | Semi-synthesis of rufomycin active derivatives from Eli Lilly and Company **(A)** Modified position from this work **(B)**.

With the development of drug-resistant tuberculosis, the discovery of new drugs or the drug-repurposed for tuberculosis is increasing recently (Furin et al., 2019). Ilamycins, also named rufomycins, comprise a representative of cycloheptapeptides with strong anti-TB activity, which were isolated from *Streptomyces atratus* and *S. islandicus* (Takita et al., 1962; Cary et al., 1971; Ma et al., 2017; Sun et al., 2020; Zhou et al., 2020). Previous studies identified the target of rufomycins, caseinolytic protein C1 (ClpC1), which was different from that of the current therapeutic drugs (Sassetti et al., 2003; Lee et al., 2016; Choules et al., 2018; Choules et al., 2019; Wolf et al., 2019). Therefore, compounds of this family are a promising drug-lead for the treatment of MRD- and XRD-TB. Moreover, for the structure-activity relationship (SAR) studies, Eli Lilly and Company firstly synthesized a series of ilamycin derivatives in 2000 (Lambooy, 2000). Anti-TB assays showed that 6 of the derivatives exhibited strong inhibitory activities against *Mtb* H37Ra (**Figure 1A**).

In recent years, our group has been focusing on the discovery and the biosynthesis of anti-infective antibiotics. Ilamycin F, isolated from a genetic engineered mutant of the deep South China Sea-derived strain *Streptomyces atratus* SCSIO ZH16, had a strong anti-TB activity against *M. tuberculosis* H37Rv with minimum inhibitory concentration (MIC) value of 1.2 μM (Ma et al., 2017). As the main metabolite of the mutant strain *S. atratus* SCSIO ZH16 Δ*ilaR,* the yield of ilamycin F is about 400–500 mg/L in its mutant. In this regard, ilamycin F is ideally utilized as a starting material for preparing new ilamycin derivatives, which will facilitate to further investigate their SAR and discover more efficient anti-TB drug leads. Herein, we report the preparation and characterization of eighteen new ilamycin F derivatives (ilamycin NJL1–NJL18) on C-33 and C-44 of ilamycin F (**Figure 1B**). Several semi-synthesized derivatives display potent anti-TB activity against *M. tuberculosis* H37Rv with fast-onset effect and low cytotoxicity.

RESULTS AND DISCUSSION

Semi-Synthesis of Ilamycin NJLs

Ilamycin F has two types of functional groups for modification, C-33 carboxyl group and C-44 hydroxyl group. With the aim of synthesizing new derivatives, several modifications in ilamycin F were introduced by acylation and esterification (**Scheme 1**). Ilamycin NJL1–NJL12 (**1**–**12**) were concisely synthesized by 1-(3-dimethylaminopropyl)-3-ethylcarbodiimide hydrochloride (EDC)/1-hydroxybenzotriazole (HOBt) assisted amidation at C-33 carboxyl group using L-amino acid methyl esters and benzylamine derivatives (**Figure 2**). The yields ranged from 74 to 83%. Moreover, according to the twin drug strategy (Contreras et al., 2008; Ibacache et al., 2018), isoniazid and N-deacetyl-linezolid, two anti-TB substrates, were respectively coupled with ilamycin F to generate ilamycin NJL13–NJL14 (**13**–**14**) using the aforementioned amidation method in 76–77% yield (**Figure 2**). The strategy was proposed to produce synergic effect by binding two targets.

The C-44 hydroxyl group of ilamycin F is another position for derivatization. Although various ether and aliphatic sidechains at C-44 were created through etherification or esterification by Eli Lilly and Company, all derivatives displayed low anti-TB activities (Lambooy, 2000). To further study SAR of ilamycin F, heteroaromatic rings, *p*-fluorophenylacetic acid and 3-(methylthio) propionic acid were introduced at the C-44 hydroxyl group (**Scheme 1**). Ilamycin NJL15–NJL18 (**15**–**18**) could be successfully obtained in the presence of EDC and 4-dimethylaminopyridine (DMAP) (**Figure 3**), but owing to low

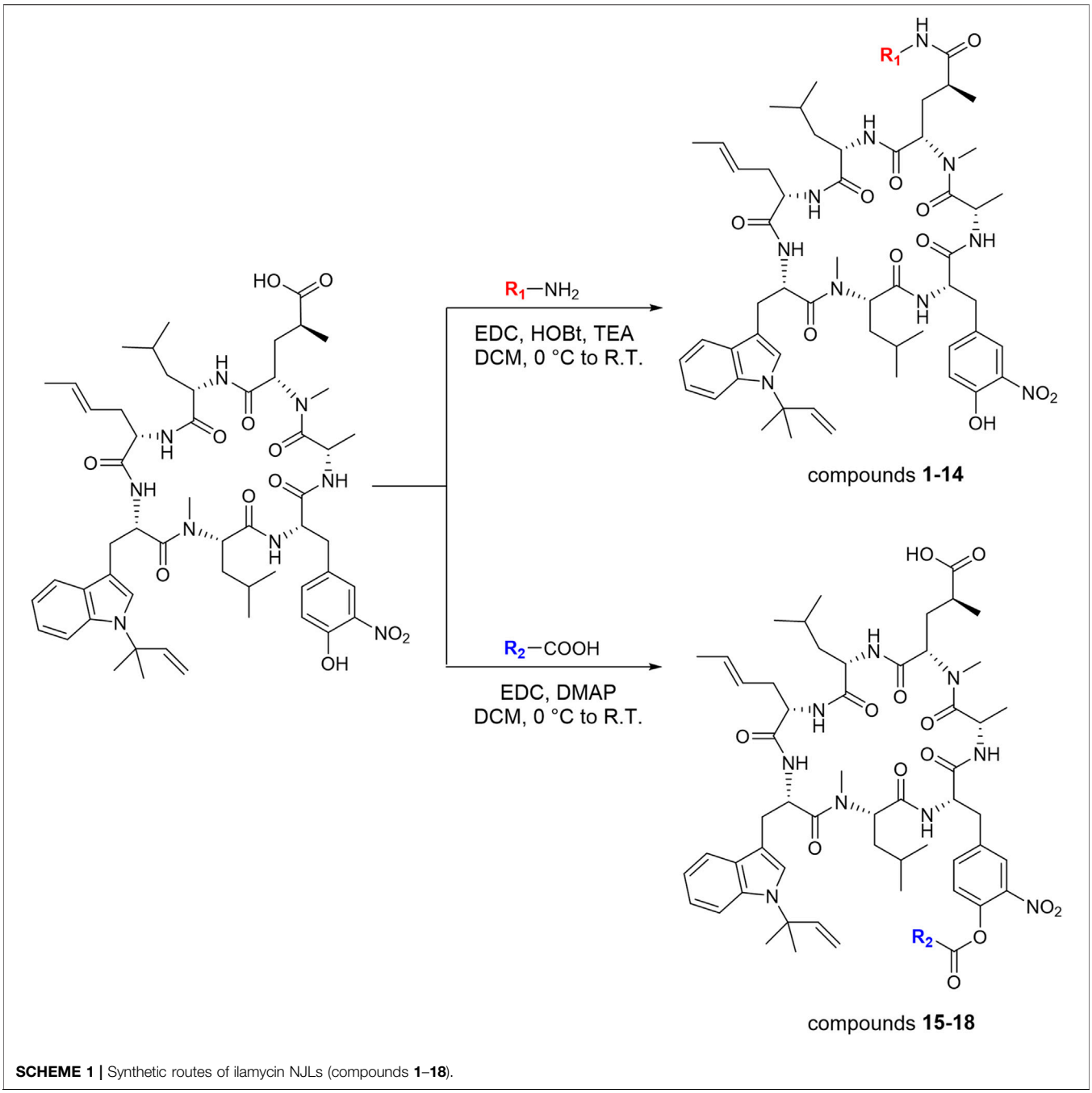

SCHEME 1 | Synthetic routes of ilamycin NJLs (compounds **1**–**18**).

nucleophilicity of the C-44 hydroxyl group, the yields of the reaction were only given to 32–40%.

Bioactivities of Ilamycin NJLs

The anti-TB activities of ilamycin NJL1–NJL18 (**1**–**18**) were evaluated against *M. tuberculosis* H37Rv, which has pathogenic and still popularly used in virulent laboratory (Camus et al., 2002; Målen et al., 2011). As depicted in **Table 1**, although basic amino acid derivatives (compounds **4**–**5**) at the C-33 had weak activities, the modification of neutral amino acid derivatives, in comparison with ilamycin F, displayed potent anti-TB activities with fast-onset effect. Compounds **1**–**3**, **6**, and **8**, showed efficient activities on day 3rd, which was higher than that of ilamycin F with 4–19 folds. Importantly, compounds **1, 6**, and **8** had slightly stronger activities than that of ilamycin F on day 14th (MIC, 1.6–1.7 μM), speculating that their modification did not change the interaction with targets, but would obviously facilitate to promoting penetration of membranes in *Mtb*. Moreover, benzylamine derivatives of ilamycin F, compounds **9**–**11**, were also exhibited the fast-onset effect on day 3rd except compound **12**. This finding indicated

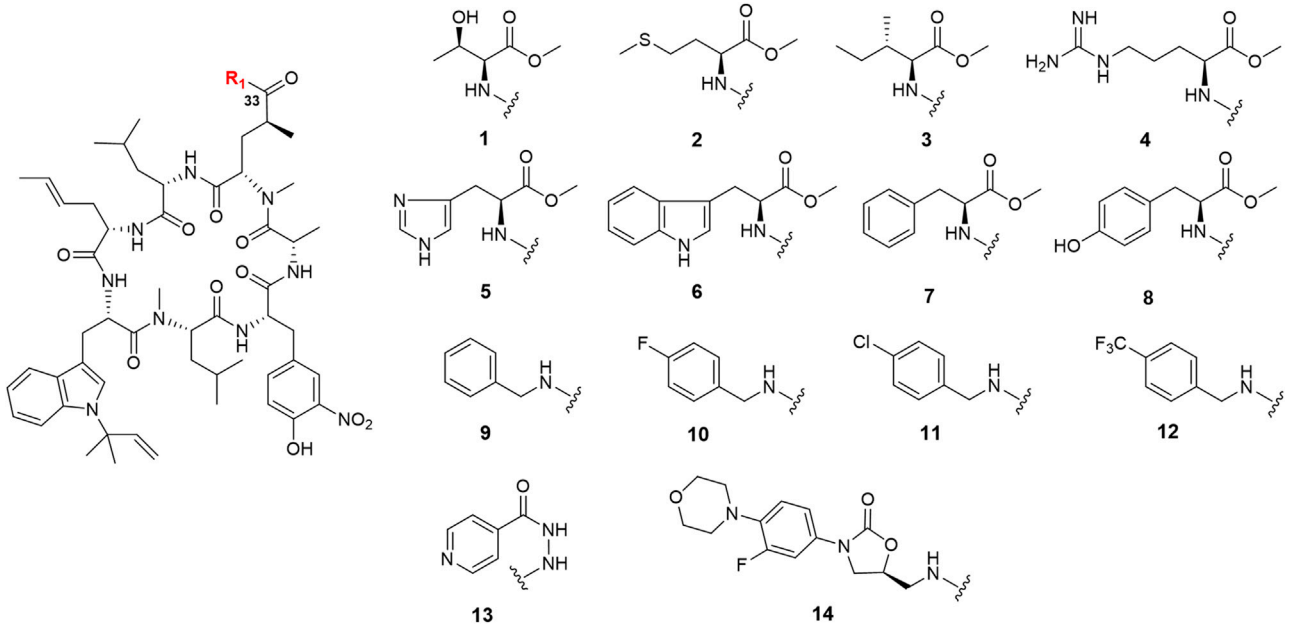

FIGURE 2 | Structures of ilamycin NJLs modified at C-33 (compounds **1**–**14**).

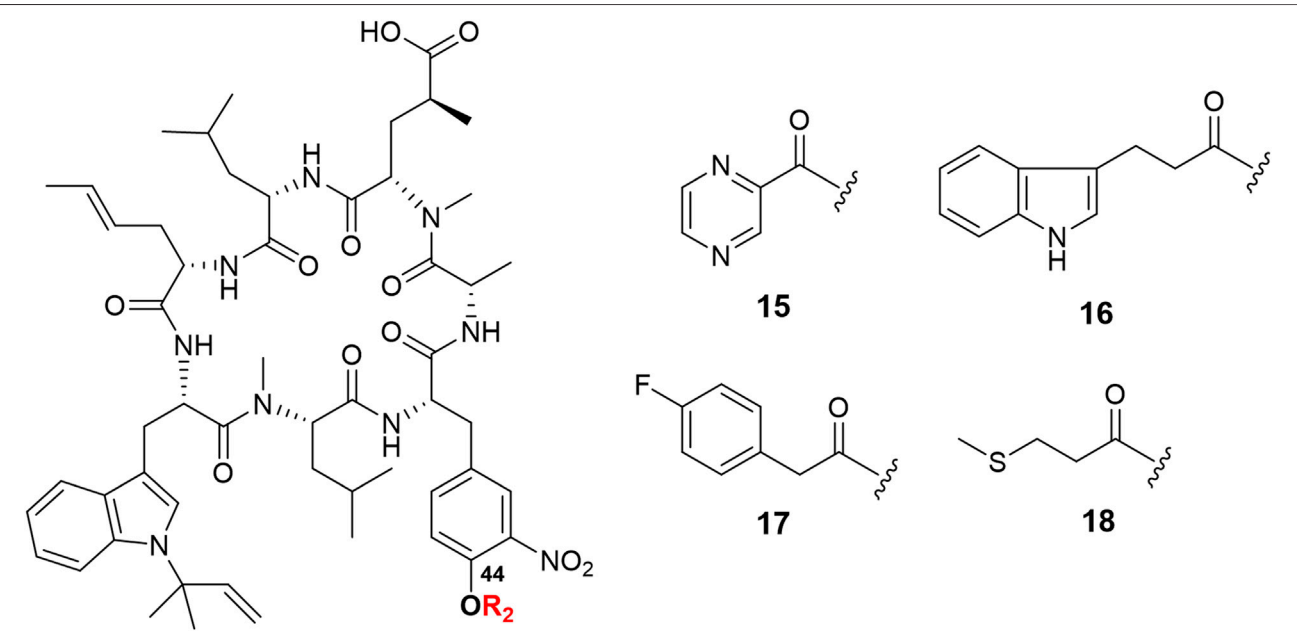

FIGURE 3 | Structures of ilamycin NJLs modified at C-44 (compounds **15**–**18**).

that benzylamine modified with a larger substituent significantly affected anti-TB activity of ilamycin derivatives. Although showed a similar activity with that of ilamycin F on day 14th, compound **10** was 2-fold more potent MIC value than that of **9** and **11**, which might result from the promotion of its lipophilicity by fluorine substituent and improved the penetration to cell membranes (Smart, 2001; Purser et al., 2008). However, the activities of compounds **13**–**14** were significantly decreased under the twin drug strategy, when a carboxyl group at the C-33 was replaced by isoniazid or N-deacetyl-linezolid. This result indicated that the construction of compounds **13**–**14** affected the binding to

TABLE 1 | Anti-tubercular activity of ilamycin NJLs (**1**–**18**) against *M. tuberculosis* H37Rv.

Compounds	MICs (μM)against H37Rv			Compounds	MICs (μM)against H37Rv		
	Day 3rd	Day 7th	Day 14th		Day 3rd	Day 7th	Day 14th
1	3.5	1.7	1.7	11	3.4	3.4	3.4
2	6.7	6.7	3.4	12	>100	>100	>100
3	6.8	6.8	6.8	13	27.6	27.6	27.6
4	26.4	26.4	26.4	14	48.5	48.5	48.5
5	26.8	26.8	26.8	15	27.9	27.9	27.9
6	1.7	1.7	1.7	16	26.4	26.4	26.4
7	26.6	13.3	6.6	17	27.2	27.2	27.2
8	1.6	1.6	1.6	18	28.0	28.0	28.0
9	3.5	3.5	3.5	ilamycin F	30.7	15.4	1.9
10	1.7	1.7	1.7		—		

TABLE 2 | IC_{50} value (μM) of ilamycin NJLs (**1**–**18**) against five human cancer cell lines and two normal cell lines.

Compounds	MCF-7	HeLa	HepG2	A549	HCT116	L02	Huvec-12
1	9.0	11.3	17.7	5.7	7.2	6.5	10.3
2	>50	>50	>50	>50	>50	>50	>50
3	>50	14.5	>50	>50	>50	12.0	>50
4	>50	26.0	>50	23.0	30.6	25.9	35.2
5	>50	>50	>50	>50	>50	>50	>50
6	>50	>50	>50	>50	>50	>50	>50
7	>50	>50	>50	>50	>50	>50	>50
8	>50	>50	>50	>50	>50	>50	>50
9	>50	>50	>50	>50	>50	>50	>50
10	>50	>50	>50	>50	>50	>50	>50
11	>50	>50	>50	>50	>50	>50	>50
12	>50	>50	>50	>50	>50	>50	>50
13	>50	>50	>50	>50	>50	>50	>50
14	>50	>50	>50	>50	>50	>50	>50
15	>50	>50	>50	>50	>50	>50	>50
16	>50	>50	>50	>50	>50	>50	>50
17	>50	>50	>50	>50	>50	>50	>50
18	>50	>50	>50	>50	>50	>50	>50
ilamycin F	32.2	31.0	>50	47.0	44.8	43.9	46.1
doxorubicin	4.0	0.7	0.6	1.5	4.0	7.7	12.0

their targets, and exhibited no synergistic effect on anti-TB activity. Additionally, compounds **15**–**18** modified at the C-44 also showed lower activities. The similar groups coupling at the C-33 with beneficial effects could not produce the same promotion at the C-44 hydroxyl group of ilamycin F. The results suggested that the hydroxyl group at C-44 might serve as a pharmacophore, which was critical in achieving anti-TB activity and also consistence with our previous discoveries (Sun et al., 2020).

To evaluate the application potential of these compounds, the cytotoxicity of ilamycin NJLs (**1**–**18**) was evaluated *in vitro* using five human cancer cell lines, including breast adenocarcinoma (MCF-7), cervical carcinoma (HeLa), hepatocellular carcinoma (HepG2), lung cancer (A549), colon cancer (HCT116); two normal cell lines including human hepatic cell line (L02) and human umbilical vein endothelial cell line (Huvec-12). Although most compounds (**2**–**18**) showed no or weak cytotoxicity, compound **1** exhibited a moderate IC_{50} value (5.7–9.0 μM) against MCF-7, A549, HCT116, and L02, which had a 3–8-fold promotion compared with that of ilamyicn F (**Table 2**). The result indicated that threonine methyl ester modified in C-33 carboxyl group of ilamycin F was favorable for the cytotoxic activity.

CONCLUSION

In this study, ilamycin F, a starting material isolated from marine-derived mutant *S. atratus* ZH16 Δ*ilaR*, was employed to semi-synthesize eighteen ilamycin F derivatives (ilamcyin NJL1–NJL18). Their inhibitory effects on *M. tuberculosis* H37Rv were tested *in vitro*. Our study revealed that compounds **1**, **6**, **8**, and **10** exhibited slightly stronger anti-TB activity (1.6–1.7 μM) with that of ilamycin F on day 14th, but displayed a 9–19-fold increased anti-TB activities compared with that of ilamycin F on day 3rd (MICs 1.6–3.5 μM), which indicated their rapid suppression effect on *M. tuberculosis*. In addition, most ilamycin NJLs had low cytotoxicity except compound **1** displayed a moderate cytotoxic activity (IC_{50}, 5.7–11.3 μM) against five human cancer cell lines and two normal cell lines. Our results will be beneficial to further exploration for

SAR of ilamycins and promote the development of anti-TB drugs.

DATA AVAILABILITY STATEMENT

The original contributions presented in the study are included in the article/**Supplementary Material**, further inquiries can be directed to the corresponding author.

AUTHOR CONTRIBUTIONS

JL conducted the chemical experiments and drafted the manuscript. ZL and TZ did the antitubercular assay. MH and HZ performed the cytotoxicity assays. CS carried out the NMR analysis. JM and JJ initiated the project and revised the manuscript.

FUNDING

This research was funded by the National Natural Science Foundation of China (82022067, 31870046, and 81973372), Key Science and Technology Project of Hainan Province (ZDKJ202018), Key-Area Research and Development Program of Guangdong Province (2020B1111030005), Key Special Project for Introduced Talents Team of Southern Marine Science and Engineering Guangdong Laboratory (Guangzhou) (GML2019ZD0406), Guangdong Provincial-level Special Funds for Promoting High-quality Economic Development (2020032), Key Science and Technology Project of Sichuan Province (19SYXHZ0025).

SUPPLEMENTARY MATERIAL

The Supplementary Material for this article can be found online at: https://www.frontiersin.org/articles/10.3389/fchem.2021.774555/full#supplementary-material

REFERENCES

Camus, J.-C., Pryor, M. J., Médigue, C., and Cole, S. T. (2002). Re-Annotation of the Genome Sequence of *Mycobacterium Tuberculosis* H37Rv. *Microbiology.* 148, 2967–2973. doi:10.1099/00221287-148-10-2967

Cary, L. W., Takita, T., and Ohnishi, M. (1971). A Study of the Secondary Structure of Ilamycin B1by 300 MHz Proton Magnetic Resonance. *FEBS Lett.* 17, 145–148. doi:10.1016/0014-5793(71)80584-7

Choules, M. P., Klein, L. L., Lankin, D. C., McAlpine, J. B., Cho, S.-H., Cheng, J., et al. (2018). Residual Complexity Does Impact Organic Chemistry and Drug Discovery: the Case of Rufomyazine and Rufomycin. *J. Org. Chem.* 83, 6664–6672. doi:10.1021/acs.joc.8b00988

Choules, M. P., Wolf, N. M., Lee, H., Anderson, J. R., Grzelak, E. M., Wang, Y., et al. (2019). Rufomycin Targets ClpC1 Proteolysis in *Mycobacterium Tuberculosis* and M. Abscessus. *Antimicrob. Agents Chemother. Agents Ch.* 63, e02204–18. doi:10.1128/AAC.02204-18

Contreras, J.-M., and Sippl, W. (2008). *Homo and Heterodimer Ligands: the Twin Drug Approach. The Practice of Medicinal Chemistry*. 3rd ed. Netherlands: Elsevier, 380–414. doi:10.1016/B978-0-12-374194-3.00018-4

Furin, J., Cox, H., and Pai, M. (2019). Tuberculosis. *The Lancet.* 393, 1642–1656. doi:10.1016/S0140-6736(19)30308-3

Horsburgh, C. R., Jr, Barry, C. E., III, and Lange, C. (2015). Treatment of Tuberculosis. *N. Engl. J. Med.* 373, 2149–2160. doi:10.1056/NEJMra1413919

Ibacache, J., Faundes, J., Montoya, M., Mejías, S., and Valderrama, J. (2018). Preparation of Novel Homodimers Derived From Cytotoxic Isoquinolinequinones. A Twin Drug Approach. *Molecules.* 23, 439–448. doi:10.3390/molecules23020439

Lambooy, P. K. (2000). *Process for the Isolation of Rufomycin Factors*. United States: Eli Lilly and Company. Available online at: http://europepmc.org/article/PAT/WO0078798.

Lee, H., and Suh, J.-W. (2016). Anti-tuberculosis lead Molecules From Natural Products Targeting *Mycobacterium Tuberculosis* ClpC1. *J. Ind. Microbiol. Biot.* 43, 205–212. doi:10.1007/s10295-015-1709-3

Målen, H., De Souza, G. A., Pathak, S., Søfteland, T., and Wiker, H. G. (2011). Comparison of Membrane Proteins of Mycobacterium TuberculosisH37Rv and H37Ra Strains. *BMC Microbiol.* 11, 1–10. doi:10.1186/1471-2180-11-18

Ma, J., Huang, H., Xie, Y., Liu, Z., Zhao, J., Zhang, C., et al. (2017). Biosynthesis of Ilamycins Featuring Unusual Building Blocks and Engineered Production of Enhanced Anti-Tuberculosis Agents. *Nat. Commun.* 8, 1–10. doi:10.1038/s41467-017-00419-5

Purser, S., Moore, P. R., Swallow, S., and Gouverneur, V. (2008). Fluorine in Medicinal Chemistry. *Chem. Soc. Rev.* 37, 320–330. doi:10.1039/B610213C

Saravanan, M., Niguse, S., Abdulkader, M., Tsegay, E., Hailekiros, H., Gebrekidan, A., et al. (2018). Review on Emergence of Drug-Resistant Tuberculosis (MDR & XDR-TB) and its Molecular Diagnosis in Ethiopia. *Microb. Pathogenesis.* 117, 237–242. doi:10.1016/j.micpath.2018.02.047

Sassetti, C. M., Boyd, D. H., and Rubin, E. J. (2003). Genes Required for Mycobacterial Growth Defined by High Density Mutagenesis. *Mol. Microbiol.* 48, 77–84. doi:10.1046/j.1365-2958.2003.03425.x

Smart, B. E. (2001). Fluorine Substituent Effects (On Bioactivity). *J. Fluorine Chem.* 109, 3–11. doi:10.1016/S0022-1139(01)00375-X

Sun, C., Liu, Z., Zhu, X., Fan, Z., Huang, X., Wu, Q., et al. (2020). Antitubercular Ilamycins From Marine-Derived Streptomyces Atratus SCSIO ZH16 ΔilaR. *J. Nat. Prod.* 83, 1646–1657. doi:10.1021/acs.jnatprod.0c00151

Takita, T., Ohi, K., Okami, Y., Maeda, K., and Umezawa, H. (1962). New Antibiotics, Ilamycins. *J. Antibiot. (Tokyo).* 15, 46–48. doi:10.11554/antibioticsa.15.1_46

Wolf, N. M., Lee, H., Choules, M. P., Pauli, G. F., Phansalkar, R., Anderson, J. R., et al. (2019). High-resolution Structure of ClpC1-Rufomycin and Ligand Binding Studies Provide a Framework to Design and Optimize Anti-Tuberculosis Leads. *ACS Infect. Dis.* 5, 829–840. doi:10.1021/acsinfecdis.8b00276

World Health Organization (2020). Global Tuberculosis Report. Available online at: https://www.who.int/teams/global-tuberculosis-programme/data.

Zhou, B., Shetye, G., Yu, Y., Santarsiero, B. D., Klein, L. L., Abad-Zapatero, C., et al. (2020). Antimycobacterial Rufomycin Analogues From *Streptomyces Atratus* Strain MJM3502. *J. Nat. Prod.* 83, 657–667. doi:10.1021/acs.jnatprod.9b01095

Conflict of Interest: The authors declare that the research was conducted in the absence of any commercial or financial relationships that could be construed as a potential conflict of interest.

The reviewer (SF) declared a past co-authorship with one of the authors (TZ) to the handling Editor.

Publisher's Note: All claims expressed in this article are solely those of the authors and do not necessarily represent those of their affiliated organizations, or those of the publisher, the editors and the reviewers. Any product that may be evaluated in this article, or claim that may be made by its manufacturer, is not guaranteed or endorsed by the publisher.

frontiers in Chemistry

ORIGINAL RESEARCH
published: 12 November 2021
doi: 10.3389/fchem.2021.772858

Polycyclic Tetramate Macrolactams—A Group of Natural Bioactive Metallophores

Ling Ding, Sheng-Da Zhang, Ahmad Kasem Haidar, Manila Bajimaya, Yaojie Guo, Thomas Ostenfeld Larsen and Lone Gram*

Department of Biotechnology and Biomedicine, Technical University of Denmark, Kongens Lyngby, Denmark

New infectious diseases and increase in drug-resistant microbial pathogens emphasize the need for antibiotics with novel mode-of-action. Tetramates represented by fungi-derived tenuazonic acid and bacterial polycyclic tetramate macrolactams (PTMs) are an important family of natural products with a broad spectrum of antimicrobial activities. Despite their potential application as new antibiotics, it remains unknown how PTMs function. In this study, genomic mining revealed that PTM biosynthetic gene clusters (BGCs) are widespread in both Gram-positive and Gram-negative bacteria, and we investigated a sponge endosymbiont *Actinoalloteichus hymeniacidonis* harboring a potential PTM-BGC. Xanthobaccin A that previously has only been isolated from a Gram-negative bacterium was obtained after a scale-up fermentation, isolation, and structure elucidation through mass spectrometry and nuclear magnetic resonance (NMR) spectroscopy. Xanthobaccin A as well as two previously reported tetramates, equisetin and ikarugamycin, exhibited antibacterial activities against *Bacillus subtilis*. In addition, these three tetramates were for the first time to be confirmed as metallophores and the stoichiometry of the complexes were shown to be Fe(III)(equisetin)$_3$/Fe(III)(equisetin)$_2$ and Fe(III)(ikarugamycin)$_2$, respectively. Meanwhile, we found that all three tetramates could reduce ferric into ferrous iron, which triggers the Fenton chemistry reaction. Their antibacterial activity was reduced by adding the radical scavenger, vitamin C. Altogether, our work demonstrates that equisetin and PTMs can act as metallophores and their antimicrobial mechanism is possibly mediated through Fenton chemistry.

Keywords: tetramate, Fenton chemistry, metallophore, PTM, antibiotics

OPEN ACCESS

Edited by:
Khaled A. Shaaban,
University of Kentucky, United States

Reviewed by:
Madan Kharel,
University of Maryland Eastern Shore, United States
Eric Nybo,
Ferris State University, United States

****Correspondence:***
Ling Ding
lidi@dtu.dk

Specialty section:
This article was submitted to Medicinal and Pharmaceutical Chemistry, a section of the journal Frontiers in Chemistry

Received: *08 September 2021*
Accepted: *25 October 2021*
Published: *12 November 2021*

Citation:
Ding L, Zhang S-D, Haidar AK, Bajimaya M, Guo Y, Larsen TO and Gram L (2021) Polycyclic Tetramate Macrolactams—A Group of Natural Bioactive Metallophores. Front. Chem. 9:772858. doi: 10.3389/fchem.2021.772858

INTRODUCTION

The increase in drug-resistant pathogenic microorganisms is a major societal challenge (Cooper and Shlaes, 2011) and the development of antibiotics with novel mode-of-action is urgently needed. Natural products represent an important source of drugs, and more than 50% of approved new antibiotics are either natural products or natural products-derived (Newman and Cragg, 2020). Therefore, one promising drug discovery strategy is to further explore microbial natural products.

Natural products with metal-chelating properties have a great potential for the development of new antibiotics. Polyphenols, quinones, 3-acyltetramic, and tetronic acids are among those natural

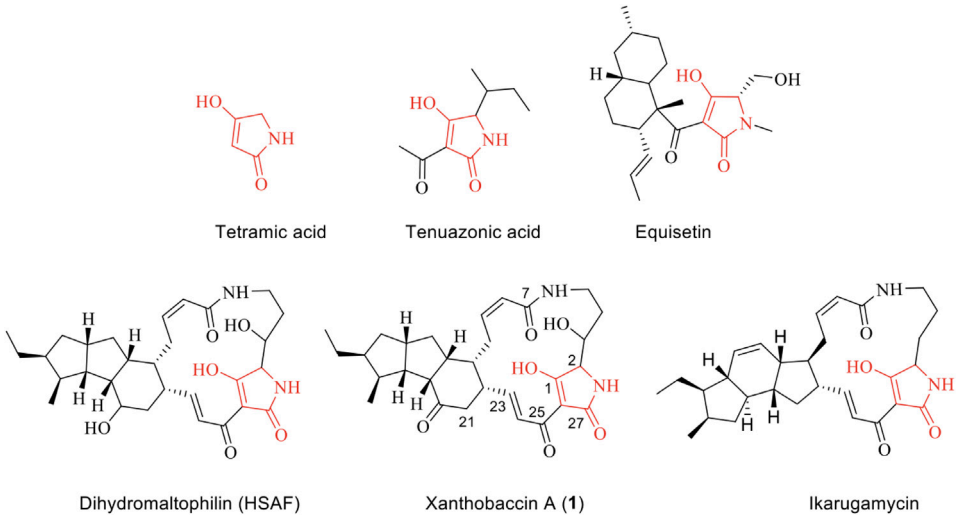

FIGURE 1 | Chemical structure of tetramic acid and selected examples of natural products containing a tetramic acid unit.

products with metal-chelating properties, and some derivatives exhibit profound activities against multidrug-resistant bacteria (Dandawate et al., 2019). For example, natural products containing a tetramate-moiety (**Figure 1**) represent an important class of bioactive compounds with a broad spectrum of antimicrobial activities. There are two well-known examples, namely the fungal natural products equisetin (Vesonder et al., 1979) and tenuazonic acid (Stickings 1959). Tenuazonic acid is a toxic constituent from *Alternaria tenuis* Auct, *Phoma sorghina*, and other phytopathogenic fungi (Laatsch 2012). Tenuazonic acid can complex with copper, iron, nickel, and magnesium ions (Lebrun et al., 1985) and it has been suggested that the biological activity of tetramates is related to their metal-complexing ability (Steyn and Rabie 1976). The crystal structure of copper bis (tenuazonate) monohydrate has been determined by X-ray crystallography (Dippenaar et al., 1977). Although enolic tautomers of tenuazonic acids exist, their crystal structure has revealed a square-planar Cu(II) complex with a Z-enol form in which the amide and acetyl oxygen atoms are bound to the metal (Dippenaar et al., 1977). The complexation of tenuazonic acid with iron(III), nickel(II), and magnesium(II) was further investigated in 1985. Mass spectroscopy and IR spectra provided evidence of stoichiometry of Fe (III)$(TA)_3$, Ni(II)$(TA)_2$, and Mg(III)$(TA)_2$ (Lebrun et al., 1985). The addition of $FeCl_3$ and $MgCl_2$ did not reverse the toxicity to bacteria or rice cells indicating that the activity is not due to deprivation of these essential metals (Lebrun et al., 1985). Herein the mode-of-action remains unknown.

In comparison to the fungal tetramates, bacteria tend to produce polycyclic tetramate macrolactams (PTM), which are an emerging class of natural products, that includes the antifungal HSAF produced by a Proteobacterium (Yu et al., 2007), the antinematode geodin A from a sponge (Capon et al., 1999), the antiprotozoal ikarugamycin from a *Streptomyces* sp. (Jomon et al., 2012), and the anticancer compounds ikarugamycins and clifednamide A from a sponge-associated *Streptomyces* sp. (Dhaneesha et al., 2019). Intriguingly, many bacterial PTM producers are involved in a beneficial association with higher organisms. Due to their biological activities, several of these microorganisms have been developed as biocontrol agents in agriculture, e.g. the HSAF-producer *Lysobacter enzymogenes* (Yu et al., 2007) and *Stenotrophomonas* sp., the latter of which lives in the sugar beet rhizosphere and produces the antifungal agent xanthobaccin A active against the host-pathogen *Pythium ultimum* (Hashidoko et al., 1999). Despite their important biological activities, the mode of action of PTMs and other tetramates remains elusive. PTMs harboring a tetramate moiety could potentially act as metal chelators, however, this has, to our knowledge, not been investigated. Hence, we aim to provide new evidence on how the larger tetramates complex with ions and how tetramates broadly function.

The starting point for the investigations was a genome-mining survey on numerous bacterial genomes, which revealed that PTMs are widespread in both Gram-positive and Gram-negative bacteria (**Supplementary Figure S1**). Among those bacteria, *Actinoalloteichus hymeniacidonis*, an endosymbiont from the sponge *Hymeniacidon perlevis* (Zhang et al., 2006) was found to harbor a potential PTM biosynthetic gene cluster (**Figure 2**). Analysis of the gene cluster showed the presence of putative genes coding for siderophore interacting proteins downstream of the key PKS-NRPS gene. This indicated that the product could be a metallophore. We, therefore cultivated the bacterium under iron-deficient conditions which led to the production of putative PTMs. From the 6 L fermentation broth, we isolated and characterized the antimicrobial component as xanthobaccin A. Further analysis revealed that xanthobaccin A, together with two other microbial tetramates, ikarugamycin and equisetin, can chelate ferric iron and reduce it to ferrous iron triggering the cascade of Fenton

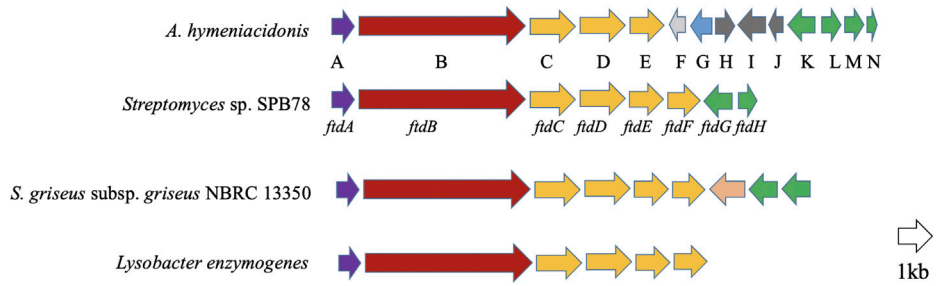

FIGURE 2 | Open reading frame (ORF) map of the possible xanthobaccin biosynthetic locus from *A. hymeniacidonis* compared to other characterized PTM clusters in *Streptomyces* sp. SPB78 (frontalamides, Blodgett et al., 2010), *S. griseus* subsp. *griseus* NBRC 13350 (frontalamide-like compounds, Luo et al., 2013) and *Lysobacter enzymogenes* (HSAF, Yu et al., 2007). Each ORF is color-coded to designate ftd orthologs. Those shown in purple encode for sterol desturase, red for hybrid PKS-NRPS, orange for oxidoreductase and green for transporters. For *A. hymeniacidonis* (**Supplementary Table S1**), there are siderophore interaction-related proteins F (siderophore-interacting protein) and G (iron-siderophore-interacting ABC transporter substrate-binding protein); H–J: proteins with unknown functions.

chemistry. In this paper, we describe the antimicrobial, iron-chelating, and antimicrobial mechanisms of xanthobaccin A together with equisetin and ikarugamycin.

MATERIALS AND METHODS

Bacterial Strains and Culture Conditions

Actinoalloteichus hymeniacidonis HPA 177T was purchased from DSMZ, Germany. *Bacillus subtilis* ATCC6051 was obtained from the research group of Professor Ákos T. Kovács, Department of Biotechnology and Biomedicine, Technical University of Denmark.

Genome Mining

To identify, annotate and analyze the secondary metabolite biosynthetic gene clusters, NCBI BLAST (Boratyn et al., 2013) and AntiSMASH 5.0 (Blin et al., 2019) were used in the genome mining process of *A. hymeniacidonis* (CP014859.1) and other PTM producers (**Supplementary Table S2**).

Accession Numbers of Source Files Used to Compare Unknown *ftd*-Like Gene Clusters in Bacterial Genomes

The following GenBank releases are sources of *ftd*-like gene clusters used in comparative analyses: *Streptomyces* sp. SPB78, GenBank accession NZ_ACEU01000453; *S. griseus* subsp. *griseus* NBRC 13350, GenBank access AP009493.1; *Lysobacter enzymogenes*, GenBank access EF028635.2.

General Chemical Experimental Procedures

NMR spectra were recorded on a Bruker Advance III 800 MHz spectrometer. Silica gel chromatography was performed on silica gel 60 (Merck, 0.04–0.063 mm, 230–400 mesh ASTM) and Sephadex LH20 (Pharmacia). Ikarugamycin and equisetin were ordered from Sigma-Aldrich. Solvents of analytical grades were ordered from VWR.

Fermentation and Isolation

To obtain sufficient amounts of metabolites for chemical characterization, *A. hymeniacidonis* was cultured in a 6 L liquid fermentation at 28°C, 200 rpm for 7 days. Slant of spores of *A. hymeniacidonis* was inoculated in a 500 ml flask containing 150 ml medium soluble starch 4 g/L, KNO_3 2 g/L, NaCl 1 g/L, $MgSO_4{\cdot}7H_2O$ 0.5 g/L, $CaCO_3$ 0.02 g/L, yeast extract 1 g/L. The culture broth was separated into supernatant and mycelia parts, respectively. Both were extracted by ethyl acetate and the organic phases were combined. Evaporation of the organic solvent yielded 1.8 g of crude extract that was partially purified in flash chromatography by silica gel chromatography using gradient solutions of dichloromethane and methanol into 10 fractions F1-10. The F7 fraction containing PTMs was further purified by semi-preparative HPLC using an XBridge RP_{18} HPLC Column 10 × 250 mm, 5 µm, a flow rate of 4 ml/min, 40.0°C. Using a 28 min multi-step method and acetonitrile and water as mobile phases the following method was applied in semi-preparative HPLC: at 0–5 min 10–50% acetonitrile, at 5–7 min 50–60% acetonitrile, at 7–15 min 60–80% acetonitrile, at 15–18 min 80–100% acetonitrile, and acetonitrile was maintained at 100% for another 5 min and followed by re-equilibration to 10% acetonitrile until 28 min. Pure compound **1** (0.8 mg) was obtained and analyzed by NMR spectroscopy.

HPLC-MS Analysis

A UHPLC–DAD–QTOF method was set up for the screening, with an injection volume of 1 µl extract. The separation was performed on a Dionex Ultimate 3000 UHPLC system (Thermo Scientific, Dionex, Sunnyvale, CA, United States) equipped with a 100 × 2.1 mm, 2.6 µm, Kinetex C_{18} column, held at a temperature of 40°C, and using a linear gradient system composed of A: water, and B: acetonitrile. The flow rate was 0.4 ml min^{-1}.

Time-of-flight detection was performed using a maXis 3G QTOF orthogonal mass spectrometer (Bruker Daltonics, Bremen, Germany) operated at a resolving power of ~50,000 full width at

half maximum FWHM. The instrument was equipped with an orthogonal electrospray ionization source, and mass spectra were recorded in the range m/z 100–1,000 as centroid spectra, with five scans per second. For calibration, 1 µl of 10 mmol sodium formate was injected at the beginning of each chromatographic run, using the divert valve 0.3–0.4 min. Data files were calibrated post-run on the average spectrum from this time segment, using the Bruker HPC high-precision calibration algorithm.

For ESI^+ the capillary voltage was maintained at 4,200 V, in the spray chamber, the gas flow to the nebulizer was set to 2.4 bar, the drying temperature was 220°C, and the drying gas flow was 12.0 L min^{-1}. Transfer optics ion-funnel energies, quadrupole energy were tuned on HT-2 toxin to minimize fragmentation. For ESI^- the settings were the same, except that the capillary voltage was maintained at −2,500 V. Ion-cooler settings were: transfer time 50 µs, radiofrequency RF 55 V peak-to-peak Vpp, and pre-pulse storage time 5 µs.

Iron-Reducing Assay

The iron II detecting agent ferrozine was used to test the iron-reducing activity of three tetramates, xanthobaccin A, equisetin, and ikarugamycin. A reaction solution comprised of 10 µl test tetramate (1 mg/ml), 10 µl ammonium iron III citrate $C_6H_8FeNO_7$ (5 mg/ml), and 20 µl aqueous ferrozine (1% wt/vol). $FeSO_4$ mixed with aqueous ferrozine (1% wt/vol) was used as a positive control. Tetramate mixed with ammonium iron III citrate was used as a negative control. All components were dissolved in ammonium chloride buffer 1 M, pH 4.5. After 5 min reaction under darkness, the reaction mixtures were analyzed by HPLC-HRMS.

Antimicrobial Assay

An agar diffusion assay was carried out to test the antimicrobial activity of tetramates against *Bacillus subtilis* ATCC 6051. Whatman Antibiotic assay discs of 6 mm were loaded with 20 µg pure tetramates with/without vitamin C (10 µg). The growth medium for *B. subtilis* was 3 g meat extract, 5 g (Bacto)-peptone, 5 g glucose, 1 L tap water, pH 7.3–7.5, 18 g agar. The test plates were prepared by pouring 14 ml of L-agar as a base layer; after solidifying, this was overlaid with 4 ml of the inoculated seed layer. Roxymycin was used as a positive antibiotic control. Pure methanol and vitamin C were used as negative controls. The plates were incubated at 37°C for 24 h, and antimicrobial activity was recorded as clear zones (in mm) of inhibition surrounding the disk. The test sample was considered active when the zone of inhibition was greater than 6 mm. The MIC assay was done by the broth dilution method according to the NCCLS (National Committee for Clinical Laboratory Standards, 1997).

RESULTS

Sponge Bacterial Endosymbiont Harbors a Tetramate Biosynthetic Gene Cluster

Actinoalloteichus hymeniacidonis HPA 177^T is a Gram-positive, rare actinomycete isolated from the marine sponge *Hymeniacidon perlevis* (Zhang et al., 2006). Our genome mining revealed that it harbored a putative PTM BGC (**Figure 2**), and the core biosynthetic PKS-NRPS protein, which exhibited 67 and 61% similarity to HSAF and frontalamide synthetase proteins, respectively. The individual genes from the PTM gene cluster are listed in **Supplementary Table S1** and the proposed biosynthetic pathway is shown in **Supplementary Figure S2**. The biosynthesis was proposed to be carried out by a hybrid iterative PKS-NRPS, and a single set of the functional domains KS-AT-DH-KR-ACP that iteratively incorporate six malonyl-CoA to form two polyene chains, which were further condensed with the two free amine groups of L-ornithine *via* the NRPS activity. This resulted in a tetramate-polyene intermediate, which was then cyclized *via* reduction by the tailoring oxidative enzymes to form the PTM skeleton. The potential biosynthetic gene cluster and the homologs of the *A. hymeniacidonis* core PKS-NRPS protein (TL08_RS13440) identified in the NCBI database and their phylogenetic relationships are depicted in **Supplementary Figure S1** and **Supplementary Table S2**, respectively.

Fermentation, Isolation, and Characterization of Bioactive Tetramates From *Actinoalloteichus hymeniacidonis*

To test whether the tetramate gene cluster identified through genome mining is functional in *A. hymeniacidonis*, we conducted a small-scale fermentation (10 ml) and confirmed the production of possible PTMs supported by LC-MS analyses (**Supplementary Figure S3**). To characterize the active compounds, *A. hymeniacidonis* was cultivated in a 6 L scale to yield a crude extract subjected to separation by chromatography on silica gel and Sephadex LH-20 columns, yielding pure compound 1 (0.8 mg).

Compound 1 was isolated as a major component. HRESIMS data of 1 ($[M + H]^+$ 511.2788, calculated for 511.2803, Δ 2.7 ppm) suggested a molecular formula of $C_{29}H_{38}N_2O_6$ and implied that it might be xanthobaccin A through AntiBase search (Laatsch, 2012). Four olefinic protons (H-8, δ 5.93; H-9, δ 5.74; H-23, δ 6.63; H-24, δ 6.97) corresponding to two double bonds were observed. A *trans* and a *cis* configuration for the two double bonds was deduced by the coupling constants (16.0 and 10.8 Hz between H23/H24 and H8/H9, respectively). In the HMBC spectrum, NH (δ 7.87, t, 5.6 Hz), H-8, and H-9 showed correlations to C-7 (δ 166.1). The ^{13}C NMR spectrum indicated the presence of a tetramate unit by the presence of signals for C-1 (δ 196.2), C-27 (δ 178.5), C-2 (δ 61.4), and C-26 (δ 99.4). The location of a carbonyl group at C-20 (δ 207.9) was established by HMBC correlations between H-12, H-21 and H-22 and C-20. The aliphatic parts of the molecule were confirmed by both COSY and HMBC correlations. The selected HMBC correlations can be seen in **Supplementary Figure S4**. Both ^1H NMR and ^{13}C NMR spectra were identical to xanthobaccin A reported in the literature (Hashidoko et al., 1999). Xanthobaccin A was firstly reported from the Gram-negative bacterium *Stenotrophomonas* sp. SB-K88 living in the rhizosphere, which exhibited high activity against the plant

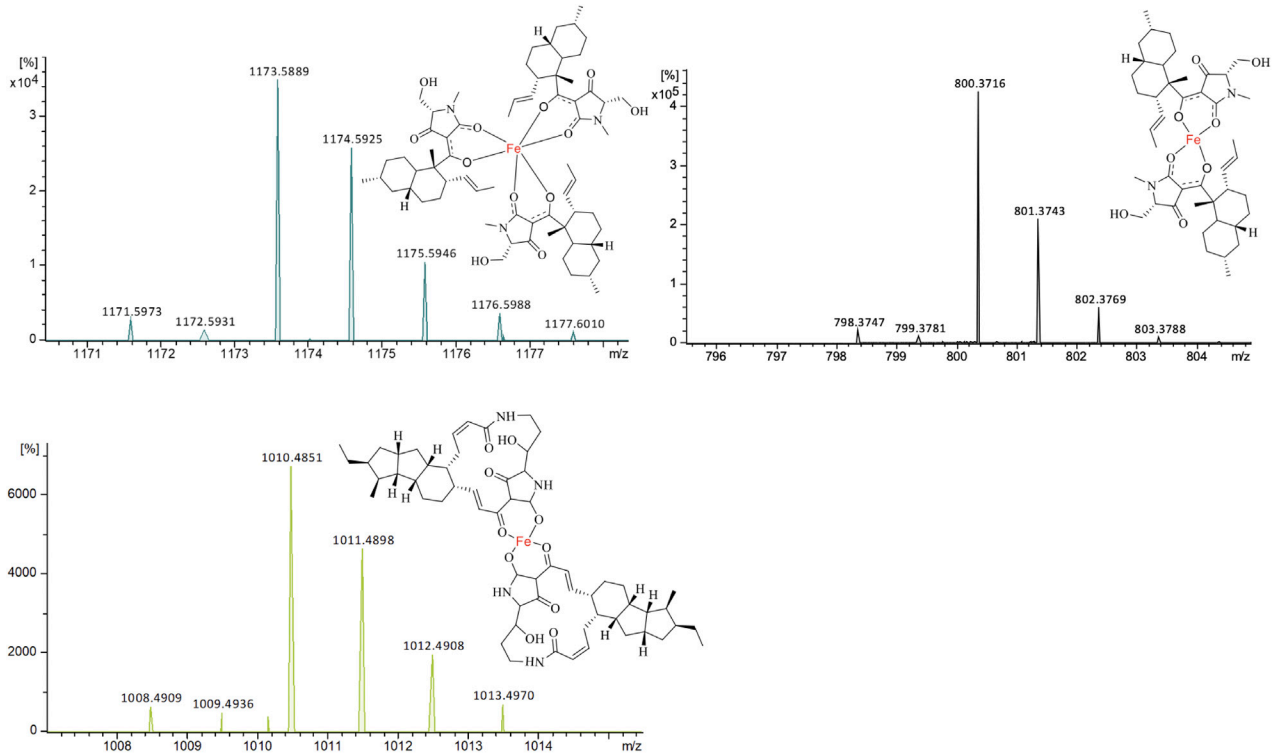

FIGURE 3 | ESIMS for the two different stoichiometries of equisetin-Fe(III) complexes and one ikarugamycin-Fe(III) complex. **(A)** $[M + H]^+$, m/z 1,171.5993, Fe(III)(equisetin)$_3$; **(B)** $[M + H]^+$, m/z 798.3747, Fe(III)(equisetin)$_2$. **(C)** $[M + H]^+$, m/z 1,008.4909, Fe(III)(ikarugamycin)$_2$.

fungal pathogen *Pythium ultimum* (Hashidoko et al., 1999). Here, for the first time, we demonstrated that xanthobaccin A is also produced by a Gram-positive bacterium associated with a sponge. Together with the discovery of the cytotoxic ikarugamycins and clifednamide A from a sponge-associated *Streptomyces* sp. (Dhaneesha et al., 2019), it indicates that sponge endosymbionts might be the true producers for those PTMs reported from sponges, such as the antinematode geodin A (Capon et al., 1999).

Antimicrobial Mechanisms of Tetramates

Xanthobaccin A was reported to be the principal active metabolite of *A. hymeniacidonis*. The compound exhibited a minimum inhibitory concentration (MIC) of 1 μg/ml against *Pythium ultimum* (Hashidoko et al., 1999). To compare the antibacterial activity of xanthobaccin A to other related tetramates, equesetin and ikarugamycin, were tested against *Bacillus subtilis*. All three tetramates had antimicrobial activity against *B. subtilis* with MIC values of 10, 0.62, 2.5 μg/ml for xanthobaccin A, equestin and ikarugamycin, respectively.

Next, we tested the ion-chelating activity of all three tetramates by adding ferric citrate to the solutions of tetramates, followed by HPLC analyses. However, it was hard to observe the corresponding stoichiometry under acidic conditions. Thus, commercially available tetramates equisetin and ikarugamycin were further analyzed for their iron complex under a neutral HPLC condition.

Through extracted ion chromatography, both Fe(III)(equisetin)$_3$ (m/z 1,171.5973 $[M + H]^+$, calc. 1,171.5993 for $C_{66}H_{90}N_3O_{12}Fe$, Δ 1.7 ppm) and Fe(III)(equisetin)$_2$ (m/z 798.3720 $[M + H]^+$, calc. $C_{44}H_{59}N_2O_8Fe$ 798.374, Δ 2.6 ppm) could be observed (**Figure 3**). It is not surprising since there are two different enolic tautomers of equisetin which lead to two or three complex structures. A higher electron density on the amide carbonyl compared to the carbonyl on the C-4 position could lead to the observation of a dominant stoichiometry under a neutral pH condition.

Different from equisetin, the relative larger tetramate ikarugamycin could form Fe(III)(ikarugamycin)$_2$ (m/z 1,008.4909 $[M + H]^+$, calc. $C_{58}H_{73}FeN_4O_8$ 1,008.4897, Δ 1.2 ppm) as the dominant iron complex (**Figure 3**). During the submission of the manuscript, another study (Yu et al., 2021) reported that HSAF could act as an iron-chelator with a similar chelating pattern. Also, the HSAF-mutant was less susceptible to oxidative stress (Yu et al., 2021).

We hypothesized that there is a similar scenario compared to the copper bis(tenuzonate) structure. Revisiting the former investigation of tenuazonic acid-Fe (III) complex revealed a similar observation, where ions derived from a loss of fragment radicals were detected (Lebrun et al., 1985). In the same investigation, a reduction process of Fe(III)(TA)3 to Fe(II)(TA)3 was proposed in the report (Lebrun et al., 1985). This led us to our hypothesis that the

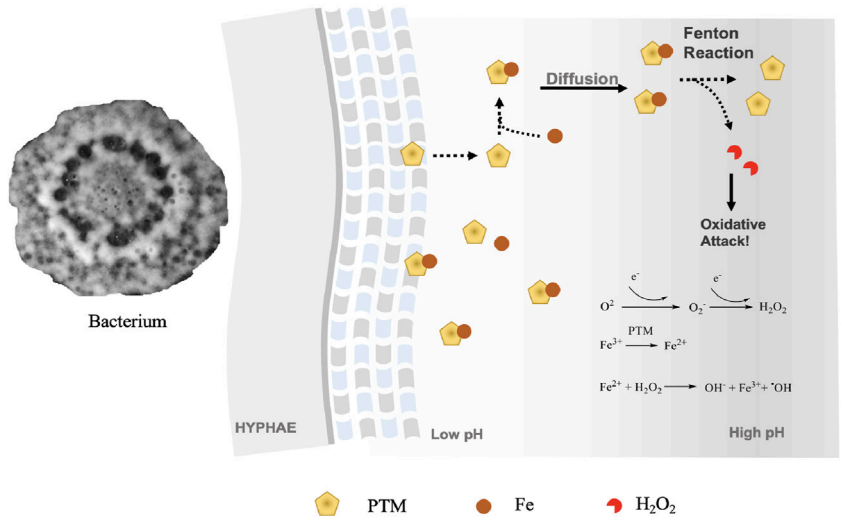

FIGURE 4 | Proposed mode-of-action of PTMs as metallophores and antibiotics. Bacteria secrete PTMs into extracellular environment. As the diffusion occurs and the pH lowers, PTMs start to reduce Fe^{3+} and initiate a Fenton's reaction. An oxidative attack could occur, where PTMs function as antibiotics.

Fenton chemistry follows the complexation of Fe(III) with tetramates.

To further address the function of tetramates, we studied the previous evidence from HSAF in *Candida albicans* IBT656, where a transcriptomics analysis was carried out. RNA-seq of PTM-treated *Candida albicans* revealed that HSAF triggered apoptosis *via* ROS-dependent pathway (Ding et al., 2016). However, the exact mechanism remains unknown.

Nevertheless, this evidence and the iron-chelating activity pointed to a possible link to Fenton chemistry, which describes the oxidative degradation of organic matter by hydrogen peroxide (H_2O_2) in the role of Fe^{2+} under acidic conditions, first discovered by H. J. Fenton in 1894. H_2O_2 is naturally produced by living organisms, from bacteria, algae to human phagocytic cells. Although H_2O_2 has limited reactivity, in the presence of Fe^{2+}, it can initiate a very strong reaction to produce high active hydroxyl radicals.

To clarify the iron-reducing activities, we carried out an iron-reducing experiment with ferrozine. As ferrozine forms a pink complex with iron II, which can be analyzed by a UV spectrometer, we determined the iron III reducing activity of the three tetramates using the ferrozine method. All tetramates showed positive results in the ferrozine test. Upon incubation of xanthobaccin A with ammonium iron III citrate and ferrozine, a ferrozine-iron II complex was detected by HPLC-HRMS, which showed a characteristic UV maximum absorption at 562 nm and formula of $C_{40}H_{28}FeN_8O_{12}S_4$ ($[M + H]^+$ m/z 995.0203, Δ-2.5ppm) (**Supplementary Figure S5**). This suggested the reduction of iron III to iron II by xanthobaccin A. It is likely that the complexation of xanthobaccin with iron II triggers Fenton chemistry (**Figure 4**) and produces reactive hydroxyl radicals as depicted in **Figure 4**. As expected, adding the radical scavenger vitamin C reduced the antibacterial effects of tetramates. After adding vitamin C, the inhibition zones were reduced from 23 to 18 mm for equisetin, and 7 to 6 mm for xanthobaccin A, respectively.

DISCUSSION

Many natural metallophores play important roles as virulence factors, signaling molecules, and regulators of oxidative stress (Johnstone and Nolan 2015). Among those metallophores with potent antimicrobial activities, tetramates could be novel potential antibiotics. Tetramic acids possessing a 3-acyl group are supposed to chelate trivalent metal ions (Markopoulos et al., 2010; Zaghouani and Nay 2016). A previous report demonstrated that anti-HIV (Miller et al., 1963), antibacterial, and antitumoral agent tenuazonic acid (Gitterman 1965) isolated from *Alternaria tenuis* could form copper salts (Rosett et al., 2015). Similarly, the antibacterial agent magnesidin from *Pseudomonas magnesiorubra* nov sp. could form metal complexes with Mg, Cu, Ni, and Fe (Kohl et al., 1974).

PTMs are an important emerging family of bioactive compounds described solely in bacteria. Their potential as an iron-chelator has, to our knowledge, not been investigated before, and we here, for the first time, demonstrated that PTMs are a group of bacterial metallophores. By an iron-reducing experiment with ferrozine, the data support that xanthobaccin A, equisestin, and ikarugamycin can induce Fenton chemistry, which could be alleviated by adding the radical scavenger vitamin C. The Fenton reaction *in vivo* appears to occur in the presence of catalytic ferrous iron, leading to the production of the most

reactive hydroxyl radicals in the biological system (Dizdaroglu 1991). The hydroxyl radical has a very short *in vivo* half-life of approximately 10^{-9} s and high reactivity (Sies 1993). It can damage virtually all types of macromolecules including carbohydrates, nucleic acids, lipids, and amino acids (Reiter et al., 1995). This makes it the most harmful free radical for the organism (Reiter et al., 1997).

Interestingly, microorganisms also use Fenton chemistry for defense, and besides tetramates, there are other examples. Co-cultivation of the model saprotrophic basidiomycete *Serpula lacrymans* with a ubiquitous terrestrial bacterium, either *Bacillus subtilis*, *Pseudomonas putida*, or *Streptomyces iranensis* could induce the production of the antibacterial compound atromentin (Tauber et al., 2016), a group of pigments that could trigger Fenton chemistry (Shah et al., 2015).

Since PTMs can be detected in both sugar beet rhizosphere soil and sponges (Nakayama, 1996; Capon et al., 1999), we hypothesize that higher organisms, can recruit bacterial PTM producers for a chemo-defense against other organisms. Given the metallophore and antibiotics activity, we propose that one potential ecological role of PTMs in the natural ecosystem is to chelate Fe^{3+} in the vicinity of hyphae at low pH, which restrains the reduction of Fe^{3+} and initiation of Fenton chemistry on-site (**Figure 4**). The piracy of neighboring Fe^{3+} causes the limitation of competing organisms. A decreasing gradient of tetramates concentration by diffusion away from the hyphae with subsequent increase in pH will result in the dissociation of Fe^{3+}-tetramate chelates, thus initiating a Fenton reaction for an oxidative attack. Given the wide existence and effective functions of Fenton chemistry in the ecosystem, tetramates producers might be developed as solutions for biocontrol against crop infections.

CONCLUSION

We isolated an antimicrobial agent xanthobaccin A from a sponge endosymbiont. For the first time, we demonstrated that bacterial PTMs can function as metallophores. Xanthobaccin A, equestin, and ikarugamycin exhibited antibacterial activity against *B. subtilis* and the effects could be alleviated by adding radical scavenger vitamin C. We demonstrated that all three tetramates could trigger Fenton chemistry, and this potentially explains why tetramates display broad biological activity. The isolation of PTMs from a sponge bacterial endophyte provides indirect evidence that the sponge-associated bacteria could be the true producers of sponge-derived PTMs. We propose that tetramates may function as a natural defense of niches by growth inhibition of other microbes via Fenton Chemistry. They could be potentially developed as effective antibiotics against drug-resistant pathogens (Samuni et al., 1983).

DATA AVAILABILITY STATEMENT

The original contributions presented in the study are included in the article/**Supplementary Material**, further inquiries can be directed to the corresponding author.

AUTHOR CONTRIBUTIONS

LD designed the experiments, S-DZ, AH, MB, and YG carried out lab experiment, TO commented on the manuscript, LD, S-DZ, and LG wrote the manuscript.

FUNDING

This work was supported by the Danish National Research Foundation DNRF137 for the Center for Microbial Secondary Metabolites CeMiSt.

ACKNOWLEDGMENTS

We thank Kasper Enemark-Rasmussen and Charlotte Held Gotfredsen for NMR measurements and Aaron John Christian Andersen for MS measurements.

SUPPLEMENTARY MATERIAL

The Supplementary Material for this article can be found online at: https://www.frontiersin.org/articles/10.3389/fchem.2021.772858/full#supplementary-material

REFERENCES

Blin, K., Shaw, S., Steinke, K., Villebro, R., Ziemert, N., Lee, S. Y., et al. (2019). AntiSMASH 5.0: Updates to the Secondary Metabolite Genome Mining Pipeline. *Nucleic Acids Res.* 47, W81–W87. doi:10.1093/nar/gkz310

Blodgett, J. A. V., Oh, D.-C., Cao, S., Currie, C. R., Kolter, R., and Clardy, J. (2010). Common Biosynthetic Origins for Polycyclic Tetramate Macrolactams from Phylogenetically Diverse Bacteria. *Proc. Natl. Acad. Sci.* 107, 11692–11697. doi:10.1073/pnas.1001513107

Boratyn, G. M., Camacho, C., Cooper, P. S., Coulouris, G., Fong, A., Ma, N., et al. (2013). BLAST: a More Efficient Report with Usability Improvements. *Nucleic Acids Res.* 41, W29–W33. doi:10.1093/nar/gkt282

Capon, R, J., Skene, C., Lacey, E., Gill, J. H., Wadsworth, D., and Friedel, T. (1999). Geodin A Magnesium Salt: A Novel Nematocide from a Southern Australian marine Sponge. *Geodia. J. Nat. Prod.* 62, 1256–1259. doi:10.1021/np990144v

Cooper, M. A., and Shlaes, D. (2011). Fix the Antibiotics Pipeline. *Nature* 472, 32. doi:10.1038/472032a

Dandawate, P., Padhye, S., Schobert, R., and Biersack, B. (2019). Discovery of Natural Products with Metal-Binding Properties as Promising Antibacterial Agents. *Expert Opin. Drug Discov.* 14, 563–576. doi:10.1080/17460441.2019.1593367

Dhaneesha, M., Hasin, O., Sivakumar, K. C., Ravinesh, R., Naman, C. B., Carmeli, S., et al. (2019). DNA Binding and Molecular Dynamic Studies of Polycyclic Tetramate Macrolactams (PTM) with Potential Anticancer Activity Isolated from a Sponge-Associated *Streptomyces Zhaozhouensis*

Subsp. Mycale Subsp. Nov. *Mar. Biotechnol.* 21, 124–137. doi:10.1007/s10126-018-9866-9

Ding, Y., Li, Z., Li, Y., Lu, C., Wang, H., Shen, Y., et al. (2016). HSAF-induced Antifungal Effects in *Candida Albicans* through ROS-Mediated Apoptosis. *RSC Adv.* 6, 30895–30904. doi:10.1039/C5RA26092B

Dippenaar, A., Holzapfel, C. W., and Boeyens, J. C. A. (1977). Crystal Structure of Copper Bis(tenuazonate) Monohydrate. *J. Cryst. Mol. Struct.* 7, 189–197. doi:10.1007/BF01371471

Dizdaroglu, M. (1991). Chemical Determination of Free Radical-Induced Damage to DNA. *Free Radic. Biol. Med.* 10, 225–242. doi:10.1016/0891-5849(91)90080-M

Gitterman, C. O. (1965). Antitumor, Cytotoxic, and Antibacterial Activities of Tenuazonic Acid and Congeneric Tetramic Acids. *J. Med. Chem.* 8, 483–486. doi:10.1021/jm00328a015

Hashidoko, Y., Nakayama, T., Homma, Y., and Tahara, S. (1999). Structure Elucidation of Xanthobaccin A, a New Antibiotic Produced from *Stenotrophomonas* Sp. Strain SB-K88. *Tetrahedron Lett.* 40, 2957–2960. doi:10.1016/S0040-4039(99)00336-6

Johnstone, T. C., and Nolan, E. M. (2015). Beyond Iron: Non-classical Biological Functions of Bacterial Siderophores. *Dalt Trans.* 44, 6320–6339. doi:10.1039/c4dt03559c

Jomon, K., Kuroda, Y., Ajisaka, M., and Sakai, H. (2012). A New Antibiotic, Ikarugamycin. *J. Antibiot.* 25, 271–280. doi:10.7164/antibiotics.25.271

Kohl, H., Bhat, S. V., Patell, J. R., Gandhi, N. M., Nazareth, J., Divekar, P. V., et al. (1974). Structure of Magnisidin, a New Magnesium-Containing Antibiotic from *Pseudomonas Magnesiorubra*. *Tetrahedron Lett.* 15, 983–986. doi:10.1016/S0040-4039(01)82385-6

Laatsch, H. (2012). *Antibase Version 4.0 - the Natural Compound Identifier*. KGaA, Weinheim: Wiley VCH.

Lebrun, M. H., Duvert, P., Gaudemer, F., Gaudemer, A., Deballon, C., and Boucly, P. (1985). Complexation of the Fungal Metabolite Tenuazonic Acid with Copper (II), Iron (III), Nickel (II), and Magnesium (II) Ions. *J. Inorg. Biochem.* 24, 167–181. doi:10.1016/0162-0134(85)85001-7

Luo, Y., Huang, H., Liang, J., Wang, M., Lu, L., Shao, Z., et al. (2013). Activation and Characterization of a Cryptic Polycyclic Tetramate Macrolactam Biosynthetic Gene Cluster. *Nat. Commun.* 4, 2894. doi:10.1038/ncomms3894

Markopoulos, J., Athanasellis, G., and Igglessi-Markopoulou, O. (2010). Tetramic and Tetronic Acids as Scaffolds in Bioinorganic and Bioorganic Chemistry. *Bioinorg Chem. Appl.*, 2010, 315056. doi:10.1155/2010/315056

Miller, F. A., Rightsel, W. A., Sloan, B. J., Ehrlich, J., French, J. C., Bartz, Q. R., et al. (1963). Antiviral Activity of Tenuazonic Acid. *Nature* 200, 1338–1339. doi:10.1038/2001338a0

Nakayama, T. (1996). *Chemical Study on Biological Control of Sugar Beet Damping-Off Disease (Jpn)*. Hokkaido: Hokkaido University.

National Committee for Clinical Laboratory Standards (1997). *Methods for Dilution Antimicrobial Susceptibility Tests for Bacteria that Grow Aerobically, Approved Standard. NCCLS Document M7-A4*. 4th ed. (Villanova, PA: Clinical and Laboratory Standards Institute, National Committee for Clinical Laboratory Standards), 26.

Newman, D. J., and Cragg, G. M. (2020). Natural Products as Sources of New Drugs over the Nearly Four Decades from 01/1981 to 09/2019. *J. Nat. Prod.* 83, 770–803. doi:10.1021/acs.jnatprod.9b01285

Reiter, R. J., Carneiro, R. C., and Oh, C. S. (1997). Melatonin in Relation to Cellular Antioxidative Defense Mechanisms. *Horm. Metab. Res.* 29, 363–372. doi:10.1055/s-2007-979057

Reiter, R. J., Melchiorri, D., Sewerynek, E., Poeggeler, B., Barlow-Walden, L., Chuang, J., et al. (1995). A Review of the Evidence Supporting Melatonin's Role as an Antioxidant. *J. Pineal Res.* 18 (1), 1–11. doi:10.1111/j.1600-079X.1995.tb00133.x

Rosett, T., Sankhala, R. H., Stickings, C. E., Taylor, M. E. U., and Thomas, R. (2015). Studies in the Biochemistry of Micro-organisms. 103. Metabolites of *Alternaria Tenuis* Auct.: Culture Filtrate Products. *Biochem. J.* 67 (3), 390–400. doi:10.1042/bj0670390

Samuni, A., Aronovitch, J., Godinger, D., Chevion, M., and Czapski, G. (1983). On the Cytotoxicity of Vitamin C and Metal Ions: A Site-specific Fenton Mechanism. *Eur. J. Biochem.* 137, 119–124. doi:10.1111/j.1432-1033.1983.tb07804.x

Shah, F., Schwenk, D., Nicolás, C., Persson, P., Hoffmeister, D., and Tunlid, A. (2015). Involutin Is an Fe^{3+} Reductant Secreted by the Ectomycorrhizal Fungus *Paxillus Involutus* during Fenton-based Decomposition of Organic Matter. *Appl. Environ. Microbiol.* 81, 8427–8433. doi:10.1128/aem.02312-15

Sies, H. (1993). Strategies of Antioxidant Defense. *Eur. J. Biochem.* 215, 213–219. doi:10.1111/j.1432-1033.1993.tb18025.x

Steyn, P. S., and Rabie, C. J. (1976). Characterization of Magnesium and Calcium Tenuazonate from P*homa Sorghina*. *Phytochemistry* 15, 1977–1979. doi:10.1016/S0031-9422(00)88860-3

Stickings, C. E. (1959). Studies in the Biochemistry of Micro-organisms. 106. Metabolites of *Alternaria Tenuis* auct.: the Structure of Tenuazonic Acid. *Biochem. J.* 72, 332–340. doi:10.1042/bj0720332

Tauber, J. P., Schroeckh, V., Shelest, E., Brakhage, A. A., and Hoffmeister, D. (2016). Bacteria Induce Pigment Formation in the Basidiomycete *Serpula lacrymans*. *Environ. Microbiol.* 18, 5218–5227. doi:10.1111/1462-2920.13558

Vesonder, R. F., Tjarks, L. W., Rohwedder, W. K., Burmeister, H. R., and Laugal, J. A. (1979). Equisetin, an Antibiotic from *Fusarium Equiseti* NRRL 5537, Identified as a Derivative of *N*-Methyl-2,4-Pyrollidone. *J. Antibiot.* 32, 759–761. doi:10.7164/antibiotics.32.759

Yu, F., Zaleta-Rivera, K., Zhu, X., Huffman, J., Millet, J. C., Harris, S. D., et al. (2007). Structure and Biosynthesis of Heat-Stable Antifungal Factor (HSAF), a Broad-Spectrum Antimycotic with a Novel Mode of Action. *Antimicrob. Agents Chemother.* 51, 64–72. doi:10.1128/AAC.00931-06

Yu, L., Li, H., Zhou, Z., Liu, F., and Du, L. (2021). An Antifungal Polycyclic Tetramate Macrolactam, Heat-Stable Antifungal Factor (HSAF), Is a Novel Oxidative Stress Modulator in *Lysobacter Enzymogenes*. *Appl. Environ. Microbiol.* 87, e03105. doi:10.1128/AEM.03105-20

Zaghouani, M., and Nay, B. (2016). 3-Acylated Tetramic and Tetronic Acids as Natural Metal Binders: Myth or Reality? *Nat. Prod. Rep.* 33, 540–548. doi:10.1039/c5np00144g

Zhang, H., Zheng, W., Huang, J., Luo, H., Jin, Y., Zhang, W., et al. (2006). *Actinoalloteichus Hymeniacidonis* Sp. nov., an Actinomycete Isolated from the marine Sponge *Hymeniacidon Perleve*. *Int. J. Syst. Evol. Microbiol.* 56, 2309–2312. doi:10.1099/ijs.0.64217-0

Conflict of Interest: The authors declare that the research was conducted in the absence of any commercial or financial relationships that could be construed as a potential conflict of interest.

Publisher's Note: All claims expressed in this article are solely those of the authors and do not necessarily represent those of their affiliated organizations, or those of the publisher, the editors, and the reviewers. Any product that may be evaluated in this article or claim that may be made by its manufacturer is not guaranteed or endorsed by the publisher.

frontiers in Chemistry

ORIGINAL RESEARCH
published: 19 November 2021
doi: 10.3389/fchem.2021.755351

Diaportones A–C: Three New Metabolites From Endophytic Fungus *Diaporthe foeniculina* BZM-15

Fenghua Kang[1,2†], Xiuxiang Lu[3†], Sha Zhang[1,2], Dekun Chen[1,2], Min Kuang[1,2], Weiwei Peng[1,2], Jianbing Tan[1,2], Kangping Xu[1,2], Zhenxing Zou[1,2] and Haibo Tan[1,2,3*]*

[1]Xiangya School of Pharmaceutical Sciences, Central South University, Changsha, China, [2]Hunan Key Laboratory of Diagnostic and Therapeutic Drug Research for Chronic Diseases, Central South University, Changsha, China, [3]South China Botanical Garden, Chinese Academy of Sciences, Guangzhou, China

Phytochemical investigation of *Diaporthe foeniculina* BZM-15 led to one new γ-butyrolactone derivative, diaportone A (**1**), one cyclopentenone derivative, diaportone B (**3**), and one monoterpene derivative, diaportone C (**5**), along with six known compounds (**2**, **4**, and **6–9**). Their structures as well as the absolute configurations were characterized by means of NMR, HRESIMS, and ECD spectroscopy and quantum chemistry calculation, respectively. Furthermore, all compounds were evaluated for their cytotoxic activity and antibacterial activity, and compounds **7** and **8** displayed significant antiproliferative effects on three human cancer cell lines (SF-268, MCF-7, and HepG2) with IC_{50} values ranging from 3.6 to 15.8 μM.

Keywords: endophytic fungus, *Diaporthe foeniculina*, *Leptospermum brachyandrum*, diaportone, structure elucidation, cytotoxicity

OPEN ACCESS

Edited by:
Yuanyuan Lu,
China Pharmaceutical University, China

Reviewed by:
Weaam Ebrahim,
Mansoura University, Egypt
Hui Zou,
Hunan Normal University, China

***Correspondence:**
Zhenxing Zou
zouzhenxing@csu.edu.cn
Haibo Tan
tanhaibo@scbg.ac.cn

[†]*These authors contributed equally to this work*

Specialty section:
This article was submitted to Organic Chemistry, a section of the journal Frontiers in Chemistry

Received: *08 August 2021*
Accepted: *27 September 2021*
Published: *19 November 2021*

Citation:
Kang F, Lu X, Zhang S, Chen D, Kuang M, Peng W, Tan J, Xu K, Zou Z and Tan H (2021) Diaportones A–C: Three New Metabolites From Endophytic Fungus Diaporthe foeniculina *BZM-15. Front. Chem. 9:755351. doi: 10.3389/fchem.2021.755351*

INTRODUCTION

Fungi are prolific producers of bioactive secondary metabolites and have contributed to improvements in human and animal health in spectacular and indispensable ways (Bills and Gloer, 2016; El-Elimat et al., 2021). They are ubiquitous in nature and often provide nutrients or protection for the host (Wani et al., 2015). Many endophytic fungi produce compounds with a novel structure and specific bioactivity for their long period of living in host tissues, which have been potential resources for novel compounds and new drugs (Jia et al., 2016; Kaul et al., 2012). *Leptospermum brachyandrum* is a famous ornamental and medicinal plant that belongs to the *Myrtaceae* family. In our previous research, three endophytes were isolated from this plant, such as *Diaporthe foeniculina*, *Eutypella scoparia*, and *Rhytidhysteron* sp., and a number of novel natural products with antibacterial or cytotoxic activity have been discovered from these endophytes (Zhang et al., 2021a; Zhang et al., 2021b; Zhang et al., 2020; Zhang et al., 2021). Simultaneously, five new 2-pyrones were isolated from *D. foeniculina* (Yu et al., 2021). With the aim of seeking new bioactive natural products from medicinal plant endophytes, chemical investigation of strain *D. foeniculina* BZM-15 was further researched and afforded to find three new metabolites, including one γ-butyrolactone derivative, diaportone A (**1**), one cyclopentenone derivative, diaportone B (**3**), and one monoterpene, diaportone C (**5**), along with six known compounds, colletolides A (**2**) (Li et al., 2019), phomotenone (**4**) (Ahmed et al., 2011), altiloxin B (**6**) (Hemberger et al., 2013), dankasterone A (**7**) (Jiao et al., 2015), 14α-hydroxyergosta-4,7,22-triene-3,6-dione (**8**) (Liu et al., 2018), and fortisterol (**9**) (Kitchawalitet al., 2014) (**Figure 1**). Herein, this report describes the isolation, structural elucidation, and biological activity of compounds **1–9**.

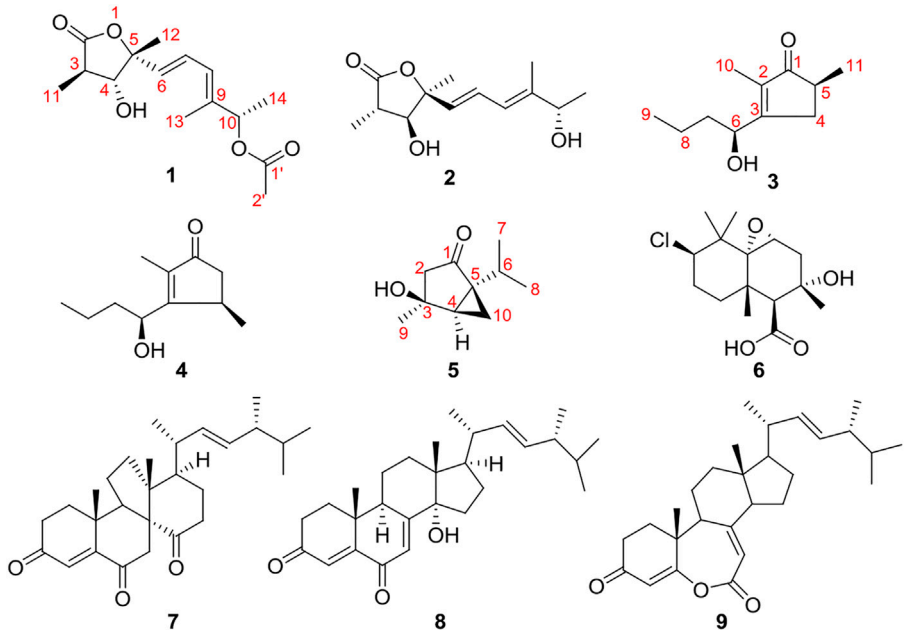

FIGURE 1 | Chemical structures of compounds **1–9**.

MATERIALS AND METHODS

General Experimental Procedures

Optical rotations were measured using an Anton Paar MCP-500 spectropolarimeter (Anton Paar, Graz, Austria). The NMR spectra were recorded on a Bruker Avance-500 spectrometer (Bruker Corporation, Fällanden, Switzerland) with TMS as an internal reference. Experimental ECD spectra in MeOH were acquired in a quartz cuvette of 1 mm optical path length on an Applied Photophysics Chirascan spectrometer. HRESIMS spectra were obtained in a Thermo MAT95XP high-resolution mass spectrometer (Thermo Fisher Scientific, Bremen, Germany). Preparative HPLC was performed on an Agilent 1260 Infinity system equipped with a DAD detector using a preparative YMC ODS C_{18} column (20 × 250 mm, 5 μm). Column chromatography was performed using silica gel (200–300 mesh, Qingdao Marine Chemical Inc., Qingdao, China) and Sephadex LH-20 gel (Pharmacia Fine Chemical Co. Ltd., Sweden). Thin-layer chromatography (TLC) was carried out on silica gel plates (Merck KGaA, Darmstadt, Germany) using various solvent systems. All solvents were purchased from Guangzhou Chemical Reagent Company, Ltd. (Guangzhou, China).

Cultivation and Culture Extraction

The fungus *D. foeniculina* BZM-15 was isolated from the plant *Leptospermum brachyandrum*, which was collected from South China Botanical Garden (SCBG), Chinese Academy of Sciences, China, in September 2016. The strain was identified as *D. foeniculina* according to the sequence analysis of rDNA ITS (internal transcribed spacer) region, which has been submitted to GenBank with the accession number of MN788609. The strain was deposited in the Laboratory of Natural Product Medicinal Chemistry, SCBG.

The fungus *D. foeniculina* BZM-15 was incubated in 200 ml of potato dextrose broth at 30°C on a rotary shaker (120 rpm) for 7 days to acquire the seed broth. Large-scale fermentation was carried out in Erlenmeyer flasks (16 × 3 L); each contained rice (200 g) and distilled water (300 ml), which were autoclaved at 121 °C for 25 min. After cooling at room temperature, seed broth was added to those Erlenmeyer flasks, which were fermented for 30 days at 28°C. After cultivation, the obtained mycelial solid medium was extracted with EtOAc (three times, 24 h for every time) at room temperature, and the extract solution was concentrated *in vacuo* to receive a crude extract (50 g).

Isolation of Compounds 1–9

The crude extract was fractionated by silica gel column chromatography ((CC) (PE-EtOAc v/v, 100:1-0:100)) to afford six main fractions (Fr.1–Fr.6). Fr.5 (7.22 g) was divided into ODS CC and eluted with MeOH-H_2O (v/v, 40–100%) to give six subfractions (Fr.5-1 to Fr.5-6). Fr.5-2 (1.94 g) was separated by Sephadex LH-20 CC, eluting with $CHCl_3$-MeOH (v/v, 1:1) to provide five subfractions (Fr.5-2-1 to Fr.5-2-5). Fr.5-2-2 (1.23 g) was chromatographed using CC on silica gel, eluted with $CHCl_3$-MeOH (v/v, 100:0-0:100), and then further purified by semipreparative HPLC with CH_3CN-H_2O (40: 60) to give compound **5** (4.0 mg). Compound **6** (5.3 mg) was obtained from Fr.5-2-3 on a semipreparative HPLC with CH_3CN-H_2O (35:65). Fr.5-3 (405.0 mg) was separated by Sephadex LH-20 CC, eluting with $CHCl_3$-MeOH (v/v, 1:1) to provide five subfractions (Fr.5-3-1 to Fr.5-3-5). Fr.5-3-1 (211.4 mg) was isolated by column chromatography on silica gel and eluted with $CHCl_3$-MeOH (v/v, 10:1-0:1) to get three fractions (Fr.5-3-1-1 to Fr.5-3-1-3). Fr.5-3-1-2 (11.4 mg) was then subjected to semipreparative HPLC with

TABLE 1 | ^{1}H (500 MHz) and ^{13}C (125 MHz) NMR spectral data of compound **1** in CD_3OD.

No	δ_H (*J* in Hz)	δ_C, type	No	δ_H (*J* in Hz)	δ_C, type
2	—	178.5, C	10	5.25, q (7.0)	76.4, CH
3	2.48, s	42.6, CH	11	1.22, d (7.0)	12.4, CH_3
4	3.80, d (10.5)	82.5, CH	12	1.51, s	25.2, CH_3
5	—	86.6, C	13	1.76, s	12.7, CH_3
6	5.92, d (15.5)	133.3, CH	14	1.34, d (6.5)	19.4, CH_3
7	6.48, dd (15.5, 10.5)	126.4, CH	1′	—	172.2, C
8	6.10, d (10.5)	126.1, CH	2′	2.03, s	21.1, CH_3
9	—	139.2, C	—	—	—

CH_3CN-H_2O (v/v, 50:50) to afford compounds **1** (8.0 mg) and **2** (6.1 mg). Fr.5-3-2 (80.3 mg) was separated by semipreparative HPLC with CH_3CN-H_2O (v/v, 50:50) to afford compounds **3** (3.9 mg) and **4** (4.3 mg).

Fr.3 (3.2 g) was subjected to CC on silica gel eluted with a gradient system of PE-EtOAc (v/v, 20:0–0:100) to afford five fractions (Fr.3-1 to Fr.3-5). Fr.3-2 (890 mg) was separated on a Sephadex LH-20 column with MeOH and then separated by preparative HPLC using CH_3CN-H_2O (80:20) to provide compounds **7** (5.8 mg) and **9** (4.4 mg). Fr.3-3 (635 mg) was purified by silica gel CC and eluted with a gradient system of CH_2Cl_2-MeOH (v/v, 100:0–0:100) to provide compound **8** (10.3 mg).

*Diaportone A (**1**)*: colorless oil; $[\alpha]_D^{25}$ – 3.7 (*c* 1.0, MeOH); UV (MeOH): λ_{max} (log ε): 238 (3.27) nm; IR ν_{max}: 3,325 and 1,635, 667 cm^{-1}; HRESIMS: *m/z* 305.1361 [M + Na] $^+$ (calcd for $C_{15}H_{22}NaO_5$, 305.1359). ^1H (500 MHz); and ^{13}C (125 MHz) NMR data, see **Table 1**.

*Diaportone B (**3**)*: yellow oil; $[\alpha]_D^{25}$ + 14.5 (*c* 0.8, MeOH); UV (MeOH): λ_{max} (log ε): 236 (3.07) nm; IR ν_{max}: 3,415, 2,960, 2,931, 2,872, 1,681, 1,639, 1,456, 1,381, 1,336, 1,172, and 1,026 cm^{-1}; HRESIMS: *m/z* 205.1206 [M + Na] $^+$ (calcd for $C_{11}H_{18}NaO_2$, 205.1199). ^1H (500 MHz); and ^{13}C (125 MHz) NMR data, see **Table 2**.

*Diaportone C (**5**)*: white solid; $[\alpha]_D^{25}$ + 10.3 (*c* 0.5, MeOH); UV (MeOH): λ_{max} (log ε): 200 (2.59) nm, 273 (1.39) nm; IR ν_{max}: 3,431, 1962, 2,873, 1708, 1,458, 1,375, 1,259, 1,182, 1,130, 1032,999,945, 758, and 682 cm^{-1}; HRESIMS: *m/z* 191.1051 [M + Na] $^+$ (calcd for $C_{10}H_{16}NaO_2$, 191.1043). ^1H (500 MHz); and ^{13}C (125 MHz) NMR data, see **Table 2**.

ECD Calculation Methods

The ECD spectra of compounds **1**, **3**, and **5** were calculated by using the Gaussian09 package (Frisch et al., 2016). Each of their configuration was optimized at the B3LYP-D3(BJ)/TZVP (IEFPCM) level of theory. The theoretic ECD spectra were calculated on the mPW1PW91/6-311G* (IEFPCM) level of theory and Boltzmann average was calculated for the spectra according to Gibbs free energy. SpecDis v1.71 was used to simulate an ECD curve with a sigma/gamma value of 0.3 eV^2 (Bruhn et al., 2013). The calculated ECD curves of compounds **1** and **3** were red shifted and blue shifted by 5 nm, respectively.

TABLE 2 | ^{1}H (500 MHz) and ^{13}C (125 MHz) NMR spectral data of compounds **3** and **5** in acetone-d_6.

No	3		5	
	δ_H (*J* in Hz)	δ_C, type	δ_H (*J* in Hz)	δ_C, type
1	—	212.2, C	—	210.6, C
2	—	134.4, C	1.88, d (17.0) 2.36, m	49.1, CH_2
3	—	173.7, C	—	71.7, C
4	2.08, m 2.98, m	34.8, CH_2	1.97, dd (7.5, 4.0)	38.4, CH
5	2.25, m	39.9, CH	—	46.1, C
6	4.75, dd (8.0, 5.5)	69.5, CH	1.88, m	27.2, CH
7	1.53, m 1.69, m	38.7 CH_2	0.95, d (7.0)	20.0, CH_3
8	1.35, m 1.45, m	19.6, CH_2	0.91, d (7.0)	19.6, CH_3
9	0.93, t (7.0)	14.6, CH_3	1.37, s	29.9, CH_3
10	1.65, s	8.7, CH_3	1.10, ddd (7.5, 5.0, 1.5) 1.36, dd (5.0, 4.5)	16.6, CH_2
11	1.08, d (7.5)	17.2, CH_3	—	—

Antibacterial Assay

Antibacterial activity of all compounds against MRSA (JCSC 3063) and *E. coli* (ATCC 8739) was tested by the broth macrodilution method on 96-well plates according to the CLSI recommendation (Li et al., 2014). Vancomycin (MIC = 1.25 μg/ml) was used as a positive control.

Cytotoxicity Assay

The cytotoxicity of all compounds against three human tumor cell lines, SF-268 (CNS cancer), MCF-7 (breast cancer), and HepG2 (hepatoma cancer), and normal cell line LX-2 was tested using the MTT assay. Adriamycin was used as a positive control. All cells were seeded into 96-well plates at 5×10^4 cells/ml and incubated at 37°C under a 5% CO_2 atmosphere for 24 h. Then, the tested compounds were added. After 72 h, MTT solution was added into each well, which was further incubated. The cell-free supernatant was removed and formazan crystals were subsequently dissolved in DMSO. Optical density (OD) was recorded at 490 nm on a microplate reader to calculate the IC_{50} values.

RESULTS AND DISCUSSION

Compound **1** was isolated as colorless oil and assigned the molecular formula $C_{15}H_{22}O_5$ as inferred from its HRESIMS ion peak at *m/z* 305.1361 [M + Na] $^+$ (calcd 305.1359 for $C_{15}H_{22}NaO_5$). The ^1H NMR spectral data (**Table 1**), in combination with the HSQC spectrum, displayed two ester carbonyl groups [δ_C 178.5 (C-2) and 172.2 (C-1′)], one conjugated diene [δ_H 5.92 (H-6), 6.48 (H-7), and 6.10 (H-8); δ_C 133.3 (C-6), 126.4 (C-7), 126.1 (C-8), and 139.2 (C-9)], two oxygenated methines [δ_H 5.25 (H-10) and 3.80 (H-4); δ_C 76.4 (C-10) and 82.5 (C-4)], one methine [δ_H 2.48 (H-3); δ_C 42.6 (C-3)], one oxygen quaternary carbon [δ_C 86.6 (C-5)], and five methyl groups [δ_H 1.22 (H-11), 1.51 (H-12), 1.76 (H-13), 1.31 (H-14),

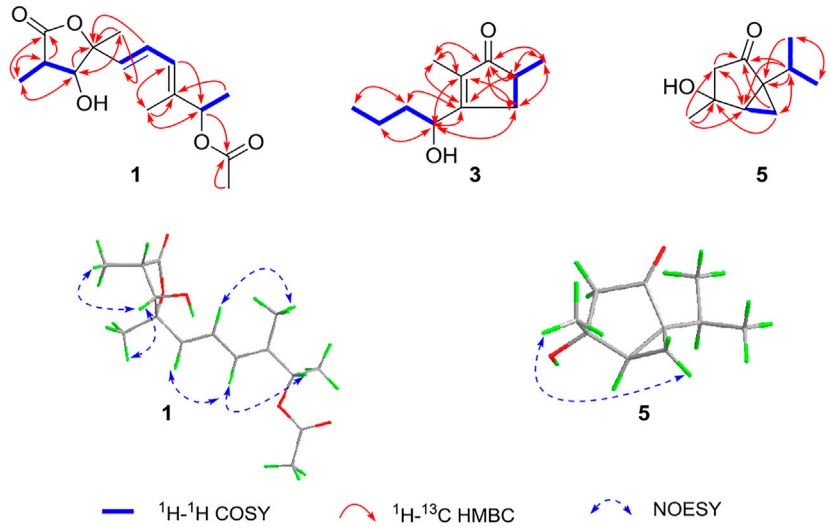

FIGURE 2 | ^{1}H-^{1}H COSY, Key HMBC, and NOESY correlations of compounds **1**, **3**, and **5**.

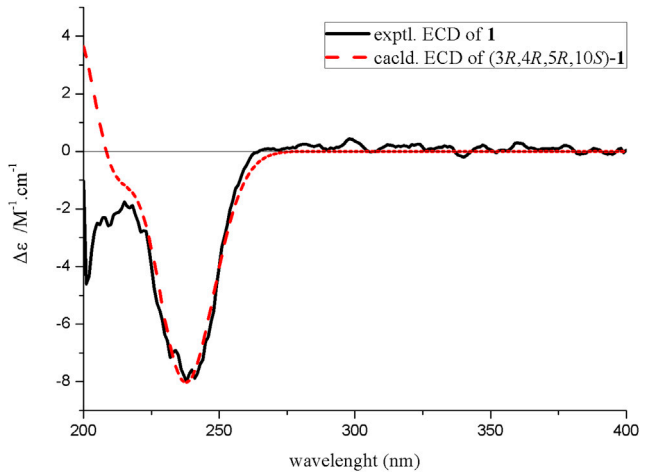

FIGURE 3 | Experimental and calculated ECD spectra of compound **1**.

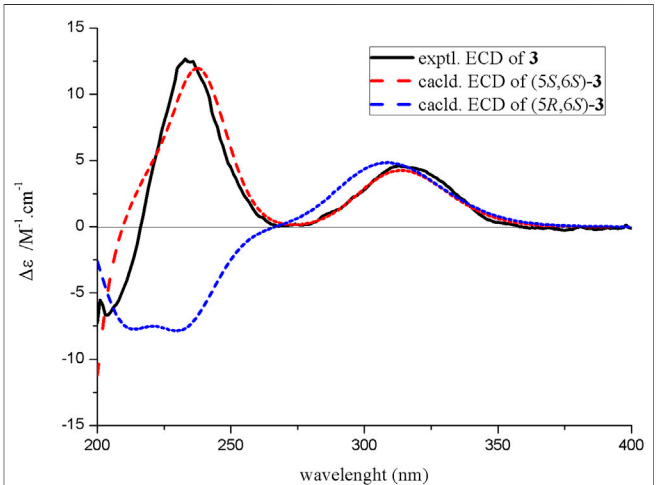

FIGURE 4 | Experimental and calculated ECD spectra of compound **3**.

and δ_H 2.03 (H-2′); δ_C 12.4 (C-11), 25.2 (C-12), 12.7 (C-13), 19.4 (C-14), and 21.1 (C-2′)].

Compared to the NMR spectra of compound **2** (**Table 1**), they shared a typical γ-butyrolactone ring bearing two methyl groups at C-3 and C-5 and a hydroxyl group at C-4. However, the spectra of compound **1** exhibited additional signals for the acetyl group, which was connected with 10-OH to form an ester. This conclusion can be proved by the correlations of H-10 with C-1′ in the HMBC spectrum. Thus, the planar structure of compound **1** was elucidated, as shown in **Figure 1**.

The relative configuration was determined by NOESY spectrum and coupling constants. The NOE correlations of H-11/H-4/H-12 indicated that 11-H_3, 4-H, and 12-H_3 were on the same side of the lactone ring. A conjugated diene moiety was determined by the large coupling constant J = 15.5 Hz between H-6 and H-7 that was *trans*-oriented and J = 10.5 Hz between H-7 and H-8 that was *cis*-oriented. In addition, the *E* confirmation of 8,9-diene was deduced from the NOE cross peaks of H-6/H-8/H-10 and H_3-13/H-7 (**Figure 2**). The chiral HPLC analysis of compound **1** revealed that it should be optically pure. The calculated ECD spectrum was consistent with its experimental ECD spectrum, suggesting the absolute configuration of compound **1** as 3*R*,4*R*,5*R*,10*S* (**Figure 3**). Thus, the structure of compound **1** was determined as a new γ-butyrolactone derivative with 6,8-hexadien-1-ol,1-acetate side chain and was named diaportone A. Notably, diaportone A possess conjugated double bond, which might be light sensitive. Moreover, it might be an artificial compound generated from the known compound **2** through acylation, although much more evidence was needed.

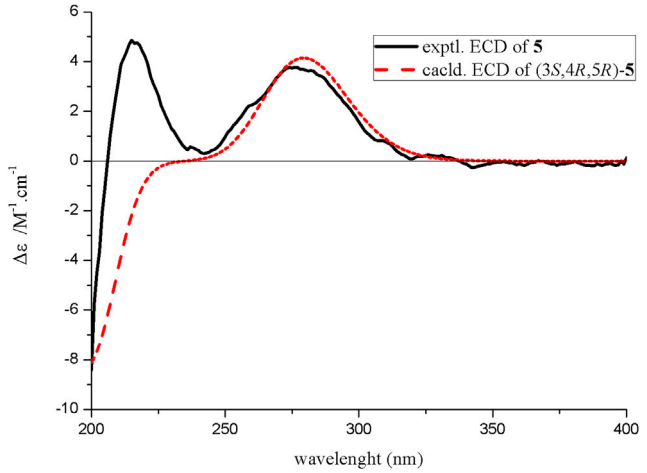

FIGURE 5 | Experimental and calculated ECD spectra of compound **5**.

Compound **3** was isolated as yellow oil. It was determined to have a molecular formula of $C_{11}H_{18}O_2$ by a combination of its HRESIMS ion peak at *m/z* 183.1388 $[M + H]^+$ (calcd 182.1307 for $C_{11}H_{19}O_2$). The ^1H and ^{13}C NMR spectroscopic data (**Table 2**) of compound **3** exhibited characteristic signals assignable to a conjugated ketone carbonyl, a tetrasubstituted olefin, two methines (one oxygenated), three methylene groups, and three methyl groups. A detailed analysis of the NMR data exhibited that compound **3** was similar to the known compound **4** (Ahmed et al., 2011) (**Table 2**) with the only difference in compound **3** being the substitution position of CH_3-11, which was deduced based on the HMBC cross peaks of H_3-11 (δ_H 1.08)/C-1 (δ_C 212.2), C-5 (δ_C 39.9), and C-4 (δ_C 34.8) (**Figure 2**). The absolute configuration of compound **3** was confirmed by the similarity between the calculated ECD curve of 5*S*,6*S* and its experimental ECD spectrum (**Figure 4**). Therefore, the structure of compound **3**, diaportone B, was defined as shown.

Compound **5** was isolated as a white solid. The molecular formula $C_{10}H_{16}O_2$ was determined by the HRESIMS ion peak at *m/z* 169.1224 $[M + H]^+$ (calcd 169.1229 for $C_{10}H_{17}O_2$). The 1D NMR data (**Table 2**) of compound **5** exhibited three methyl groups, two methylene groups, two methines, two sp^3 nonprotonated carbons (one oxygenated), and one ketone carbonyl. Comparison of NMR data with those of dihydroxysabinane (Lin et al., 2009) revealed a high degree of similarity skeleton, where the only obvious difference is in the presence of a carbonyl group at C-1 in compound **5** instead of a hydroxyl group in dihydroxysabinane. This deduction was confirmed by the HMBC correlations of C-1 with H-2 (δ_H 1.88 and 2.36), H-6 (δ_H 1.88), and H-10 (δ_H 1.36 and 1.10) and obvious low-field chemical shift of C-1 (δ_C 210.9) (**Figure 2**).

The relative configuration of compound **5** was determined by the analysis of ROESY spectral data (**Figure 2**). The methylene (CH_2-10) and the hydroxyl groups at the chiral carbons (C-3) were assigned as β-oriented and the methyl groups (CH_3-9) and the methine (CH-6) should be α-oriented due to the presence of the ROESY correlation of H-4 with H_3-9. The above data supported the presence of two possible enantiomers (3*S*,4*R*,5*R*)-**5** and (3*R*,4*S*,5*S*)-**5**. To determine the absolute configuration of compound **5**, the ECD calculation was performed. Its experimental ECD spectrum of compound **5** was in good agreement with the calculated ECD spectrum for 3*S*,4*R*,5*R* (**Figure 5**). Therefore, the structure of compound **5** was determined and given the trivial name diaportone C.

TABLE 3 | Cytotoxicity of compounds **1–9** against three human cancer cell lines.

Compounds	IC_{50}[a] (μM)				SI Values[b]
	SF268	MCF-7	HepG2	LX-2	
1–6, **9**	> 40	> 40	> 40	> 40	NA
7	6.7 ± 0.7	3.6 ± 1.1	4.9 ± 0.9	> 40	> 6
8	8.3 ± 0.5	11.4 ± 0.3	15.8 ± 1.3	> 40	> 5
Adriamycin[c]	1.9 ± 0.03	1.5 ± 0.01	2.2 ± 0.03	> 40	> 21

[a]*Results are the mean ± SD (n = 3).*
[b]*Safety index (SI) value = IC_{50} for LX-2 cell line/IC_{50} for SF286 cell line.*
[c]*Positive control.*
NA, not active.

Finally, the cytotoxic activities of all compounds inhibited three human cancer cell lines (SF-268, MCF-7, and HepG2), and antibacterial activities against MRSA and *E. coli* were evaluated. As show in **Table 3**, compounds **7** and **8** showed different potency of cytotoxicity against the three cell lines, with IC_{50} values ranging from 3.6 to 15.8 μM, whereas they were not active on the normal cell line LX-2. Unfortunately, none of the compounds showed any antibacterial activities against MRSA and *E. coli* at a concentration of 100 μg/ml.

CONCLUSION

A phytochemical investigation into *D. foeniculina* BZM-15 resulted in the isolation and structural elucidation of three undescribed and six known compounds. Their structures including absolute configurations were determined by extensive physicochemical and spectroscopic analysis, as well as by ECD calculation. Cytotoxicity assays found that compounds **7** and **8** showed good cell inhibition against three human cancer cell lines (SF-268, MCF-7, and HepG2). This result enriched the study on the chemical constituents of *D. foeniculina* and validated that endophytic fungi remained a rich source of structurally/biologically new compounds.

DATA AVAILABILITY STATEMENT

The original contributions presented in the study are included in the article/**Supplementary Material**; further inquiries can be directed to the corresponding authors.

AUTHOR CONTRIBUTIONS

HT and ZZ conceived and designed the experiments. FK, XL, and WP were responsible for the isolation of compounds. FK and SZ

elucidated the structures. DC, JT, and MK tested the pharmacological activity of the compounds. FK, SZ, and KX interpreted the data, and wrote the article. All authors read and approved the final manuscript.

FUNDING

This research were funded by the National Natural Science Foundation of China (No. 8217131312, 81773602), Natural Science Foundation of Guangdong Province (2019A1515011694), Natural Science Foundation of Hunan Province (No. 2021JJ30917), Guangdong Special Support Program (2017TQ04R599), Youth Innovation Promotion Association of CAS (2020342), High-tech Industry Science and Technology Innovation Project of Hunan Province (2020GK4083), Foundation of Key Laboratory of Plant Resources Conservation and Sustainable Utilization, South China Botanical Garden, Chinese Academy of Sciences, and the Open Sharing Fund for the Large-scale Instruments and Equipments of Central South University.

SUPPLEMENTARY MATERIAL

The Supplementary Material for this article can be found online at: https://www.frontiersin.org/articles/10.3389/fchem.2021.755351/full#supplementary-material

REFERENCES

Ahmed, I., Hussain, H., Schulz, B., Draeger, S., Padula, D., Pescitelli, G., et al. (2011). Three New Antimicrobial Metabolites from the Endophytic Fungus *Phomopsis* Sp. *Eur. J. Org. Chem.* 2011, 2867–2873. doi:10.1002/ejoc.201100158

Bills, G. F., and Gloer, J. B. (2016). Biologically Active Secondary Metabolites from the Fungi. *Microbiol. Spectr.* 4, 1–32. doi:10.1128/microbiolspec.FUNK-0009-2016

Bruhn, T., Schaumloffel, A., Hemberger, Y., and Bringmann, G. (2013). SpecDis: Quantifying the Comparison of Calculated and Experimental Electronic Circular Dichroism Spectra. *Chirality* 25, 243–249. doi:10.1002/chir.22138

El-Elimat, T., Raja, H. A., Figueroa, M., Sharie, A. H. A., Bunch, R. L., and Oberlies, N. H. (2021). Freshwater Fungi as a Source of Chemical Diversity: A Review. *J. Nat. Prod.* 84, 898–916. doi:10.1021/ACS.JNATPROD.0C01340

Frisch, M. J., Trucks, G. W., Schlegel, H. B., Scuseria, G. E., Robb, M. A., Cheeseman, J. R., et al. (2016). *G*aussian 16, Revision B.01. Wallingford CT: Gaussian, Inc.

Hemberger, Y., Xu, J., Wray, V., Proksch, P., Wu, J., and Bringmann, G. (2013). Pestalotiopens A and B: Stereochemically Challenging Flexible Sesquiterpene-Cyclopaldic Acid Hybrids from *Pestalotiopsis* Sp. *Chem.-Eur. J.* 19, 15556–15564. doi:10.1002/chin.20141719810.1002/chem.201302204

Jia, M., Chen, L., Xin, H. L., Zheng, C. J., Rahman, K., Han, T., et al. (2016). A Friendly Relationship between Endophytic Fungi and Medicinal Plants: A Systematic Review. *Front. Microbiol.* 7, 906. doi:10.3389/fmicb.2016.00906

Jiao, Y., Li, G., Wang, H. Y., Liu, J., Li, X. B., Zhang, L. L., et al. (2015). New Metabolites from Endolichenic Fungus *Pleosporales* Sp. *Chem. Biodivers.* 12, 1095–1104. doi:10.1002/cbdv.201400279

Kaul, S., Gupta, S., Ahmed, M., and Dhar, M. K. (2012). Endophytic Fungi from Medicinal Plants: a Treasure hunt for Bioactive Metabolites. *Phytochem. Rev.* 11, 487–505. doi:10.1007/s11101-012-9260-6

Kitchawalit, S., Kanokmedhakul, K., Kanokmedhakul, S., and Soytong, K. (2014). A New Benzyl Ester and Ergosterol Derivatives from the Fungus Gymnoascus Reessii. *Nat. Prod. Res.* 28, 1045–1051. doi:10.1080/14786419.2014.903478

Li, C. R., Zhai, Q. Q., Wang, X. K., Hu, X. X., Li, G. Q., Zhang, W. X., et al. (2014). *In Vivo* antibacterial Activity of MRX-I, a New Oxazolidinone. *Antimicrob. Agents Chemother.* 58, 2418–2421. doi:10.1128/AAC.01526-13

Li, Y., Wei, W., Wang, R. L., Liu, F., Wang, Y. K., Li, R., et al. (2019). Colletolides A and B, Two New γ-butyrolactone Derivatives from the Endophytic Fungus *Colletotrichum Gloeosporioides*. *Phytochem. Lett.* 33, 90–93. doi:10.1016/j.phytol.2019.08.004

Lin, T., Lin, X., Lu, C. H., Hu, Z. Y., Huang, W. Y., Huang, Y. J., et al. (2009). Secondary Metabolites of *Phomopsis* Sp. XZ-26, an Endophytic Fungus from *Camptothecaacuminate*. *Eur. J. Org. Chem.* 2009, 2975–2982. doi:10.1002/ejoc.200801021

Liu, M. T., Sun, W. G., Wang, J. P., He, Y., Zhang, J. W., Li, F. L., et al. (2018). Bioactive Secondary Metabolites from the marine-associated Fungus *Aspergillus terreus*. *Bioorg. Chem.* 80, 525–530. doi:10.1016/j.bioorg.2018.06.029

Wani, Z. A., Ashraf, N., Mohiuddin, T., and Riyaz-Ul-Hassan, S. (2015). Plant-endophyte Symbiosis, an Ecological Perspective. *Appl. Microbiol. Biot.* 99, 2955–2965. doi:10.1016/j.bioorg.2018.06.02910.1007/s00253-015-6487-3

Yu, Z. H., Lu, X. X., Choi, J., Deng, S. L., Xiong, B. H., Zhang, W. G., et al. (2021). 2-Pyrones from Endophytic Fungus *Diaporthe Foeniculina* BZM-15. *Nat. Prod. Res.* Published Online. doi:10.1080/14786419.2021.1904400

Zhang, S., Kang, F. H., Tan, J. B., Chen, D. K., Kuang, M., Wang, W. X., et al. (2021a). (±)-Rhytidhymarins A and B, Two Pairs of New Isocoumarin Derivatives from Endophytic Fungus *Rhytidhysteron* Sp. BZM-9. *New J. Chem.* 45, 12700→12704. doi:10.1039/d1nj01993g

Zhang, S., Wang, W. X., Tan, J. B., Kang, F. H., Chen, D. K., Xu, K. P., et al. (2021b). Rhytidhyesters A-D, Four New Chlorinated Cyclopentene Derivatives from the Endophytic Fungus *Rhytidhysteron* Sp. BZM-9. *Planta Med.* 87, 489–497. doi:10.1055/a-1429-3396

Zhang, W. G., Lu, X. X., Huo, L. Q., Zhang, S., Chen, Y., Zou, Z., et al. (2021). Sesquiterpenes and Steroids from an Endophytic *Eutypella Scoparia*. *J. Nat. Prod.* 84, 1715–1724. doi:10.1021/acs.jnatprod.0c01167

Zhang, W. G., Wang, M. M., Zhang, S., Xu, K. P., ShanTan, G., Qiu, S. X., et al. (2020). Eutyscoparols A-G, Polyketide Derivatives from Endophytic Fungus *Eutypella Scoparia* SCBG-8. *Fitoterapia* 146, 104681. doi:10.1016/j.fitote.2020.104681

Conflict of Interest: The authors declare that the research was conducted in the absence of any commercial or financial relationships that could be construed as a potential conflict of interest.

Publisher's Note: All claims expressed in this article are solely those of the authors and do not necessarily represent those of their affiliated organizations, or those of the publisher, the editors, and the reviewers. Any product that may be evaluated in this article, or claim that may be made by its manufacturer, is not guaranteed or endorsed by the publisher.

frontiers in Chemistry

ORIGINAL RESEARCH
published: 25 November 2021
doi: 10.3389/fchem.2021.780304

Acorenone C: A New Spiro-Sesquiterpene from a Mangrove-Associated Fungus, *Pseudofusicoccum* sp. J003

Shujie Jia, Xiangdong Su, Wensi Yan, Meifang Wu, Yichuang Wu, Jielang Lu, Xin He, Xin Ding and Yongbo Xue*

School of Pharmaceutical Sciences (Shenzhen), Shenzhen Campus of Sun Yat-sen University, Shenzhen, China

Mangrove-derived endophytes are rich in bioactive secondary metabolites with a variety of biological activities. Recently, a fungus *Pseudofusicoccum* sp. J003 was first isolated by our research group from mangrove species *Sonneratia apetala* Buch.-Ham. The subsequent chemical investigation of the methanol extract of the culture broth of this strain has led to the isolation of a new sesquiterpenoid named acorenone C **(1)**, two alkaloids **(2–3)**, four phenolic compounds **(4–7)**, and four steroid derivatives **(8–11)**. The new structure of **1** was established by extensive spectroscopic analysis, including 1D, 2D NMR spectroscopy, and HRESIMS. Its absolute configuration was elucidated by experimental ECD and ECD calculation. The *in vitro* AChE inhibitory, anti-inflammatory, and cytotoxic activities of the selected compounds were evaluated. The results showed that compound **1** showed mild AChE inhibitory activity, with an inhibition rate of 23.34% at the concentration of 50 μM. Compound **9** exerted a significant inhibitory effect against nitric oxide (NO) production in LPS-stimulated RAW 264.7 mouse macrophages, with an inhibition rate of 72.89% at the concentration of 25 μM, better than that of positive control L-NMMA. Compound **9** also displayed obvious inhibition effects on the growth of two human tumor cell lines, HL-60 and SW480 (inhibition rates 98.68 ± 0.97% and 60.40 ± 4.51%, respectively). The antimicrobial activities of the compounds **(1–11)** against *Escherichia coli*, *Bacillus subtilis*, *Staphylococcus aureus*, and *Pseudomonas aeruginosa* were also tested; however, none of them showed antimicrobial activities.

Keywords: ***Pseudofusicoccum*** **sp.,** ***Sonneratia apetala*** **Buch.-Ham., sesquiterpenoid, anti-inflammation, acetylcholinesterase**

OPEN ACCESS

Edited by:
Khaled A. Shaaban,
University of Kentucky, United States

Reviewed by:
Mohamed Shaaban,
National Research Center, Egypt
Vivekanandan Subramanian,
University of Kentucky, United States

***Correspondence:**
Yongbo Xue
xueyb@mail.sysu.edu.cn

Specialty section:
This article was submitted to Medicinal and Pharmaceutical Chemistry, a section of the journal Frontiers in Chemistry

Received: *20 September 2021*
Accepted: *25 October 2021*
Published: *25 November 2021*

Citation:
Jia S, Su X, Yan W, Wu M, Wu Y, Lu J, He X, Ding X and Xue Y (2021) Acorenone C: A New Spiro-Sesquiterpene from a Mangrove-Associated Fungus, Pseudofusicoccum *sp. J003. Front. Chem. 9:780304. doi: 10.3389/fchem.2021.780304*

INTRODUCTION

The great diversity of creatures in the ocean was found to be a rich reservoir of candidates for drug development (Sigwart et al., 2021). To date, more than 35,000 marine natural products have already been discovered, which have a higher rate of successful drug discovery than other naturally occurring compounds (Lyu et al., 2021; Sigwart et al., 2021). Mangroves are an intertidal wetland ecosystem spreading across low-latitude tropical and subtropical regions, which are found to have potential to control coastal erosion and protect coastal land. The ingredients produced by mangrove plant species may play a role in helping them survive from universally unfavorable factors (Bandaranayake, 2002). Many types of natural products have been identified from mangroves and their endophytes,

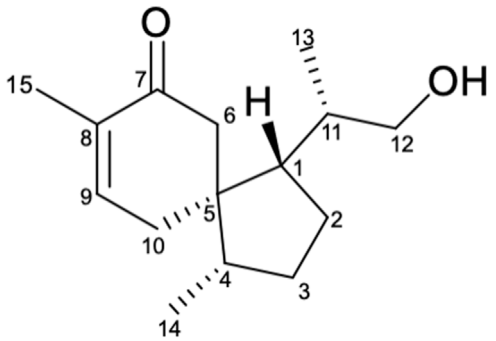

FIGURE 1 | Structure of compound 1.

including heterocyclic compounds, benzofurans, alkaloids, lignin, polysaccharides, fatty acids, lipids, anthocyanins, flavonoids, phenols and quinones, tannins, limonin, terpenoids, steroids, and saponins (Carroll et al., 2020).

Recently, our research group aimed at structurally diverse natural products from the mangroves and their endophytes for pharmaceutical drug discovery. As a small- to medium-sized columnar true mangrove, the plant species *Sonneratia apetala* Buch.-Ham. is native to South Asia and Southeast Asia and has been cultivated in Guangdong and Hainan provinces, China (Hossain et al., 2016). *S. apetala* has versatile pharmacological effects, for example, the extracts of barks and leaves of *S. apetala* exhibited antibacterial, antioxidant, anti-diabetic, and anti-cancer activities (Patra et al., 2015). However, the endophytes of *S. apetala* were scarcely investigated.

In this work, a fungus *Pseudofusicoccum* sp. J003 was isolated from the fruit of *S. apetala* for the first time. Previous studies on the secondary metabolites obtained from the genus *Pseudofusicoccum* by other research groups revealed the presence of phenolic compounds (Abba et al., 2018), cyclopeptides, and rotenoids (Sobreira et al., 2018). In our study, the chemical investigation into the methanol extract of this strain by repeated column chromatography over silica gel, Sephadex LH-20, RP-C_{18} silica, and semi-preparative HPLC resulted in the isolation of a new sesquiterpenoid **(1)** (**Figure 1**), two alkaloids **(2–3)**, four phenolic compounds **(4–7)**, and four steroid derivatives **(8–11)**. Herein, the isolation, structure determination of isolated compounds, and evaluation of their *in vitro* anti-inflammatory, antimicrobial, cytotoxic, and AChE inhibitory activities were described.

MATERIALS AND METHODS

General Experimental Procedures

The optical rotations, CD, and FT-IR spectra were measured with a Perkin-Elmer 341 polarimeter (PerkinElmer, Waltham, MA, USA), JASCO J-810 spectrometer (Jasco Corporation, Japan), Bruker Vertex 70 FT-IR spectrophotometer (Bruker, Karlsruhe, Germany), respectively. The UV spectrum was recorded using a Waters e2695 spectrophotometer (Waters, Massachusetts, USA) equipped with a DAD and a 1-cm-path length cell. Samples in methanol solution were scanned from 190 to 400 nm in 1-nm steps. The structure characterization of the obtained compound was based on 1D NMR (^{1}H, ^{13}C) and 2D NMR (COSY, HSQC, HMBC, and NOESY) data, recorded on the Bruker AM-400, AM-500, and AM-700 NMR spectrometers (Bruker, Karlsruhe, Germany) with TMS as internal standard, respectively. The detailed parameters for the NMR data of all isolates are provided (see Supporting Information, **Supplementary Figures S3–S9**; **Supplementary Figures S11–S30**). Chemical shifts (δ) were expressed in ppm with reference to the solvent signals. HRESIMS data were acquired on a Thermo Fisher LTQ XL LC/MS (Thermo Fisher, Palo Alto, CA, USA). Semi-preparative HPLC was performed on an Agilent 1220 apparatus equipped with a UV detector with a semi-preparative column (RP-C_{18}, 5 μm, 250 × 10 mm, Welch Materials, Inc.). Column chromatography was performed using silica gel (200–300 mesh and 80–120 mesh, Qingdao Marine Chemical Co., Ltd., Qingdao, China) and Sephadex^{TM} LH-20 gel (40–70 μm; Merck, Darmstadt, Germany). Fractions were monitored by TLC (GF254, Qingdao Marine Chemical Co., Ltd., Qingdao), and spots were visualized by heating silica gel plates sprayed with 10% H_2SO_4 in EtOH. All solvents were of analytical grade (Guangzhou Chemical Regents Company, Ltd., Guangzhou, China).

Fungal Isolation and Fermentation

The fungal strain *Pseudofusicoccum* sp. J003 was isolated from the fruit of *Sonneratia apetala* Buch.-Ham., which was collected at a wetland of Nansha district, Guangzhou, China, in September 2020. The sequence data for this strain have been submitted to the GenBank under accession no. MZ854244. The fungal strain was deposited on 20% aqueous glycerol stock in a −80°C freezer at the School of Pharmaceutical Sciences (Shenzhen), Shenzhen Campus of Sun Yat-sen University, Shenzhen, China. The strain was cultured on potato dextrose agar for 5 days at 28°C. Agar plates, including the strain, were cut into small pieces, and then these pieces were inoculated in a tissue culture bottle (150 × 350 ml) on a solid rice medium (40 g of rice and 35 ml of distilled water) and cultured at room temperature for 30 days.

Extraction and Isolation of Secondary Metabolites

Cultural media were extracted with methanol three times. Methanol was removed by reduced pressure evaporation at 45°C, and the remaining aqueous phase was extracted 4 times with ethyl acetate. The ethyl acetate layer was concentrated under reduced pressure to yield a brown extract (60.0 g). The crude extract was introduced to a silica gel chromatography column (CC) and eluted with petroleum ether/ethyl acetate (35:1→0:1) to obtain seven fractions (Fr. 1–Fr. 7). Fr. 2 (7.3 g) was separated into 7 subfractions (Fr. 2.1–Fr. 2.7) using silica gel CC and eluted with *n*-hexane/2-propanol. Fr. 2.2 (102.3 mg) was purified by semi-preparative HPLC (100% MeOH, 3.0 ml/min) to yield 4 (21.6 mg, t_R 24.5 min). Fr. 2.6 (800.5 mg) was purified by semi-preparative HPLC (45% MeOH/H_2O, v/v, 3.0 ml/min) to yield 5

TABLE 1 | ^{1}H and ^{13}C NMR data for 1 (Record in CD_3OD, *J* in Hz).

No.	δ_H	δ_C
1	1.66 m	52.2
2a	1.54 m	23.6
2b	1.65 m	
3a	1.32 m	30.8
3b	1.83 m	
4	1.67 m	46.6
5		50.0
6a	2.63 d (16.5)	49.8
6b	2.24 d (16.5)	
7		203.2
8		136.1
9	6.82 t like (3.9)	147.1
10a	2.36 dm (19.4)	27.4
10b	2.22 dm (19.4)	
11	1.76 m	36.3
12a	3.36 m	68.5
12b	3.38 m	
13	0.91 d (6.7)	14.7
14	0.84 d (6.8)	17.4
15	1.75 s	15.4

(1.3 mg, t_R 8.5 min). Fr. 2.4 (113.0 mg) and Fr. 2.7 (220.7 mg) were separated by repeated CC over silica gel to yield 10 (3.4 mg) and 9 (6.7 mg). Fr. 4 (500.5 mg) was separated with repeated silica gel CC to yield six fractions (Fr. 4.1–Fr. 4.6) and then subjected subfraction Fr. 4.3 (268.3 mg) to a Sephadex LH-20 CC ($CHCl_2$–MeOH, 1:1) to afford three parts (Fr. 4.4a–Fr. 4.4c). Fr. 4.4b (43.2 mg) was purified by semi-preparative HPLC (100% MeOH/H_2O, v/v, 3.0 ml/min) to yield 8 (14.0 mg, t_R 14.5 min). Fr. 4.4c (55.8 mg) was purified by semi-preparative HPLC (70% MeOH/H_2O, v/v, 3.0 ml/min) to yield 1 (2.0 mg, t_R 23.1 min). Fr. 5 (18.9 g) was separated with repeated Sephadex LH-20 CC (MeOH) to yield 6 (7.1 mg) and 7 (90.0 mg). Fr. 7 (7.7 g) was separated with repeated silica gel CC and eluted with CH_2Cl_2/MeOH and *n*-hexane/2-propanol to yield 2 (22.0 mg), 3 (20.0 mg), and 11 (10.0 mg).

Acorenone C 1) Colorless oil; $[\alpha]_D^{29}$ −34.6 (*c* 0.1, MeOH); UV (MeOH) λ_{max} (log ε) 233 (1.2) nm; CD (0.10 mM, MeOH) λ_{max} (Δε) 213 (−1.72), 244 (+9.25) nm; IR ν_{max} 3,429, 2,951, 2,922, 2,872, 1,663, 1,456, 1,381, 1,369, 1,248, 1,034 cm^{-1}; ^{1}H NMR and ^{13}C NMR data (see **Table 1**); HRESIMS $[M + Na]^+$ *m/z* 259.1679 (calcd. for $C_{15}H_{24}O_2Na$, 259.1669).

Anti-AChE Assay

Acetylcholinesterase (AChE) inhibitory activity of the compounds isolated was assayed by the spectrophotometric method with slight modification (Ellman et al., 1961). *S*-Acetylthiocholine iodide, *S*-butyrylthiocholine iodide, 5,5′-dithio-bis-(2-nitrobenzoic) acid (DTNB, Ellman's reagent), and acetylcholinesterase derived from human erythrocytes were purchased from Sigma Chemical. The compounds were dissolved in DMSO. The reaction mixture (totally 200 μL) containing phosphate buffer (pH 8.0), a test compound (50 μM), and acetyl cholinesterase (0.02 U/mL) was incubated for 20 min (37°C). Then the reaction was initiated by the addition of 40 μL of a solution containing DTNB (0.625 mM) and acetylthiocholine iodide (0.625 mM) for AChE inhibitory activity assay, respectively. The hydrolysis of acetylthiocholine was monitored at 405 nm every 30 s for 1 h. Tacrine was used as a positive control with a final concentration of 0.333 μM. All the reactions were performed in triplicate. The percentage inhibition was calculated as follows: % inhibition = (E–S)/E × 100 (E is the activity of the enzyme without the test compound and S is the activity of the enzyme with the test compound).

Anti-Inflammatory Assay

The RAW 264.7 cells (2×10^5 cells/well) were incubated in 96-well culture plates with or without 1 μg/ml LPS (Sigma Chemical Co., USA) for 24 h in the presence or absence of the test compounds. Aliquots of supernatants (50 μL) were then reacted with 100 μL Griess reagent (Sigma Chemical Co., USA). The absorbance was measured at 570 nm by using the Synergy TMHT Microplate Reader (BioTek Instruments Inc., USA). In the study, L-NMMA (Sigma Chemical Co., USA) was used as a positive control. In the remaining medium, an MTT assay was carried out to determine whether the suppressive effect was related to cell viability. The inhibitory rate of NO production = (NO level of blank control – NO level of test samples)/NO level of blank control. The percentage of NO production was evaluated by measuring the amount of nitrate concentration in the supernatants with Griess reagent, as described previously (Wu et al., 2017).

Cytotoxicity Assay

Five human cancer cell lines, including the A549 lung cancer cell line, the HL-60 human myeloid leukemia cell line, the MCF-7 breast cancer cell line, the SMMC-7721 human hepatocarcinoma cell line, and the SW-480 human pancreatic carcinoma were used. Cells were cultured in RPMI-1640 or DMEM medium, supplemented with 10% fetal bovine serum and 5% CO_2 at 37°C. The cytotoxicity assay was performed using an MTTS 3-(4,5-dimethylthiazol-2-yl)-5(3-carboxymethoxyphenyl)-2-(4-sulfopheny)-2H-tetrazolium) method in 96-well microplates, as reported previously (Liu et al., 2012), with slight modification. In brief, 100 μL of adherent cells were seeded into each well of the 96-well culture plates and allowed to adhere for 12 h before adding the test compounds, while suspended cells were seeded into wells at a density of 1×10^5 cells/mL just prior to the addition of the test compounds. Each tumor cell line was exposed to the test compound at concentrations of 40 μM in triplicates for 48 h. Wells with DMSO were used as negative controls, and Taxol and DDP were used as positive controls. After treatment of the compounds, cell viability was detected by a microplate reader at λ = 492 nm.

Antimicrobial Assay

Compounds 1–11 were evaluated for their antimicrobial activities against *Escherichia coli*, *Bacillus subtilis*, *Staphylococcus aureus*, and *Pseudomonas aeruginosa*. The antimicrobial assay was conducted by the previously described method (Zhang et al., 2019). The sample to be tested was added into a 96-well culture plate, and the maximum concentration of the used compounds was 250 μg/ml. Bacteria liquid was added to each well until the

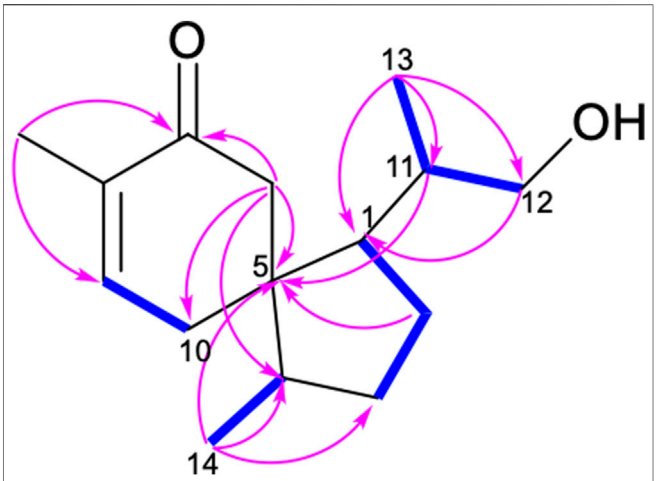

FIGURE 2 | Key COSY (bolds, blue) and HMBC (arrows, pink) correlations of 1.

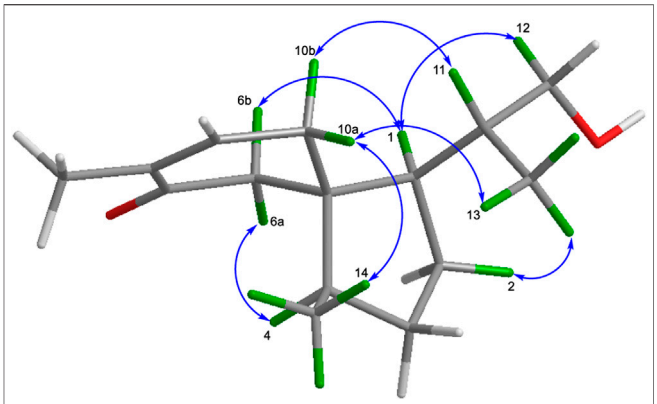

FIGURE 3 | Key NOESY correlations of compounds 1.

final concentration is 5×10^5 CFU/ml. It was then incubated at 37°C for 24 h, and the OD value at 595 nm was measured by the microplate reader, and the medium blank control was used in the experiment.

RESULTS AND DISCUSSION

Identification of Compounds

Compound 1 was obtained as colorless oil. Its molecular formula was determined to be $C_{15}H_{24}O_2$ based on the deprotonated ion peak $[M + Na]^+$ at *m/z* 259.1679 $[M + Na]^+$ (calcd for 259.1669) in the (+)-HRESIMS, indicating 4 degrees of unsaturation. The IR spectrum showed characteristic absorption bands of hydroxyl (3,429 cm^{-1}) and the carbonyl groups (1,662 cm^{-1}). The ^{13}C NMR and DEPT spectra of **1** (**Table 1**) showed 15 carbon signals, including three methyls, five methylenes (including oxygenated methylene at δc 68.5), three methine groups, two olefinic carbon signals (δc 147.1 and 136.1), an aliphatic quaternary carbon, and a carbonyl carbon (δ_C 203.2). The ^1H NMR spectrum of 1 (**Table 1**) displayed the presence of an olefinic proton resonated at δ_H 6.82 (t like, $J = 3.9$ Hz), two methyl group doublets at 0.91 (d, $J = 6.7$ Hz) and 0.84 (d, $J = 6.8$ Hz), and two oxygenated methine protons at δ_H 3.36 and 3.38. Apart from the two degrees of unsaturation occupied by the carbonyl group and a double bond, the remaining degrees of unsaturation suggested that compound **1** should be a dicyclic sesquiterpenoid (Amandine et al., 2017).

The ^1H-^1H COSY spectrum of **1** indicated the presence of spin systems of (HO)CH_2(12)-CH(11)-CH_3(13) and CH(1)-CH_2(2)-CH_2(3)-CH(4)-CH_3(14) (**Figure 2**). In the HMBC spectrum, the HMBC interactions from H-13 (δ_H 0.91) and H-12 (δ_H 3.36 and 3.38) to C-11 (δ_C 36.3) and C-1 (δ_C 52.2) revealed the direct C–C linkage from C-11 to C-1 (**Figure 2**). Subsequently, the HMBC correlations of H-2 and H-11 with C-5 (δ_C 50.0) and of H-14 with C-3, C-4, and C-5 indicated the presence of a methyl cyclopentane substructure with a 1-propanol substituted at C-1. The spin system of = CH(9)–CH_2(10) observed from the ^1H–^1H COSY spectrum of 1, together with the key HMBC correlations from H_3-15 (δ_H 1.75) to C-7 (δ_C 203.2)/C-8 (δ_C 136.1)/C-9 (δ_C 147.1), from H-6 (δ_H 2.24 and 2.63) to C-5/C-8/C-10, collaborated with the methyl cyclohexane substructure decorated by an *α,β*-unsaturated ketone functionality. Based on the aforementioned pieces of evidence, the crucial HMBC correlations from H-6 and H-10 to C-1, C-4, and C-5 and from H-1 and H-4 to C-5, C-6, and C-10 constructed the gross structure of **1**, featuring a spiro[4,5]decane scaffold. The planar structure of 1 was thus deduced as shown (**Figure 2**), resembling the (3*S*)-1,4-epi-3-hydroxyacorenone (Calva et al., 2017).

The relative configurations of **1** were elucidated by the observation of its NOESY spectrum. The NOESY correlations of H-10a with H_3-13 and H_3-14, and Me-13/H-2a revealed that H-10a, H_3-13, and H_3-14 were co-facial and provisionally assigned to be *α*-oriented. Accordingly, the NOESY cross-peaks of H-11/H-10b, H-1/H-6b, H-6a/H-4, and H-1/H-12a indicated the *β*-orientation of H-1, H-4, and H-11. The relative stereochemistries at C-1, C-4, C-5, and C-11 of **1** were thus determined (**Figure 3**). Therefore, as for the absolute configuration of **1**, two possible enantiomers (**Figures 4A,B**) were presented (**Figure 4**).

To further determine the absolute stereochemistry of **1**, the electronic circular dichroism (ECD) (for detailed procedures, see SI) calculation of the two possible enantiomers (**Figures 5A,B**; **Figures 4**, **5**) was performed using Gaussian 09 and figured using GaussView 5.0 (Dennington et al., 2009; Frisch et al., 2009). Conformation search *via* molecular mechanics calculations was conducted in Discovery Studio 3.5 Client, with an MMFF force field with a 20 kcal/mol upper energy limit (Smith and Goodman, 2010). The optimized conformation geometries and thermodynamic parameters of the selected conformations were provided. The predominant conformers were subsequently optimized at the B3LYP/6-31G(d,p) level. The theoretical calculation of ECD was performed using a time-dependent density functional theory (TDDFT) at the B3LYP/6-31G(d,p) level in MeOH with the PCM model. The calculated spectrum of 1b (1*S*,4*S*,5*R*,11*S*) agreed with the experimental data, showing

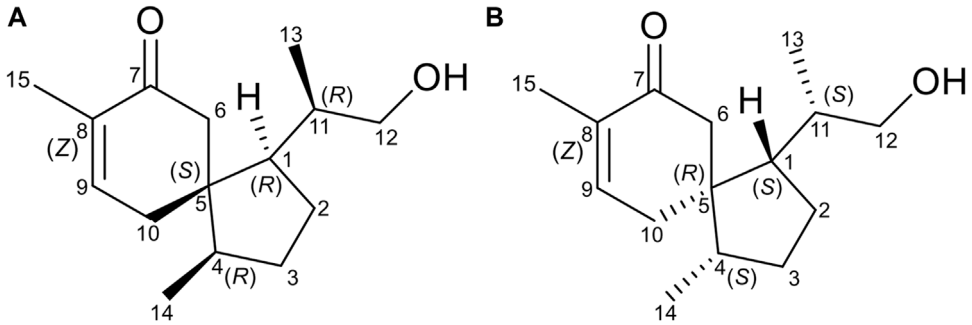

FIGURE 4 | Two possible enantiomers of compound 1 [**(A)** (1*R*,4*R*,5*S*,11*R*) and **(B)** (1*S*,4*S*,5*R*,11*S*)].

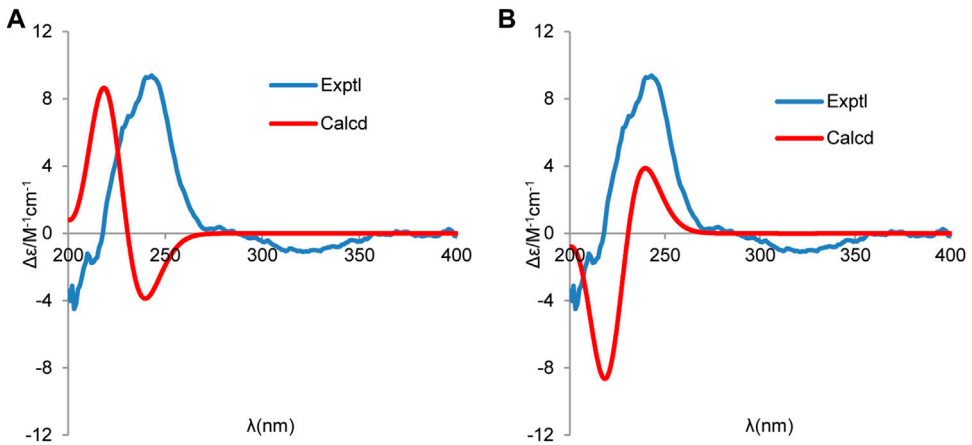

FIGURE 5 | Experimental and calculated ECD spectra of **(A)** (1*R*,4*R*,5*S*,11*R*) and **(B)** (1*S*,4*S*,5*R*,11*S*) (red, calculated at the B3LYP-PCM/6-31G(d,p)//B3LYP/6-31G (d,p) level in CH_3OH; blue, experimental in CH_3OH).

TABLE 2 | AChE inhibitory activity of compound 1.

Compound	Concentration (*μ*M)	Inhibition (%)[a]
1	50	23.34 ± 3.53
Tacrine[b]	0.333	58.99 ± 1.67

[a]*All compounds examined in a set of triplicated experiment.*
[b]*Positive control.*

TABLE 3 | Inhibitory activities of compounds **1**–**4**, **6**–**9**, and **11** on LPS-stimulated NO production.

Compound	Concentration (μM)	NO production inhibition (%)[a]
1	50	−1.05 ± 1.24
2	50	−3.51 ± 1.67
3	50	−0.18 ± 2.74
4	50	−9.74 ± 2.67
6	50	6.14 ± 0.66
7	50	−3.33 ± 2.19
8	50	−1.58 ± 0.79
9	25	72.89 ± 0.71
11	50	3.16 ± 1.58
L-NMMA[b]	50	52.59 ± 0.99

[a]*All compounds examined in a set of triplicated experiment.*
[b]*Positive control.*

a negative Cotton effect (CE) at 213 nm and a strong positive CE at 244 nm (**Figure 5**). Consequently, the structure of **1** was determined to be (1*S*,4*S*,5*R*)-1-((*S*)-1-hydroxypropan-2-yl)-4,8-dimethylspiro [4.5]dec-8-en-7-one, and a trivial acorenone C was given.

Ten known compounds, uracil **(2)** (Xing et al., 2020), cyclo-(L-Pro-L-Tyr) **(3)** (Jayatilake et al., 1996), bis-(2-ethylhexyl) terephthalate **(4)** (Firdovsi et al., 2007), 4-hydroxybenzaldehyde **(5)** (Shataer et al., 2020), 2-phenylethanol **(6)** (Guerrini et al., 2011), 4-hydroxyphenethyl-alcohol **(7)** (Wei et al., 2013), estigmast-4-en-6β-ol-3-ona **(8)** (Correia et al., 2003), ergosterol **(9)** (Zhang et al., 2002), ergosterol peroxide **(10)** (Hybelbauerová et al., 2008), and cerevisterol **(11)** (Kang et al., 2017) were also isolated from *Pseudofusicoccum* sp. J003. The structures of these compounds **(2–11)** were elucidated by comparing the spectral data to those reported in the references.

TABLE 4 | *In vitro* cytotoxic activity (cell inhibition (%)) of compounds **8**, **9**, and **11** against five human tumor cell lines[a]

Compound	Concentration (μM)	HL-60	A-549	SMMC-7721	MCF-7	SW480
8	40	27.90 ± 3.58	49.58 ± 0.49	35.73 ± 1.37	9.26 ± 1.67	15.06 ± 1.99
9	40	98.68 ± 0.97	48.25 ± 1.14	46.26 ± 1.63	21.92 ± 1.61	60.40 ± 4.51
11	40	20.22 ± 3.11	7.00 ± 2.01	27.91 ± 1.05	21.17 ± 3.50	10.87 ± 0.36
DDP[b]	40	79.06 ± 0.38	84.65 ± 1.00	82.78 ± 0.73	63.55 ± 2.90	78.73 ± 0.62
Taxol[b]	5	54.62 ± 0.46	53.00 ± 0.50	74.50 ± 0.43	58.63 ± 0.58	61.72 ± 2.15

[a]*All compounds examined in a set of triplicated experiment.*
[b]*Positive control.*

Biological Activity

According to the literature, acorenone analogs usually have AChE inhibitory activity (Calva et al., 2017). The AChE inhibition effect of new compound **1** was tested. It exhibited mild inhibitory activity against AChE with an inhibition rate of 23.34% ± 3.53 at the concentration of 50 μM (**Table 2**). To further test *in vitro* anti-inflammatory activity, compounds **1–4**, **6–9**, and **11** were evaluated for their inhibitory activities against LPS-induced nitric oxide (NO) production in RAW 264.7 mouse macrophages, of which compound **9** showed obvious inhibitory activity, with an inhibition rate of 72.89% ± 0.71 at the concentration of 25 μM (**Table 3**). Since steroid derivatives were reported to have cytotoxic properties against tumor cells (Bok et al., 1999), compounds **8**, **9**, and **11** were selected to test their cytotoxic activities against five human cancer cell lines, including HL-60, A549, MCF-7, SMMC-7721, and SW480, of which compound **9** inhibited the proliferation of tumor cells HL-60, with an inhibition rate of 98.68% ± 0.97 and SW480 with an inhibition rate of 60.40% ± 4.51 at a concentration of 40 μM, respectively (**Table 4**). The antimicrobial activity of compounds **1–11** was also evaluated against the bacteria *S. aureus*, *B. subtilis*, *P. aeruginosa*, and *E. coli*. However, all of them were found to be devoid of significant activity (MIC >250 μg/ml).

CONCLUSION

Mangroves with significant ecological significance and biodiversity have attracted broad interest from scientific communities. In this research, a new sesquiterpenoid called acorenone C **(1)**, along with ten known compounds **(2–11)**, was identified from the culture medium of an endophyte *Pseudofusicoccum* sp. J003, a fungus isolated from a mangrove species *S. apetala*. In addition, compounds **1–6** and **8–11** were identified from the genus *Pseudofusicoccum* for the first time. Their structures were established by extensive spectroscopic analyses, including 1D, 2D NMR spectroscopy, and HRESIMS, as well as ECD calculation. In the vitro bioassays, compound **1** showed mild AChE inhibitory activity, with an inhibition rate of 23.34% at the concentration of 50 μM. Compound **9** exerted a significant inhibitory effect against nitric oxide (NO) production in LPS-stimulated RAW 264.7 mouse macrophages, with an inhibition rate of 72.89% at the concentration of 25 μM, better than that of positive control L-NMMA. Compound **9** also displayed obvious inhibition effects on the growth of two human tumor cell lines HL-60 and SW480 (inhibition rates of 98.68 ± 0.97% and 60.40 ± 4.51%, respectively). The antimicrobial activities of the compounds **(1–11)** against *Escherichia coli*, *Bacillus subtilis*, *Staphylococcus aureus*, and *Pseudomonas aeruginosa* were also tested; however, none of them showed antimicrobial activities. This work will add new bioactive marine natural products from microbes of mangrove plants.

DATA AVAILABILITY STATEMENT

The datasets presented in this study can be found in online repositories. The names of the repository/repositories and accession number(s) can be found below: https://www.ncbi.nlm.nih.gov/genbank/ MZ854244

AUTHOR CONTRIBUTIONS

SJ conducted the main experiments and prepared the manuscript. SJ and WY were responsible for the isolation of compounds. SJ and XD did the antibacterial assay. SJ and XS conducted the anti-AChE assay. SJ, JL, and MW performed the anti-inflammatory assay. YW and XH did the cytotoxicity assay. SJ, XS, and YX identified the structures. XS and YX revised the manuscript. YX initiated the project and oversaw the research. All authors approved the submission of the manuscript for publication.

FUNDING

This research was financially supported by the National Natural Science Foundation of China (Nos. 31770379 and 21977120), the Key Basic Research Programme of the Science, Technology and Innovation Commission of Shenzhen Municipality (JCYJ20200109142215045), the Hundred Talents Program of Sun Yat-sen University (No. 75110-18841218). We express our sincere thanks to Xiaonian Li and Jianchao Chen for their helpful assistance in NMR measurement.

SUPPLEMENTARY MATERIAL

The Supplementary Material for this article can be found online at: https://www.frontiersin.org/articles/10.3389/fchem.2021.780304/full#supplementary-material

REFERENCES

Abba, C., Eze, M. P., Nwachukwu, C., Okoye, F., Eboka, C., Eze, P., et al. (2018). Phenolic Compounds from Endophytic *Pseudofusicoccum* Sp. Isolated from *Annona Muricata*. *Tjnpr* 2, 332–337. doi:10.26538/tjnpr/v2i7.6

André, A., Wojtowicz, N., Touré, K., Stien, D., and Eparvier, V. (2017). New Acorane Sesquiterpenes Isolated from the Endophytic Fungus *Colletotrichum Gloeosporioides* SNB-GSS07. *Tetrahedron Lett.* 58, 1269–1272. doi:10.1016/j.tetlet.2017.02.024

Bandaranayake, W. M. (2002). Bioactivities, Bioactive Compounds and Chemical Constituents of Mangrove Plants. *Wetl. Ecol. Manag.* 10, 421–452. doi:10.1023/A:1021397624349

Bok, J. W., Lermer, L., Chilton, J., Klingeman, H. G., and Towers, G. H. N. (1999). Antitumor Sterols from the Mycelia of *Cordyceps Sinensis*. *Phytochemistry* 51 (7), 891–898. doi:10.1016/s0031-9422(99)00128-4

Calva, J., Bec, N., Gilardoni, G., Larroque, C., Cartuche, L., Bicchi, C., et al. (2017). Acorenone B: AChE and BChE Inhibitor as a Major Compound of the Essential Oil Distilled from the Ecuadorian Species Niphogeton Dissecta (Benth.) J.F. Macbr. *Pharmaceuticals* 10, 84. doi:10.3390/ph10040084

Carroll, A. R., Copp, B. R., Davis, R. A., Keyzers, R. A., and Prinsep, M. R. (2020). Marine Natural Products. *Nat. Prod. Rep.* 37, 175–223. doi:10.1039/C9NP00069K

Correia, S. d. J., David, J. P., and David, J. M. (2003). Constituintes das cascas de Tapirira guianensis (Anacardiaceae). *Quím. Nova* 26, 36–38. doi:10.1590/S0100-40422003000100008

Dennington, R., Keith, T., and Millam, J. (2009). *Gauss View*. Version 5. Shawnee Mission: Semichem Inc.

Ellman, G. L., Courtney, K. D., Andres, V., and Featherstone, R. M. (1961). A New and Rapid Colorimetric Determination of Acetylcholinesterase Activity. *Biochem. Pharmacol.* 7, 88–95. doi:10.1016/0006-2952(61)90145-9

Firdovsi, S. T., Yagoub, M., and Parvin, A. E. (2007). Transesterification Reaction of Dimethyl Terephthalate by 2-Ethylhexanol in the Presence of Heterogeneous Catalysts under Solvent-free Condition. *Chin. J. Chem.* 25, 246–249. doi:10.1002/cjoc.200790049

Frisch, M. J., Trucks, G. W., Schlegel, H. B., Scuseria, G. E., Robb, M. A., Cheeseman, J. R., et al. (2009). *Gaussian 09*. Wallingford, CT: Gaussian, Inc.

Guerrini, A., Rossi, D., Paganetto, G., Tognolini, M., Muzzoli, M., Romagnoli, C., et al. (2011). Chemical Characterization (GC/MS and NMR Fingerprinting) and Bioactivities of South-African Pelargonium Capitatum (L.) L' Her. (Geraniaceae) Essential Oil. *Chem. Biodiversity* 8, 624–642. doi:10.1002/cbdv.201000045

Hossain, S. J., Iftekharuzzaman, M., Haque, M. A., Saha, B., Moniruzzaman, M., Rahman, M. M., et al. (2016). Nutrient Compositions, Antioxidant Activity, and Common Phenolics ofSonneratia apetala(Buch.-Ham.) Fruit. *Int. J. Food Prop.* 19, 1080–1092. doi:10.1080/10942912.2015.1055361

Hybelbauerová, S., Sejbal, J., Dračínský, M., Hahnová, A., and Koutek, B. (2008). Chemical Constituents ofStereum Subtomentosum and Two Other Birch-Associated Basidiomycetes: An Interspecies Comparative Study. *C&B* 5 (5), 743–750. doi:10.1002/cbdv.200890070

Jayatilake, G. S., Thornton, M. P., Leonard, A. C., Grimwade, J. E., and Baker, B. J. (1996). Metabolites from an Antarctic Sponge-Associated Bacterium, *Pseudomonas aeruginosa*. *J. Nat. Prod.* 59, 293–296. doi:10.1021/np960095b

Kang, X., Xu, Y., Chen, G., and Wen, L. (2017). Study on Screening of Endophytic Fungi from *Cyclosorus Parasiticus* for Antibacterial Activity and Secondary Metabolites from the Active Fungus *Pestalotiopsis* Sp. CYC38. *J. Guangdong Pharm. Univ.* 33, 1–5. doi:10.16809/j.cnki.2096-3653.2016102401

Liu, X., Xue, Y.-B., Dong, K., Li, X.-N., Li, Y., Pu, J.-X., et al. (2012). Three New Ent-Kaurane Diterpenoids from *Isodon Rubescens* and Their Cytotoxicities. *Chin. J. Nat. Medicines* 10, 464–470. doi:10.1016/S1875-5364(12)60088-0

Lyu, C., Chen, T., Qiang, B., Liu, N., Wang, H., Zhang, L., et al. (2021). CMNPD: a Comprehensive marine Natural Products Database towards Facilitating Drug Discovery from the Ocean. *Nucleic Acids Res.* 49, D509–D515. doi:10.1093/nar/gkaa763

Patra, J. K., Das, S. K., and Thatoi, H. (2015). Phytochemical Profiling and Bioactivity of a Mangrove Plant, *Sonneratia Apetala*, from Odisha Coast of India. *Chin. J. Integr. Med.* 21, 274–285. doi:10.1007/s11655-014-1854-y

Shataer, D., Abdulla, R., Ma, Q. L., Liu, G. Y., and Aisa, H. A. (2020). Chemical Composition of Extract of *Corylus Avellana* Shells. *Chem. Nat. Compd.* 56, 338–340. doi:10.1007/s10600-020-03024-z

Sigwart, J. D., Blasiak, R., Jaspars, M., Jouffray, J.-B., and Tasdemir, D. (2021). Unlocking the Potential of marine Biodiscovery. *Nat. Prod. Rep.* 38, 1235–1242. doi:10.1039/d0np00067a

Smith, S. G., and Goodman, J. M. (2010). Assigning Stereochemistry to Single Diastereoisomers by Giao Nmr Calculation: The Dp4 Probability. *J. Am. Chem. Soc.* 132, 12946–12959. doi:10.1021/ja105035r

Sobreira, A. C. M., Pinto, F. d. C. L., Florêncio, K. G. D., Wilke, D. V., Staats, C. C., Streit, R. d. A. S., et al. (2018). Endophytic Fungus *Pseudofusicoccum Stromaticum* Produces Cyclopeptides and Plant-Related Bioactive Rotenoids. *RSC Adv.* 8, 35575–35586. doi:10.1039/c8ra06824k

Wei, S.-S., He, J.-B., and Yan, Y.-M. (2013). Studies on the Chemical Constituents of *Tenodera sinensis Saussure* Egg. *J. Int. Pharm. Res.* 32, 257–258. doi:10.13506/j.cnki.jpr.2013.05.013

Wu, Y., Xie, S.-S., Hu, Z.-X., Wu, Z.-D., Guo, Y., Zhang, J.-W., et al. (2017). Triterpenoids from Whole Plants of *Phyllanthus Urinaria*. *Chin. Herbal Medicines* 9, 193–196. doi:10.1016/S1674-6384(17)60095-9

Xing, Z., Wu, X., Zhao, J., Zhao, X., Zhu, X., Wang, Y., et al. (2020). Isolation and Identification of Induced Systemic Resistance Determinants from *Bacillus Simplex* Sneb545 against *Heterodera glycines*. *Sci. Rep.* 10, 11586. doi:10.1038/s41598-020-68548-4

Zhang, N., Shi, Z., Guo, Y., Xie, S., Qiao, Y., Li, X.-N., et al. (2019). The Absolute Configurations of Hyperilongenols A-C: Rare 12,13-Seco-Spirocyclic Polycyclic Polyprenylated Acylphloroglucinols with Enolizable β,β′-tricarbonyl Systems from Hypericum Longistylum Oliv. *Org. Chem. Front.* 6, 1491–1502. doi:10.1039/C9QO00245F

Zhang, Y., Mills, G. L., and Nair, M. G. (2002). Cyclooxygenase Inhibitory and Antioxidant Compounds from the Mycelia of the Edible Mushroom *Grifola Frondosa*. *J. Agric. Food Chem.* 50, 7581–7585. doi:10.1021/jf0257648

Conflict of Interest: The authors declare that the research was conducted in the absence of any commercial or financial relationships that could be construed as a potential conflict of interest.

Publisher's Note: All claims expressed in this article are solely those of the authors and do not necessarily represent those of their affiliated organizations, or those of the publisher, the editors, and the reviewers. Any product that may be evaluated in this article, or claim that may be made by its manufacturer, is not guaranteed or endorsed by the publisher.

frontiers in Chemistry

ORIGINAL RESEARCH
published: 16 December 2021
doi: 10.3389/fchem.2021.785431

The Oxidation Cascade of a Rare Multifunctional P450 Enzyme Involved in Asperterpenoid A Biosynthesis

Hui-Yun Huang[1], Jia-Hua Huang[2], Yong-Heng Wang[1], Dan Hu[1], Yong-Jun Lu[3], Zhi-Gang She[4], Guo-Dong Chen[1], Xin-Sheng Yao[1,2] and Hao Gao[1]**

[1]Institute of Traditional Chinese Medicine and Natural Products, College of Pharmacy/Guangdong Province Key Laboratory of Pharmacodynamic Constituents of TCM and New Drugs Research, Jinan University, Guangzhou, China, [2]School of Traditional Chinese Materia Medica, Shenyang Pharmaceutical University, Shenyang, China, [3]School of Life Sciences, Sun Yat-sen University, Guangzhou, China, [4]School of Chemistry, Sun Yat-sen University, Guangzhou, China

The cytochrome P450 enzymes (P450s or CYPs) are heme-containing enzymes which catalyze a wide range of oxidation reactions in nature. In our previous study, a rare multifunctional P450 AstB was found, which can dually oxidize two methyl groups (C-19 and C-21) of preasperterpenoid A to asperterpenoid A with 3-carboxyl and 11-hydroxymethyl groups. However, the oxidation order of C-19 and C-21 catalyzed by AstB is unclear. In order to reveal this oxidation order, probable pathways catalyzed by AstB were proposed, and the oxidation order of C-19 and C-21 was obtained by quantum chemistry calculations. The potential intermediates (three new asperterpenoids D–F, **1**–**3**) were obtained through the chemical investigation on the extract of the transformant strain and chemical conversions, which were used as the standards to detect their existences in the extract of the transformant strain with HPLC-MS. Combined with the quantum chemistry calculation and the HPLC-MS analysis, the catalyzed order of AstB in asperterpenoid A biosynthesis was revealed. Furthermore, the *m*PTPB inhibition of obtained asperterpenoids was evaluated, and the results showed that 3-carboxyl and the oxidation station of C-21 would be the key factors for *m*PTPB inhibition of asperterpenoids.

Keywords: multifunctional P450s, methyl oxidation, asperterpenoids, *m*PTPB inhibition, oxidation cascade

OPEN ACCESS

Edited by:
Xiachang Wang,
Nanjing University of Chinese Medicine, China

Reviewed by:
Giovanna Di Nardo,
University of Turin, Italy
Ahmed M. Sayed,
AlMaaqal University, Iraq

****Correspondence:***
Guo-Dong Chen
chgdtong@163.com
Hao Gao
tghao@jnu.deu.cn

Specialty section:
This article was submitted to Medicinal and Pharmaceutical Chemistry, a section of the journal Frontiers in Chemistry

Received: *29 September 2021*
Accepted: *15 November 2021*
Published: *16 December 2021*

Citation:
Huang H-Y, Huang J-H, Wang Y-H, Hu D, Lu Y-J, She Z-G, Chen G-D, Yao X-S and Gao H (2021) The Oxidation Cascade of a Rare Multifunctional P450 Enzyme Involved in Asperterpenoid A Biosynthesis. Front. Chem. 9:785431. doi: 10.3389/fchem.2021.785431

INTRODUCTION

Cytochrome P450 enzymes (P450s or CYPs) are a kind of enzyme catalyzing a wide range of oxidation reactions at the specific site of molecules, which play an important role in the metabolism of organisms (Sheng et al., 2009) and the biosynthesis of natural products with potent bioactivity (Jiang et al., 2021; Lin et al., 2019). For examples, human P450c11 catalyzes the generation of cortisol (one of glucocorticoids in human organisms) from 11-deoxycortisol (Bertram et al., 2012). P450 2D6 is in charge for the transformation of codeine to morphine (one of the famous analgesics) (Kramlinger et al., 2015). TwCYP712K1 performs the three-step oxidation of fridelin to polpunonic acid in celastrol (a potent anticancer and anti-obesity natural product from *Tripterygium wilfordii* Hook. f) (Zhou et al., 2021). More and more research studies have found that some P450s can be involved in the oxidation reactions with multiple sites of molecules (Bai et al., 2020; Child et al., 2019; Erickson et al., 2007; Yanni et al., 2008; Zeng et al., 2019) and catalyze non-oxidation reactions (Bai et al., 2020; Keyler et al., 2003; Long and Dolan,

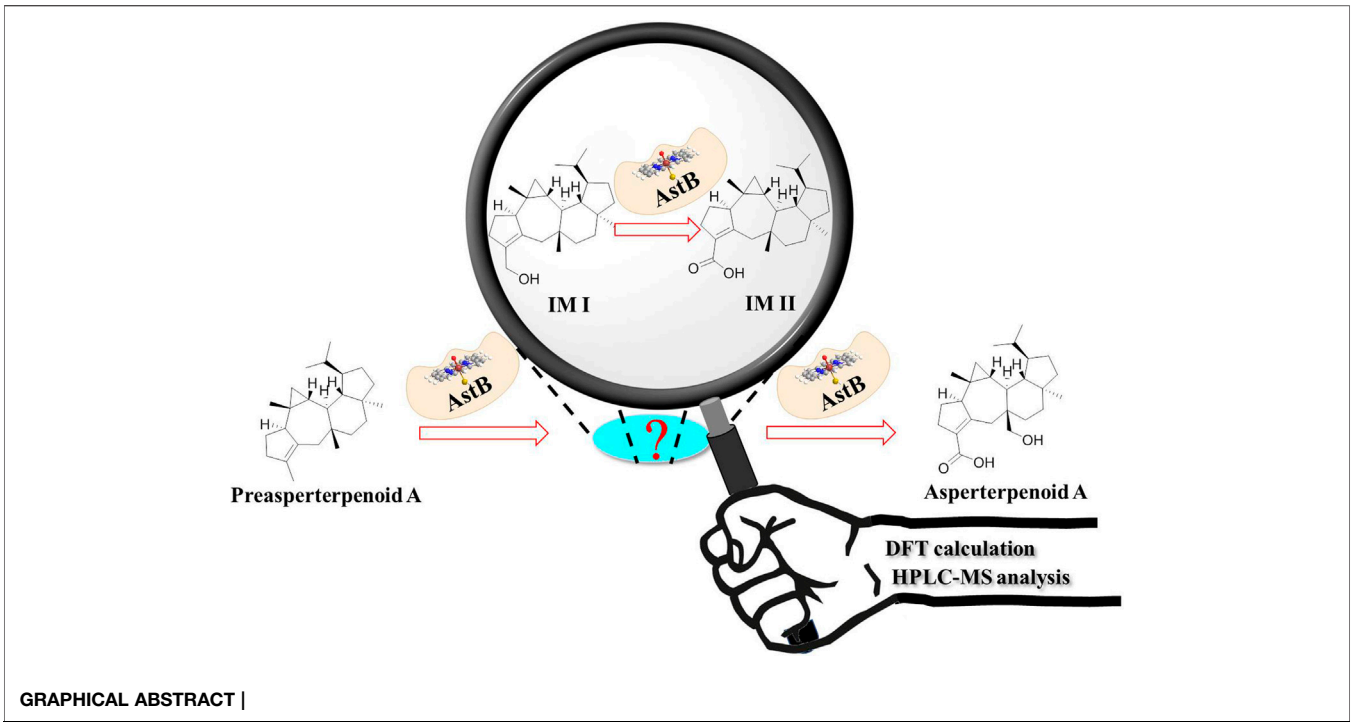

GRAPHICAL ABSTRACT |

2001; Peyronneau et al., 2012), which are classified as multifunctional P450s. In reported multifunctional P450 family, only few oxidation cascades have been demonstrated (Cochrane and Vederas, 2014; Erickson et al., 2007; Mendez et al., 2014; Moses et al., 2015; Narita et al., 2016; Zeng et al., 2019).

In our search of bioactive compounds from fungi through genome mining (Huang et al., 2019; Zhang et al., 2020), a rare oxidation multifunctional P450 AstB was found, which was solely responsible for the transformation of preasperterpenoid A to asperterpenoid A (the molecule with 3-carboxyl and 11-hydroxymethyl groups) *via* C-19 and C-21 oxidations of preasperterpenoid A (**Figure 1**). Furthermore, asperterpenoids A (IC_{50} = 2.16 μM) and B (the molecule with 3,11-dicarboxyl, IC_{50} = 2.50 μM) presented the potent inhibition against *Mycobacterium tuberculosis* protein tyrosine phosphatase B (*m*PTPB, a virulence factor secreted by *M. tuberculosis* and can facilitate the establishment of tuberculosis infection and pathogenesis) (Huang et al., 2013; Huang et al., 2019). However, the oxidation order of C-19 and C-21 catalyzed by AstB remained obscure because no intermediate in the generation of asperterpenoid A was obtained from the heterologously expressed *astBC*-harboring transformant strain (*Aspergillus oryzae*) with the previous fermentation condition (Huang et al., 2019). Therefore, the quantum chemistry calculations of the oxidation order of C-19 and C-21, the acquirements of the potential intermediates, and the HPLC-MS detection of the potential intermediates in the transformant strain were carried out. In addition, the *m*PTPB inhibition of obtained asperterpenoids was also evaluated.

MATERIALS AND METHODS

General Experimental Procedures

Methanol (MeOH) was purchased from Yuwang Industrial Co. Ltd. (Yucheng, China). Acetonitrile (MeCN) and acetone were obtained from Oceanpak Alexative Chemical Co. Ltd. (Gothenburg, Sweden). Cyclohexane and ethyl acetate (EtOAc) were analytical grade from Fine Chemical Co. Ltd. (Tianjin, China). The biochemical reagents and kits used in this study were purchased from TaKaRa Bio Inc. (Dalian, China), Thermo Fisher Scientific Inc. (Shenzhen, China), and Sangon Biotech Co. Ltd. (Shanghai, China), unless noted otherwise.

UV data, IR data, and optical rotations were, respectively, measured on the JASCO V-550 UV/vis spectrometer, JASCO FT/IR-4600 plus spectrometer, and JASCO P2000 digital polarimeter from JASCO International Co. Ltd. (Tokyo, Japan). ECD spectra were recorded in MeOH using a JASCO J-810 spectrophotometer (Jasco International Co. Ltd., Tokyo, Japan) at room temperature. The HRESIMS data were obtained on a Waters Micromass Q-TOF mass spectrometer from Waters Corporation (Milford, United States). 1D and 2D NMR spectra were recorded with the Bruker AV 600 spectrometer from Bruker BioSpin Group (Faellanden, Switzerland) using the solvent signals ($CDCl_3$: δ_H 7.26/δ_C 77.0) as the reference. Analytical HPLC was performed on a Thermo Fisher HPLC system equipped with an Ultimate 3000 pump, an Ultimate 3000 diode array detector, an Ultimate 3000 column compartment, an Ultimate 3000 autosampler (Thermo Fisher, United States), and an Alltech (Grace) 2000ES evaporative light scattering detector (Alltech, United States) using a COSMOSIL 3C18-EB column (4.6 mm i.d. × 150 mm, 3 μm) with a linear gradient of 50–100% H_2O

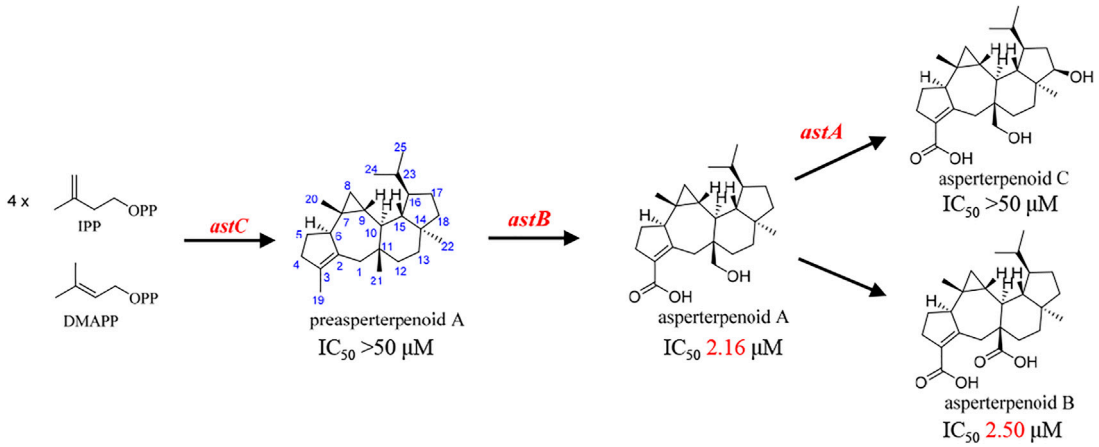

FIGURE 1 | Biosynthesis and IC_{50} value (*m*PTPB inhibitions) of the reported asperterpenoids.

(0.1% formic acid)-MeCN (0.1% formic acid) in 25 min followed by 100% MeCN (0.1% formic acid) for 35 min at 1 ml min^{-1}. The semi-preparative HPLC was performed on an Ultimate 3000 HPLC system (Thermo Fisher) with a YMC-Pack ODS-A column (10.0 mm i.d. × 250 mm, 5 μm). Column chromatography (CC) was carried out on silica gels (200–300 mesh) (Qingdao Haiyang Chemical Group Corporation, Qingdao, China).

Density Functional Theory Calculation of Hydrogen Abstraction Catalyzed by AstB

The computational reaction model (105 atoms) consisted of the two parts: 1) preasperterpenoid A and 2) Cpd I [see **Figure 3**, a brief P450 enzyme including a truncated heme and a thiolate axial ligand (SH-)]. Geometries for all the stationary points, including the reactant complex (RC), product complex (PC), and transition state (TS), were fully optimized in the gas phase using the M06 method in conjugation of the SDD(Fe)/6-31G*(C, H, O, N, and S) basis set (Fukui, 1981; Hratchian and Schlegel, 2004). (For details, see **Supplementary Information S1**.)

Fungal Source, Fermentation Condition Investigation, Extraction, and Isolation of Asperterpenoid D (1)

The strain of the *A. oryzae* transformant harboring *astBC* was obtained in previous study (Huang et al., 2019). The fungal strain was inoculated into 10 ml DPY medium (2% dextrin, 1% polypeptone, 0.5% yeast extract, 0.05% $MgSO_4{\cdot}7H_2O$, 0.5% KH_2PO_4, and 0.01% adenine) and was cultured at 28°C and 200 rpm for 2 days as the seed broth. Then the broth was transferred into 15 Erlenmeyer flasks (500 ml), each containing 100 ml of fermentation medium and grown at 28°C and 200 rpm. The screening of the fermentation conditions was carried out through bifactor analysis with culture media (rice, ME, PDB, GPY, and maltose media) and fermentation days (3, 5, and 7 days for liquid media and 10, 20, and 45 days for the rice medium, respectively) as variable factors. The rice medium contained 70 g of rice and 105 ml distilled H_2O on each flask; ME medium contained 2% malt extract, 1% polypeptone, and 2% starch; PDB medium contained 20% potato and 2% dextrose; GPY medium contained 2% starch, 0.5% peptone, and 0.2% yeast extract; maltose medium contained 3% starch, 0.15% yeast extract, 0.1% $MgSO_4$, 0.25% malt extract, 0.2% KH_2PO_4, and 0.4% $CaCO_3$ (**Supplementary Figures S6–S10**). Through the screening of fermented conditions, the intermediate II (asperterpenoid D, **1**) was found in rice, GPY, PDB, ME, and maltose media, respectively (**Supplementary Figures S6–S11**, **Figure 4**). Then fermentation was carried out in 30 Erlenmeyer flasks (500 ml), each containing 100 ml of ME medium. After autoclaving at 121°C for 30 min, each flask was inoculated with 10 ml of the seed broth and cultured at 28°C and 200 rpm for 3 days.

Mycelia were harvested by filtration and extracted with acetone (2 L). The extraction was repeated for three times, and the extract was dried under reduced pressure to obtain a crude extract (4.7 g). Then the crude extract was fractionated in a dried column vacuum chromatography system filled with silica gel, using cyclohexane (100%), cyclohexane-AcOEt (98:2), cyclohexane-AcOEt (90:10), AcOEt (100%), and MeOH (100%) to obtain fractions of 126.8, 20.5, 676.3, 544.1, and 700.6 mg, respectively. The fraction eluted with cyclohexane-AcOEt (98:2) was subjected to semi-preparative HPLC, using MeCN-H_2O (90:10, v/v) containing 0.1% formic acid at a flow rate of 3 ml min^{-1} to yield asperterpenoid D (**1**) (t_R: 13.8 min, 7.9 mg).

The Preparations of Asperterpenoids E (2) and F (3)

Asperterpenoid E (IM-I, **2**) preparation: a magnetically stirred mixture of asperterpenoid D (**1**) (20 mg, 0.05 mmol) in dry THF (tetrahydrofuran) (10 ml) was treated with $LiAlH_4$ (18.89 mg, 0.50 mmol), and the ensuing gray suspension was stirred at 85°C under a balloon of nitrogen for 48 h

TABLE 1 | ^{1}H (600 MHz) and ^{13}C NMR (150 MHz) data of compounds **1–3** in $CDCl_3$.

	1		2		3	
Position	**δ_C, type**	**δ_H, (*J* in Hz)[a]**	**δ_C, type**	**δ_H, (*J* in Hz)[a]**	**δ_C, type**	**δ_H, (*J* in Hz)[a]**
1	47.9, CH_2	a: 3.57, d (13.4)	47.0, CH_2	a: 2.44, d (13.9)	41.6, CH_2	a: 2.94, d (13.7)
	—	b: 1.79, d (13.4)	—	b: 1.71, d (13.9)	—	b: 1.45, d (13.7)
2	162.1, C	—	134.7, C	—	135.6, C	—
3	126.4, C	—	140.6, C	—	140.7, C	—
4	33.1, CH_2	a: 2.63	33.7, CH_2	a: 2.48	35.5, CH_2	a: 2.63
	—	b: 2.55, br dd (16.0, 9.8)	—	b: 2.33	—	b: 2.13, ddd (15.8, 9.6, 2.6)
5	26.0, CH_2	a: 1.98, br dd (13.0, 7.5)	26.2, CH_2	a: 1.97, br dd (13.1, 7.4)	26.6, CH_2	a: 1.98. br dd (13.1, 7.2)
	—	b: 1.90, dq (13.0, 9.4)	—	b: 1.85, dq (13.0, 9.4)	—	b: 1.86, dq (13.1, 9.4)
6	56.8, CH	2.30, br d (8.7)	54.6, CH	2.17, br d (9.0)	55.4, CH	2.18, br d (8.8)
7	21.5, C	—	22.1, C	—	22.6, C	—
8	25.5, CH_2	a: 0.61, dd (8.4, 4.2)	25.1, CH_2	a: 0.55, dd (8.3, 4.2)	25.8, CH_2	a: 0.60, dd (8.4, 4.3)
	—	b: 0.37, br t (4.7)	—	b: 0.33, dd (5.2, 4.2)	—	b: 0.33, br t (4.9)
9	29.8, CH	0.22	29.4, CH	0.10	29.1, CH	0.06, ddd (10.5, 8.4, 5.6)
10	47.7, CH	1.21	47.2, CH	1.19	47.7, CH	1.34, t (11.1)
11	40.4, C	—	39.2, C	—	43.9, C	—
12	39.3, CH_2	a: 1.61	39.3, CH_2	a: 1.60	30.0, CH_2	a: 1.91
	—	b: 1.39	—	b: 1.33	—	b: 1.24
13	35.9, CH_2	a: 1.40	35.9, CH_2	a: 1.45	35.7, CH_2	a: 1.47
	—	b: 1.31	—	b: 1.31	—	b: 1.27
14	43.0, C	—	42.9, C	—	42.8, C	—
15	50.9, CH	1.21	51.0, CH	1.19	51.4, CH	1.16, t (11.0)
16	45.4, CH	1.77	45.3, CH	1.76	45.6, CH	1.73, tdd (10.5, 4.3, 3.1)
17	22.4, CH_2	a: 1.60	22.2, CH_2	a: 1.61	22.2, CH_2	a: 1.60
	—	b: 1.45	—	b: 1.45	—	b: 1.44
18	40.1, CH_2	a: 1.37	40.0, CH_2	a: 1.35	39.9, CH_2	a: 1.37
	—	b: 1.00	—	b: 0.99	—	b: 1.00
19	171.6, C	—	59.0, CH_2	a: 4.25, d (11.1)	59.2, CH_2	a: 4.40, d (12.5)
	—	—	—	b: 4.17, d (11.1)	—	b: 3.98, d (12.5)
20	20.8, CH_3	0.93, s	20.7, CH_3	0.85, s	21.0, CH_3	0.95, s
21	20.1, CH_3	0.94, s	20.4, CH_3	0.90, s	61.3, CH_2	a: 3.69, d (10.9)
	—	—	—	—	—	b: 3.62, d (10.9)
22	17.8, CH_3	0.74, s	17.6, CH_3	0.73, s	17.7, CH_3	0.76, s
23	28.5, CH	2.30	28.4, CH	2.33	28.3, CH	2.27
24	23.3, CH_3	0.86, d (6.6)	23.2, CH_3	0.86, d (6.6)	23.1, CH_3	0.85, d (6.9)
25	15.3, CH_3	0.78, d (6.6)	15.1, CH_3	0.76, d (6.6)	15.0, CH_3	0.74, d (6.9)

[a]*Indiscernible signals from overlap or the complex multiplicity are reported without designating multiplicity.*

then extracted with water/ethyl acetate. The organic layer was concentrated under reduced pressure, and the residue was isolated by semi-preparative HPLC (YMC-Pack ODS-A column, 3 ml min^{-1}) with isocratic elution of 85% MeCN-H_2O containing 0.1% formic acid to yield **2** (t_R: 62.0 min, 5.0 mg).

Asperterpenoid F (IM-IV, **3**) preparation: A magnetically stirred mixture of asperterpenoid A (40 mg, 0.10 mmol) in dry THF (10 ml) was treated with $LiAlH_4$ (36.22 mg, 0.96 mmol), and the ensuing gray suspension was stirred at 85°C under a balloon of nitrogen for 48 h then extracted with water/ethyl acetate. The organic layer was concentrated under reduced pressure, and the residue was isolated by semi-preparative HPLC (YMC-Pack ODS-A column, 3 ml min^{-1}) with isocratic elution of 85% MeCN-H_2O containing 0.1% formic acid to yield **3** (t_R: 27.0 min, 17.7 mg).

Structural Characterizations of 1–3

Asperterpenoid D (**1**): amorphous white powder; ^{1}H and ^{13}C NMR (see **Table 1**); $[\alpha]_D^{24}$ +85.5 (*c* 0.20, MeOH); UV (MeOH) λ_{max} (log ε) 203 (3.79) and 235 (3.96); ECD λ_{nm} ($\Delta\varepsilon$) (MeOH) 211 (+1.46) and 243 (−2.84) nm; IR (KBr) ν_{max} 3,278, 3,049, 2,956, 2,927, 2,870, 2,837, 1,740, 1,679, 1,629, 1,458, 1,383, 1,287, 1,267, 948, and 936 cm^{-1}; HRESIMS (positive) *m/z* 371.2934 $[M + H]^+$ (calcd. for $C_{25}H_{39}O_2$, 371.2950) (**Supplementary Table S2**, **Supplementary Figures S14–S23**).

Asperterpenoid E (**2**): amorphous white powder; ^{1}H and ^{13}C NMR (see **Table 1**); $[\alpha]_D^{24}$ +64.0 (*c* 0.20, MeOH); UV (MeOH) λ_{max} (log ε) 203 (4.03) and 252 (4.27); ECD λ_{nm} ($\Delta\varepsilon$) (MeOH) 208 (+2.19), 236 (−0.35), 263 (+4.08), and 330 (−1.60) nm; IR (KBr) ν_{max} 3,411, 2,955, 2,927, 2,871, 2,855, 1,704, 1,602, 1,460, and 1,384 cm^{-1}; HRESIMS (positive) *m/z* 339.3036 $[M + H–H_2O]^+$ (calcd. for $C_{25}H_{39}$, 339.3046). (**Supplementary Table S4**, **Supplementary Figures S26–S35**).

Asperterpenoid F (**3**): amorphous white powder; ^{1}H and ^{13}C NMR (see **Table 1**); $[\alpha]_D^{24}$ +36.5 (*c* 0.23, MeOH); UV (MeOH) λ_{max} (log ε) 208 (3.17) and 257 (3.59); ECD λ_{nm} ($\Delta\varepsilon$) (MeOH) 207 (+2.76), 233 (−0.03), 261 (+0.96), and 338 (−0.43) nm; IR (KBr) ν_{max} 3,316, 2,953, 2,930, 2,890, 1,672, 1,461, 1,379, and 1,023 cm^{-1}; HRESIMS (positive) *m/z* 395.2917 $[M + Na]^+$ (calcd. for $C_{25}H_{40}O_2Na$, 395.2921) (**Supplementary Table S5**, **Supplementary Figures S36–S45**).

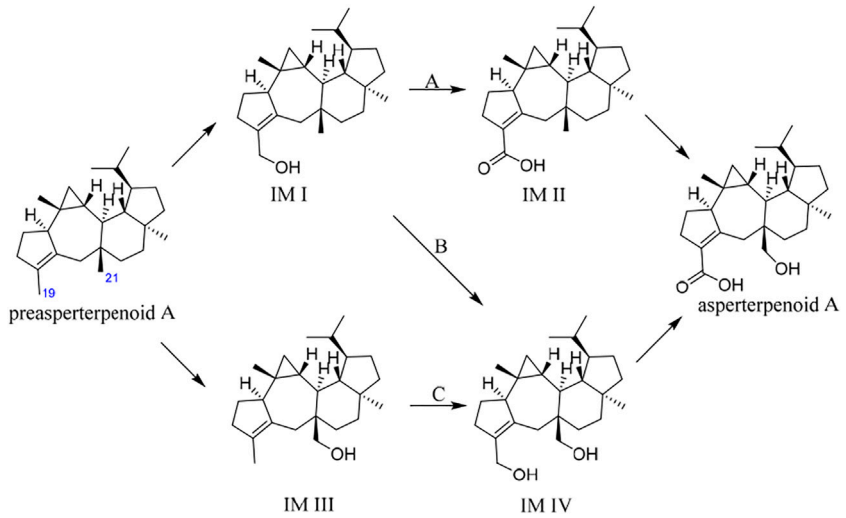

FIGURE 2 | Three possible routes for AstB enzyme catalyzing oxidations.

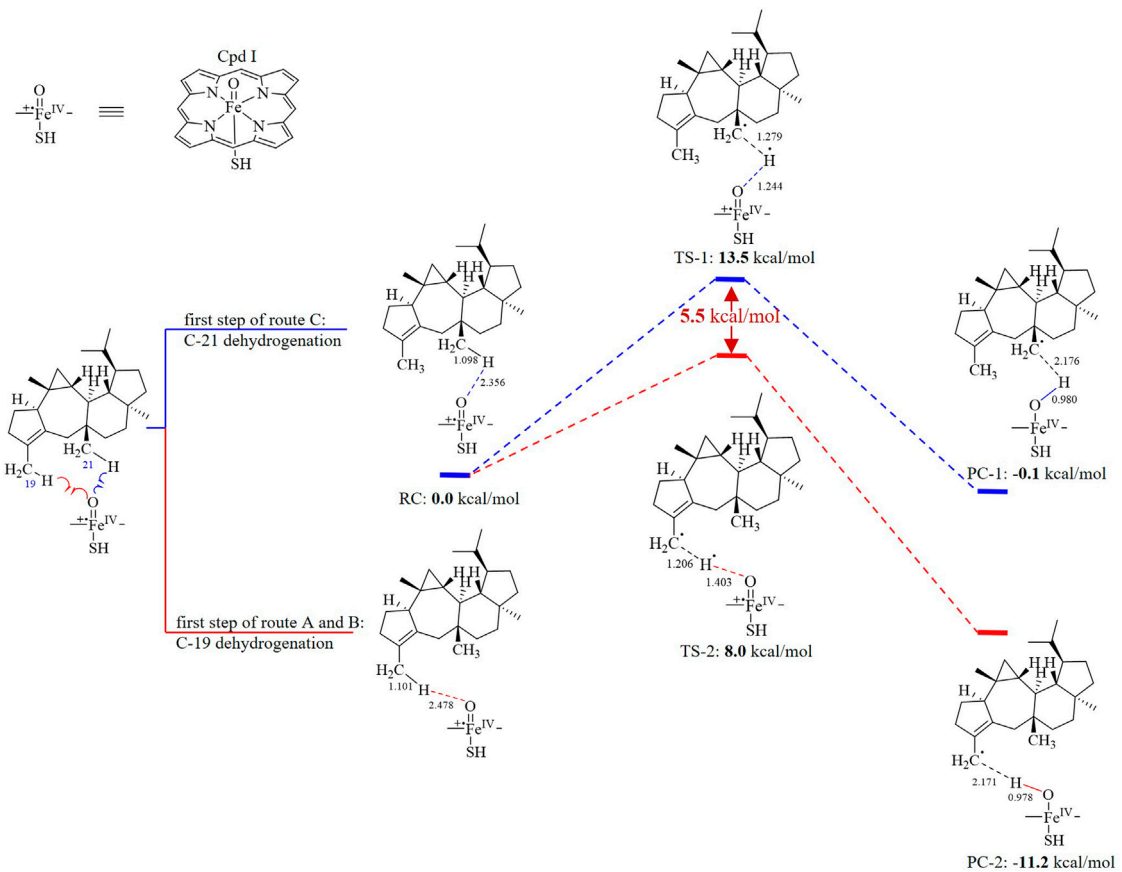

FIGURE 3 | Dehydrogenation energy calculations of C-19 dehydrogenation (first step of route A and B) and C-21 dehydrogenation (first step of route C).

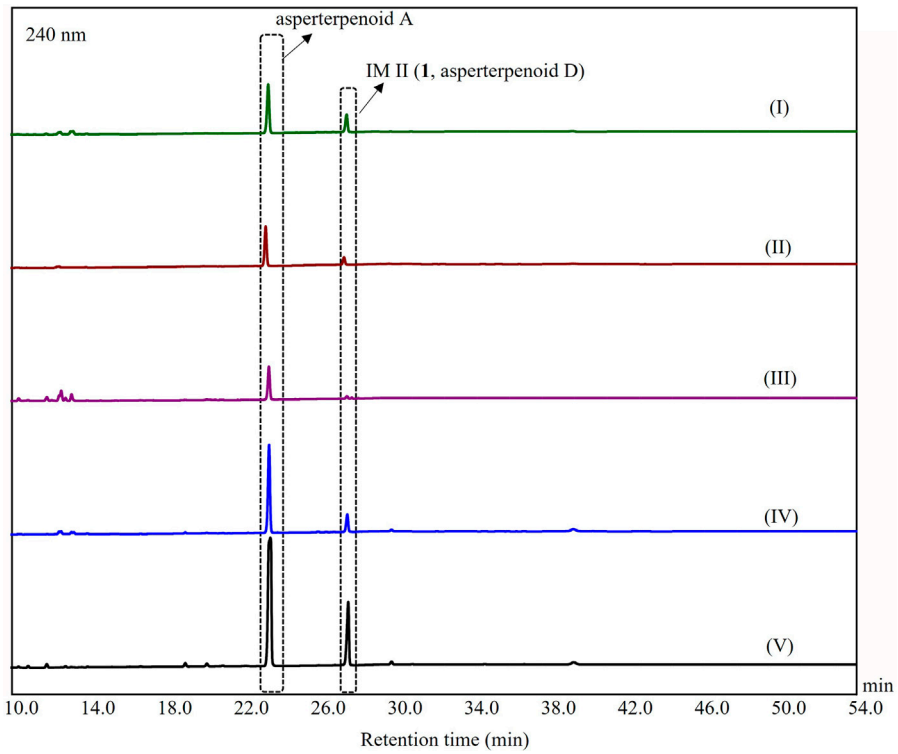

FIGURE 4 | HPLC analysis of metabolites from *A. oryzae* transformants harboring *astBC*. (I) The strain was cultured in the GPY medium for 3 days, (II) the strain was cultured in the PDB medium for 3 days, (III) the strain was cultured in the rice medium for 10 days, (IV) the strain was cultured in the maltose medium for 3 days, and (V) the strain was cultured in the ME medium for 3 days.

RESULTS AND DISCUSSION

It is known that hydroxymethyl is a common intermediate in oxidation of a methyl group to carboxyl, such as 12-OH-(-)-JAMe (the intermediate derived from (-)-JAMe) as the key intermediate in the generation of 12-COOH-(-)-JAMe (Kombrink, 2012). Because the oxidation orders of 3- and 11-methyls to hydroxymethyls and 3-hydroxymethyl to 3-carboxyl are unclear, there would be four potential intermediates, leading to three possible oxidation routes (A, B, and C) for the generation of asperterpenoid A from preasperterpenoid A catalyzed by AstB (**Figure 2**).

To the best of our knowledge, the hydrogen atoms of allyl carbons are generally more active and easier to leave than those of other kinds of carbons (Zerth et al., 2003). Based on this, it is proposed that the route A would exist in the transformation of preasperterpenoid A to asperterpenoid A catalyzed by AstB because C-19 (allyl carbon) oxidation is theoretically prior to C-21 oxidation in the route A. In order to confirm this inference, the DFT calculations were carried out (Denningtonll TK et al., 2003; Frisch GWT et al., 2013; Fukui, 1981; Hratchian and Schlegel, 2004; Sansen et al., 2007; Tao et al., 2015).

The oxidation first occurring at C-19 or C-21 is decided by the Gibbs free energy barriers of C-19 and C-21 dehydrogenations. Based on the DFT calculations (**Figure 3**), the free energy barriers of C-19 (transition state 2, TS-2) and C-21 (transition state 1, TS-1) dehydrogenations were predicted to be 8.0 and 13.5 kcal/mol, respectively. Therefore, the energy gap of two dehydrogenations was 5.5 kcal/mol (the probability of the occurrence of C-19 dehydrogenation was 99.99%), which indicated that C-19 oxidation would be the first step in the oxidations catalyzed by AstB. The calculation results also confirmed that the hydrogen atoms of allyl carbons are easier to leave than those of other kinds of carbons. In addition, H-19 in IM I would be easier to leave rather than H-21 because of the inductive effect from 19-hydroxyl group. Therefore, the 3-hydroxymethyl group of IM I would be subsequently oxidized to form IM II, rather than to form IM IV. These results were consistent with our inference that the route A would exist in the oxidations of AstB. (For details, see **Supplementary Information S1**).

In order to confirm the results from the DFT calculations, the acquirement of the key intermediates was necessary. In our previous study, no intermediate was observed in the extract of the heterologous expressed *astBC*-harboring transformant strain (*A. oryzae*), which would be resulted from the fermentation without an appropriate condition or the trace amount of the intermediates (Huang et al., 2019). According to this, the screening of the fermentation conditions was carried out using a bifactor analysis with a culture medium (rice, GPY, PDB, ME, and maltose media) and fermentation days (3, 5, and 7 days for liquid media and 10, 20, and 45 days for rice medium) as variable factors. (For details, see **Supplementary Information S2**, **Supplementary Figures**

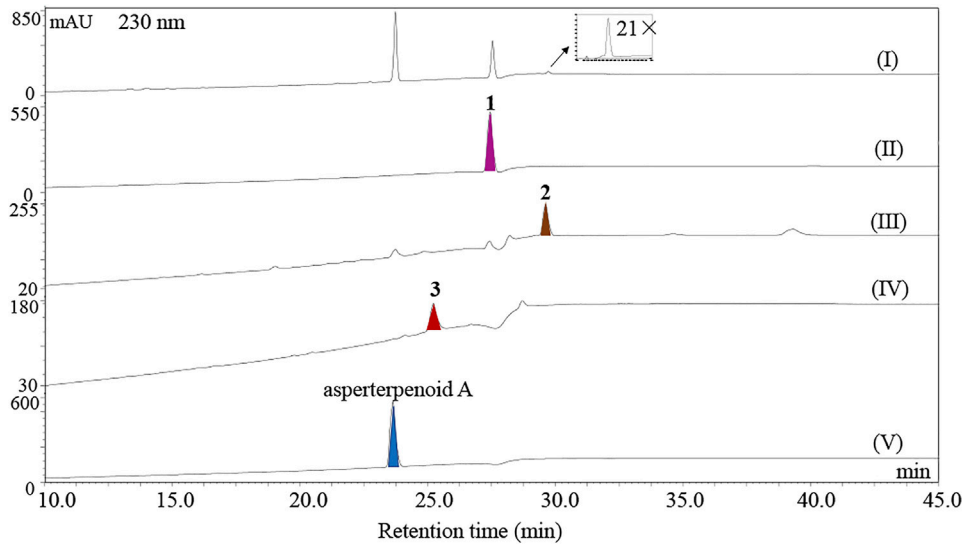

FIGURE 5 | HPLC analysis of metabolites. (I) HPLC chromatogram of the extract of the *A. oryzae* transformants harboring *astBC* cultured in the ME medium for 3 days, (II–V) HPLC chromatograms of asperterpenoid D (**1**), asperterpenoid E (**2**), asperterpenoid F (**3**), and asperterpenoid A.

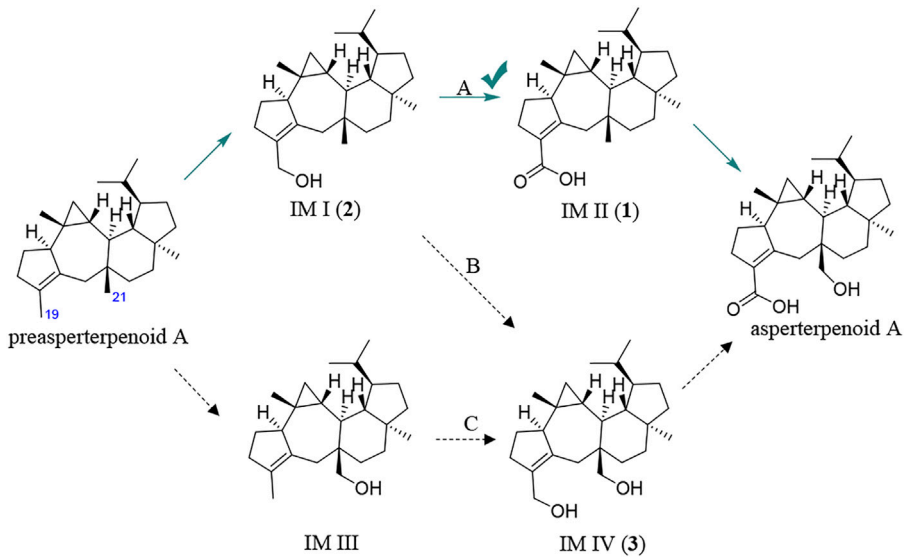

FIGURE 6 | Main pathway for AstB enzyme catalyzing oxidations.

S6–S10.) An additional chromatographic peak was observed when the strain was fermented with rice, GPY, PDB, maltose, and ME media, respectively. Among them, the peak in the extract of the fermentation using ME medium with 3 days was the most obvious (**Figure 4**). The HPLC-MS analysis showed that the peak would be a new asperterpenoid (the positive ion peak at *m/z* 353.39 $[M + H - H_2O]^+$) (**Supplementary Figure S11**). After the isolation of this additional chromatographic peak through the large-scale fermentation with the ME medium for 3 days, the peak compound (**1**) was obtained. Based on the detailed NMR analysis (**Supplementary Table S2**, **Supplementary Figures S18–S23**) combined with ECD calculation (**Supplementary Information S4.2**, **Supplementary Figures S24, S25**), the structure of **1** was determined as a new asperterpenoid with 3-methyl oxidized to 3-carboxyl, which was IM II in route A and named as asperterpenoid D. The result confirmed the existence of route A in the oxidations catalyzed by AstB.

Furthermore, the potential intermediates IM I and IM IV were prepared with the artificial reduction from

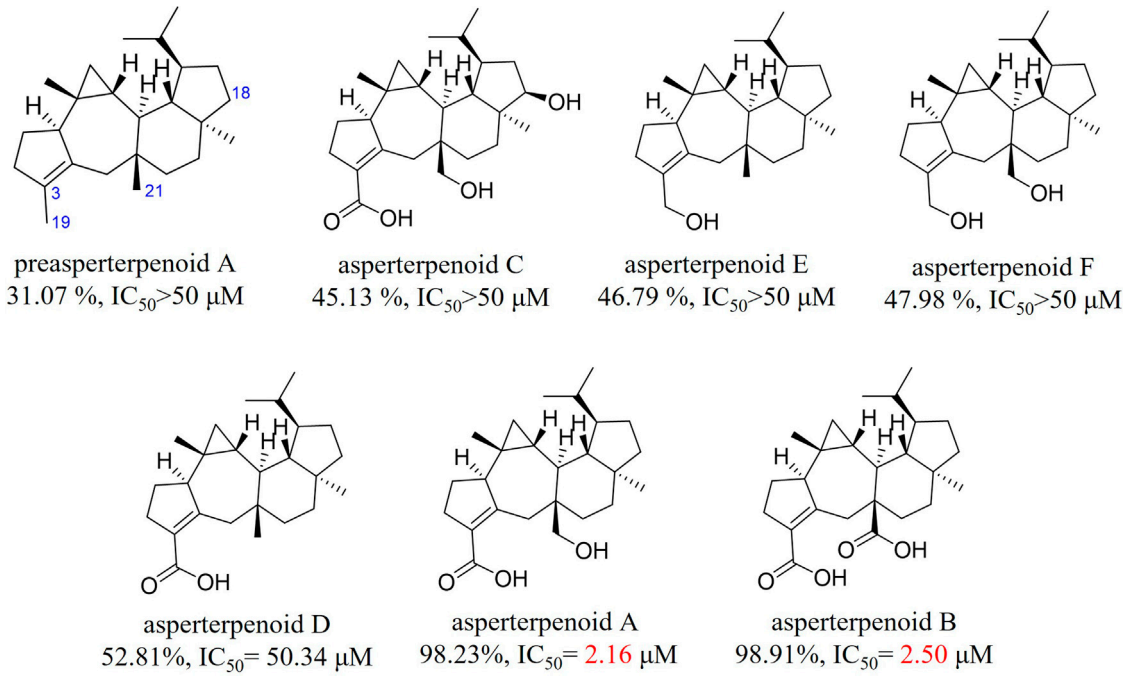

FIGURE 7 | *m*PTPB inhibition at 50 μM and IC_{50} value of asperterpenoids.

asperterpenoid D and asperterpenoid A because the potential intermediates IM I and IM IV were the biosynthetic precursors of asperterpenoid D and asperterpenoid A in the relevant proposed route. After reduction from asperterpenoid D with $LiAlH_4$, the potential intermediate IM I (**2**, named asperterpenoid E) was obtained, and its structure was confirmed as a new asperterpenoid with 3-methyl oxidized to 3-methylol based the detailed analyses of NMR data (**Supplementary Table S4**, **Supplementary Figures S26–S35**). By the same way, the potential intermediate IM IV (**3**, named asperterpenoid F) was also obtained, and its structure was identified by the detailed analyses of NMR (**Supplementary Table S5**, **Supplementary Figures S36–S45**). Through HPLC-MS analysis with compounds **1–3** and asperterpenoid A as standards (HPLC analysis see **Figure 5**, HPLC-MS analysis see **Supplementary Figures S12, S13**), a tiny chromatographic peak (t_R = 29.6 min) was identified as asperterpenoid E (**2**) in the HPLC chromatogram of the *astBC*-harboring transformant strain (*A. oryzae*) in the ME medium cultured for 3 days (see **Figure 5I**, **Supplementary Information S3**, **Supplementary Figure S12**). In the HPLC-MS analysis, however, there was no peak with the same retention time and ion peak as asperterpenoid F (**3**) in the extract of the *astBC*-harboring transformant strain (*A. oryzae*) (see **Supplementary Figure S13**), indicating that **3** would not exist. These experiment data supported that the route A was the oxidization cascade of AstB (**Figure 6**).

In the previous study, it was found that asperterpenoids A and B showed potent inhibition against *m*PTPB and 18-hydroxyl would weaken the inhibition (Huang et al., 2019). For the abstention of asperterpenoids with 3-hydroxymethyl, the relationship between the oxidation stations of C-19 and C-21 in asperterpenoids and their *m*PTPB inhibition was unknown. In this research, the *m*PTPB inhibition of three new asperterpenoids (**1–3**, asperterpenoids D–F) and five known asperterpenoids (preasperterpenoid A and asperterpenoids A–C) was evaluated (**Figure 7**, detail see **Supplementary Information S7**, **Supplementary Table S6**). Among these new asperterpenoids, only asperterpenoid D (**2**) presented the *m*PTPB inhibition (IC_{50} = 50.34 μM), which was weaker than those of asperterpenoids A and B. The data clearly showed that 3-carboxyl and the oxidation station of C-21 were essential for *m*PTPB inhibition of asperterpenoids.

In conclusion, the oxidation cascade of a rare multifunctional P450 enzyme (AstB) was cleared based on the combination of the quantum chemistry calculations and the experiments of obtaining the potential intermediates and the HPLC-MS detection of the potential intermediates. Furthermore, the relationship between the oxidation stations of C-19 and C-21 in asperterpenoids and their *m*PTPB inhibition was also revealed.

DATA AVAILABILITY STATEMENT

The original contributions presented in the study are included in the article/**Supplementary Material**; further inquiries can be directed to the corresponding authors.

AUTHOR CONTRIBUTIONS

This study was designed and supported by HG, X-SY, and G-DC. The isolations, structural elucidations, calculated ECD, and the fungal fermentation were performed by H-YH and J-HH. Density functional theory (DFT) calculation of hydrogen abstraction catalyzed by AstB was performed by H-YH and Y-HW. The anti-*m*PTPB assay was performed by Y-JL and Z-GS. The transformant strains were supplied by J-HH and DH. The manuscript was written by H-YH and G-DC. The paper was revised by HG.

FUNDING

This work was financially supported by grants from National Key Research and Development Program of China (2018YFA0903200/2018YFA0903201), the National Natural Science Foundation of China (81925037 and 81973213), National High-level Personnel of Special Support Program (2017RA2259), the 111 Project of Ministry of Education of the People's Republic of China (B13038), Guangdong Natural Science Funds for Distinguished Young Scholar (2017A03036027, China), Local Innovative and Research Teams Project of Guangdong Pearl River Talents Program (2017BT01Y036, China), and K. C. Wong Education Foundation (G-DC, 2021, China). The calculations were supported by the high-performance computing platform of Jinan University.

SUPPLEMENTARY MATERIAL

The Supplementary Material for this article can be found online at: https://www.frontiersin.org/articles/10.3389/fchem.2021.785431/full#supplementary-material

REFERENCES

Bai, X. B., Guo, H., Chen, D. D., Yang, Q., Tao, J., and Liu, W. (2020). Isolation and Structure Determination of Two New Nosiheptide-Type Compounds Provide Insights into the Function of the Cytochrome P450 Oxygenase NocV in Nocathiacin Biosynthesis. *Org. Chem. Front.* 7, 584–589. doi:10.1039/c9qo01328h

Bertram, G. K., Susan, B. M., and Anthony, J. T. (2012). *Basic & Clinic Pharmacology*. New York, NY: McGraw Hill.

Child, S. A., Rossi, V. P., and Bell, S. G. (2019). Selective ω-1 Oxidation of Fatty Acids by CYP147G1 from *Mycobacterium marinum*. *Biochim. Biophys. Acta (Bba) - Gen. Subjects* 1863, 408–417. doi:10.1016/j.bbagen.2018.11.013

Cochrane, R. V. K., and Vederas, J. C. (2014). Highly Selective but Multifunctional Oxygenases in Secondary Metabolism. *Acc. Chem. Res.* 47, 3148–3161. doi:10.1021/ar500242c

Denningtonll TK, R., Millam, J., Eppinnett, K., Hovell, W. L., and Gilliland, R. (2003). *Gauss View*. version 3.0. Wallingford, CT: Gaussian Inc.

Erickson, D. A., Hollfelder, S., Tenge, J., Gohdes, M., Burkhardt, J. J., and Krieter, P. A. (2007). *In Vitro* metabolism of the Analgesic Bicifadine in the Mouse, Rat, Monkey, and Human. *Drug Metab. Dispos.* 35, 2232–2241. doi:10.1124/dmd.107.016055

Frisch GWT, M. J., Schlegel, H. B., Scuseria, G. E., Robb, M. A., Cheeseman, J. R., Scalmani, G., et al. (2013). *Gaussian 09, Revisin D01*. Wallingford, CT: Gaussian Inc.

Fukui, k. (1981). The Path of Chemical Reactions - The IRC Approach. *Acc. Chem. Res.* 14, 363–368. doi:10.1021/ar00072a001

Hratchian, H. P., and Schlegel, H. B. (2004). Accurate Reaction Paths Using a Hessian Based Predictor-Corrector Integrator. *J. Chem. Phys.* 120, 9918–9924. doi:10.1063/1.1724823

Huang, J.-H., Lv, J.-M., Wang, Q.-Z., Zou, J., Lu, Y.-J., Wang, Q.-L., et al. (2019). Biosynthesis of an Anti- Tuberculosis Sesterterpenoid Asperterpenoid A. *Org. Biomol. Chem.* 17, 248–251. doi:10.1039/c8ob02832j

Huang, X.-S., Huang, H.-B., Li, H.-X., Sun, X.-F., Huang, H.-R., Lu, Y.-J., et al. (2013). Asperterpenoid A, a New Sesterterpenoid as an Inhibitor of mycobacterium Tuberculosis Protein Tyrosine Phosphatase B from the Culture of *Aspergillus* sp. 16-5c. *Org. Lett.* 15, 721–723. doi:10.1021/ol303549c

Jiang, F.-L., Gong, T., Chen, J.-J., Chen, T.-J., Yang, J.-L., and Zhu, P. (2021). Synthetic Biology of Plants-Derived Medicinal Natural Products. *Chin. J. Biotechnol.* 37, 1931–1951. doi:10.13345/j.cjb.210138

Keyler, D., Pentel, P. R., Kuehl, G., Collins, G., and Murphy, S. E. (2003). Effects of Nicotine Infusion on the Metabolism of the Tobacco Carcinogen 4-(methylnitrosamino)-1-(3-Pyridyl)-L-Butanone (NNK) in Rats. *Cancer Lett.* 202, 1–9. doi:10.1016/j.canlet.2003.07.004

Kombrink, E. (2012). Chemical and Genetic Exploration of Jasmonate Biosynthesis and Signaling Paths. *Planta* 236, 1351–1366. doi:10.1007/s00425-012-1705-z

Kramlinger, V. M., Rojas, M. A., Kanamori, T., and Guengerich, F. P. (2015). Cytochrome P450 3A Enzymes Catalyze the O-6-Demethylation of Thebaine, a Key Step in Endogenous Mammalian Morphine Biosynthesis. *J. Biol. Chem.* 290, 20200–20210. doi:10.1074/jbc.M115.665331

Lin, H. C., Hewage, R. T., Lu, Y. C., and Chooi, Y. H. (2019). Biosynthesis of Bioactive Natural Products from Basidiomycota. *Org. Biomol. Chem.* 17, 1027–1036. doi:10.1039/c8ob02774a

Long, L., and Dolan, M. E. (2001). Role of Cytochrome P450 Isoenzymes in Metabolism of O-6-Benzylguanine: Implications for Dacarbazine Activation. *Clin. Cancer Res.* 7, 4239–4244.

Mendez, C., Baginsky, C., Hedden, P., Gong, F., Caru, M., and Rojas, M. C. (2014). Gibberellin Oxidase Activities in *Bradyrhizobium japonicum* Bacteroids. *Phytochemistry* 98, 101–109. doi:10.1016/j.phytochem.2013.11.013

Moses, T., Pollier, J., Faizal, A., Apers, S., Pieters, L., Thevelein, J. M., et al. (2015). Unraveling the Triterpenoid Saponin Biosynthesis of the African Shrub *Maesa lanceolata*. *Mol. Plant* 8, 122–135. doi:10.1016/j.molp.2014.11.004

Narita, K., Chiba, R., Minami, A., Kodama, M., Fujii, I., Gomi, K., et al. (2016). Multiple Oxidative Modifications in the Ophiobolin Biosynthesis: P450 Oxidations Found in Genome Mining. *Org. Lett.* 18, 1980–1983. doi:10.1021/acs.orglett.6b00552

Peyronneau, M. A., Saba, W., Dolle, F., Goutal, S., Coulon, C., Bottlaender, M., et al. (2012). Difficulties in Dopamine Transporter Radioligand PET Analysis: the Example of LBT-999 Using [F-18] and [C-11] Labelling Part II: Metabolism Studies. *Nucl. Med. Biol.* 39, 347–359. doi:10.1016/j.nucmedbio.2011.09.006

Sansen, S., Yano, J. K., Reynald, R. L., Schoch, G. A., Griffin, K. J., Stout, C. D., et al. (2007). Adaptations for the Oxidation of Polycyclic Aromatic Hydrocarbons Exhibited by the Structure of Human P450 1a2. *J. Biol. Chem.* 282, 14348–14355. doi:10.1074/jbc.M611692200

Sheng, X., Zhang, H.-M., Hollenberg, P. F., and Newcomb, M. (2009). Kinetic Isotope Effects in Hydroxylation Reactions Effected by Cytochrome P450 Compounds I Implicate Multiple Electrophilic Oxidants for P450-Catalyzed Oxidations. *Biochem* 48, 1620–1627. doi:10.1021/bi802279d

Tao, J., Kang, Y., Xue, Z.-Y., Wang, Y.-T., Zhang, Y., Chen, Q., et al. (2015). Theoretical Study on the N-Demethylation Mechanism of Theobromine Catalyzed by P450 Isoenzyme 1a2. *J. Mol. Graph.* 61, 123–132. doi:10.1016/j.jmgm.2015.06.017

Yanni, S. B., Annaert, P. P., Augustijns, P., Bridges, A., Gao, Y., Benjamin, D. K., et al. (2008). Role of Flavin-Containing Monooxygenase in Oxidative

Metabolism of Voriconazole by Human Liver Microsomes. *Drug Metab. Dispos.* 36, 1119–1125. doi:10.1124/dmd.107.019646

Zeng, H.-C., Yin, G.-P., Wei, Q., Li, D.-H., Wang, Y., Hu, Y.-C., et al. (2019). Unprecedented [5.5.5.6]Dioxafenestrane Ring Construction in Fungal Insecticidal Sesquiterpene Biosynthesis. *Angew. Chem. Int. Edit.* 58, 6569–6573. doi:10.1002/anie.201813722

Zerth, H. M., Leonard, N. M., Mohan, R. S., Leonard, N. M., and Mohan, R. S. (2003). Synthesis of Homoallyl Ethers via Allylation of Acetals in Ionic Liquids Catalyzed by Trimethylsilyl Trifluoromethanesulfonate. *Org. Lett.* 5, 55–57. doi:10.1021/ol0271739

Zhang, W.-Y., Zhong, Y., Yu, Y., Shi, D.-F., Huang, H.-Y., Tang, X.-L., et al. (2020). 4-Hydroxy Pyridones from Heterologous Expression and Cultivation of the Native Host. *J. Nat. Prod.* 83, 3338–3346. doi:10.1021/acs.jnatprod.0c00675

Zhou, J.-W., Hu, T.-Y., Liu, Y., Tu, L.-C., Song, Y.-D., Lu, Y., et al. (2021). Cytochrome P450 Catalyses the 29-Carboxyl Group Formation of Celastrol. *Phytochemistry* 190, 112868. doi:10.1016/j.phytochem.2021.112868

Conflict of Interest: The authors declare that the research was conducted in the absence of any commercial or financial relationships that could be construed as a potential conflict of interest.

Publisher's Note: All claims expressed in this article are solely those of the authors and do not necessarily represent those of their affiliated organizations, or those of the publisher, the editors, and the reviewers. Any product that may be evaluated in this article, or claim that may be made by its manufacturer, is not guaranteed or endorsed by the publisher.

frontiers in Chemistry

ORIGINAL RESEARCH
published: 16 December 2021
doi: 10.3389/fchem.2021.797858

Humulane-Type Macrocyclic Sesquiterpenoids From the Endophytic Fungus *Penicillium* sp. of *Carica papaya*

Fu-Run Wang[1,2†], Li Yang[1†], Fan-Dong Kong[4†], Qing-Yun Ma[1], Qing-Yi Xie[1], You-Gen Wu[2], Hao-Fu Dai[5], Ping Chen[2], Na Xiao[3]* and You-Xing Zhao[1]**

[1]Haikou Key Laboratory for Research and Utilization of Tropical Natural Products, Institute of Tropical Bioscience and Biotechnology, CATAS, Haikou, China, [2]Key Laboratory for Quality Regulation of Tropical Horticultural Crops of Hainan Province, College of Horticulture, Hainan University, Haikou, China, [3]State Key Laboratory of Crop Biology, College of Agronomy, Shandong Agriculture University, Tai'an, Shandong, China, [4]Key Laboratory of Chemistry and Engineering of Forest Products, State Ethnic Affairs Commission, Guangxi Key Laboratory of Chemistry and Engineering of Forest Products, Guangxi Collaborative Innovation Center for Chemistry and Engineering of Forest Products, School of Chemistry and Chemical Engineering, Guangxi University for Nationalities, Nanning, China, [5]Hainan Institute for Tropical Agricultural Resources, CATAS, Haikou, China

OPEN ACCESS

Edited by:
Xiachang Wang,
Nanjing University of Chinese Medicine, China

Reviewed by:
Weaam Ebrahim,
Mansoura University, Egypt
Sherif S. Ebada,
Ain Shams University, Egypt
Orazio Taglialatela-Scafati,
University of Naples Federico II, Italy

***Correspondence:**
Ping Chen
chenping08213@163.com
Na Xiao
xiaona198707@126.com
You-Xing Zhao
zhaoyouxing@itbb.org.cn

[†]These authors have contributed equally to this work

Specialty section:
This article was submitted to Organic Chemistry, a section of the journal Frontiers in Chemistry

Received: 19 October 2021
Accepted: 15 November 2021
Published: 16 December 2021

Citation:
Wang F-R, Yang L, Kong F-D, Ma Q-Y, Xie Q-Y, Wu Y-G, Dai H-F, Chen P, Xiao N and Zhao Y-X (2021) Humulane-Type Macrocyclic Sesquiterpenoids From the Endophytic Fungus Penicillium sp. of Carica papaya. Front. Chem. 9:797858. doi: 10.3389/fchem.2021.797858

Three new humulane-type sesquiterpenoids, penirolide A (**1**), penirolide B (**2**), and 10-acetyl-phomanoxide (**3**), together with three known compounds aurasperone A (**4**), pughiinin A (**5**), and cyclo(L-Leu-L-Phe) (**6**) were isolated from the endophytic fungus *Penicillium* sp. derived from the leaves of *Carica papaya* L. Their structures including their absolute configurations were determined based on the analysis of NMR and HRESIMS spectra, NMR chemical shifts, and ECD calculations. Compounds **2**, **3**, **5**, and **6** significantly inhibited glucagon-induced hepatic glucose production, with EC_{50} values of 33.3, 36.1, 18.8, and 32.1 μM, respectively. Further study revealed that compounds **2**, **3**, **5**, and **6** inhibited hepatic glucose production by suppression of glucagon-induced cAMP accumulation.

Keywords: endophytic fungus, *Penicillium* sp., humulane-type sesquiterpenoid, anti-diabetic activity, cAMP accumulation

INTRODUCTION

Endophytic fungi, living in plants but non-pathogenic, have been proven to be promising sources of secondary metabolites with unusual structures as well as intriguing pharmacology activities, and become interesting and important resources for drug discovery (Strobel, 2003; Uzma et al., 2018; Gupta et al., 2020; Zhang et al., 2006). In recent years, increasing attention has been attracted to metabolite profiles of endophytic fungi from medicinal plants (Kaul et al., 2012). Papaya, *Carica papaya* L. (papaya), an edible and medicinal plant cultivated in tropical and subtropical regions, has been used as topical dressings for ulcer and dermatitis treatment, has gastrointestinal uses such as anti-helminthic and antibacterial activity treatments, has been used as anti-arthritis treatment, and has traditional uses for fertility control (Krishna et al., 2008; Pinnamaneni, 2017).

In our continuing search for structurally novel and biologically active secondary metabolites from endophytic fungi, three new humulane-type sesquiterpenoids, penirolides A (**1**) and B (**2**), and 10-acetyl-phomanoxide (**3**), were isolated from the endophytic fungus *Penicillium* sp. derived from the leaves of papaya. Humulane-type sesquiterpenoids, an uncommon type of compounds featuring an 11-membered macrocycle, were found in plants, liverworts, and fungi, and exhibited various

bioactivities including antibacterial, antifungal, cytotoxic, and immunosuppressive activities (Liao et al., 2013; Luo et al., 2006; Toyota et al., 2004). Due to the flexible 11-membered macrocycle in the molecule, elucidation of the stereochemistry of humulane-type sesquiterpenoids is very challenging. Chiral derivatization and chemical conversions were successfully applied to clarify their configurations (Liao et al., 2013). However, limited amounts of sample available hampers broad use of these methods in the structural elucidation of natural products. Quantum calculations of NMR shifts represents a simple, useful, and fast alternative in address complex stereochemical problems by comparing experimental and computed values using parameters (Lodewyk et al., 2012; Grimblat and Sarotti, 2016), such as correlation coefficient, mean absolute error (MAE), corrected mean absolute error (CMAE), CP3 parameter (Smith and Goodman, 2009), DP4 probability (Smith and Goodman, 2010), or its improved version, DP4+ probability (Grimblat et al., 2015), avoiding chemical derivatization. In our effort to determine the configurations of the new humulane-type sesquiterpenoids (**1**–**3**), extensive spectroscopic analysis including 1D and 2D NMR spectra, NMR chemical shift calculations coupled with DP4+ probability analysis, and ECD calculations were utilized. In addition, all the isolates were evaluated for their anti-diabetic activity on a glucagon-induced glucose production model in mouse hepatocytes. Herein, the isolation, structural elucidation, and biological activities of compounds **1**–**6** **Figure 1** were reported.

RESULTS AND DISCUSSION

Compound **1** was isolated as yellow oil. Its molecular formula was determined as $C_{15}H_{26}O_4$ from the positive ion peak at *m/z* 293.1723 $[M + Na]^+$ (calcd for $C_{15}H_{26}NaO_4$, 293.1723), requiring three indices of hydrogen deficiency. The ^{1}H NMR spectrum (**Table 1**) showed signals for two olefinic protons (δ_H 5.47 and 5.43), three methylenes (δ_H 1.27–2.28), three oxygenated methines (δ_H 2.93, 3.43, and 3.44), and four methyls (δ_H 1.06, 1.08, 1.11, and 1.24). The ^{13}C NMR spectrum revealed the presence of 15 carbons, which were classified by HSQC spectrum as one double bond (δ_C 122.8 and 144.7), three methylenes (δ_C 38.1, 45.1, and 45.6), three oxygenated methines (δ_C 75.6, 80.3, and 63.7), three quaternary carbons (δ_C 36.1, 67.1, and 75.6) including two oxygenated, and four methyls (δ_C 16.5, 22.3, 26.7, and 28.5). The ^{1}H–^{1}H COSY spectrum of **1** presented three coupling spin systems, H-7*α*/H-7*β*–H-8, H-3*α*/H-3*β*–H-4–H-5, and H-10–H-11α/H-11β–H-1 (**Figure 2**). The HMBC correlations (**Figure 2**) from C<u>H</u>$_3$-13 (δ_H 1.06, s)/C<u>H</u>$_3$-14 (1.11, s) to C-5 (δ_C 144.7), C-6 (δ_C 36.1), and C-7 (δ_C 45.1), from H-7*α* (δ_H 1.91, s)/H-7*β* (δ_H 1.27, s) to C-5, from C<u>H</u>$_3$-12 (1.08, s) to C-1 (δ_C 80.3), C-2 (δ_C 75.6), and C-3 (δ_C 45.6), from H-3*α* (δ_H 2.20, s)/H-3*β* (δ_H 2.28, s) to C-1, and from C<u>H</u>$_3$-15 (1.24, s) to C-8 (δ_C 63.7), C-9 (δ_C 67.1), and C-10 (δ_C 75.6) connected the three coupling spin systems and formed the Humulane-type sesquiterpenoid skeleton. The olefinic bond and the macrocycle accounted for two indices of hydrogen deficiency. The remaining one degree of unsaturation together with the analysis of the chemical shift of C-8 and C-9 suggested the existence of oxirane ring at positions 8 and 9.

The vicinal coupling constant (J = 15.8 Hz) between H-4 and H-5 assigned the *E* configured Δ^4 double bond. In the ROESY spectrum, the key correlation of CH_3-15 with H-8 (δ_H 2.93) indicated that CH_3-15 and H-8 were cofacial (**Figure 3**). However, due to the flexibility of the 11-membered ring and the signals overlap (e.g., H-1 and H-10), the relative configuration of other stereocenters (C-1, C-2, and C-10) on the ring could not be fully determined by ROESY spectrum. Thus, we performed theoretical NMR chemical shifts calculations of eight diastereomers (**Figure 4**) of **1** at mPW1PW91-SCRF/6-311G(d,p)//B3LYP-D3BJ/6-31G(d) theoretical level in methanol with the GIAO method (Wolinski et al., 1990). The calculated ^{13}C and ^{1}H NMR chemical shifts of (1*S**,2*S**,8*R**,9*S**,10*R**)-**1** showed the best agreement with the experimental values. Furthermore, DP4+ analysis (Grimblat et al., 2015) predicted that (1*S**,2*S**,8*R**,9*S**,10*R**)-**1** was the most likely candidates with 100% probability. The absolute configuration of **1** was assigned by the ECD calculation (**Figure 5**). The calculated ECD curve of (1*S*,2*S*,8*R*,9*S*,10*R*)-**1** matched well with the experimental curve, establishing the absolute configuration of **1** as 1*S*,2*S*,8*R*,9*S*,10*R*. Collectively, compound **1** was identified as shown in **Figure 1** and named penirolide A.

Compound **2** was isolated as yellow oil. Its molecular formula was determined as $C_{17}H_{28}O_4$ from the positive ion at *m/z* 319.1882 $[M + Na]^+$ (calcd for $C_{17}H_{28}NaO_4$, 319.1880) in the HRESIMS, corresponding to four degrees of unsaturation. The ^{1}H NMR spectrum (**Table 1**) showed resonances for one olefinic proton (δ_H 5.61), three sp^3 methines (δ_H 1.01, 2.93, and 3.04), five methyls (δ_H 0.87, 0.98, 1.15, 1.81, and 2.01), and three methylenes in which one methylene has exceptionally upfield chemical shifts (δ_H 0.53 and 0.38), suggesting the existence of a cyclopropane unit. The ^{13}C NMR spectrum (**Table 1**) revealed the presence of 17 carbons comprising five methyls, three methylenes, five methines (including one olefinic and three oxygenated), and four non-protonated carbons (including one olefinic and one carbonyl). Three coupling spin systems, H-1–H-11*α*/H-11*β*, H-3*α*/H-3*β*–H-4–H-5, and H-7*α*/H-7*β*–H-8, could be deduced from the ^{1}H-^{1}H COSY correlations (**Figure 2**). In the HMBC spectrum, correlations of CH_3-12 (δ_H 0.87, s) with C-2 (δ_C 25.8), C-3 (δ_C 14.6), and C-4 (δ_C 24.5) indicated the presence of C-2–C-3–C-4 cyclopropane moiety, which connected with C-1 as established by the correlations from H-1 (δ_H 3.04) to C-2 and C-3. The HMBC correlations (**Figure 2**) from two methyls, C<u>H</u>$_3$-13 (δ_H 1.15) and C<u>H</u>$_3$-14 (δ_H 0.98), to C-5 (δ_C 72.7), C-6 (δ_C 39.4), and C-7 (δ_C 38.9), from H-5 (δ_H 2.93) to C-7 (δ_C 38.9), and from C<u>H</u>$_3$-15 (δ_H 1.81) to C-8 (δ_C 126.8), C-9 (δ_C 132.2), and C-10 (δ_C 68.6) constructed a 10-membered ring with two geminal methyls at C-6 and one methyl at C-9, which fused with the above noted cyclopropane ring through C-2/C-3. Additional HMBC correlations from C<u>H</u>$_3$-17 (δ_H 2.01) and H-10 (δ_H 5.61) to carbonyl C-16 (δ_C 170.3) enable attachment of an acetyl group to the C-10.

TABLE 1 | ^{1}H (500 MHz) and ^{13}C NMR (125 MHz) data for compounds **1**–**3** (δ in ppm, J in Hz).

No	1[a]		2[b]		3[b]	
	δ_H	δ_C	δ_H	δ_C	δ_H	δ_C
1	3.43, t (7.7)	80.3, CH	3.04, dd (11.1, 4.5)	78.9, CH	2.71, dd (13.3, 3.0)	59.7, CH
2		75.6, C		25.8, C		59.6, C
3α	2.20, dd (14.0, 9.5)	45.6, CH_2	0.53, dd (9.9, 4.4)	14.6, CH_2	2.66, dd, (12.3,3.2)	42.9, CH_2
3β	2.28, dd (14.0, 4.4)		0.38, dd (5.7, 4.4)		0.63, dd (12.3, 10.5)	
4	5.47, ddd (15.8, 9.6, 4.3)	122.8, CH	1.01, dt (10.0, 5.7)	24.5, CH	2.76, ddd (10.2, 3.6, 2.4)	52.6, CH
5	5.43, dd (15.8, 1.1)	144.7, CH	2.93, d (6.1)	72.7, CH	2.33, d (2.4)	65.9, CH
6		36.1, C		39.4, C		34.4, C
7α	1.91, dd (13.7, 3.0)	45.1, CH_2	1.76, ddd (14.6, 4.4, 2.3)	38.9, CH_2	1.92, ddd (14.8, 4.3, 2.2)	38.7, CH_2
7β	1.27, dd (13.7, 11.4)		2.58, t (13.6)		2.62, m	
8	2.93 dd (11.4, 3.0)	63.7, CH	5.46, dd (12.6, 3.3)	126.8, CH	5.44, dd (12.5, 3.3)	127.7, CH
9		67.1, C		132.2, C		132.6, C
10	3.44, t (5.6)	75.6, CH	5.61, d (10.4)	68.6, CH	5.86, dd (12.0, 3.0)	68.7, CH
11α	2.01, dt (15.6, 1.6)	38.1, CH_2	2.25, dt (14.0, 10.8)	36.4, CH_2	1.78, m	31.1, CH_2
11β	1.22, ddd (15.6, 8.2, 5.9)		1.83, dd (14.0, 4.5)		2.26, dt (14.0, 3.0)	
12	1.08, s	22.3, CH_3	0.87, s	12.6, CH_3	1.27, s	18.2, CH_3
13	1.06, s	28.5, CH_3	0.98, s	21.9, CH_3	1.12, s	29.7, CH_3
14	1.11, s	26.7, CH_3	1.15, s	25.9, CH_3	0.77, s	17.9, CH_3
15	1.24, s	16.5, CH_3	1.81, brs	18.4, CH_3	1.71, brs	18.7, CH_3
16				170.3, C		170.1, C
17			2.01, s	21.5, CH_3	2.05, s	21.3, CH_3

[a]*In MeOD.*
[b]*In $CDCl_3$.*

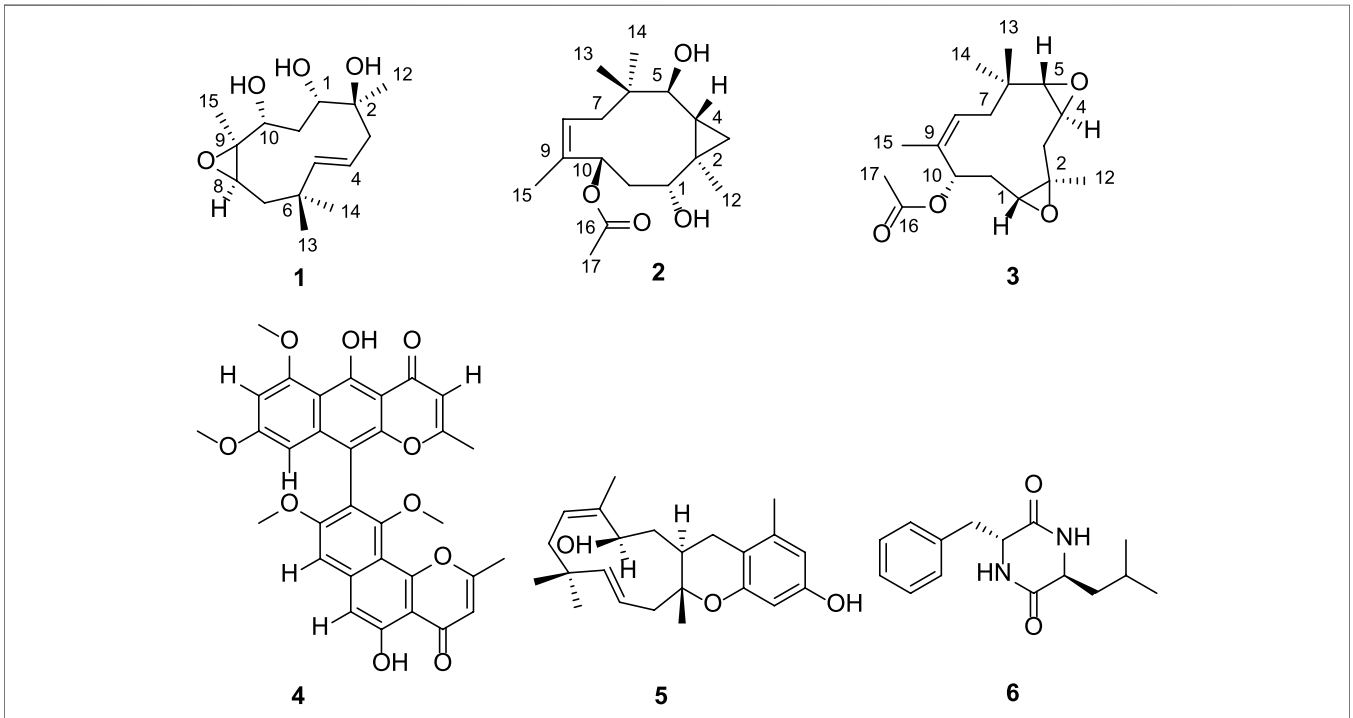

FIGURE 1 | The structures of compounds **1**–**6**.

The relative configuration of **2** was initially assigned by ROESY correlations. The ROESY correlations (**Figure 3**) of C$\underline{H}_3$-15 with H-8 (δ_H 5.46) and H-10 with H-7α (δ_H 1.76)/H-7β (δ_H 2.58) indicated *Z* geometry for the Δ^8 double bond. The sequential ROESY correlations of H-10/H-4/H-1/H-3β placed these protons on the same face the ring. The C$\underline{H}_3$-12 showed ROESY correlations with H-3α and H-5, suggesting that they were located on the face opposite to H-4. However, relative configuration assignment only based on ROESY correlations is usually not reliable enough in conformationally flexible molecules

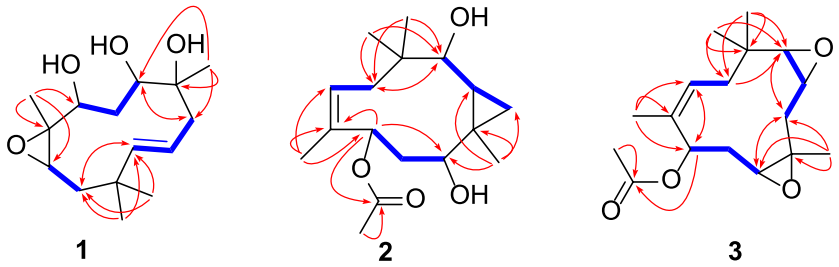

FIGURE 2 | Key ^{1}H-^{1}H COSY (blue bold lines) and HMBC (red arrows) correlations of compounds **1**–**3**.

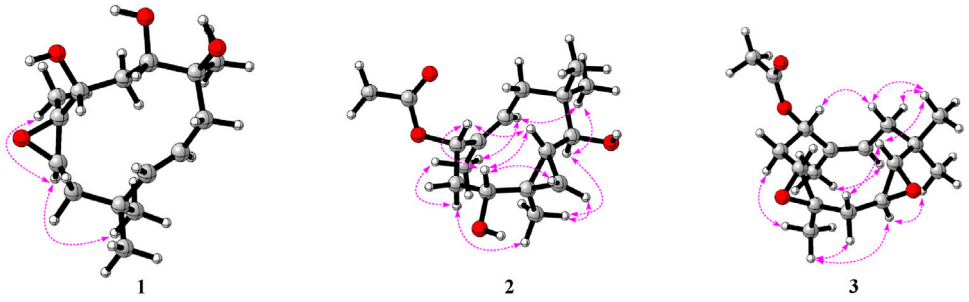

FIGURE 3 | Key ROESY correlations of compounds **1**–**3**.

such as macrocycles. In order to irrefutably determine the relative configuration of the chiral centers (C-1, C-5, and C-10) on the macrocycle of **2**, eight possible diastereomers of **2** were applied to theoretical calculations of NMR chemical shifts followed by DP4+ analysis (**Figure 6**). The calculated chemical shifts of (1*R**,2*R**,4*R**,5*S**,10*S**)-**2** showed best agreement with the experimental values among the possible diastereomers and (1*R**,2*R**,4*R**,5*S**,10*S**)-**2** possessed 100% DP4+ probability (Grimblat et al., 2015), indicating that (1*R**,2*R**,4*R**,5*S**,10*S**)-**2** was the most likely candidate structure. The ECD calculation was further employed to clarify the absolute configuration of **2**. The calculated ECD curve of (1*R*,2*R*,4*R*,5*S*,10*S*)-**2** well fitted with the experimental one (**Figure 7**), defining the stereochemistry of **2** as 1*R*,2*R*,4*R*,5*S*,10*S*. Accordingly, compound **2** was elucidated as shown in **Figure 1** and named penirolide B.

Compound **3** was obtained as yellow oil and its molecular formula of $C_{17}H_{26}O_4$ was assigned by HRESIMS positive ion peak at 317.1723 $[M + Na]^+$ (calcd for $C_{17}H_{26}NaO_4$, 317.1723), indicating five degrees of unsaturation. The ^{1}H NMR spectrum (**Table 1**) displayed signals for one olefinic proton (δ_H 5.44), four sp^3 methines (δ_H 2.71, 2.76, 2.33, and 5.86), five methyls (δ_H 0.77, 1.12, 1.27, 1.71, and 2.05), and three methylenes. The ^{13}C NMR spectrum (**Table 1**) showed resonances for 17 carbons ascribed by HSQC spectrum as five methyls, three methylenes, five methines (including one olefinic and three oxygenated), and four non-protonated carbons (including one olefinic and one carbonyl). These NMR data were very similar to that of phomanoxide (Zhang et al., 2015) whose structure was confirmed by x-ray crystallography, with the only difference being the presence of an additional acetyl group [δ_H 2.05 (s, 3H), δ_C 21.3, CH_3-17; δ_C 170.1, C-16] in **3**. The deshielded shift of C-10 (δ_C 68.7; $\Delta\delta_C$ 2.1) in **3** relative to that of phomanoxide indicated that the acetyl attached at C-10, which was supported by the HMBC correlations from C$\underline{H}_3$-17 and H-10 (δ_H 5.86) to carbonyl C-16 (**Figure 2**).

In the ROESY spectrum of **3**, the correlations of C$\underline{H}_3$-12 with H-3α, H-4, and H-11α suggested that these protons resided on the same face of the molecule. Cross peak of H-3β/H-5 indicated that the two protons were cofacial (**Figure 3**). The large coupling constant $J_{H\text{-}10\text{–}H\text{-}11\alpha}$ = 12.0 Hz demonstrated that H-10 and H-11α were *trans* oriented. Therefore, the relative configuration was proposed as 1*R**,2*R**,4*S**,5*S**,10*S**, which was further confirmed by the NMR chemical shift calculation (**Figure 8**) and its similar NMR data to that of phomanoxide. The 1*R*,2*R*,4*S*,5*S*,10*S* configuration for **3** was established based on its well-matched experimental and calculated ECD curves (**Figure 9**). Thus, the structure of **3** was elucidated as depicted in **Figure 1** and named 10-acetyl-phomanoxide.

In addition, three known compounds, aurasperone A (**4**) (Campos et al., 2005), pughiinin A (**5**) (Pittayakhajonwut et al., 2002), and cyclo(L-Leu-L-Phe) (**6**) (Stark and Hofmann, 2005), were identified by comparison of their NMR data with literature data.

The liver plays a major role in whole body glucose metabolism by maintaining a balance between glucose production and glucose storage. Excessive hepatic glucose production contributes substantially to diabetes, and it is proposed that suppression of

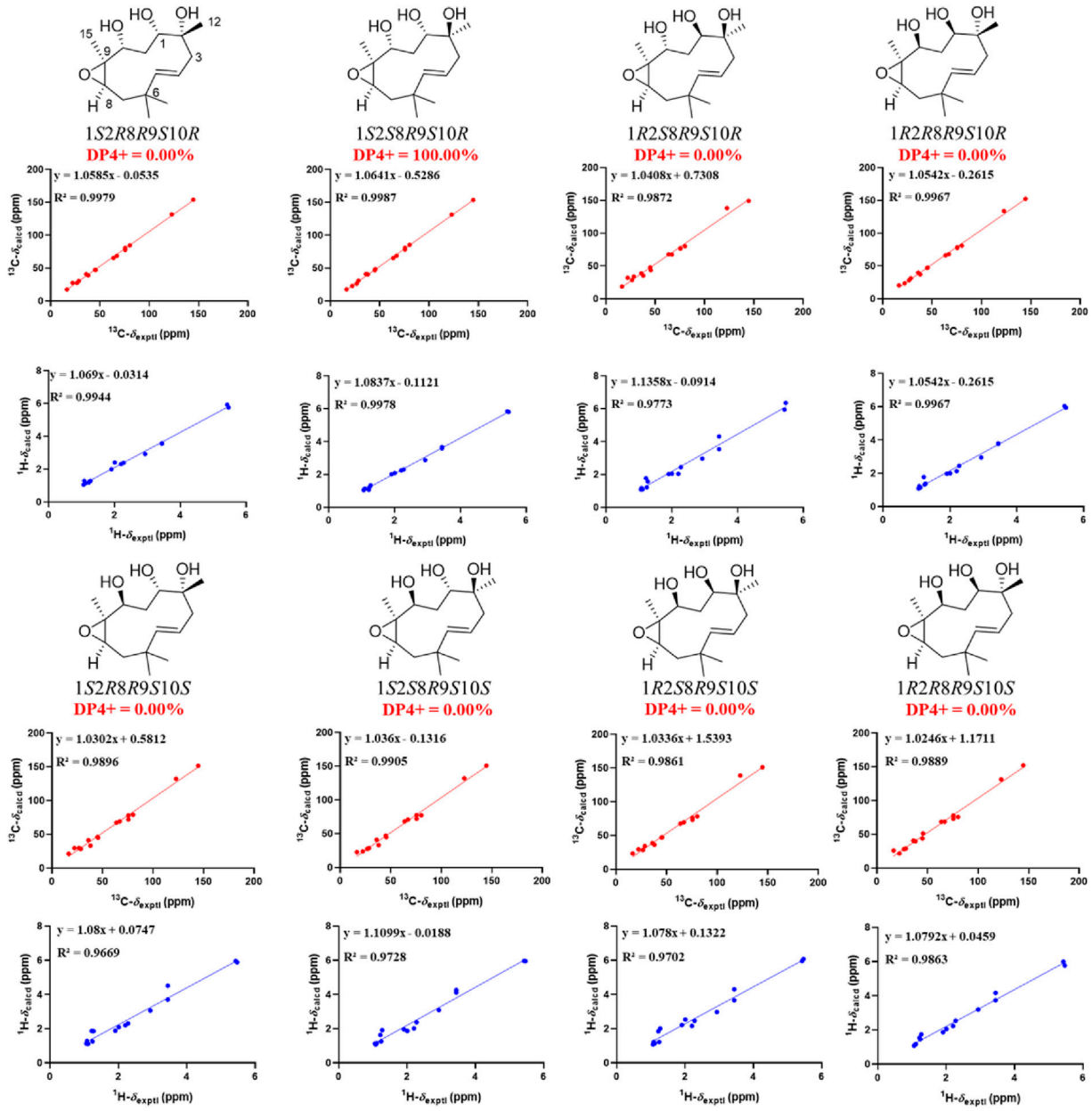

FIGURE 4 | Linear regression analysis between experimental and calculated ^{13}C and ^{1}H NMR chemical shifts of isomers of **1**.

hepatic glucose production may provide therapeutic advantages for the control of diabetes (Xiao et al., 2017; Liao et al., 2021). To investigate the anti-diabetic effect of the six compounds, we examined the glucose production in hepatocytes. Compounds **2**, **3**, **5**, and **6** significantly inhibited glucagon-induced hepatic glucose production, with EC_{50} values of 33.3, 36.1, 18.8, and 32.1 μM, respectively, while it was >200 μM for Compounds **1** and **4**, and 2.3 μM for the positive control metformin (**Figure 10A**). In response to glucagon, cAMP is a second messenger to initiate glucagon signaling cascades in hepatic glucose production. Compounds **2**, **3**, **5**, and **6** treatment suppressed cAMP accumulation (**Figure 10B**). These results indicated that compounds **2, 3, 5,** and **6** inhibited hepatic glucose production by suppression glucagon-induced cAMP accumulation.

MATERIALS AND METHODS

General Experimental Procedures

Optical rotations were measured with a JASCO P-1020 digital polarimeter. The infrared spectra were recorded on a Shimadzu UV2550 spectrophotometer (Shimadzu, Kyoto, Japan). The mass spectrometric (HRESIMS) data were acquired using an API QSTAR Pulsar mass spectrometer (Bruker, Bremen, Germany).

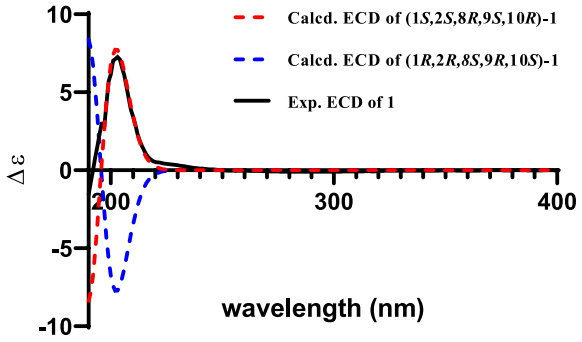

FIGURE 5 | Experimental spectrum of **1** in methanol and calculated ECD spectra of (1*S*,2*S*,8*R*,9*S*,10*R*)-**1** and (1*R*,2*R*,8*S*,9*R*,10*S*)-**1**.

Semipreparative high-performance liquid chromatography (HPLC) equipped with octadecyl silane (ODS) column (Cosmosil ODS-A, 10 × 250 nm, 5 μm, 4 ml/min) was used to isolate compounds. The solvents used to the preparative HPLC, such as methanol, acetonitrile, hexane, and ethanol were of chromatographic grade (Concord Technology Co. Ltd., Tianjin, China). The solvents used to the extraction or isolation of the columns, such as ethyl acetate, methanol, chloroform, and methanol, were of analytical pure (Concord Technology Co. Ltd., Tianjin, China). The NMR spectra were recorded with a Bruker AV-500 spectrometer (Bruker, Bremen, Germany) using TMS as an internal standard. Silica gel (60–80 and 200–300 mesh; Qingdao Haiyang Chemical Co. Ltd., Qingdao, China) and Rp-C18 (20–45 μm; Fuji Silysia Chemical Ltd., Durham, NC, United States) were used for column chromatography.

Fungal Material

The fungus *Penicillium* sp. was isolated from healthy papaya leaves collected in Haikou, Hainan Province, People's Republic of China, and identified by sequence analysis of the ITS region of rDNA (GenBank No. MT729953). A voucher strain was deposited in the Institute of Tropical Bioscience and Biotechnology.

Fermentation and Isolation

Plugs of agar with mycelium were cut from solid medium and transferred aseptically to a 1,000-ml Erlenmeyer flask, containing 300 ml of liquid medium (glucose 10 g/L, maltose 20 g/L, monosodium glutamate 10 g/L, yeast extract 3 g/L, corn starch 1 g/L, mannitol 20 g/L, $MgSO_4$ 0.3 g/L, and KH_2PO_4 0.5 g/L). The whole culture broth (45 L) was harvested and filtered to yield the mycelium cake and liquid broth. The mycelium cake and liquid broth were extracted by EtOAc three times. The two EtOAc extracts were evaporated under reduced pressure and combined based on their similar metabolite profiles provided by HPLC analysis, affording a total of 12 g of EtOAc extract. The extract was separated by silica gel column eluted with different ratios of Petroleum ether-EtOAc (8:1, 6:1, 4:1, 2:1, 1:1, and 0:1) to afford six fractions (Fr.1–6). Fr.4 (0.52 g) was purified by a Rp-C_{18} silica gel column (MeOH-H_2O, 70%–30%), followed by semi-preparative HPLC (MeCN-H_2O, containing 0.1% Formic acid, 50:50, v/v, 4.0 ml min^{-1}) to obtain compounds **1** (7.0 mg, t_R = 9.5 min) and **2** (4.6 mg, t_R = 6.5 min). Fr.3 (1.03 g) was applied to a Rp-C_{18} silica gel column chromatography (MeOH-H_2O, 50%–50%) and semi-preparative HPLC (MeCN-H_2O, containing 0.1% Formic acid, 20:80, v/v, 4.0 ml min^{-1}) to obtain compound **3** (4.8 mg, t_R = 9.6 min). Fr.6 (1.01 g) was subjected to a Rp-C_{18} silica gel column chromatography (MeOH-H_2O, 80–20%) to obtain three subfractions (Fr.6.1–Fr.6.3), Compounds **4** (18.3 mg, t_R = 8.3 min) and **5** (18.2 mg, t_R = 7.5 min) were obtained from Fr.6.1 by semi-preparative HPLC (MeCN-H_2O, containing 0.1% formic acid, 75:25, v/v, 4.0 ml min^{-1}). Fr.6.3 (0.33 g) was subjected to semi-preparative HPLC (MeCN-H_2O, containing 0.1% formic acid, 15:85, v/v, 4.0 ml min^{-1}) to afford **6** (3.2 mg, t_R = 10.5 min).

Penirolide A (1)

Yellow oily; [⍰]25D −9.0 (*c* 0.1, MeOH); UV (CH_3OH) λ_{max} (logε): 206 (2.52) nm; ECD (CH_3OH) λ_{max} ($\Delta\varepsilon$): 203 (7.25) nm; IR(KBr) ν_{max}: 3,414, 2,962, 2,872, 1,727, 1,668, 1,453,1,384, 1,285, 1,200, 1,091, 1,065, 990 cm^{-1}; ^1H and ^{13}C NMR spectral data, **Table 1**; HRESIMS *m/z* 293.1723 ($[M + Na]^+$ (calcd for $C_{15}H_{26}NaO_4$, 293.1723).

Penirolide B (2)

Yellow oily; [⍰]25D +3.0 (*c* 0.1, MeOH); UV (CH_3OH) λ_{max} (logε): 205 (2.56) nm; ECD (CH_3OH) λ_{max} ($\Delta\varepsilon$): 202 (8.09) nm; IR(KBr) ν_{max}: 3,422, 2,960, 1,728, 1,453, 1,373, 1,248, 1,050, 960 cm^{-1}; ^1H and ^{13}C NMR spectral data, **Table 1**; HRESIMS *m/z* 319.1882 $[M + Na]^+$ (calcd for $C_{17}H_{28}NaO_4$, 319.1880).

10-Acetyl-phomanoxide (3)

Yellow oily; [⍰]25D +31.9 (*c* 0.1, MeOH); UV (CH_3OH) λ_{max} (logε): 205 (2.55) nm; ECD (CH_3OH) λ_{max} ($\Delta\varepsilon$): 203 (10.12) nm; IR(KBr) ν_{max}: 3,442, 2,961, 2,929, 1,736, 1,380, 1,242, 1,024 cm^{-1}; ^1H and ^{13}C NMR spectral data, **Table 1**; HRESIMS *m/z* 317.1723 $[M + Na]^+$ (calcd for $C_{17}H_{26}NaO_4$, 317.1723).

NMR and ECD Calculations

The conformations of the isomers of compounds **1**–**3** were generated by iMTD-GC method embedded in Crest program (Pracht et al., 2020). Two conformations with the root-mean-square (RMS) distance and energy deviation of 0.5 Å and 0.25 kcal/mol, respectively, were considered as duplicates and one

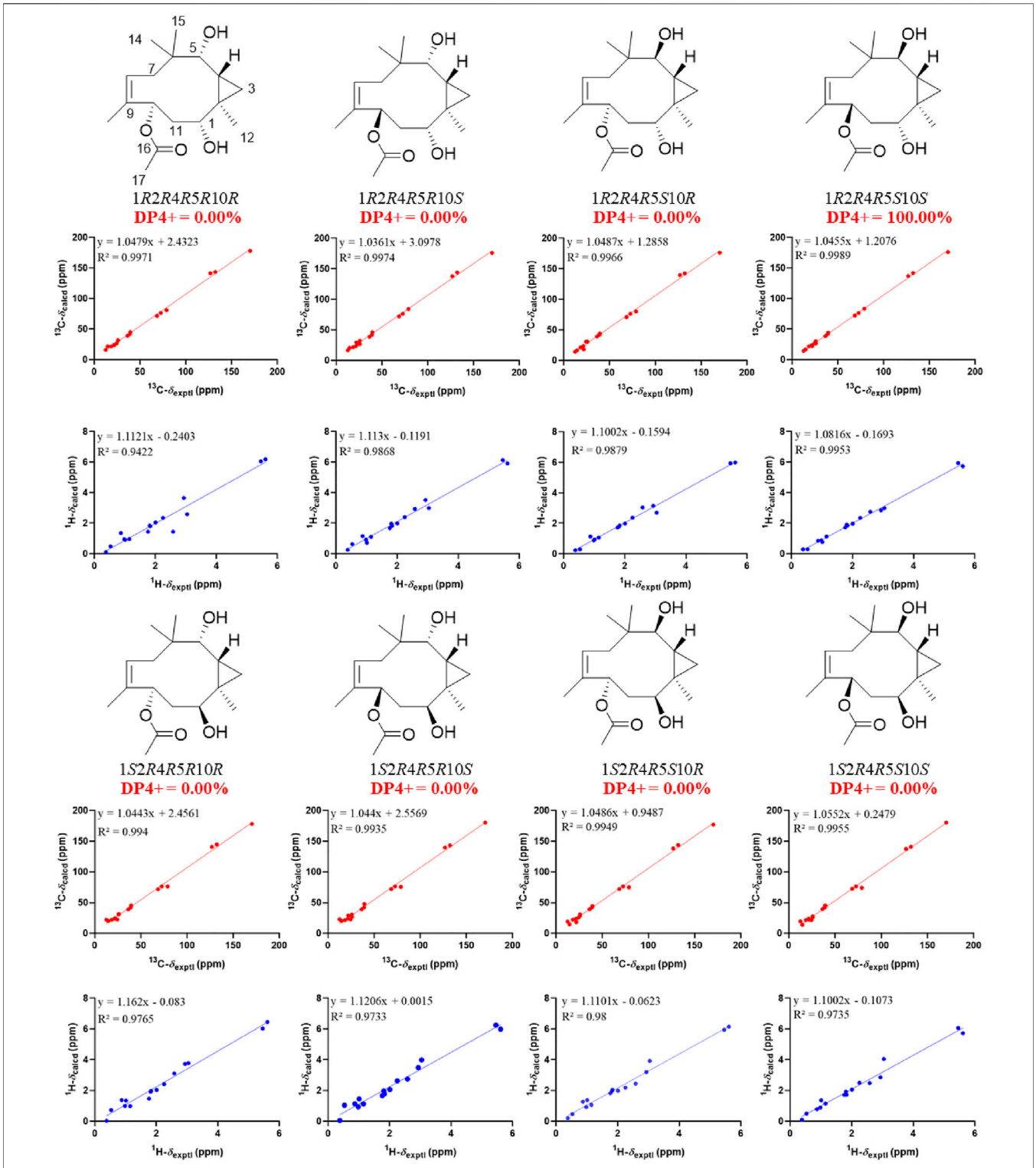

FIGURE 6 | Linear regression analysis between experimental and calculated ^{13}C and ^{1}H NMR chemical shifts of isomers of **2**.

of them was removed. Density functional theory calculations were performed with the Gaussian 16 package (Frisch et al., 2019). The remaining conformers with population over 1% were optimized at the B3LYP-D3BJ/6-31G(d) level in gas phase and the conformers within an energy window of 3 kcal/mol were kept. Then, these conformers were refined by re-optimizations at the B3LYP-D3BJ/6-

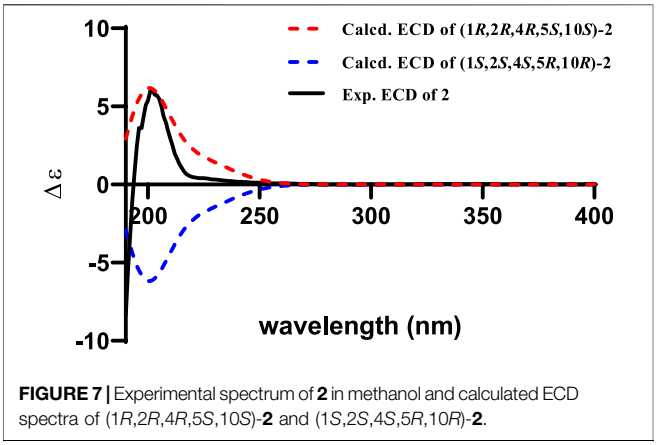

FIGURE 7 | Experimental spectrum of **2** in methanol and calculated ECD spectra of (1*R*,2*R*,4*R*,5*S*,10*S*)-**2** and (1*S*,2*S*,4*S*,5*R*,10*R*)-**2**.

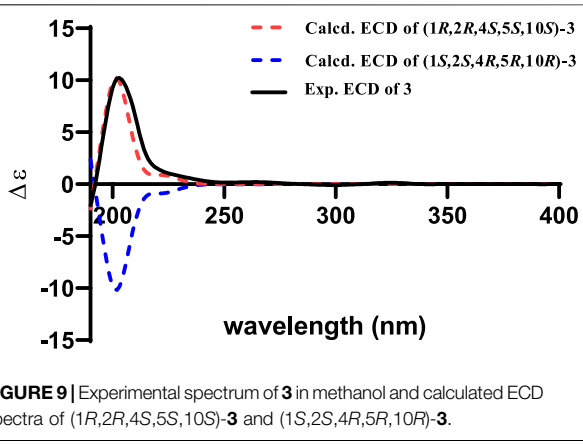

FIGURE 9 | Experimental spectrum of **3** in methanol and calculated ECD spectra of (1*R*,2*R*,4*S*,5*S*,10*S*)-**3** and (1*S*,2*S*,4*R*,5*R*,10*R*)-**3**.

311G(d,p) level with the IEFPCM solvent model in methanol for **1** and chloroform for **2** and **3**, and frequency analysis of all optimized conformations was also performed at the same level of theory to ensure that no imaginary frequencies were present, confirming that the optimized structures were minima on their potential energy surfaces. NMR shielding tensors were calculated with the GIAO method (Wolinski et al., 1990) at the mPW1PW91/6-311G(d,p) level with the IEFPCM solvent model in methanol for **1** and chloroform for **2** and **3**. The calculated isotropic magnetic shielding constants (σ) were Boltzmann averaged according to their Gibbs free energies. The shielding constants were converted into chemical shifts by referencing to TMS at 0 ppm according to the formula $\delta cal = \sigma TMS - \sigma cal$, where the σTMS (the shielding constant of TMS) was calculated at the same level. For each candidate, the parameters a and b of the linear regression $\delta cal = a\delta exp + b$; the correlation coefficient, R^2; the mean absolute error (MAE) defined as $\Sigma n\ |\delta cal - \delta exp|/n$; and the corrected mean absolute error, CMAE, defined as $\Sigma n\ |\delta corr - \delta exp|/n$, where $\delta corr = (\delta cal - b)/a$, were calculated. DP4+ probability analysis was performed using the calculated NMR shielding tensors with DP4+ excel file (Grimblat et al., 2015). ECD spectra were calculated by the TDDFT methodology at the B3LYP/def2TZVP utilizing IEFPCM in methanol. The final ECD spectra were simulated by averaging the spectra of lowest energy conformers according to the Boltzmann distribution theory and their relative Gibbs free energy (ΔG) using SpecDis 1.71 (Bruhn et al., 2013) with $\sigma = 0.30$ eV and uv shift = 5 nm for **1** and 10 nm for **2** and **3**, respectively.

Primary Mouse Hepatocytes

Male C57BL/6J mice (6 weeks old) were purchased from Pengyue Laboratory Animal Company (Jinan, China). Animal care and experiments were approved by the Animal Ethics Committee of

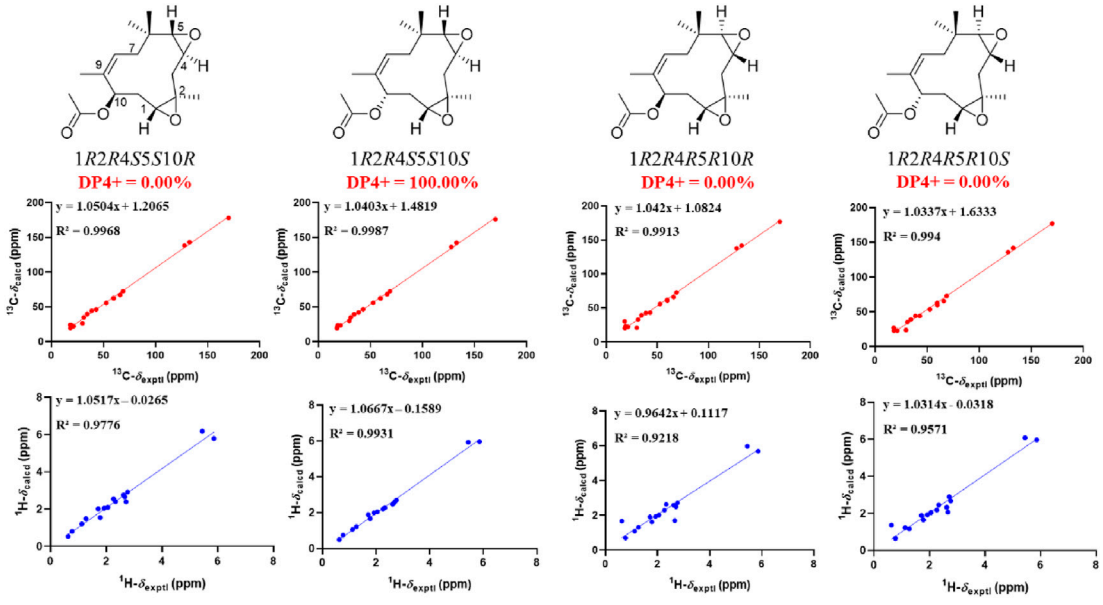

FIGURE 8 | Linear regression analysis between experimental and calculated ^{13}C and ^{1}H NMR chemical shifts of isomers of **3**.

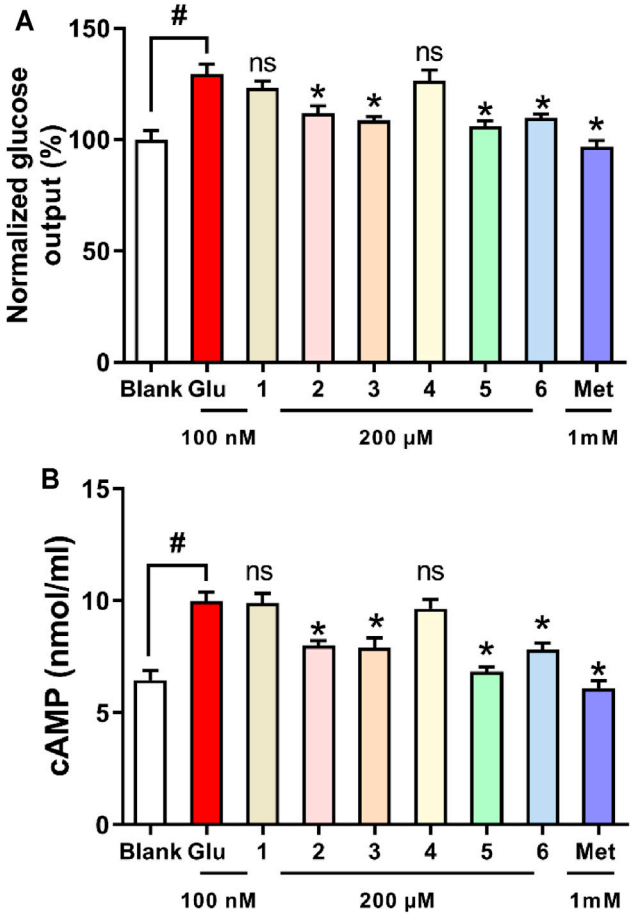

FIGURE 10 | Effects of compounds **1**–**6** on glucagon-induced hepatic glucose production **(A)** and cAMP accumulation **(B)** in mouse hepatocytes. *$p < 0.05$ and #$p < 0.05$ as compared with the blank group and group treated with glucagon, respectively.

Shandong Agriculture University. Primary mouse hepatocytes were prepared as previously described (Xiao et al., 2017). Briefly, fasted C57BL/6J male mice were anesthetized and livers were washed with Krebs-HEPES and digested with collagenase IV by perfusion through the inferior vena cava at 3 ml/min. Then, the whole liver was removed 6 min later, and hepatocytes were extracted in DMEM with 10% FBS. After filtering, cells were resuspended and cultured in 96- or 48-well plates. Then, the cells were treated as indicated.

Measurement of Cell Viability and Glucose Production in Hepatocytes

Primary mouse hepatocytes were seeded in a 96-well plate and treated with 100 nM glucagon and various concentrations of test compounds (1–200 μM) for 24 h. After that, cell viability was assessed by the MTT method (Pan et al., 2021). For the determination of glucose production, hepatocytes were incubated in KRB solution containing relevant substrates (10 mM pyruvate, 100 nM glucagon) or indicated compounds (1, 5, 10, 100, and 200 μM) for 6 h. Then, the cell supernatant was collected for glucose analysis using the commercial kit.

Measurement of cAMP Production

Hepatocytes were incubated with the indicated compounds and stimulated with glucagon (100 nM) for 2 h, lysed in cell lysis buffer, and the supernatant was harvested for the assays of cAMP (Xiao et al., 2017). All data were expressed as the mean ± SD from at least three independent experiments.

DATA AVAILABILITY STATEMENT

The original contributions presented in the study are included in the article/**Supplementary Material**. Further inquiries can be directed to the corresponding authors.

AUTHOR CONTRIBUTIONS

Y-XZ and PC contributed to the conception and design of the study. LY and F-DK determined the planar structures and absolute configurations, and wrote the draft of the manuscript. F-RW and Q-YM undertook the isolation and purification of all compounds. NX contributed to bioactivity assay. Q-YX undertook collection and identification of strain work. Y-GW and H-FD improved the manuscript. All authors contributed to manuscript revision as well as read and approved the submitted version.

FUNDING

This research was supported by the Natural Science Foundation of Hainan Province (2019CXTD411), the Financial Fund of the Ministry of Agriculture and Rural Affairs, P. R. of China (NFZX2021), the Natural Science Foundation of Shandong Province (ZR2019BH080), the National Natural Science Foundation of China (82004014), the China Agriculture Research System (CARS-21), and the Central Public-Interest Scientific Institution Basal Research Fund for Chinese Academy of Tropical Agricultural Sciences (1630052017002 and 1630052021019).

SUPPLEMENTARY MATERIAL

The Supplementary Material for this article can be found online at: https://www.frontiersin.org/articles/10.3389/fchem.2021.797858/full#supplementary-material

REFERENCES

Bruhn, T., Schaumlöffel, A., Hemberger, Y., and Bringmann, G. (2013). SpecDis: Quantifying the Comparison of Calculated and Experimental Electronic Circular Dichroism Spectra. *Chirality* 25, 243–249. doi:10.1002/chir.22138

Campos, F. R., Barison, A., Daolio, C., Ferreira, A. G., and Rodrigues-Fo, E. (2005). Complete1H and13C NMR Assignments of Aurasperone A and Fonsecinone A, Two Bis-Naphthopyrones Produced by Aspergillus Aculeatus. *Magn. Reson. Chem.* 43, 962–965. doi:10.1002/mrc.1654

Frisch, M. J., Trucks, G. W., Schlegel, H. B., Scuseria, G. E., Robb, M. A., Cheeseman, J. R., et al. (2019). *Gaussian 16, Revision C.01*. Wallingford CT: Gaussian, Inc.

Grimblat, N., and Sarotti, A. M. (2016). Computational Chemistry to the Rescue: Modern Toolboxes for the Assignment of Complex Molecules by GIAO NMR Calculations. *Chem. Eur. J.* 22, 12246–12261. doi:10.1002/chem.201601150

Grimblat, N., Zanardi, M. M., and Sarotti, A. M. (2015). Beyond DP4: An Improved Probability for the Stereochemical Assignment of Isomeric Compounds Using Quantum Chemical Calculations of NMR Shifts. *J. Org. Chem.* 80, 12526–12534. doi:10.1021/acs.joc.5b02396

Gupta, S., Chaturvedi, P., Kulkarni, M. G., and Van Staden, J. (2020). A Critical Review on Exploiting the Pharmaceutical Potential of Plant Endophytic Fungi. *Biotechnol. Adv.* 39, 107462. doi:10.1016/j.biotechadv.2019.107462

Kaul, S., Gupta, S., Ahmed, M., and Dhar, M. K. (2012). Endophytic Fungi from Medicinal Plants: A Treasure Hunt for Bioactive Metabolites. *Phytochem. Rev.* 11, 487–505. doi:10.1007/s11101-012-9260-6

Krishna, K. L., Paridhavi, M., and Patel, J. A. (2008). Review on Nutritional, Medicinal and Pharmacological Properties of Papaya (Carica Papaya Linn.). *Nat. Prod. Radiance* 7, 364–363.

Liao, C.-S., Tang, C.-P., Yao, S., and Ye, Y. (2013). Humulane-type Sesquiterpenoids from Pilea Cavaleriei Subsp. Crenata. *Org. Biomol. Chem.* 11, 4840–4846. doi:10.1039/C3OB40872H

Liao, W., Yang, W., Shen, Z., Ai, W., Pan, Q., Sun, Y., et al. (2021). Heme Oxygenase-1 Regulates Ferrous Iron and Foxo1 in Control of Hepatic Gluconeogenesis. *Diabetes* 70, 696–709. doi:10.2337/db20-0954

Lodewyk, M. W., Siebert, M. R., and Tantillo, D. J. (2012). Computational Prediction of 1H and 13C Chemical Shifts: A Useful Tool for Natural Product, Mechanistic, and Synthetic Organic Chemistry. *Chem. Rev.* 112, 1839–1862. doi:10.1021/cr200106v

Luo, D.-Q., Gao, Y., Gao, J. M., Wang, F., Yang, X. L., Liu, J. K., et al. (2006). Humulane-type Sesquiterpenoids from the Mushroom Lactarius Mitissimus. *J. Nat. Prod.* 69, 1354–1357. doi:10.1021/np060153l

Pan, G., Zhao, Y., Ren, S., Liu, F., Xu, Q., Pan, W., et al. (2021). Indole-terpenoids with Anti-inflammatory Activities from Penicillium Sp. HFF16 Associated with the Rhizosphere Soil of Cynanchum Bungei Decne. *Front. Microbiol.* 12, 710364. doi:10.3389/fmicb.2021.710364

Pinnamaneni, R. (2017). Nutritional and Medicinal Value of Papaya (Carica Papaya Linn.). *Wjpps* 6, 2559–2578. doi:10.20959/wjpps20178-9947

Pittayakhajonwut, P., Theerasilp, M., Kongsaeree, P., Rungrod, A., Tanticharoen, M., and Thebtaranonth, Y. (2002). Pughiinin A, a Sesquiterpene from the FungusKionochaeta pughiiBCC 3878. *Planta Med.* 68, 1017–1019. doi:10.1055/s-2002-35653

Pracht, P., Bohle, F., and Grimme, S. (2020). Automated Exploration of the Low-Energy Chemical Space with Fast Quantum Chemical Methods. *Phys. Chem. Chem. Phys.* 22, 7169–7192. doi:10.1039/C9CP06869D

Smith, S. G., and Goodman, J. M. (2010). Assigning Stereochemistry to Single Diastereoisomers by GIAO NMR Calculation: The DP4 Probability. *J. Am. Chem. Soc.* 132, 12946–12959. doi:10.1021/ja105035r

Smith, S. G., and Goodman, J. M. (2009). Assigning the Stereochemistry of Pairs of Diastereoisomers Using GIAO NMR Shift Calculation. *J. Org. Chem.* 74, 4597–4607. doi:10.1021/jo900408d

Stark, T., and Hofmann, T. (2005). Structures, Sensory Activity, and Dose/Response Functions of 2,5-Diketopiperazines in Roasted Cocoa Nibs (Theobroma Cacao). *J. Agric. Food Chem.* 53, 7222–7231. doi:10.1021/jf051313m

Strobel, G. A. (2003). Endophytes as Sources of Bioactive Products. *Microbes Infect.* 5, 535–544. doi:10.1016/S1286-4579(03)00073-X

Toyota, M., Omatsu, I., Braggins, J., and Asakawa, Y. (2004). New Humulane-type Sesquiterpenes from the Liverworts Tylimanthus Tenellus and Marchantia Emarginata Subsp. Tosana. *Chem. Pharm. Bull.* 52, 481–484. doi:10.1248/cpb.52.481

Uzma, F., Mohan, C. D., Hashem, A., Konappa, N. M., Rangappa, S., Kamath, P. V., et al. (2018). Endophytic Fungi-Alternative Sources of Cytotoxic Compounds: A Review. *Front. Pharmacol.* 9, 309. doi:10.3389/fphar.2018.00309

Wolinski, K., Hinton, J. F., and Pulay, P. (1990). Efficient Implementation of the Gauge-independent Atomic Orbital Method for NMR Chemical Shift Calculations. *J. Am. Chem. Soc.* 112, 8251–8260. doi:10.1021/ja00179a005

Xiao, N., Lou, M.-D., Lu, Y.-T., Yang, L.-L., Liu, Q., Liu, B., et al. (2017). Ginsenoside Rg5 Attenuates Hepatic Glucagon Response via Suppression of Succinate-Associated HIF-1α Induction in HFD-Fed Mice. *Diabetologia* 60, 1084–1093. doi:10.1007/s00125-017-4238-y

Zhang, H. W., Song, Y. C., and Tan, R. X. (2006). Biology and Chemistry of Endophytes. *Nat. Prod. Rep.* 23, 753–771. doi:10.1039/B609472B

Zhang, J., Liu, L., Wang, B., Zhang, Y., Wang, L., Liu, X., et al. (2015). Phomanolides A and B from the Fungus Phoma sp.: Meroterpenoids Derived from a Putative Tropolonic Sesquiterpene via Hetero-Diels-Alder Reactions. *J. Nat. Prod.* 78, 3058–3066. doi:10.1021/acs.jnatprod.5b00969

Conflict of Interest: The authors declare that the research was conducted in the absence of any commercial or financial relationships that could be construed as a potential conflict of interest.

frontiers in Chemistry

ORIGINAL RESEARCH
published: 23 December 2021
doi: 10.3389/fchem.2021.802279

Discovery of Mycothiogranaticins from *Streptomyces vietnamensis* GIMV4.0001 and the Regulatory Effect of Mycothiol on the Granaticin Biosynthesis

Ming-Rong Deng[1*†], *Yan Li*[1†], *Xiao Luo*[1], *Xiang-Ling Zheng*[1], *Yuchan Chen*, *Yu-Lian Zhang*[1], *Weimin Zhang*, *Hao Zhou*[2*] and *Honghui Zhu*[1*]

[1]*Key Laboratory of Agricultural Microbiomics and Precision Application — Ministry of Agriculture and Rural Affairs, Guangdong Provincial Key Laboratory of Microbial Culture Collection and Application, State Key Laboratory of Applied Microbiology Southern China, Guangdong Microbial Culture Collection Center (GDMCC), Institute of Microbiology, Guangdong Academy of Sciences, Guangzhou, China,* [2]*Key Laboratory of Functional Molecules Analysis and Biotransformation of Universities in Yunnan Province, School of Chemical Science and Technology, Yunnan University, Kunming, China*

OPEN ACCESS

Edited by:
Xiachang Wang,
Nanjing University of Chinese Medicine, China

Reviewed by:
Xuhua Mo,
Qingdao Agricultural University, China
Weaam Ebrahim,
Mansoura University, Egypt
Doralyn S. Dalisay,
University of San Agustin, Philippines

***Correspondence:**
Ming-Rong Deng
dengmr@gdim.cn
Hao Zhou
haozhou@ynu.edu.cn
Honghui Zhu
zhuhh@gdim.cn

†These authors have contributed equally to this work and share first authorship

Specialty section:
This article was submitted to Medicinal and Pharmaceutical Chemistry, a section of the journal Frontiers in Chemistry

Received: *26 October 2021*
Accepted: *06 December 2021*
Published: *23 December 2021*

Citation:
Deng M-R, Li Y, Luo X, Zheng X-L, Chen Y, Zhang Y-L, Zhang W, Zhou H and Zhu H (2021) Discovery of Mycothiogranaticins from Streptomyces vietnamensis GIMV4.0001 and the Regulatory Effect of Mycothiol on the Granaticin Biosynthesis. Front. Chem. 9:802279. doi: 10.3389/fchem.2021.802279

Granaticins are benzoisochromanequinone polyketides with remarkable antibacterial and anticancer activities. Three sulfur-containing granaticin congeners, mycothiogranaticins A (**1**), B (**2**) and granaticin MA (**3**) were discovered from a granaticin-producing strain of *Streptomyces vietnamensis* GIMV4.0001. Two of them were structurally determined with mycothiol or N-acetylcysteine moieties and found to be bio-actively reluctant. Disruption of the *mshA* gene (*SVTN_RS20640*) that encodes the D-inositol-3-phosphate glycosyltransferase crucial for mycothiol biosynthesis, fully abolished the production of mycothiogranaticins. The result substantiated that the newly discovered mycothiogranaticins are consequences of the combination of the granaticin and mycothiol biosynthetic pathways. The overall granaticin production of the Δ*mshA* mutant strain was unexpectedly decreased by at least more than 50%, while similar production level of granaticins to that of the wild type strain was observed in an mycothiol-S transferase gene (*SVTN_RS22215*) disruptant Δ*mst*. These results indicated that the mycothiol deficiency was responsible for the decreased production of granaticins. Mycothiol may positively regulate the biosynthesis of granaticin possibly by maintaining the cellular redox balance. To the best of our knowledge, this is the first report that mycothiol can not only be a direct building block of polyketides but also play a regulatory role in the polyketide biosynthesis.

Keywords: mycothiol, MshA, MST, regulation, *Streptomyces vietnamensis*, granaticin, actinomycete, sulfur-containing polyketide

INTRODUCTION

Bacterial aromatic polyketides are pharmaceutically important natural products with remarkable structural diversity, some of which have been developed and most commonly used as antibiotics and anticancer drugs, such as oxytetracycline, tetracenomycin, doxorubicin and aclacinomycin. Therefore, deeper explorations of the structural diversity of bacterial aromatic polyketides would

enable this class of compounds as continuous sources for drug development. Sulfur incorporation can significantly expand the structural diversity and bioactivities of many naturally occurring molecules (Hai et al., 2021), many sulfur-containing natural products, such as penicillin and ixabepilone, have been approved for clinic therapy. However, bacterial sulfur-containing aromatic polyketides are relatively rare, with only a few examples reported over the past decades (Etoh et al., 1987; Ohta et al., 1987; Rohr and Zeeck, 1987; Miyata et al., 1992; Aoyama et al., 1993; Carney et al., 1997; Kulanthaivel et al., 1999; Sasaki et al., 2010; Taguchi et al., 2013; Wang et al., 2013; Woo et al., 2013; Taguchi et al., 2015; Bilyk et al., 2016; Che et al., 2016; Xie et al., 2016; Nakashima et al., 2017; Matsuo et al., 2019a; Bae et al., 2019; Matsuo et al., 2019b; He et al., 2019; Fang et al., 2020; Cao et al., 2021). Amongst these reports, naquihexcin A could inhibit the proliferation of the adriamycin resistant human breast cancer (Che et al., 2016); nanaomycin K showed an inhibitory effect on the epithelial-mesenchymal transition (Matsuo et al., 2019a); and naquihexcin E exhibited a notable anti-HIV activity (He et al., 2019). These suggested promising potentials of these privileged sulfur-containing polyketides for drug development.

Granaticins are members of the benzoisochromanequinone (BIQ) polyketides (**Figure 1**), showing a wide range of biological activities on both microbes and higher organisms. They are highly active against Gram-positive bacteria and protozoa and exhibit cytotoxicity against many cancer cell lines *in vitro* at nM to μM levels as well as P-388 lymphocytic leukemia in mice (Corbaz et al., 1957; Chang et al., 1975; Elson et al., 1988). Granaticins inhibit bacteria by interfering with $tRNA^{Leu}$ aminoacylation process resulting in failure to synthesize proteins and RNAs (Ogilvie et al., 1975a; b). The cytotoxicity was reported initially to be attributed to the inhibition of ribosomal RNA maturation (Heinstein, 1982). More recently, granaticins were found to specifically inhibit farnesyltransferase (Iwasaki and Omura, 2007), inosine 5′-monophosphate dehydrogenase (Ren et al., 2008) and cell division cycle 7 kinase (Frattini et al., 2011), which are important targets for the development of anticancer drugs (Ratcliffe, 2006; Agrawal and Somani, 2009; Swords et al., 2010). Therefore, granaticins are the highest ranked BIQ members with clinical potentials.

Streptomyces vietnamensis is a recently designated species that can produce granaticins (Zhu et al., 2007; Deng et al., 2011a). The metabolites from the granaticin pathway of this strain were systematically characterized (Deng et al., 2020). Here we report the discovery of three sulfur-containing granaticin congeners, mycothiogranaticins A (**1**), B (**2**) and granaticin MA (**3**), from *S. vietnamensis* GIMV4.0001, and the involvement of mycothiol in the granaticin biosynthesis, serving as both a structural building block and a biosynthetic regulator.

MATERIALS AND METHODS

Strains, Plasmids, Biochemicals and Growth Conditions

Strains, plasmids, and polymerase chain reaction (PCR) primers used in this study were listed in **Supplementary Table S1, S2**, respectively. *Escherichia coli* NEB Turbo was used for general cloning and plasmid preparation. *E. coli* ET12567/pUZ8002 (MacNeil et al., 1992) was used as the donor host for intergeneric conjugation. *S. vietnamensis* GIMV4.0001 (Zhu et al., 2007) is a wild-type granaticin (**4**) producer. The temperature-sensitive plasmid pKC1139 (Bierman et al., 1992) was used for generating the in-frame disruption plasmids pKC-Δ*mshA* and pKC-Δ*mst*. The integrative plasmid pSET-KasO* (Pan et al., 2017) was used for the gene complementation purpose. PCR primers were ordered from and synthesized by GENEWIZ. Phanta Max Super-Fidelity DNA polymerase and ClonExpress MultiS One Step Cloning Kit were purchased from Vazyme Biotech Co., Ltd, China, and the reactions were performed according to the manufacturer's procedures. Kits for gel extraction and plasmid preparation were products of Magen Co., Ltd (China). Other common biochemicals and medium components were purchased from standard commercial sources. DNA sequencing was performed by GENEWIZ. *E. coli* strains containing plasmids were cultured in LB medium at 37 °C, with shaking at 200 rpm, supplemented with appropriate antibiotics as required. *Streptomyces* strains were grown at 28 °C on ISP2 agar medium for sporulation or in liquid YEME medium (0.3% yeast extract, 0.5% tryptone, 0.3% malt extract, 1% glucose, 5 mM $MgCl_2$) for growth of mycelium, isolation of total DNA and granaticin (**4**) production. The liquid Gauze's synthetic medium No.1 was also used for parallel analysis of granaticin (**4**) production. *E. coli-Streptomyces* conjugations were performed on IPS4 agar medium.

Fermentation, Isolation and Structural Elucidation

The seed cultures were prepared from 2-days fermentation broths rotationally incubated at 220 rpm and 28 °C in the liquid YEME medium. For large-scale fermentation (20 L), fifty 2000-mL baffled flasks containing 400 mL of liquid YEME with 5% (in volume) seed culture were incubated under the foresaid conditions for 6 days. At the end of the fermentation, 5% (w/v) resins (Amberlite® XAD16, Shanghai Macklin Biochemical Co., Ltd, China) were added into the cultures, and a 3-h extended incubation with rotation was applied to allow the metabolites to be absorbed into the resins. Then the resins were harvested, cleaned and air-dried. Methanol was used for extraction. The organic extracts were concentrated *in vacuo*. The crude extract was fractionated on a silica gel column and eluted with a stepwise gradient of CH_2Cl_2–CH_3OH (100:0, 98:2, 96:4, 94:6, 92:8, 9:1, 8:2, 7:3, 1:1, 0:100). The elution volume was 200 mL for each gradient. The eluents were analysed by TLC and then combined. The combined fractions were further analysed by LC-MS. The fractions that contain the interested *m/z* values were further chromatographed over a preparative reversed-phase HPLC column (Waters XBridge® Prep C18 10 μm OBD, 19 × 250 mm) with a gradient elution (13 mL/min) of CH_3OH in H_2O containing 0.1% formic acid. The targeted subfractions were then passed through several rounds of semipreparative HPLC (Agilent ZORBAX Stable Bond 80Å Phenyl Column, 9.4 × 250 mm, 5 μm) to obtain pure compounds. Compounds **1** and **3**

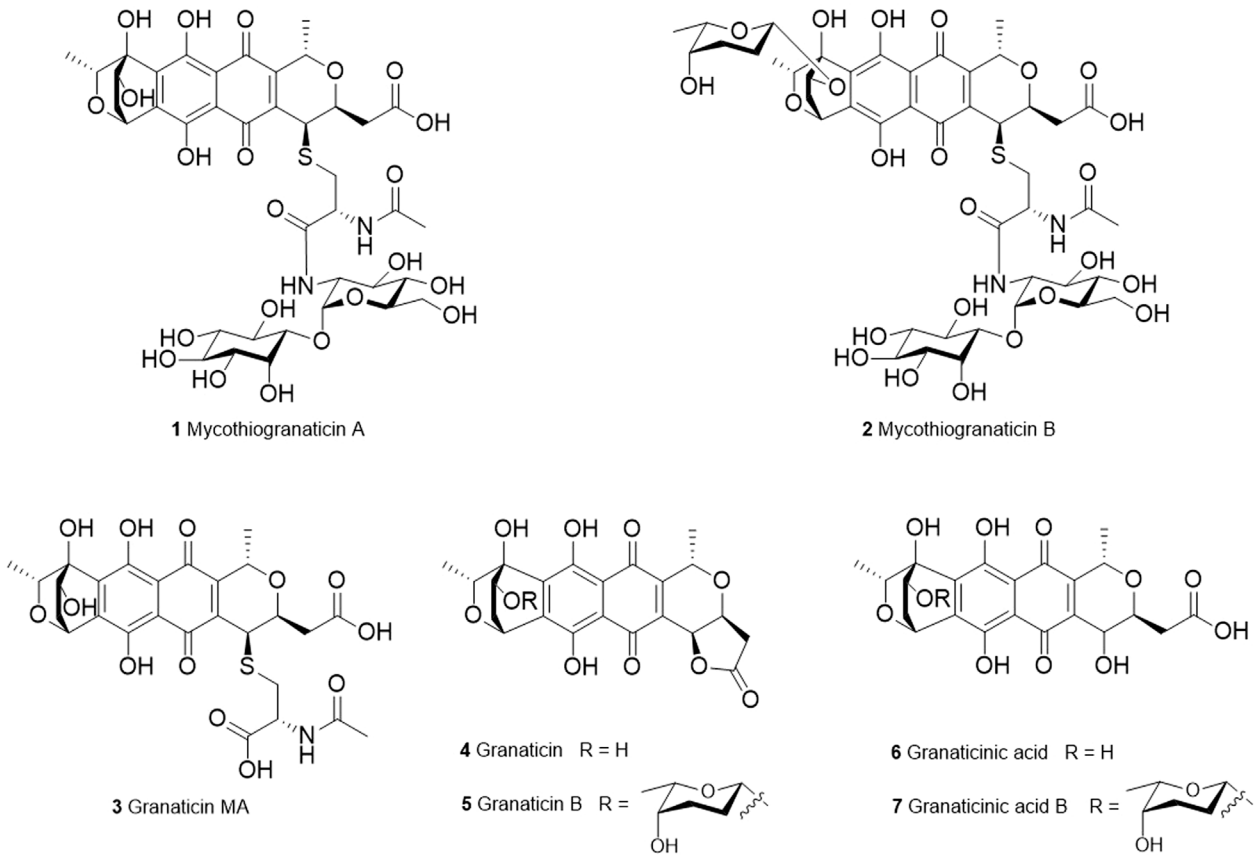

FIGURE 1 | Structures of granaticins and mycothiogranaticins.

were purified with retention times of 10.6 and 17 min, respectively, using an isocratic elution (2.5 mL/min) of 55% CH_3OH in H_2O containing 0.1% formic acid. The retention time of compound **2** was 11.2 min when using a 15-min gradient elution (3 mL/min) from 60–100% CH_3OH in H_2O containing 0.1% formic acid. The ^1H and ^{13}C NMR spectra were done on either a Bruker Avance III HD 600 MHz or Avance III Ultrashield 700 MHz with QCI Cryoprobe spectrometer at 298 K. Optical rotations were measured with an Anton-Paar's MCP500 polarimeter. The experimental CD spectrum of compound **1** was collected in methanol at a concentration of 0.5 mg/mL on an Applied Photophysics Chirascan spectrometer using a quartz cell with path length of 10 mm. The ECD calculation was performed by using the density functional theory (DFT) with the Gaussian 09 package (Frisch et al., 2009). The preliminary conformational distributions search was performed *via* molecular mechanics using the MM+ method implemented in CONFLEX version 8.0 software. The obtained conformers were optimized at the B3LYP/6-31G level using Gaussian 09 software to give the energy-minimized conformers. Methanol was used as a solvent with the polarizable continuum model (PCM). Then, the optimized conformers were subjected to the calculations of ECD spectra using TDDFT at the B3LYP/6-31G (d, p) level. The overall calculated ECD curves were weighted by Boltzmann distribution (with a half-bandwidth of 0.35 eV) with a UV correction of 15 nm. The calculated ECD spectra were produced by SpecDis 1.64 software (Bruhn et al., 2013). The structures and absolute configurations were elucidated on the basis of extensive spectroscopic analyses including UV, MS, NMR and ECD spectra, and together with consideration of their biogenetic origins.

Antibacterial and Cytotoxic Activity Assays

The minimum inhibitory concentrations (MICs) were determined using a 96-well plate format with Müller-Hinton (MH) broth (Wiegand et al., 2008). Cells of each strain at log-phase growth stage were adjusted to an $OD_{600} = 0.5$, then 100-fold diluted with MH broth. The diluted cell broth was pipetted with a volume of 98 μL into each well. Two microliters of each compound, serially diluted in DMSO, were added to each well. DMSO was used as negative control, and vancomycin and granaticin as positive controls. The MIC values were determined after incubation for 18 h either at 37 °C for *Staphylococcus aureus* or at 30 °C for *Micrococcus luteus*. Each MIC determination was performed in triplicate. A sulforhodamine B (SRB) colorimetric assay (Vichai and Kirtikara, 2006) was used to assess the potential cytotoxicity against the SF-268, MCF-7, HepG-2 and A549 cell lines. Cells (180 μL) with a density of 3×10^4 cells/mL were seeded onto 96-

well plates and incubated for 24 h at 37 °C, 5% CO_2. Then 20 μL of compounds with various concentrations were added into the wells. Plates were further incubated for 72 h. After incubation, cell monolayers were fixed with 50% (wt/v) trichloroacetic acid (50 μL) and stained for 30 min with 0.4% (wt/v) SRB dissolved in 1% acetic acid. Unbound dye was removed by washing repeatedly with 1% acetic acid. The protein-bound dye was dissolved in 10 mM Tris base solution (200 μL) for OD determination at 570 nm using a microplate reader. Cisplatin was used as a positive control. Granaticin was also assessed for comparison purpose. All data were obtained in triplicate and are presented as means ± S.D. IC_{50} values were calculated with the SigmaPlot 14.0 software using a non-linear curve-fitting method.

Chemical Analysis and Assessment of Biomass and Overall Production of Granaticins

LC-MS analysis was carried out, with an ESI source in negative ion mode, on an Agilent 6230 TOF mass spectrometry coupled to 1290 Infinity LC System equipped with an Agilent ZORBAX SB-C18 column (1.8 μm, 3.0 × 5.0 mm). Liquid chromatography for LC-MS analysis was performed using a 20 min solvent gradient (0.25 mL/min) from 10–100% CH_3OH in H_2O containing 0.1% formic acid. Yields of the four main products, granaticin (**4**), granaticin B (**5**), granaticinic acid (**6**) and granaticinic acid B (**7**) were used for assessment of the overall production of granaticins. Standard calibration curves for each product were generated by using the pure compounds (**Supplementary Figure S1**). The biomass was measured by using a volume of 20 mL of fermentation broth for each. All the tests were done in triplicate.

Genetic Manipulation of *S. vietnamensis*

The *mshA* gene encodes the D-inositol-3-phosphate glycosyltransferase catalyzing the first step of mycothiol biosynthesis, and the *mst* gene dictates the mycothiol-S transferase catalyzing the transfer of mycothiol to various substrates (Newton et al., 2003; Newton et al., 2011). The protein sequences of *mshA* (*SCO4204*) from *S. coelicolor* A3 (2) (Park et al., 2006) and *Rv0443* from *Mycobacterium tuberculosis* H37Rv were used to BLAST against the genome sequence of *S. vietnamensis* GIMV4.0001 (Deng et al., 2015). The *SVTN_RS20640* gene, encoding a protein whose sequence shares an identity of nearly 80% with SCO4204, was preferentially considered as the *mshA* gene in *S. vietnamensis* (**Supplementary Figure S2**). The *SVTN_RS22215* gene, whose product was predicted to belong to the DinB superfamily, was the only candidate *mst* gene sharing 52.8% identity to Rv0443 (**Supplementary Figure S3**).

To construct the in-frame deletion mutant Δ*mshA*, two 1.7-kb DNA fragments flanking the *mshA* gene (*SVTN_RS20640*) were amplified using the primer pairs Sv-MshALF/R and Sv-MshARF/R. The plasmid pKC1139 was double digested with *Hin*dIII and *Eco*RI. The linearized plasmid together with the two PCR-amplified homologous arms were assembled by using a ClonExpress® MultiS One Step Cloning Kit, affording the disruption plasmid pKC-Δ*mshA*. The recombinant plasmid pKC-Δ*mshA* was then subjected to sequencing to ensure that no mutations were introduced during the construction process. After passing through the non-methylating *E. coli* ET12567/pUZ8002, pKC-Δ*mshA* was introduced into *S. vietnamensis* GIMV4.0001 by intergeneric conjugation, following the established procedure (Deng et al., 2011b). Exconjugants were picked and re-streaked on the ISP2 agar plates supplemented with 30 μg/mL apramycin and then grown at 28 °C for 2 days. Colonies were inoculated into liquid YEME medium and rotationally incubated at 37 °C for 1 day to lose the temperature-sensitive plasmid. The cultures were then diluted and spread on plate. The colonies that are sensitive to apramycin were picked and subjected to DNA isolation and PCR validation. For further verification, two overlapping PCR fragments amplified with the primer pairs V-MshALOF/V-MshARIR and V-MshALIF/V-MshAROR were subjected to sequencing to make sure that no unintended mutations were introduced during the homologous recombination process (**Supplementary Figure S18**). The Δ*mst* mutant was generated in a similar way. For the complementation of *mshA*, a 1.4 kb DNA fragment containing the full-length coding sequence of *mshA* (*SVTN_RS20640*) and the putative ribosomal binding sequence was amplified by PCR with the primer pair Com-MshF/R. The amplified fragment was assembled into pSET-KasO* between *Afl*II and *Spe*I sites by using a ClonExpress kit. The resulting plasmid pSET-*mshA* was introduced into the Δ*mshA* mutant with the same method as described above. Screening of the desired complementary colony followed the standard procedure.

RESULTS

Discovery of Sulfur-Containing Granaticin Congeners from *S. vietnamensis* GIMV4.0001

In our continuous studies on the granaticin biosynthesis, we noticed that there were two new minor peaks which possess characteristic UV absorptions of granaticins in some batches of fermentation in the liquid YEME medium. LC-MS analysis showed that the *m/z* values of the two minor peaks are 929.2501 $[M–H]^-$ (**Supplementary Figure S4**) and 1043.3189 $[M–H]^-$ (**Supplementary Figure S5**), respectively. Because the *m/z* values are different from the known granaticin congeners, we decided to isolate these compounds. During the isolation process, compound **3** came into our sights with a *m/z* value of 606.1285 $[M–H]^-$ (**Supplementary Figure S6**) and granaticin-type UV absorption characteristics. Compound **3** couldn't be detected by either HPLC or LC-MS in the samples of the direct fermentation broths or crude extracts of *S. vietnamensis*. It could only be detected after at least one round of silica gel separation. Therefore, compound **3** should be considered as a degradation product. Although the suggested molecular weight of compound **3** is as same as the compound 4-deoxy-4-S-(N-acetylcysteinyl) granaticinic acid (granaticin MA) which was reported nearly 40 years ago (Kormann et al., 1984), the NMR data and

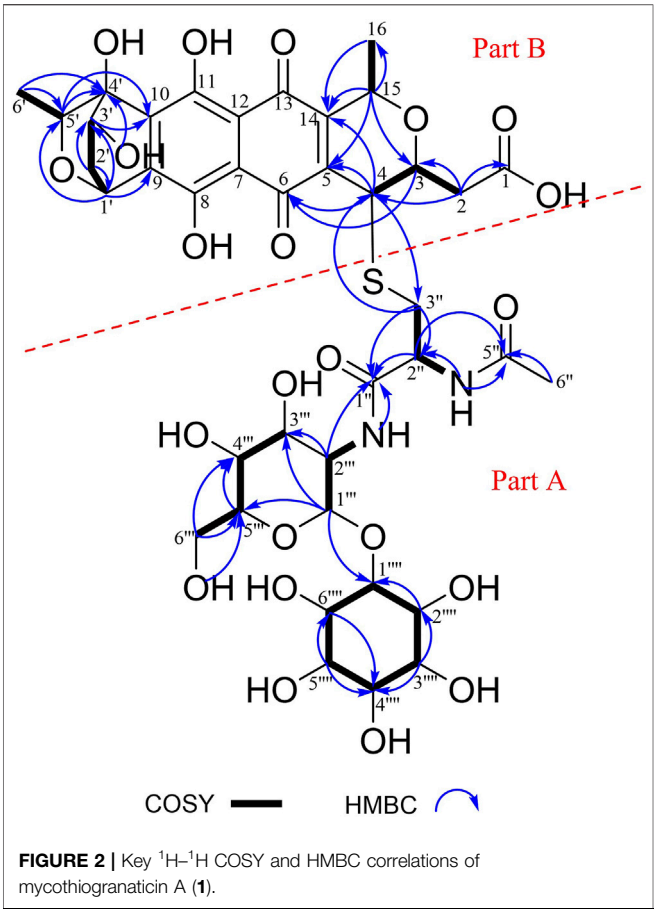

FIGURE 2 | Key ^{1}H–^{1}H COSY and HMBC correlations of mycothiograna ticin A (**1**).

absolute configuration of granaticin MA were unavailable. It prompted us to purify it and collect the necessary spectrum data.

Compound **1** (2.06 mg/L) was obtained as a red powder $[\alpha]_D^{25}$ -21.5 (*c* 0.016, CH_3OH). Its molecular formula was established as $C_{39}H_{50}N_2O_{22}S$ by HR-ESI-MS at *m/z* 929.2501 $[M - H]^-$ (calcd. 929.2503), corresponding to sixteen degrees of unsaturation. The ^{1}H and ^{13}C NMR spectra (**Supplementary Table S3**), coupled with HSQC analysis, showed signals of three methyls, four methylenes, eighteen methines and fourteen quaternary carbons (**Supplementary Figure S7–12**). The signals of six methines [(δ_H 3.18, δ_C 80.2, C-1′′′′), (δ_H 3.91, δ_C 71.6, C-2′′′′), (δ_H 3.09, δ_C 71.6, C-3′′′′), (δ_H 3.34, δ_C 72.4, C-4′′′′), (δ_H 2.93, δ_C 74.8, C-5′′′′), (δ_H 3.53, δ_C 72.1, C-6′′′′)] were typical of an inositol moiety, further confirmed by the ^{1}H–^{1}H COSY correlations of H-1′′′′/H-2′′′′/H-3′′′′/H-4′′′′/H-5′′′′/H-6′′′′/H-1′′′′ (**Figure 2**). The signals of five methines [(δ_H 4.83, δ_C 98.6, C-1′′′), (δ_H 3.64, δ_C 54.0, C-2′′′), (δ_H 3.53, δ_C 70.9, C-3′′′), (δ_H 3.10, δ_C 70.7, C-4′′′), (δ_H 3.67, δ_C 72.9, C-5′′′)] and one methylene (δ_H 3.44, δ_C 60.8, C-6′′′) indicated the presence of an α-glucosamine moiety, which was verified by ^{1}H–^{1}H COSY correlations of H-1′′′/H-2′′′/NH-2′′′ and H-3′′′/H-4′′′/H-5′′′/H-6′′′, along with the key HMBC correlations from H-1′′′ to C-3′′′ and C-5′′′, and from H-2′′′ to C-3′′′. The ^{1}H–^{1}H COSY correlations of H-3′′/H-2′′/NH-2″ and the key HMBC correlations from H-2″ to C-1″ and C-5″, from NH-2″ and H-6″ to C-5″ confirmed the presence of an N-acetylcysteine moiety. Further analysis of the NMR data suggested that compound **1** contains a same moiety (part A in **Figure 2**) with nanaomycin H (Nakashima et al., 2017). The fragment could be verified by the key HMBC correlations from H-1′′′ to C-1′′′′, from NH-2′′′ and H-2′′′ to C-1′′. Apart from the signals for the part A, the remaining signals (**Supplementary Table S3**) closely resembled those of dihydrograna ticin (Arnone et al., 1979), except for the presence of a methine group at C-4 of compound **1** instead of a methylene group in dihydrograna ticin. These findings suggested that part A and part B were linked through a sulfur atom between C-3″ and C-4. This deduction was confirmed by the HMBC correlations from H_2-3″ to C-4 and from H-4 to C-3′′. Comprehensive analysis of ^{1}H–^{1}H COSY and HMBC spectra of compound **1** led to the establishment of its planar structure as depicted in **Figure 2**.

In the NOESY spectrum (**Figure 3**), the observation of the NOE interactions of H-3/H_3-16 revealed the same relative configuration of the right unit of part B of compound **1** to dihydrograna ticin. Meanwhile, the NOESY correlations of H-3′/H-5′ and H-1′/H-6′ suggested the same relative configuration of the left unit of part B (**Figure 1**). Unfortunately, no NOESY correlations supported the relative configuration between the left and the right units of part B. However, the previously identified granaticin congeners from *S. vietnamensis* GIMV4.0001 have the same absolute configuration with the reported granaticins from *S. violaceoruber* Tü22 (Deng et al., 2011a). And the only biosynthetic gene cluster of granaticin residing in the genome of *S. vietnamensis* GIMV4.0001 shares identical organization and high sequence homology with that of *S. violaceoruber* Tü22. In view of biosynthesis, the absolute configuration of part B of compound **1** should be identical to that of dihydrograna ticin except for C-4. As for part A, till now, all the identified mycothiol S-conjugates share the same absolute configuration with mycothiol and the genetic engineering result further supported our conclusion that the part A of compound **1** share the same absolute configuration with mycothiol. Based on the above discussion, the absolute configuration of C-4 was determined as *R* by the NOESY correlation of H-3/H-4. This deduction was further verified by ECD/TDDFT computations on the two possible stereoisomers, (4*S*)-**1** and (4*R*)-**1**. As shown in **Figure 4**, the calculated ECD curve of (4*S*)-**1** showed the identical Cotton effects (CEs) as the experimental ECD curve for compound **1**. Consequently, the whole structure of compound **1** was established as shown in **Figure 1**, named as mycothiograna ticin A.

Compound **2** was prone to degrade during the purification process. Comparing the peaks of compounds **1** and **2** that showed in the HPLC profiles (**Figure 5A**), one would intuitively believe that the production titer of compound **2** should be greater than that of compound **1**. However, we regrettably did not obtain pure enough compound **2** to collect the NMR data. Compound **2** could turn into compound **1** rather rapidly, particularly at the stage of semi-preparation HPLC where 0.1% formic acid must be added into the mobile phase to enable the compounds to peak normally (**Supplementary Figure S13**). The molecular formula of compound **2** could be established as $C_{45}H_{60}N_2O_{24}S$ with

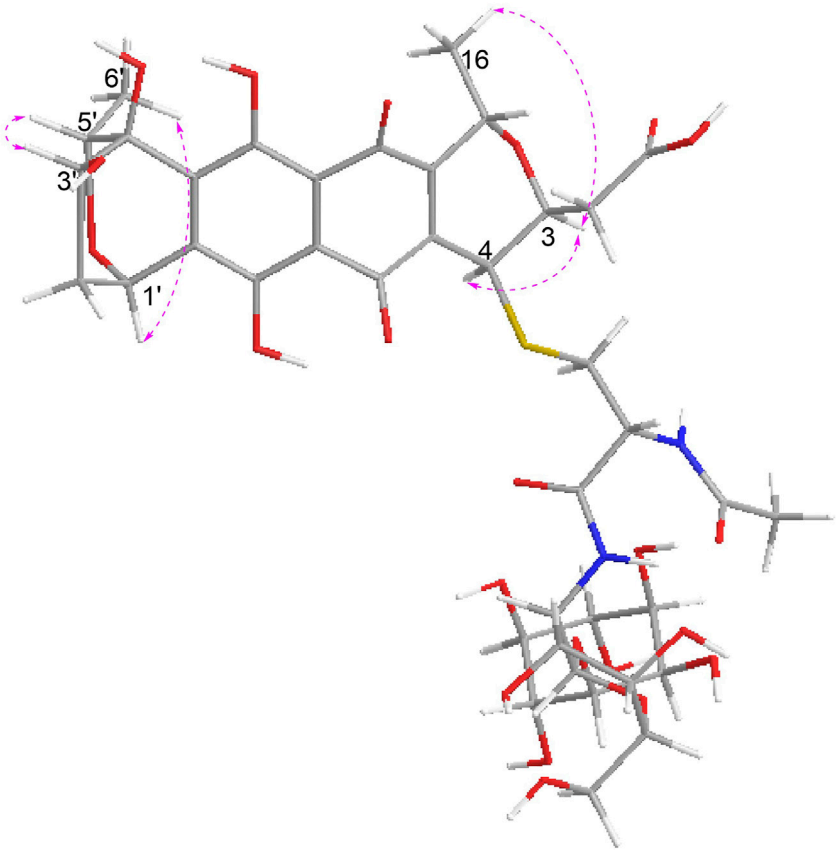

FIGURE 3 | Key NOE correlations of mycothiograna ticin A (**1**).

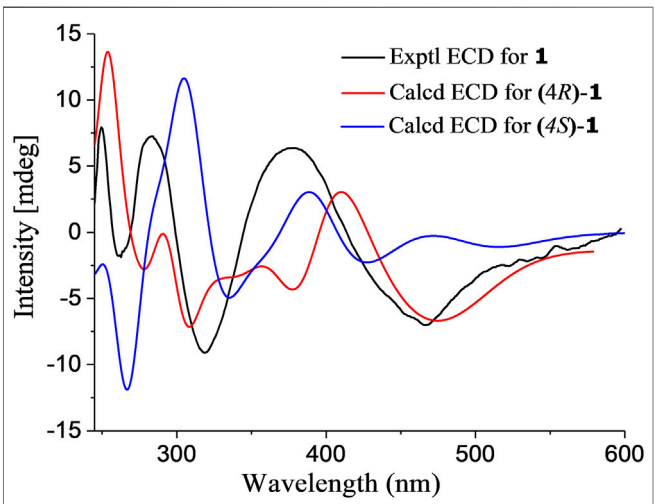

FIGURE 4 | Experimental and calculated ECD spectra of mycothiograna ticin A (**1**).

HR-ESI-MS data (exptl. *m/z* 1043.3189 $[M - H]^-$; calcd. 1043.3184) (**Supplementary Figure S14**). When compound **2** was converted to compound **1**, the molecular weight was reduced by 114 Da, which is as same as in the situation of the conversion of granaticin B (**5**) into granaticin (**4**). The rhodinose moiety of granaticin B (**5**) is connected to the first sugar by an O-glycosidic bond, and this glycosidic bond is hypersensitive to acid and base. The reduction of 114 Da in molecular weight corresponded to the loss of the rhodinose moiety. This led us to speculate that compound **2** is a mycothiol S-conjugate of dihydrograna ticin B. Indeed, in the HRESI-MS/MS analysis, the major daughter peaks between compounds **2** and **1** shared either the same or a range of differences from 114.0672 to 114.0685 in *m/z* values (**Supplementary Figure S15**). This result is consistent with the expected conversion of the mycothiol S-conjugate of dihydrograna ticin B into the mycothiol S-conjugate of dihydrograna ticin. The MS/MS fragmentation mechanisms were proposed (**Supplementary Figure S16**). Thus, compound **2** was named as mycothiograna ticin B, and its proposed structure was shown in **Figure 1**.

Compound **3** (0.39 mg/L) was isolated as a red powder $[\alpha]_D^{25}$ -654.0 (*c* 0.010, CH_3OH). Its molecular formula was established as $C_{27}H_{29}NO_{13}S$ by HR-ESI-MS at *m/z* 606.1285 $[M - H]^-$ (calcd. 606.1287). The 1D NMR spectroscopic data of compound **3** (**Supplementary Table S4**) were highly similar to those of compound **1**, except that the inositol and α-glucosamine

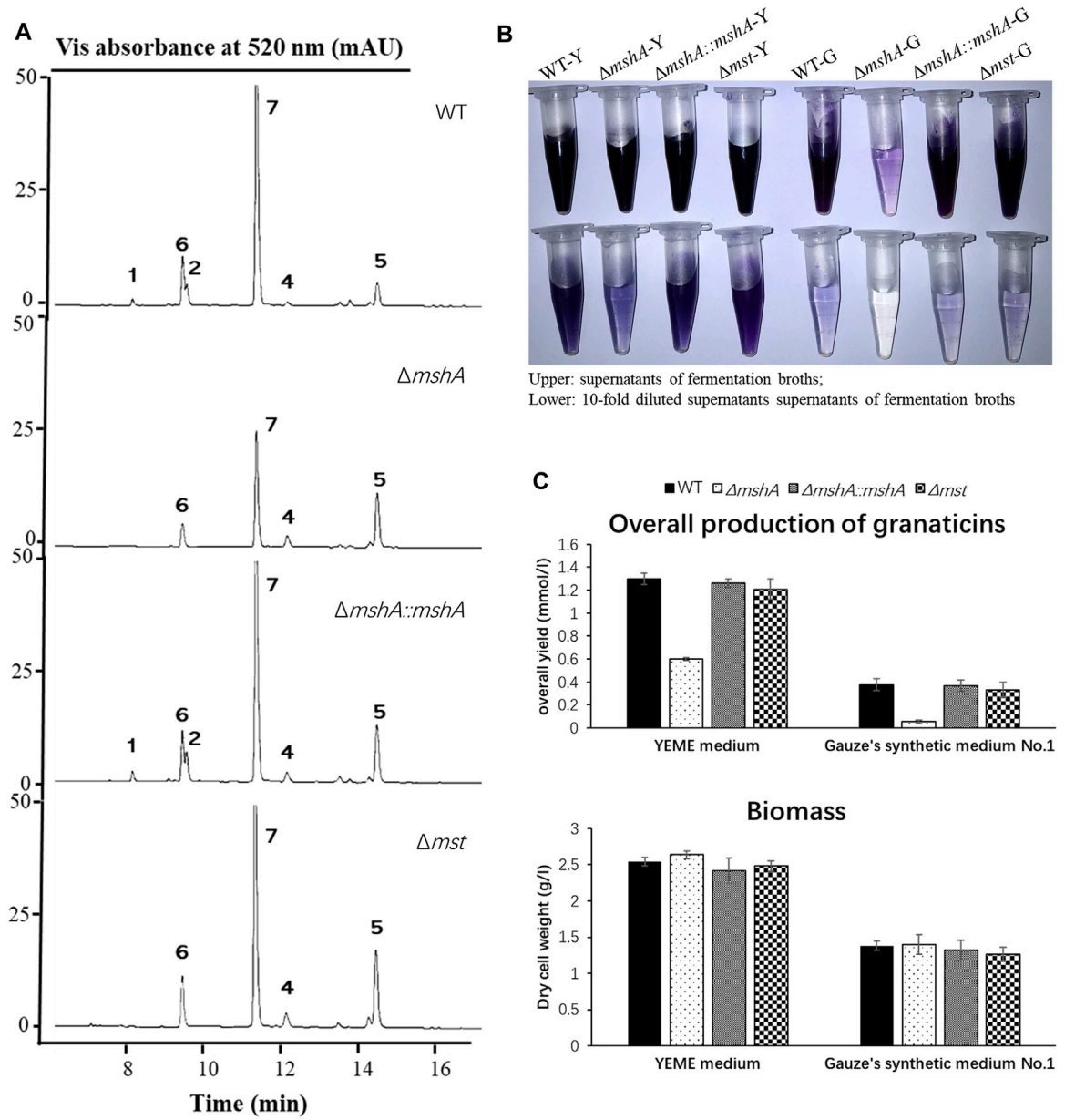

FIGURE 5 | Effects of disruptions of the *mshA* and *mst* genes on the production of granaticins. **(A)** HPLC profiling of the *Streptomyces vietnamensis* wild type and genetically manipulated strains. Note that granaticin MA (**3**) might be a degradation product of mycothiograna ticin A (**1**) and could not be detected in the fermentation broth under the standard procedures. **(B)** The supernatants and diluted supernatants of the *S. vietnamensis* strains in different media. WT-Y, Δ*mshA*-Y, Δ*mshA*::*mshA*-Y, Δ*mst*-Y, WT-G, Δ*mshA*-G, Δ*mshA*::*mshA*-G and Δ*mst*-G stand for the wild-type (WT), mutant Δ*mshA*, complementary strain Δ*mshA*::*mshA* and mutant Δ*mst* in the YEME (Y) or Gauze's synthetic No.1 (G) media, respectively. Tris-EDTA buffer (pH 8.0) was used for dilution. **(C)** The overall yields of granaticins and biomass of the wild type, mutant and complementary strains.

moieties were absent and a carboxyl signal at C-1″ (δ_C 173.8) was present. Further analyses of NMR data, including COSY and HMBC experiments (**Supplementary Figure S17**), elucidated the structure of compound **3** as 4-deoxy-4-S-(N-acetylcysteinyl) granaticinic acid (granaticin MA) (Kormann et al., 1984). Its absolute configuration was deduced as compound **1** by comprehensive consideration NMR data, biogenesis and genetic engineering result.

Mycothiograna ticin A (**1**) and granaticin MA (**3**) were tested for their potential antibacterial and cytotoxic activities. As shown in **Supplementary Table S5**, these two compounds, in comparison to granaticin (**4**), exhibited dramatically decreased activities against all the tested strains, and no inhibitory effects were observed against all the tested cancer cell lines (HL-60, MCF-7, HepG-2 and A549) and the LX-2 human hepatic stellate cell line (**Supplementary Table S6**).

Gene Disruption Revealing Mycothiol as both a Structural Building Block and a Regulator in the Granaticin Biosynthesis

Mycothiol could be involved in antibiotic biosynthesis as exemplified by the biosynthesis of lincomycin A (Zhao et al., 2015). To investigate whether the biosynthesis of mycothiogranaticins is mycothiol pathway-dependent, we set out to generate an in-frame deletion mutant Δ*mshA*. The *mshA* gene was reported to be essential for mycothiol biosynthesis in *S. coelicolor* A3 (2) (Park et al., 2006) and other actinomycetes (Newton et al., 2003; Vilchèze et al., 2008). A BLAST analysis revealed that *SVTN_RS20640* is the best candidate gene of *mshA* (**Supplementary Figure S2**). Successful in-frame deletion of *mshA* (*SVTN_RS20640*) was verified by PCR confirmation of its genotype (**Supplementary Figure S18**). The mutant Δ*mshA* apparently produced much less blue pigment in the fermentation broth and no mycothiogranaticin A (**1**) or B (**2**) could be detected by HPLC analysis (**Figures 5A, B**). Reintroduction of *mshA* (*SVTN_RS20640*) into the mutant Δ*mshA* resulted in restoring the dark blue pigmentation of the fermentation broth and production of mycothiogranaticin A (**1**) and B (**2**) in the complementary strain Δ*mshA*::*mshA* (**Figures 5A, B**). The results suggested that the mycothiol moiety presented in mycothiogranaticins A (**1**) and B (**2**) is originated from the mycothiol pathway.

Mycothiol is a glutathione counterpart in many actinobacteria, and it is involved in cellular detoxification. The *mst* gene, encoding the mycothiol-S transferase, was reported to catalyze the conjugation of mycothiol to electrophiles to form mycothiol-electrophile conjugates (Newton et al., 2011). To further investigate the biosynthetic mechanism of mycothiogranaticins, *SVTN_RS22215*, the only *mst* candidate gene, was subjected to deletion. The genotype of the deletion mutant Δ*mst* (*SVTN_RS22215*) was confirmed by PCR and sequcencing (**Supplementary Figure S19**). Disruption of *SVTN_RS22215* would not affect the biosynthesis of both granaticin and mycothiol, but interrupt the conjugation step of mycothiol to granaticins. Indeed, the deletion mutant Δ*mst* didn't show any reduced pigmentation of the fermentation broth (**Figure 5B**), but mycothiogranaticin A (**1**) and B (**2**) were absent from it (**Figure 5A**). The result showed that the mycothiol-S transferase is key for productions of mycothiogranaticins, suggesting that the biosynthesis of mycothiogranaticins relies on the mycothiol-dependent detoxification pathway, and that the incorporation of mycothiol into the granaticin chromophore should be the final step.

As mentioned earlier, disruption of *SVTN_RS20640* led much reduced pigmentation of the fermentation broth of the mutant strain Δ*mshA* (**Figure 5B)**, suggesting a negative effect on the granaticin production. The overall production of granaticins of the mutant strain Δ*mshA* were reduced by more than 50% in the YEME liquid and 80% in the Gauze's synthetic medium No.1 liquid, respectively, while the complementary strain Δ*mshA*::*mshA* and the mutant strain Δ*mst* gave similar production levels to that of the wild type strain (**Figure 5C**). Theoretically, disruption of *mshA* (*SVTN_RS20640*) would result in mycothiol deficiency in the mutant strain Δ*mshA*. Considering the important role of mycothiol in maintaining the redox balance of the cytoplasm in *Actinobacteria* (Newton et al., 1996; Loi et al., 2015), the potential deleterious effect of the *mshA* deletion on cell growth and in turn reduction of the granaticin production should be examined. The growth of each strain was assessed by dry cell weighting. The result showed, however, the growth of the mutant strain Δ*mshA* was not impaired, comparing with that of the wild-type strain (**Figure 5C**). This suggested that the decreased production of granaticins in the mutant strain Δ*mshA* was correlated with the mycothiol deficiency. Mycothiol might possess a positive regulatory effect on the biosynthesis of granaticin.

DISCUSSION

A few of new granaticin congeners have been discovered in recent years (Jiang et al., 2014; Lv et al., 2019). Till now, the only sulfur-containing granaticin congener, granaticin MA, was reported nearly 4 decades ago (Kormann et al., 1984), but the NMR and bioactivity data were unavailable for the research community. In the current study, we discovered three granaticin congeners with mycothiol or N-acetylcysteine moieties, including granaticin MA, from *S. vietnamensis* GIMV4.0001. Sulfur incorporation can not only expand the structural diversity of molecules, but also endow them distinct bioactivities. For example, the S-bridged polyketide dimmer naquihexcin E possesses anti-HIV activity, whereas the antiviral activity of the non-sulfur-containing monomer naquihexcin K was not reported (He et al., 2019). More closely related examples are nanaomycin H, I and J (Nakashima et al., 2017; Matsuo et al., 2019a). Nanaomycin A and granaticin (**4**) are close BIQ members, and share the same stereo configuration (3*R*, 15*S*) in the pyran ring and only differ at the C-8 position of the lateral aromatic ring in the BIQ chromophores where the hydrogen atom in nanaomycin A is substituted by a hydroxyl group in granaticin (**4**). Like mycothiogranaticins, nanaomycin H, I and J contain mycothiol-derived moieties. While nanaomycin A shows strong antibacterial and cytotoxic activities, these sulfur-containing analogs showed, in contrast, no or weak antibacterial or anticancer bioactivities in the initial assay (Nakashima et al., 2017; Matsuo et al., 2019b). However, further bioactivity screening revealed that all these congeners possess epithelial-mesenchymal transition (EMT) inhibition activity showing potentials in invasive cancer therapy (Omura et al., 2018; Nakanishi et al., 2019). In spite of weak antibacterial activities and no cytotoxic activities revealed in the current study, mycothiogranaticin A (**1**) and granaticin MA (**3**) are still open for more bioactivity screening, particularly the evaluation of EMT inhibition activity, in consideration of the high similarity in structure between mycothiogranaticins and the mycothiol-derived nanaomycins.

Although more and more sulfur-containing aromatic polyketides of bacterial origin, including sulfur-bridged dimers and mycothiol-derived monomers, have been discovered in recent years, the knowledge on the sulfur incorporation mechanism involved remains limited. Researchers proposed the recruitment of the

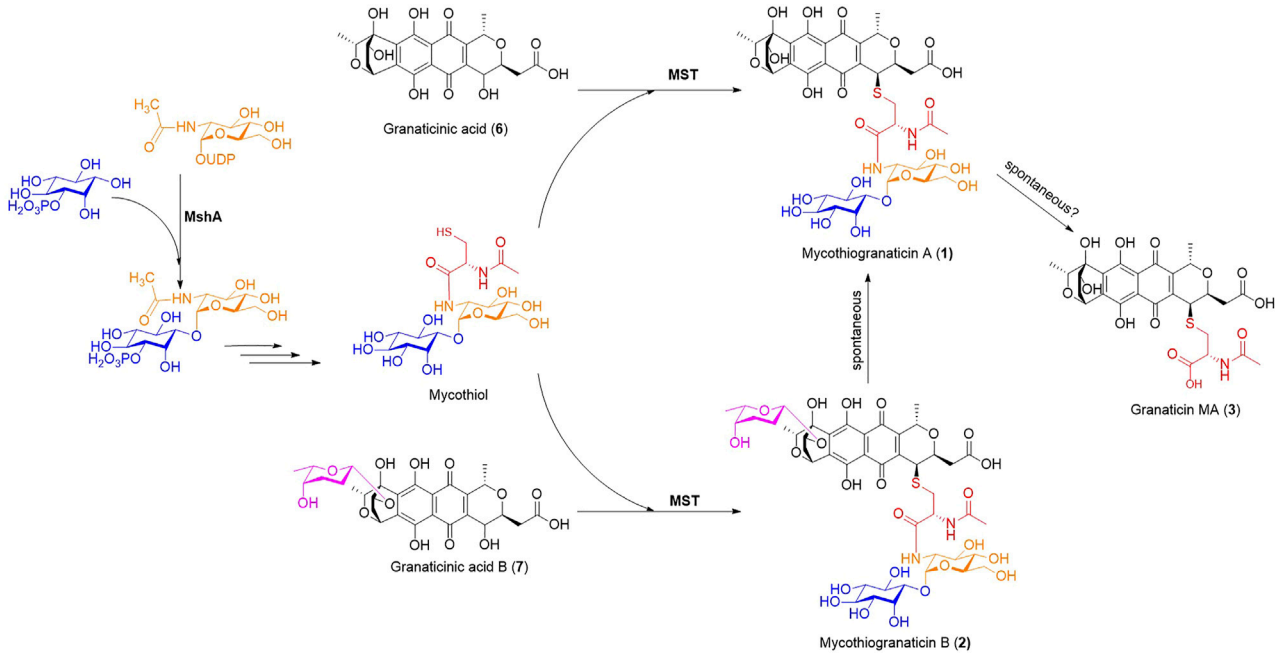

FIGURE 6 | The proposed biosynthetic pathway of mycothiogranaticins. MshA, D-inositol-3-phosphate glycosyltransferase; MST, mycothiol-S transferase.

mycothiol-dependent detoxification pathway for their biosynthesis (Wang et al., 2013; Fang et al., 2020). This assumption seems reasonable but has never been experimentally confirmed. A recent report showed that inorganic sulfur can be directly introduced into the polyketide chromophore to form sulfur-bridged dimers by nonenzymatic reactions (Cao et al., 2021), suggesting diverse sulfur incorporation mechanisms. In this study, we provided experimental evidence, for the first time, that mycothiogranaticins are derived from the mycothiol-dependent detoxification pathway. The proposed biosynthetic pathway was shown in **Figure 6**.

Mycothiol functions as a thiol-redox buffer to contribute to maintain the reduced state of the cytoplasm and mediates detoxification of both xenobiotic and endobiotic electrophilic compounds, resulting in mycothiol S-conjugates (Newton et al., 1996; Loi et al., 2015). Taking into account of the involvement of mycothiol in the biosynthesis and the reluctance of bioactivities, mycothiogranaticins should be recognized as detoxification products of granaticins by the producer. Surprisingly, disruption of *mshA* (*SVTN_RS20640*) reduced the granaticin production by at least more than 50%. Because reintroduction of *mshA* (*SVTN_RS20640*) into the Δ*mshA* mutant can restore the production level to that of the wild type, and disruption of *mst* (*SVTN_RS22215*) didn't alter the overall yield of granaticins, mycothiol deficiency should account for the reduction in the Δ*mshA* mutant. This suggested that mycothiol is involved in positively tunning the production of granaticin. To the best of our knowledge, this is the first report that mycothiol can not only directly incorporate into polyketide structures, but also play an important regulatory role on polyketide biosynthesis.

Although we currently cannot figure out the underlying mechanism, the *soxR*-like *gra-orf20* gene, lying within the granaticin biosynthetic gene cluster, may serve as a clue for further investigation. In *E. coli*, the transcriptional factor SoxR, acting as a redox sensor system, governs a global defense against specific types of oxidative stress (Pomposiello and Demple, 2001). When oxidative stress occurs, the oxidized SoxR activates the transcription of the *soxS* gene which in turn activates the whole response regulon. In our previous study, disruption of *gra-orf20* unexpectedly led a three-fold increase of granaticin production, showing that this *soxR*-like gene played a negative regulatory role in the granaticin biosynthesis, probably by sensing the redox state of the cytoplasm, but the exact mechanism remains unknown (Deng M. et al., 2011). Because mycothiol is a major redox buffering agent in many actinomycetes, disruption of *mshA* (*SVTN_RS20640*) would result in mycothiol deficiency in the Δ*mshA* mutant and render this mutant more vulnerable to oxidative stress. In this situation, the SoxR homolog, Gra-ORF20, would be more easily and strongly activated, and in turn suppress the granaticin biosynthesis.

CONCLUSION

Sulfur-containing polyketides of bacterial origin have received increasing attention from the fields of discovery and biosynthesis of natural products. In the current study, we discovered three sulfur-containing granaticin analogs, mycothiogranaticins A (**1**), B (**2**) and granaticin MA (**3**) from *S. vietnamensis* GIMV4.0001. The structure of mycothiogranaticin A (**1**) was determined by the comprehensive analysis of MS, NMR, ECD calculations and biosynthetic studies. The mycothiogranaticin A (**1**) and

granaticin MA (**3**) showed dramatically decreased antibacterial activities and no cytotoxic activities. Gene disruptions suggested that the biosynthesis of mycothiogranaticins is mycothiol-dependent, providing experimental evidence, for the first time, for the biological origin of sulfur in this category of sulfur-containing polyketides. In addition, mycothiol was unexpectedly found to be involved in positive regulation of the biosynthesis of granaticins, probably by maintaining the cellular redox balance. To the best of our knowledge, this is the first report that mycothiol can not only be a building block of polyketides but also play a regulatory role in the polyketide biosynthesis.

DATA AVAILABILITY STATEMENT

The original contributions presented in the study are included in the article/**Supplementary Material**, further inquiries can be directed to the corresponding authors.

AUTHOR CONTRIBUTIONS

HZ, HZ and M-RD designed the research. M-RD and YL performed most of the experiments. XL did part of the genetic works. X-LZ, YC, Y-LZ and WZ contributed to fermentation, chemical isolation and bioassay. M-RD wrote the manuscript. HZ and HZ revised the manuscript. All authors contributed to the article and approved the submitted version.

FUNDING

This work was financially supported by the National Natural Science Foundation of China (Grant Nos. 32070047 and 31470188), the Guangdong Science and Technology Program (Grant Nos. 2016A010105013 and 2019B030316017) and a strategic research and consulting project of Chinese Academy of Engineering (2012-XZ-8).

ACKNOWLEDGMENTS

We are grateful to Guohui Pan at the Institute of Microbiology, Chinese Academy of Sciences for kindly providing the plasmid pSET-KasO*.

SUPPLEMENTARY MATERIAL

The Supplementary Material for this article can be found online at: https://www.frontiersin.org/articles/10.3389/fchem.2021.802279/full#supplementary-material

REFERENCES

Agrawal, A., and Somani, R. (2009). Farnesyltransferase Inhibitor as Anticancer Agent. *Mrmc* 9, 638–652. doi:10.2174/138955709788452702

Aoyama, T., Zhao, W., Kojima, F., Muraoka, Y., Naganawa, H., Takeuhi, T., et al. (1993). Cysfluoretin, a New Inhibitor of Glutathione S-Transferase, Produced by *Streptomyces* sp. MI384-DF12. *J. Antibiot.* 46 (9), 1471–1474. doi:10.7164/antibiotics.46.1471

Arnone, A., Camarda, L., Cardillo, R., Fronza, G., Merlini, L., Mondelli, R., et al. (1979). ^{13}C-NMR. Analysis of Dihydrogranaticin Methyl Ester. A Case of Mixed Biogenesis. *Helv. Chim. Acta* 62 (1), 30–33. doi:10.1002/hlca.19790620105

Bae, M., An, J. S., Bae, E. S., Oh, J., Park, S. H., Lim, Y., et al. (2019). Donghaesulfins A and B, Dimeric Benz[*a*]anthracene Thioethers from Volcanic Island Derived *Streptomyces* sp. *Org. Lett.* 21 (10), 3635–3639. doi:10.1021/acs.orglett.9b01057

Bierman, M., Logan, R., O'Brien, K., Seno, E. T., Nagaraja Rao, R., and Schoner, B. E. (1992). Plasmid Cloning Vectors for the Conjugal Transfer of DNA from *Escherichia coli* to *Streptomyces* spp. *Gene* 116 (1), 43–49. doi:10.1016/0378-1119(92)90627-2

Bilyk, O., Sekurova, O. N., Zotchev, S. B., and Luzhetskyy, A. (2016). Cloning and Heterologous Expression of the Grecocycline Biosynthetic Gene Cluster. *PLOS ONE* 11 (7), e0158682. doi:10.1371/journal.pone.0158682

Bruhn, T., Schaumlöffel, A., Hemberger, Y., and Bringmann, G. (2013). SpecDis: Quantifying the Comparison of Calculated and Experimental Electronic Circular Dichroism Spectra. *Chirality* 25 (4), 243–249. doi:10.1002/chir.22138

Cao, M., Zheng, C., Yang, D., Kalkreuter, E., Adhikari, A., Liu, Y. C., et al. (2021). Cryptic Sulfur Incorporation in Thioangucycline Biosynthesis. *Angew. Chem. Int. Ed.* 60 (13), 7140–7147. doi:10.1002/anie.202015570

Carney, J. R., Hong, S.-T., and Gould, S. J. (1997). Seongomycin: A New Sulfur-Containing Benzo[*b*]fluorene Derived from Genes Clustered with Those for Kinamycin Biosynthesis. *Tetrahedron Lett.* 38 (18), 3139–3142. doi:10.1016/S0040-4039(97)00616-3

Chang, C.-J., Floss, H. G., Soong, P., and Chang, C.-T. (1975). Identity of the Antitumor Antibiotic Litmomycin with Granaticin A. *J. Antibiot.* 28 (2), 156. doi:10.7164/antibiotics.28.156

Che, Q., Tan, H., Han, X., Zhang, X., Gu, Q., Zhu, T., et al. (2016). Naquihexcin A, a S-Bridged Pyranonaphthoquinone Dimer Bearing an Unsaturated Hexuronic Acid Moiety from a Sponge-Derived *Streptomyces* sp. HDN-10-293. *Org. Lett.* 18 (14), 3358–3361. doi:10.1021/acs.orglett.6b01485

Corbaz, R., Ettlinger, L., Gäumann, E., Kalvoda, J., Keller-Schierlein, W., Kradolfer, F., et al. (1957). Stoffwechselprodukte von Actinomyceten. 9. Mitteilung. Granaticin. *Hca* 40 (5), 1262–1269. doi:10.1002/hlca.19570400518

Deng, M., Guo, J., Huang, Y., and Zhu, H. (2011c). Function of the Granaticin Biosynthetic Gene *orf20* from *Streptomyces vietnamensis*. *Wei Sheng Wu Xue Bao* 51 (3), 402–409.

Deng, M.-R., Guo, J., Li, X., Zhu, C.-H., and Zhu, H.-H. (2011a). Granaticins and Their Biosynthetic Gene Cluster from *Streptomyces vietnamensis*: Evidence of Horizontal Gene Transfer. *Antonie van Leeuwenhoek* 100 (4), 607–617. doi:10.1007/s10482-011-9615-9

Deng, M.-R., Guo, J., Ma, L.-Y., Li, Y.-X., Feng, G.-D., Mo, C.-Y., et al. (2015). Complete Genome Sequence of *Streptomyces vietnamensis* GIMV4.0001^{T}, a Genetically Manipulable Producer of the Benzoisochromanequinone Antibiotic Granaticin. *J. Biotechnol.* 200, 6–7. doi:10.1016/j.jbiotec.2015.02.009

Deng, M.-R., Guo, J., and Zhu, H.-H. (2011b). *Streptomyces vietnamensis* GIMV4.0001: a Granaticin-Producing Strain that Can Be Readily Genetically Manipulated. *J. Antibiot.* 64 (4), 345–347. doi:10.1038/ja.2011.3

Deng, M.-R., Li, Y., He, H.-H., Zhou, X., Zheng, X.-L., Wang, Y.-H., et al. (2020). An Aberrant Metabolic Flow toward Early Shunt Products in the Granaticin Biosynthetic Machinery of *Streptomyces vietnamensis* GIMV4.0001. *J. Antibiot.* 73 (4), 260–264. doi:10.1038/s41429-019-0267-8

Elson, A. L., Box, S. J., and Gilpin, M. L. (1988). New Quinone Antibiotics of the Granaticin Type, Isolated from *Streptomyces lateritius*. I. Production, Isolation and Properties. *J. Antibiot.* 41 (4), 570–572. doi:10.7164/antibiotics.41.570

Etoh, H., Iguchi, M., Nagasawa, T., Tani, Y., Yamada, H., and Fukami, H. (1987). Structures of Rhodonocardins Produced by a *Nocardia* sp. *Agric. Biol. Chem.* 51 (7), 1819–1824. doi:10.1080/00021369.1987.10868282

Fang, Z., Jiang, X., Zhang, Q., Zhang, L., Zhang, W., Yang, C., et al. (2020). S-bridged Thioether and Structure-Diversified Angucyclinone Derivatives from the South China Sea-Derived *Micromonospora echinospora* SCSIO 04089. *J. Nat. Prod.* 83 (10), 3122–3130. doi:10.1021/acs.jnatprod.0c00719

Frattini, M. G., Djaballah, H., and Kelly, T. J. (2011). *Cdc7 Kinase Inhibitors and Uses Thereof*. U.S. Patent No 11,045,446 (Washington, DC: U.S. Patent and Trademark Office).

Frisch, M. J., Trucks, G. W., Schlegel, H. B., Scuseria, G. E., Robb, M. A., Cheeseman, J. R., et al. (2009). *Gaussian 09 Revision D.01*. Wallingford, CT: Gaussian, Inc.

Hai, Y., Wei, M.-Y., Wang, C.-Y., Gu, Y.-C., and Shao, C.-L. (2021). The Intriguing Chemistry and Biology of Sulfur-Containing Natural Products from Marine Microorganisms (1987-2020). *Mar. Life Sci. Technol.* 3 (4), 488–518. doi:10.1007/s42995-021-00101-2

He, X., Wang, Y., Luo, R.-H., Yang, L.-M., Wang, L., Guo, D., et al. (2019). Dimeric Pyranonaphthoquinone Glycosides with Anti-HIV and Cytotoxic Activities from a Soil-Derived *Streptomyces*. *J. Nat. Prod.* 82 (7), 1813–1819. doi:10.1021/acs.jnatprod.9b00022

Heinstein, P. (1982). Mechanism of Action of Granaticin: Inhibition of Ribosomal RNA Maturation and Cell Cycle Specificity. *J. Pharm. Sci.* 71 (2), 197–200. doi:10.1002/jps.2600710215

Iwasaki, S., and Ōmura, S. (2007). Search for Protein Farnesyltransferase Inhibitors of Microbial Origin: Our Strategy and Results as Well as the Results Obtained by Other Groups. *J. Antibiot.* 60 (1), 1–12. doi:10.1038/ja.2007.1

Jiang, B., Li, S., Zhao, W., Li, T., Zuo, L., Nan, Y., et al. (2014). 6-Deoxy-13-hydroxy-8,11-dione-dihydrogranaticin B, an Intermediate in Granaticin Biosynthesis, from *Streptomyces* sp. CPCC 200532. *J. Nat. Prod.* 77 (9), 2130–2133. doi:10.1021/np500138k

Kormann, E., Pape, H., and Münster, D. (1984). "Modification of the Antibiotic Granaticin A by the Producting Organism *Streptomyces violaceoruber* Tü 7," in *Third European Congress of Biotechnology* (Weinheim, Germany: Verlag Chemie), 105–109.

Kulanthaivel, P., Perun, T. J., Belvo, M. D., Strobel, R. J., Paul, D. C., and Williams, D. C. (1999). Novel Naphthoquinones from a *Streptomyces* sp. *J. Antibiot.* 52 (3), 256–262. doi:10.7164/antibiotics.52.256

Loi, V. V., Rossius, M., and Antelmann, H. (2015). Redox Regulation by Reversible Protein S-Thiolation in Bacteria. *Front. Microbiol.* 6 (187). doi:10.3389/fmicb.2015.00187

Lv, Q., Fan, Y., Tao, G., Fu, P., Zhai, J., Ye, B., et al. (2019). Sekgranaticin, a SEK34b-Granaticin Hybrid Polyketide from *Streptomyces* sp. 166#. *J. Org. Chem.* 84 (14), 9087–9092. doi:10.1021/acs.joc.9b01022

MacNeil, D. J., Gewain, K. M., Ruby, C. L., Dezeny, G., Gibbons, P. H., and MacNeil, T. (1992). Analysis of *Streptomyces avermitilis* Genes Required for Avermectin Biosynthesis Utilizing a Novel Integration Vector. *Gene* 111 (1), 61–68. doi:10.1016/0378-1119(92)90603-M

Matsuo, H., Nakanishi, J., Noguchi, Y., Kitagawa, K., Shigemura, K., Sunazuka, T., et al. (2020a). Nanaomycin K, a New Epithelial-Mesenchymal Transition Inhibitor Produced by the Actinomycete "*Streptomyces rosa* subsp. *notoensis*" OS-3966. *J. Biosci. Bioeng.* 129, 291–295. doi:10.1016/j.jbiosc.2019.09.007

Matsuo, H., Noguchi, Y., Také, A., Nakanishi, J., Shigemura, K., Sunazuka, T., et al. (2019b). Nanaomycin I and J: New Nanaomycins Generated by Mycothiol-Mediated Compounds from "*Streptomyces rosa* subsp. *notoensis*" OS-3966. *J. Biosci. Bioeng.* 127 (5), 549–553. doi:10.1016/j.jbiosc.2018.10.013

Miyata, S., Ohhata, N., Murai, H., Masui, Y., Ezaki, M., Takase, S., et al. (1992). WS009 A and B, New Endothelin Receptor Antagonists Isolated from *Streptomyces* sp. No. 89009. I. Taxonomy, Fermentation, Isolation, Physico-Chemical Properties and Biological Activities. *J. Antibiot.* 45 (7), 1029–1040. doi:10.7164/antibiotics.45.1029

Nakanishi, J., Sugiyama, K., Matsuo, H., Takahashi, Y., Omura, S., and Nakashima, T. (2019). An Application of Photoactivatable Substrate for the Evaluation of Epithelial-Mesenchymal Transition Inhibitors. *Anal. Sci.* 35 (1), 65–69. doi:10.2116/analsci.18SDP07

Nakashima, T., Kimura, T., Miyano, R., Matsuo, H., Hirose, T., Kimishima, A., et al. (2017). Nanaomycin H: a New Nanaomycin Analog. *J. Biosci. Bioeng.* 123 (6), 765–770. doi:10.1016/j.jbiosc.2017.01.011

Newton, G. L., Arnold, K., Price, M. S., Sherrill, C., Delcardayre, S. B., Aharonowitz, Y., et al. (1996). Distribution of Thiols in Microorganisms: Mycothiol Is a Major Thiol in Most Actinomycetes. *J. Bacteriol.* 178 (7), 1990–1995. doi:10.1128/jb.178.7.1990-1995.1996

Newton, G. L., Koledin, T., Gorovitz, B., Rawat, M., Fahey, R. C., and Av-Gay, Y. (2003). The Glycosyltransferase Gene Encoding the Enzyme Catalyzing the First Step of Mycothiol Biosynthesis (*mshA*). *J. Bacteriol.* 185 (11), 3476–3479. doi:10.1128/jb.185.11.3476-3479.2003

Newton, G. L., Leung, S. S., Wakabayashi, J. I., Rawat, M., and Fahey, R. C. (2011). The DinB Superfamily Includes Novel Mycothiol, Bacillithiol, and Glutathione S-Transferases. *Biochemistry* 50 (49), 10751–10760. doi:10.1021/bi201460j

Ogilvie, A., Wiebauer, K., and Kersten, W. (1975a). Inhibition of Leucyl-Transfer Ribonucleic Acid Synthetase in *Bacillus subtilis* by Granaticin. *Biochem. J.* 152 (3), 511–515. doi:10.1042/bj1520511

Ogilvie, A., Wiebauer, K., and Kersten, W. (1975b). Stringent Control of Ribonucleic Acid Synthesis in *Bacillus subtilis* Treated with Granaticin. *Biochem. J.* 152 (3), 517–522. doi:10.1042/bj1520517

Ohta, K., Kasahara, F., Ishimaru, T., Wada, Y., Kanamaru, T., and Okazaki, H. (1987). Structures of Fibrostatins, New Inhibitors of Prolyl Hydroxylase. *J. Antibiot.* 40 (9), 1239–1248. doi:10.7164/antibiotics.40.1239

Omura, S., Takahashi, Y., Nakashima, T., Matsumoto, A., Nakanishi, J., and Matsuo, H. (2018). *Epithelial-mesenchymal Transition Induced Cell Inhibitor*. PCT Patent No WO2018056470A1 (Geneva: World Intellectual Property Organization).

Pan, G., Xu, Z., Guo, Z., HindraMa, M., Ma, M., Yang, D., et al. (2017). Discovery of the Leinamycin Family of Natural Products by Mining Actinobacterial Genomes. *Proc. Natl. Acad. Sci. USA* 114 (52), E11131–E11140. doi:10.1073/pnas.1716245115

Park, J. H., Cha, C. J., and Roe, J. H. (2006). Identification of Genes for Mycothiol Biosynthesis in *Streptomyces coelicolor* A3(2). *J. Microbiol.* 44 (1), 121–125.

Pomposiello, P. J., and Demple, B. (2001). Redox-Operated Genetic Switches: the SoxR and OxyR Transcription Factors. *Trends Biotechnol.* 19 (3), 109–114. doi:10.1016/S0167-7799(00)01542-0

Ratcliffe, A. J. (2006). Inosine 5′-monophosphate Dehydrogenase Inhibitors for the Treatment of Autoimmune Diseases. *Curr. Opin. Drug Discov. Devel* 9 (5), 595–605.

Ren, X., Zheng, Z. H., Lu, X. H., Zhang, X. L., Zhu, J. T., Fan, Y. L., et al. (2008). "Studies on N01WB-352A, B, the IMPDH Inhibitors," in Proceedings of Annual Conference of Chinese Pharmaceutical Association and the Eighth Chinese Pharmacist's Week, Shijiazhuang, China, 539–544.

Rohr, J., and Zeeck, A. (1987). Metabolic Products of Microorganisms. 240 Urdamycins, New Angucycline Antibiotics from *Streptomyces fradiae*. II Structural Studies of Urdamycins B to F. *J. Antibiot.* 40 (4), 459–467. doi:10.7164/antibiotics.40.459

Sasaki, E., Ogasawara, Y., and Liu, H.-w. (2010). A Biosynthetic Pathway for BE-7585A, a 2-Thiosugar-Containing Angucycline-Type Natural Product. *J. Am. Chem. Soc.* 132 (21), 7405–7417. doi:10.1021/ja1014037

Swords, R., Mahalingam, D., O'Dwyer, M., Santocanale, C., Kelly, K., Carew, J., et al. (2010). Cdc7 Kinase - A New Target for Drug Development. *Eur. J. Cancer* 46 (1), 33–40. doi:10.1016/j.ejca.2009.09.020

Taguchi, T., Maruyama, T., Sawa, R., Igarashi, M., Okamoto, S., and Ichinose, K. (2015). Structure and Biosynthetic Implication of 5*R*-(N-Acetyl-L-Cysteinyl)-14*S*-Hydroxy-Dihydrokalafungin from a Mutant of the *actVA-ORF4* Gene for Actinorhodin Biosynthesis in *Streptomyces coelicolor* A3(2). *J. Antibiot.* 68 (7), 481–483. doi:10.1038/ja.2015.13

Taguchi, T., Yabe, M., Odaki, H., Shinozaki, M., Metsä-Ketelä, M., Arai, T., et al. (2013). Biosynthetic Conclusions from the Functional Dissection of Oxygenases for Biosynthesis of Actinorhodin and Related *Streptomyces* Antibiotics. *Chem. Biol.* 20 (4), 510–520. doi:10.1016/j.chembiol.2013.03.007

Vichai, V., and Kirtikara, K. (2006). Sulforhodamine B Colorimetric Assay for Cytotoxicity Screening. *Nat. Protoc.* 1 (3), 1112–1116. doi:10.1038/nprot.2006.179

Vilchèze, C., Av-Gay, Y., Attarian, R., Liu, Z., Hazbón, M. H., Colangeli, R., et al. (2008). Mycothiol Biosynthesis Is Essential for Ethionamide Susceptibility in *Mycobacterium tuberculosis*. *Mol. Microbiol.* 69 (5), 1316–1329. doi:10.1111/j.1365-2958.2008.06365.x

Wang, X., Shaaban, K. A., Elshahawi, S. I., Ponomareva, L. V., Sunkara, M., Zhang, Y., et al. (2013). Frenolicins C-G, Pyranonaphthoquinones from *Streptomyces* sp. RM-4-15. *J. Nat. Prod.* 76 (8), 1441–1447. doi:10.1021/np400231r

Wiegand, I., Hilpert, K., and Hancock, R. E. W. (2008). Agar and Broth Dilution Methods to Determine the Minimal Inhibitory Concentration (MIC) of Antimicrobial Substances. *Nat. Protoc.* 3 (2), 163–175. doi:10.1038/nprot.2007.521

Woo, C. M., Gholap, S. L., and Herzon, S. B. (2013). Insights into Lomaiviticin Biosynthesis. Isolation and Structure Elucidation of (−)-Homoseongomycin. *J. Nat. Prod.* 76 (7), 1238–1241. doi:10.1021/np400355h

Xie, Z., Zhou, L., Guo, L., Yang, X., Qu, G., Wu, C., et al. (2016). Grisemycin, a Bridged Angucyclinone with a Methylsulfinyl Moiety from a Marine-Derived *Streptomyces* sp. *Org. Lett.* 18 (6), 1402–1405. doi:10.1021/acs.orglett.6b00332

Zhao, Q., Wang, M., Xu, D., Zhang, Q., and Liu, W. (2015). Metabolic Coupling of Two Small-Molecule Thiols Programs the Biosynthesis of Lincomycin A. *Nature* 518 (7537), 115–119. doi:10.1038/nature14137

Zhu, H.-h., Guo, J., Yao, Q., Yang, S.-z., Deng, M.-r., Phuong, L. T. B., et al. (2007). *Streptomyces vietnamensis* sp. nov., a Streptomycete with Violet-Blue Diffusible Pigment Isolated from Soil in Vietnam. *Int. J. Syst. Evol. Microbiol.* 57 (8), 1770–1774. doi:10.1099/ijs.0.64774-0

Conflict of Interest: The authors declare that the research was conducted in the absence of any commercial or financial relationships that could be construed as a potential conflict of interest.

frontiers in Chemistry

ORIGINAL RESEARCH
published: 14 February 2022
doi: 10.3389/fchem.2022.826615

Antioxidant Aryl-Substituted Phthalan Derivatives Produced by Endophytic Fungus *Cytospora rhizophorae*

Hongxin Liu[1], Zhaoming Liu[1], Yanjiang Zhang[2], Yuchan Chen[1], Huan Wang[2,3], Haibo Tan[2,3] and Weimin Zhang[1]**

[1]State Key Laboratory of Applied Microbiology Southern China, Guangdong Provincial Key Laboratory of Microbial Culture Collection and Application, Guangdong Open Laboratory of Applied Microbiology, Institute of Microbiology, Guangdong Academy of Sciences, Guangzhou, China, [2]National Engineering Research Center of Navel Orange, Gannan Normal University, Ganzhou, China, [3]Key Laboratory of South China Agricultural Plant Molecular Analysis and Genetic Improvement, Guangdong Provincial Key Laboratory of Applied Botany, South China Botanical Garden, Chinese Academy of Sciences, Guangzhou, China

Six new phthalan derivatives cytorhizophins D-I (1-6) as well as three known derivatives cytorhizophin C, pestacin and rhizophol B were isolated from *Cytospora rhizophorae.* Among them, cytorhizophins D-E (1-2) and F-G (3-4) were two pairs of diastereoisomers, all of them featuring a 1-phenyl-1,3-dihydroisobenzofuran scaffold with a highly oxygenated *O*-linked isopentenyl unit. Besides, cytorhizophins H-I (5-6) represent the first examples of phthalide family with fascinating 6/6/6/5 tetracyclic ring system fusing as unprecedented furo [4,3,2-*kl*]xanthen-2 (10b*H*)-one skeleton. The structures of the new phthalan derivatives were extensively confirmed by detail spectroscopic analysis. The partial absolute configurations of compounds 1-6 were established through electronic circular dichroism (ECD) calculations. Moreover, compounds 1-4 showed remarkable antioxidant activities with EC_{50} values ranging from 5.86 to 26.80 μM, which were better than or comparable to that of ascorbic acid (positive control).

Keywords: *Cytospora rhizophorae*, endophytic fungus, antioxidtant activity, *Gynochthodes officinalis*, cytorhizophin

OPEN ACCESS

Edited by:
Yuanyuan Lu,
China Pharmaceutical University, China

Reviewed by:
Xishan Huang,
Guangxi Normal University, China
Chunmao Yuan,
Key Laboratory of Chemistry for Natural Products of Guizhou Province (CAS), China

****Correspondence:***
Haibo Tan
tanhaibo@scbg.ac.cn
Weimin Zhang
wmzhang@gdim.cn

Specialty section:
This article was submitted to Organic Chemistry, a section of the journal Frontiers in Chemistry

Received: *01 December 2021*
Accepted: *24 January 2022*
Published: *14 February 2022*

Citation:
Liu H, Liu Z, Zhang Y, Chen Y, Wang H, Tan H and Zhang W (2022) Antioxidant Aryl-Substituted Phthalan Derivatives Produced by Endophytic Fungus Cytospora rhizophorae. Front. Chem. 10:826615. doi: 10.3389/fchem.2022.826615

INTRODUCTION

The free radicals and reactive oxygen species (ROS) were highly reactive intermediates widely existing in human body, which can react with human biomolecules including lipids, proteins, DNA, etc, thus causing seriously detrimental health effects, such as neurodegenerative diseases, atherosclerosis, liver cirrhosis, cataracts, diabetes, and cancer (Kang et al., 2007; López-Alarcónand Denicola, 2013). With the aim to clear up the oxidative stress resulting by excess amounts of ROS, numerous remarkable results have been reported in the past decades (Cerutti, 1985; Halliwell, 1987; Breimer, 1990; Ding et al., 1999; Grisham et al., 2000; Aitken et al., 2012; Russell and Cotter, 2015; El-Hawary et al., 2019; Kusio et al., 2020). Among them, antioxidant was respected as one of the most efficient therapeutic strategies against human diseases related to oxidative damage by ROS (Beckman et al., 1992; Taniguchi et al., 1993).

In the repertoire of pharmaceutical antioxidant discovery and achievements, natural products exampled by astaxanthin, vitamins, as well as carotenoids have played extremely significant roles (Quiñones, et al., 2012). Additionally, many attentions have been continuously paid to the discovery of natural antioxidants. Consequently, more and more nature-originated antioxidants were emerged and widely used in functional foods, pharmaceutical drugs, and industrial cosmetics (Mussard et al., 2019; Wen et al., 2017). Polyphenols represent a characteristic family of natural-based organic

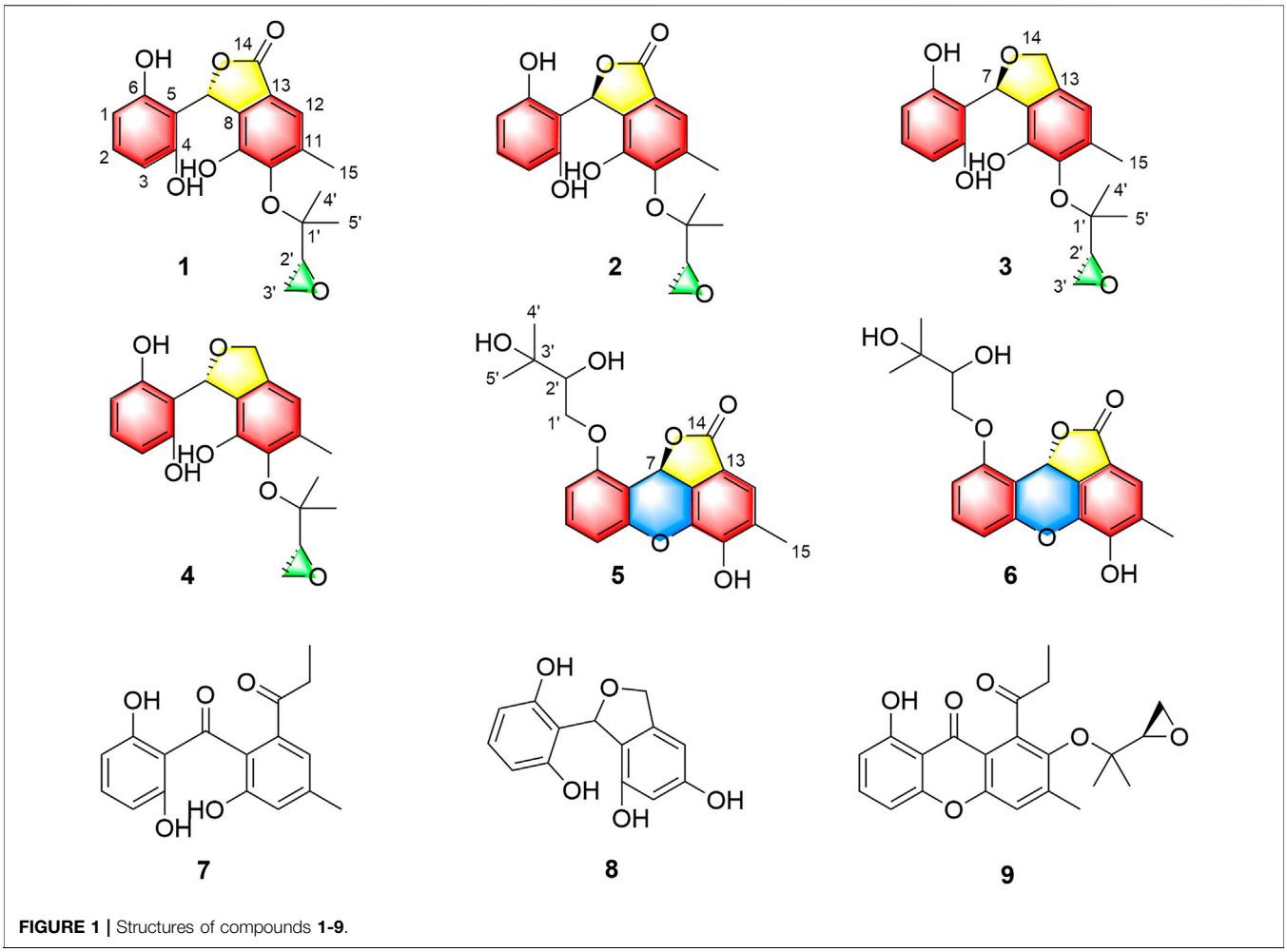

FIGURE 1 | Structures of compounds **1-9**.

compounds with strong antioxidant activities (Dao et al., 2020; Bodoira and Maestri, 2020). Phthalans featured by a core isobenzofuran skeleton were a typical class of phenols, which have dramatically attracted many medicinal scientists attributable to their affluent structure diversities, novel architecture complexities, and significant pharmaceutical activities in recent years (Naito and Kaneko, 1969; Strobel et al., 2002; Harper et al., 2003; Kapoor et al., 2003; Fotso et al., 2008). Especially, the 1-phenyl-phthalan moiety is frequently encountered in numerous natural products and commercially available drugs or drug lead compounds. Their fascinating biological activities and novel structural features rendered them appealing targets for the natural product and pharmaceutical communities.

As a part of our continuing program to discover structurally unique natural products with significantly biological potentials from the endophytic fungi (Liu et al., 2017; Liu et al., 2019a; Liu H.-X. et al., 2019; Chen et al., 2019), an endophytic fungus, *Cytospora rhizophorae* A761, was obtained from the stem of *Gynochthodes officinalis* (F.C.How) Razafim. and B. Bremer (basionym: *Morinda officinalis*). The chemical investigation on the liquid culture of *C. rhizophorae* has resulted in the successful purification of six novel polyphenolic natural products cytorhizophins D-I (**1**-**6**) as well as three known derivatives cytorhizophin C (**7**) (Liu et al., 2019c), pestacin (**8**) (Harper et al., 2003) and rhizophol B (**9**) (Liu et al., 2019c) (**Figure 1**). Cytorhizophins D-E (**1**-**2**) and F-G (**3**-**4**) were two pairs of diastereoisomers, all of them featured a 1-phenyl-1,3-dihydroisobenzofuran scaffold with a highly oxygenated isopentenyl unit. Cytorhizophins H-I (**5**-**6**) represent the first examples of phthalide family with a fascinating 6/6/6/5 tetracyclic ring system fusing as unprecedented furo [4,3,2-*kl*]xanthen-2 (10b*H*)-one skeleton. Herein, the details of the extraction, purification, structure elucidation, and antioxidant activity of cytorhizophins D-I were described.

MATERIALS AND METHODS

General Experimental Procedures

The general experimental procedures were described in supporting information.

Fungal Material

The information of fungal material used in this study were identical to that of the previous descriptions (Liu et al., 2019a).

TABLE 1 | ^{1}H (600 MHz) and ^{13}C (150 MHz) NMR data of **1** and **2** in CD_3COCD_3.

No	1		2	
	δ_H	δ_C	δ_H	δ_C
1	6.38, d, 8.1	106.9, CH[a]	6.38, d, 8.1	106.8, CH[a]
2	6.98, t, 8.1	130.4, C	6.99, t, 8.1	130.4, C
3	6.38, d, 8.1	106.9, CH[a]	6.38, d, 8.1	106.8, CH[a]
4		157.9, C		157.9, C
5		108.4, C		108.3, C
6		157.9 C		157.9, C
7	7.12, s	75.7, CH	7.16, s	75.7, CH
8		111.9, C		112.0, C
9		152.0, C		151.9, C
10		141.2, C		141.0, C
11		142.7, C		142.7, C
12	6.74, s	117.4, CH	6.74, s	117.3, CH
13		145.1, C		145.3, C
14		171.7, C		171.1, C
15	2.31, s	17.9, CH_3	2.28, s	17.9, CH_3
1′		82.2, C		81.6, C
2′	3.13, dd, 4.2, 2.7	56.8, CH	3.17, dd, 4.2, 2.7	56.5, CH
3a′	2.69, m	43.9, CH_2	2.61, m	43.9, CH_2
3b′	2.55, dd, 4.2, 2.7		2.51, dd, 4.2, 2.7	
4′	1.20, s	23.7, CH_3	1.22, s	22.1, CH_3
5	1.14, s	21.0, CH_3	1.17, s	21.9, CH_3

[a]*Detected by HMBC.*

Extraction and Isolation

The strain *Cytospora rhizophorae* A761 was kept for 7 days at 28°C and 120 r/m on a rotary shaker in 150 flasks (1,000 ml) containing 500 ml of potato dextrose broth (potato 20%, glucose 2%, K_2HPO_4 0.3%, $MgSO_4$•$7H_2O$ 0.15%, vitamin B 10 mg/L). The fermented broth (75 L) was filtered through cheesecloth to give the broth and mycelia. The fermented broth were subjected to macroporous resin D101 column with ethanol as eluent. The EtOH fraction was concentrated under a vacuum to yield a dark brown gum (37 g). The crude extract was subjected to reversed-phase silica gel C_{18} using step gradient elution with MeOH/H_2O, 60%→100% to afford six fractions (Fr.): Fr.1-Fr.6.

Then, Fr. 2 (8.92 g) was separated by silica gel flash CC (*n*-hexane/EtOAc, 20:1→1:1, v/v) to give nine subfractions (Fr.2-1 to Fr.2-9). Fr.2-5 (166.2 mg) was subjected to CC on Sephadex LH-20 (CH_2Cl_2/MeOH, 1:1, v/v) to give four sub-fractions (Fr. 2-5-1 to Fr. 2-5-4). Fr. 2-5-4 was further purified by silica gel flash column chromatography (*n*-hexane/EtOAc, 10:1→1:1, v/v) to give **8** (9.0 mg). Fr.2-7 (3.07 g) was subjected to CC on Sephadex LH-20 (CH_2Cl_2/MeOH, 1:1, v/v) to give ten sub-fractions (Fr. 2-7-1 to Fr. 2-7-10). Fr. 2-7-5 was purified by silica gel flash column chromatography and further purified by semipreparative HPLC (MeOH/H_2O, 60:40, v/v, 3 ml/min) to give **9** (5.0 mg). Fr. 2-7-6 was divided into five sub-fractions (Fr.2-7-6-1 to Fr. 2-7-6-5) by silica gel flash column chromatography (*n*-hexane/EtOAc, 10:1→1:1, v/v). Fr. 2-7-6-5 was further separated by semipreparative HPLC (MeOH/H_2O, 73:27, v/v, 3 ml/min) to give four sub-fractions (Fr. 2-7-6-5-1 to Fr. 2-7-6-5-4). Fr. 2-7-6-5-2 (10 mg, t_R = 8.3 min) was purified by semipreparative HPLC equipped with a Chiralpak IC column (*n*-hexane 95%/isopropyl alcohol, 7:3, 3 ml/min) to obtain **3** (5.0 mg, t_R = 8.6 min) and **4** (2.5 mg, t_R = 9.0 min).

Fr. Three was further purified by CC over reversed-phase silica gel C_{18} (MeOH/H_2O, 20%→100%) to give five subfractions (Fr.3-1 to Fr.3-5). Fr.3-2 (2.0 g) was divided into seven sub-fractions (Fr. 3-2-1 to Fr. 3-2-7) by Sephadex LH-20 (CH_2Cl_2/MeOH, 1:1, v/v). Fr. 3-2-1 was further purified by repeated silica gel and semi-preparative HPLC (ACN/H_2O, 50:50, v/v, 3 ml/min) to obtain compound **7** (2.0 mg, t_R = 12.0 min). Fr. 3-2-2 was subjected by silica gel CC (*n*-hexane/EtOAc, 5:1→1:2, v/v) to yield four sub-fractions (Fr.3-2-2-1 to Fr. 3-2-2-4). Fr. 3-2-2-1 was purified by semipreparative HPLC (MeOH/H_2O, 60:40, v/v, 3 ml/min) to give a mixture (10 mg, t_R = 8.9 min). The mixture was further separated by HPLC (Chiralpak IC column, *n*-hexane 95%/isopropyl alcohol, 4:1, 3 ml/min) to obtain **2** (4.0 mg, t_R = 20.8 min) and **1** (4.0 mg, t_R = 25.1 min).

Fr.3-4 (1.3 g) was separated by silica gel flash CC (*n*-hexane/EtOAc, 5:1→1:5, v/v) to yield twelve sub-fractions (Fr.3-3-1 to Fr. 3-3-12). Compound **5** (3.0 mg, t_R = 14.0 min) was obtained from Fr. 3-3-10 by semipreparative HPLC (MeOH/H_2O, 60:40, v/v, 3 ml/min). Fr.3-4 (2.8 g) was separated by Sephadex LH-20 (CH_2Cl_2/MeOH, 1:1, v/v) to give seven sub-fractions (Fr. 3-4-1 to Fr. 3-4-7). Fr. 3-4-4 was divided into four sub-fractions (Fr.3-4-4-1 to Fr. 3-4-4-4) by silica gel flash CC (*n*-hexane/EtOAc, 2:1→1:2, v/v). Fr. 3-4-4-2 was purified by HPLC (ACN/H_2O, 55:45, v/v, 2 ml/min) to yield compound **6** (4.0 mg, t_R = 18.7 min).

Cytorhizophin D (**1**): yellow powder $[\alpha]_D^{25}$ = +34.0 (*c* 0.12, MeOH); CD (MeOH, 0.4 mg/ml): 206 (−5.3), 214 (+40.5), 230 (+8.6), 247 (−18.2), 260 (+1.9), 288 (−2.3), 306 (−1.7) nm; UV (MeOH) λ_{max} (log ε) 213 (5.35), 311 (4.23) nm; IR ν_{max} 3,230, 2,927, 1716, 1,616, 1,472, 1,015, 887, 794 cm^{-1}. For ^{1}H and ^{13}C NMR, see **Table 1**; HRESIMS: *m/z* 373.1285 $[M + H]^+$ (calcd for $C_{20}H_{21}O_7$, 373.1282).

TABLE 2 | ^{1}H (600 MHz) and ^{13}C (150 MHz) NMR data of **3** and **4** in CD_3COCD_3.

No	3		4	
	δ_H	δ_C	δ_H	δ_C
1	6.40, d, 8.1	108.0, CH	6.40, d, 8.1	108.0, CH
2	6.96, t. 8.1	129.0, CH	6.96, t. 8.1	129.0, CH
3	6.40, d, 8.1	108.0, CH	6.40, d, 8.1	108.0, CH
4		156.0, C		156.0, C
5		112.2, C		112.2, C
6		156.0, C		156.0, C
7	6.78, br s	79.3 CH	6.79, br s	79.3 CH
8		125.0, C		125.0, C
9		147.5, C		147.5, C
10		140.6, C		140.6, C
11		133.9, C		133.9, C
12	6.51, s	117.4, CH	6.51, s	117.4, CH
13		135.4, C		135.4, C
14	5.52, dd, 12.2, 2.4	72.3, CH_2	5.49, dd, 12.2, 2.3	72.3, CH_2
14	5.10, dd, 12.2, 2.4		5.15, dd, 12.2, 2.3	
15	2.21, s	16.8, CH_3	2.21, s	16.7, CH_3
1′		80.3, C		80.3, C
2′	3.16, dd, 4.5, 2.7	57.2, CH	3.17, dd, 4.5, 2.7	57.3, CH
3a′	2.75, t, 4.5	44.0, CH_2	2.76, t, 4.5	44.0, CH_2
3b′	2.70, dd, 4.5, 2.7		2.69, dd, 4.5, 2.7	
4′	1.27, s	23.3, CH_3	1.27, s	23.2, CH_3
5′	1.19, s	21.7, CH_3	1.18, s	21.6, CH_3

TABLE 3 | ^{1}H (600 MHz) and ^{13}C (150 MHz) NMR data of **5** and **6** in CD_3COCD_3.

No	5		6	
	δ_H	δ_C	δ_H	δ_C
1	6.76, d, 8.1	106.3, CH	6.62, d, 8.1	111.8, CH
2	7.07, t, 8.1	129.4, C	7.10, t, 8.1	130.1, C
3	6.38, d, 8.1	106.3, CH	6.47, d, 8.1	115.3, CH
4		156.5, C		156.5, C
5		113.1, C		111.6, C
6		158.3, C		160.5, C
7	7.28, s	76.0, CH	7.04, s	75.6, CH
8		141.0, C		141.5, C
9		144.8, C		143.5, C
10		151.2, C		151.3, C
11		142.5, C		142.6, C
12	6.71, s	118.2, CH	6.75, s	118.0, CH
13		111.0, C		111.5, C
14		171.3, C		171.3, C
15	2.24, s	19.0, CH_3	2.27, s	18.0, CH_3
1′a	4.70, dd, 12.4, 4.3	70.0, CH_2	4.52, d, 11.8	79.9, CH_2
1′b	4.26, dd, 12.4, 8.9		4.33, dd, 11.8, 5.0	
2′	3.89, dd, 8.8, 4.3	72.9, CH	4.16, t, 5.0	79.1, CH
3′		86.0, C		84.3, C
4′	1.44, s	28.3, CH_3	1.35, s	21.5, CH_3
5′	1.38, s	18.5, CH_3	1.25, s	22.5, CH_3

Cytorhizophin E (**2**): yellow powder $[\alpha]_D^{25}$ = −22.3 (*c* 0.02, MeOH); CD (MeOH, 0.3 mg/ml): 206 (+3.8), 214 (−33.5), 231 (−5.3), 247 (+12.9), 262 (−2.3), 288 (+0.9), 308 (+0.6) nm; UV (MeOH) λ_{max} (log ε) 213 (5.33), 310 (4.26) nm; IR ν_{max} 3,236, 2,926, 1715, 1,614, 1,470, 1,427, 1,268, 1,233, 1,198, 1,162, 1,017, 977, 903, 885, 795, 752, 739 cm^{-1}. For ^{1}H and ^{13}C NMR, see **Table 1**; HRESIMS: *m/z* 373.1281 $[M + H]^+$ (calcd for $C_{20}H_{21}O_7$; 373.1282).

Cytorhizophin F (**3**): yellow powder $[\alpha]_D^{25}$ = +127 (*c* 0.02, MeOH); CD (MeOH, 0.15 mg/ml): 207 (+108.0), 238 (−2.4), 286 (−5.2) nm; UV (MeOH) λ_{max} (log ε) 284 (4.15) nm; IR ν_{max} 3,415, 2,953, 1,616, 1,597, 1,472, 1,285, 1,225, 1,140, 1,225, 1,015, 926, 887, 864, 826, 795, 753, 738 cm^{-1}. For ^{1}H and ^{13}C NMR, see **Table 2**; HRESIMS: *m/z* 359.1497 $[M + H]^+$ (calcd for $C_{20}H_{23}O_6$, 359.1489).

Cytorhizophin G (**4**): yellow powder $[\alpha]_D^{25}$ = −76 (*c* 0.08, MeOH); CD (MeOH, 0.10 mg/ml): 207 (−75.3), 238 (+2.7), 287 (+4.7) nm; UV (MeOH) λ_{max} (log ε) 282 (4.07) nm; IR ν_{max} 3,290, 1,616, 1,474, 1,472, 1,225, 1,015, 887, 795 cm^{-1}. For ^{1}H and ^{13}C NMR, see **Table 2**; HRESIMS: *m/z* 359.1493 $[M + H]^+$ (calcd for $C_{20}H_{23}O_6$, 359.1489).

Cytorhizophin H (**5**): pale yellow powder $[\alpha]_D^{25}$ = −117.5 (*c* 0.06, MeOH); CD (MeOH, 0.2 mg/ml): 202 (+42.2), 214 (−33.5), 235 (−4.2), 243 (−8.7) nm; UV (MeOH) λ_{max} (log ε) 311 (4.01), 282 (3.90) nm; IR ν_{max} 3,303, 2,828, 1715, 1,462, 1,423, 1,281, 1,236, 1,192, 1,144, 1,045, 1,011, 902, 786 cm^{-1}. For ^{1}H and ^{13}C NMR, see **Table 3**; HRESIMS: *m/z* 373.1285 $[M + H]^+$ (calcd for $C_{20}H_{21}O_7$, 373.1282).

Cytorhizophin I (**6**): pale yellow powder $[\alpha]_D^{25}$ = −39.3 (*c* 0.02, MeOH); CD (MeOH, 0.2 mg/ml): 200 (−38.5), 214 (−30.2), 237 (−3.3), 243 (+7.4) nm; UV (MeOH) λ_{max} (log ε) 310 (3.87), 284 (3.84) nm; IR ν_{max} 3,302, 1,472, 1,238, 1,016, 903, 677, 600, 592, 556 cm^{-1}. For ^{1}H and ^{13}C NMR, see **Table 3**; HRESIMS: *m/z* 373.1284 $[M + H]^+$ (calcd for $C_{20}H_{21}O_7$, 373.1282).

DPPH Photometric Assay

The DPPH photometric assay were carried out according to our previously established method (Zhong et al., 2020).

RESULTS AND DISCUSSION

Cytorhizophin D (**1**) was purified as a yellow powder, and the molecular formula of **1** had been established as $C_{20}H_{20}O_7$ by HRESIMS with an obvious ion peak discovered at *m/z* 373.1285 ($[M + H]^+$, calcd for $C_{20}H_{21}O_7$, 373.1282). The IR spectrum of **1** displayed prominent resonance bands at 3,230 and 1,716 cm^{-1}, clarifying the existence of hydroxy and carbonyl functionality. The ^{1}H NMR spectrum of **1** exhibited four downshifted protons at δ_H 6.74 (1H, s, H-12), δ_H 6.98 (1H, t, *J* = 8.2 Hz, H-2), 6.38 (1H, d, *J* = 8.2 Hz, H-1), and 6.38 (1H, d, *J* = 8.2 Hz, H-3), which were responsive for two independent benzenoid rings. Moreover, the signals for three methyl groups [δ_H 1.14 (3H, s), 1.20 (3H, s), 2.31 (3H, s)] signals were also observed in its ^{1}H NMR spectrum. Additionally, the ^{13}C NMR data (**Table 1**) coupling with HSQC data of **1** further identified 20 carbon signals, which could be readily differentiated to three methyls, two methylenes, six methines, as well as nine quaternary carbons with a carbonyl moiety (δ_C 171.7).

Two spin systems of C-1/C-2/C-3 and C-2′/C-3′ were successfully assigned by carefully analysis of the ^{1}H-^{1}H COSY spectrum of **1** (**Figure 2**). As referring to the fragment C-1/C-2/C-3, the critical HMBC correlative signals from H-1 to C-3 and C-5, H-2 to C-4 and C-6 in conjunction with consideration of the overlapping NMR data of C-1/C-3 as well as C-2/C-4 confirmed the presence of a symmetric aromatic ring. Moreover, the conclusive HMBC correlative signals from H_3-15 to C-10, C-11, and C-12 as well as H-12 to C-8, C-10 and C-14 revealed the existence of the ring B. The linkage of rings A and B *via* C-7 methine was successfully verified by the unambiguous HMBC correlations from H-7 to C-4, C-6, C-9, and C-13. The five-membered lactone ring C was then established with the aid of the conclusive HMBC correlations from the critical proton H-7 to C-13 and C-14. Moreover, the key HMBC correlations from H-7 to

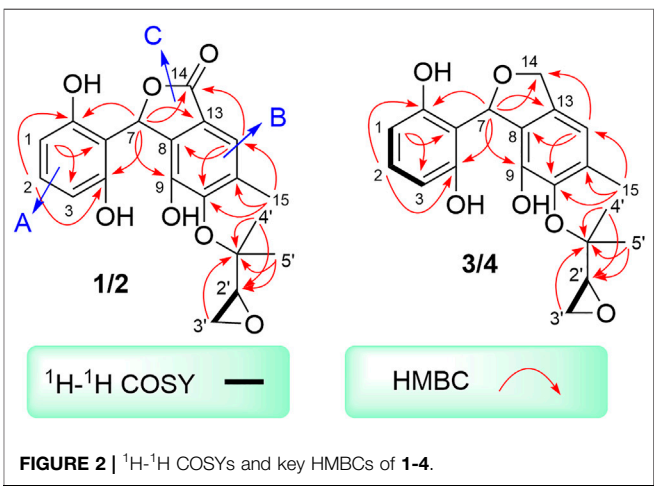

FIGURE 2 | ^{1}H-^{1}H COSYs and key HMBCs of **1-4**.

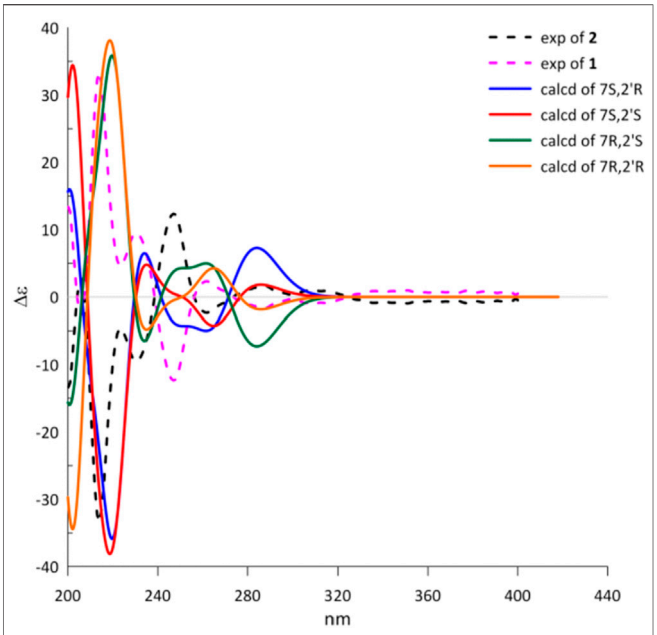

FIGURE 3 | Experimental and calculated ECD spectra of **1** and **2**.

C-9, and H-12 to C-14 concluded that the lactone ring C was fused with the benzene ring B to construct the key phthalide core.

Furthermore, with the aid of the spin fragment C-2′/C-3′, a highly oxygenated isopentyl unit was strongly suggested to connect with the phthalide core through an ether bond in **1**, answering for the informative HMBC correlations from the methyl protons H_3-4′ to C-1′, C-2′ together with H_3-5′ to C-1′, C-2′. Moreover, there was an epoxy ring in the isopentyl unit, which could be further concluded through the high-field shift of C-2′ (δ_C 56.8) and C-3′ (δ_C 43.9) together with the molecular formula. Because the lack of direct HMBC correlations from the isopentyl unit and the ring B, the location of isopentyl moiety could be readily assigned at C-10 position by comparing the carbon resonance shifts of the C-9 (δ_C 152.0) and C-11 (δ_C 142.7) along with the definitive NOESY correlations from methyls H_3-4′ and H_3-5′ to H_3-15. Consequentially, the planar structure of **1** was finally elucidated as outlined in **Figure 1**.

Cytorhizophin E (**2**) was obtained as a yellow powder and found to possess a molecular formula of $C_{20}H_{20}O_7$ based on the HRESIMS ion peak at *m/z* 373.1281 $[M + H]^+$, indicating eleven indices of hydrogen deficiency. The IR spectrum of **2** was quite similar to that of **1**. The inspection of the NMR data (**Table 1**) of **2** with those of **1** demonstrated that **2** displayed close similarity with **1**. The obvious differences were the chemical shifts of the H-7 (δ_H 7.16 ppm for **1** versus 7.12 ppm for **2**), H-15 (δ_H 2.31 ppm for **1** versus 2.28 ppm for **2**), H-2′ (δ_H 3.13 ppm for **1** versus 3.17 ppm for **2**), H-3′ (δ_H 2.69, 2.55 ppm for **1** versus 2.61, 2.51 ppm for **2**), H_3-4′ (δ_H 1.20 ppm for **1** versus 1.22 ppm for **2**), and H_3-5′ (δ_H 1.14 ppm for **1** versus 1.17 ppm for **2**), which strongly concluded that the compounds **1** and **2** should be a pair of diastereoisomers.

To determine the absolute configuration of **1** and **2**, the experimental and TDDFT calculated circular dichroism (CD) spectra at cam-b3lyp/def2svp level were performed. The calculated ECD spectrum with 7*R* configuration showed very excellent similarities to those of the experimental CD spectrum of **1** as shown in **Figure 3**. Thus, the absolute configuration at C-7 of **1** was rationally assigned as *R*. Moreover, the calculated ECD Cotton effects of the 7*S* enantiomer were well agreement with those in the experimental ECD spectrum of **2**. Cytorhizophins D (**1**) and E (**2**) possessed a couple of distant stereogenic centers at C-7 and C-2′ positions, which made the establishment for the absolute configuration of C-2′ to be challenged. The absolute configuration of C-2′ was deducted as *R* as that of the co-isolated compound rhizophol B, which was confirmed by X-ray diffraction (Liu Z. et al., 2019). Therefore, the absolute stereochemistries for **1** and **2** were clarified as 7*R*,2′*R* and 7*S*,2′*R*.

Cytorhizophin F (**3**) was also afforded as a yellow powder. The molecular formula of **3** was confirmed as $C_{20}H_{22}O_6$ by its (+)-HRESIMS *m/z* 359.1497 $[M + H]^+$. The 1D NMR spectroscopic data of the natural product **3** showed a collection of typical resonance signals responsive for a 1,2,3-trisubstituted benzene ring and an isopentyl unit, which showed very close similarity to the structure of **1**. After a detail inspection and interpretation of 1D NMR spectra of **3**, it could readily disclose that its planar structure should be closely similar to that of **1**, and the major difference between them was the absence of carbonyl group in compound **3**. This conclusion further strengthened on the basis of the signals for the *O*-substituted methylene [δ_C 72.3, δ_H 5.10 (dd, *J* = 2.4, 12.2 Hz), 5.22 (dd, *J* = 2.4, 12.2 Hz)] in **3** instead of a carbonyl functionality in **1**. Moreover, the informative HMBC correlative signals from H-7 to C-4, C-6, C-9, C-13, and C-14 could further strengthen this deduction. Thus, the planar structure of **3** was completely elucidated as depicted in **Figure 1**.

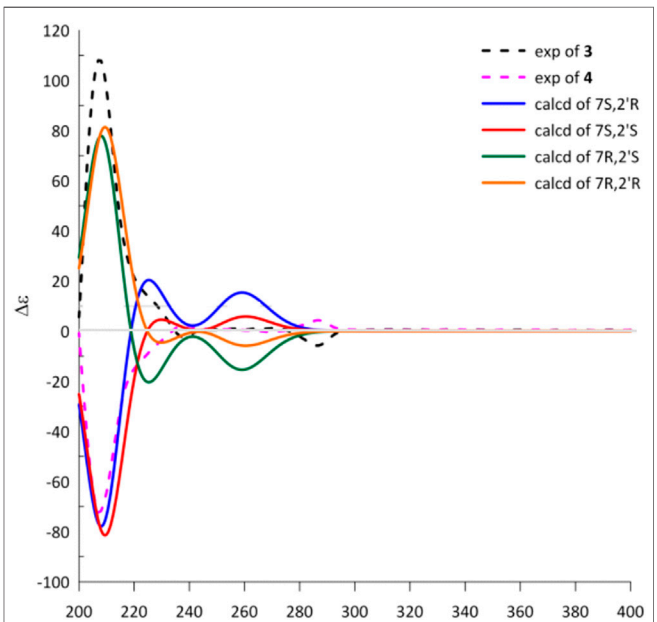

FIGURE 4 | Experimental and calculated ECD spectra of **3** and **4**.

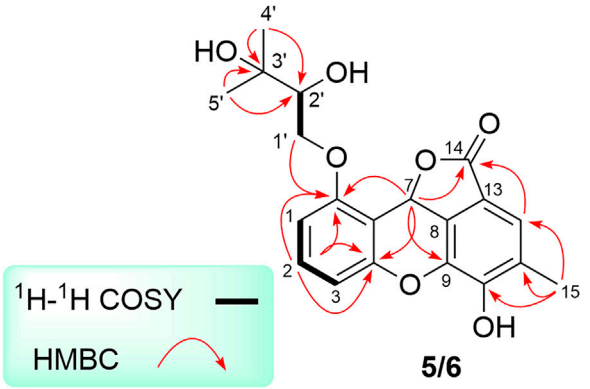

FIGURE 5 | Key ^{1}H-^{1}H COSY, and HMBC correlations of **5** and **6**.

Cytorhizophin G (**4**) was obtained to be a yellow powder and had same molecular formula with that of **3** as determined by its HREIMS ion peak at *m/z* 359.1493 $[M + H]^+$, revealing ten degrees of unsaturation. Obviously, the ^{13}C NMR spectroscopic data and HSQC spectrum of **4** collectively suggested 20 carbon signals, and all of them showed very similar chemical shifts to those of **3**. Their little differences between chemical shifts implied that they shared the same planar structure. For compound **4**, the Cotton effects in the ECD spectrum were almost direct contrary to those of **3**, suggesting that **4** should share the opposite configuration at C-7 position comparing with **3**, attributed to the slight contribution of C-2′ chiral center. The configuration of chiral center for C-7 was further confirmed by ECD calculations in **Figure 4**. The results showed that the theoretical ECD curve for 7*R* agreed with the experimental plot of **3**, 7*S* was matched with the experimental plot of **4**. Therefore, the absolute configurations of **3** and **4** were successfully established as 7*R*,2′*R*, 7*S*,2′*R*, correspondingly.

Cytorhizophin H (**5**) was isolated as a pale yellow powder and assigned an HRESIMS ion peak at *m/z* 373.1285 $[M + H]^+$ ($C_{20}H_{21}O_7$, calcd 373.1282), which perfectly agreed the molecular formula of $C_{20}H_{20}O_7$ and showed 11 degrees of hydrogen deficiency. The ^{1}H NMR spectrum of **5** exhibited four aromatic protons [δ_H 7.28 (1H, s, H-12), 7.07 (1H, t, *J* = 8.1 Hz, H-2), 6.76 (1H, d, *J* = 8.1 Hz, H-1), 6.38 (1H, d, *J* = 8.1 Hz, H-3)] as well as the characteristic proton resonance signals of three methyls [δ_H 2.24 (3H, s, H_3-15), 1.44 (3H, s, H_3-4′), 1.38 (3H, s, H_3-5′)].

Analysis of 1D as well as 2D NMR spectra including COSY, HSQC, and HMBC could readily finish the preliminary construction of the planar structure of **5** as shown in **Figure 5**. Firstly, the obvious HMBC correlations from H-1 to C-3 and C-5, H-2 to C-4 and C-6 along with the pivotal spin system C-1/C-2/C-3 successfully evidenced the presence of a 1,2,3-trisubstituted aromatic ring A. Secondly, as referring to the other spin system of C-1′/C-2′, the existence of a highly oxygenated C-5 isopentyl unit was then verified with the aid of the HMBC correlative signals from H_3-4′ to C-2′ and C-3′, H_3-5′ to C-2′ and C-3′. Moreover, the location of isopentyl functionality had been assigned to attach at C-6 position in the ring A through the C-1′-O-C-6 ether bond, attributable to the decisive HMBC cross-peak from H-1′ to C-6. Additionally, the resulting penta-substituted ring B was finally established and clarified by the HMBC correlations from H-12 to C-8, C-10 and C-14, H_3-15 to C-10, C-11, and C-12. Taking the degrees of unsaturation into account, the assignment of a benzopyran ring between C-4 and C-9 *via* a fused oxygen bridge was eventually verified. Moreover, the asymmetrical ^{1}H and ^{13}C NMR signals for the typical trisubstituted aromatic ring C further strengthened the conclusion. Therefore, the planar structure of **5** was determined and established to possess a fascinating 6/6/6/5 tetracyclic ring system fusing as unusual furo [4,3,2-*kl*]xanthen-2 (10bH)-one skeleton and showed in **Figure 1**.

Cytorhizophin I (**6**) was separated as a pale yellow powder and assigned an HRESIMS ion peak at *m/z* 373.1285 $[M + H]^+$ (calcd for $C_{20}H_{21}O_7$, 373.1282), which perfectly agreed with the molecular formula of $C_{20}H_{20}O_7$ and showed 11 degrees of hydrogen deficiency. The ^{1}H NMR spectrum of **6** exhibited four aromatic protons [δ_H 6.75 (1H, s, H-10), 7.10 (1H, t, *J* = 8.1 Hz, H-2), 6.62 (1H, d, *J* = 8.1 Hz, H-1), and 6.47 (1H, d, *J* = 8.1 Hz, H-3)], suggesting the existence of two phenyl rings. Interestingly, close comparison of the NMR data of compounds **5** and **6** as shown in **Table 3** indicated that these two compounds ought to share a significantly similar core structure. The further HMBC correlations analysis collectively pointed to that the compounds **5** and **6** were a pair of diastereoisomers.

The natural products **5** and **6** possessed two distant stereocenters C-7 and C-2′. In order to establish their absolute configurations of diastereoisomers **5** and **6**, the effort towards theoretical ECD calculation at b3lyp/6-311 + *g* (d,p) level were performed. The results revealed that the

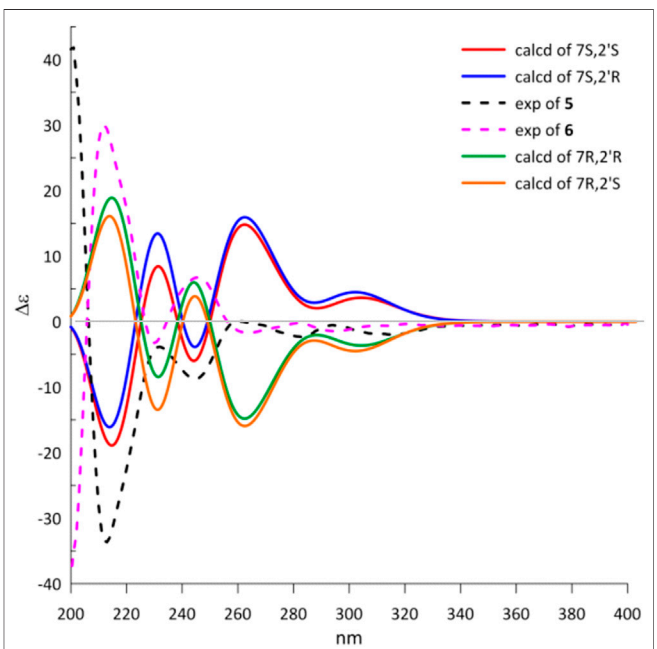

FIGURE 6 | Experimental and calculated ECD spectra of **5** and **6**.

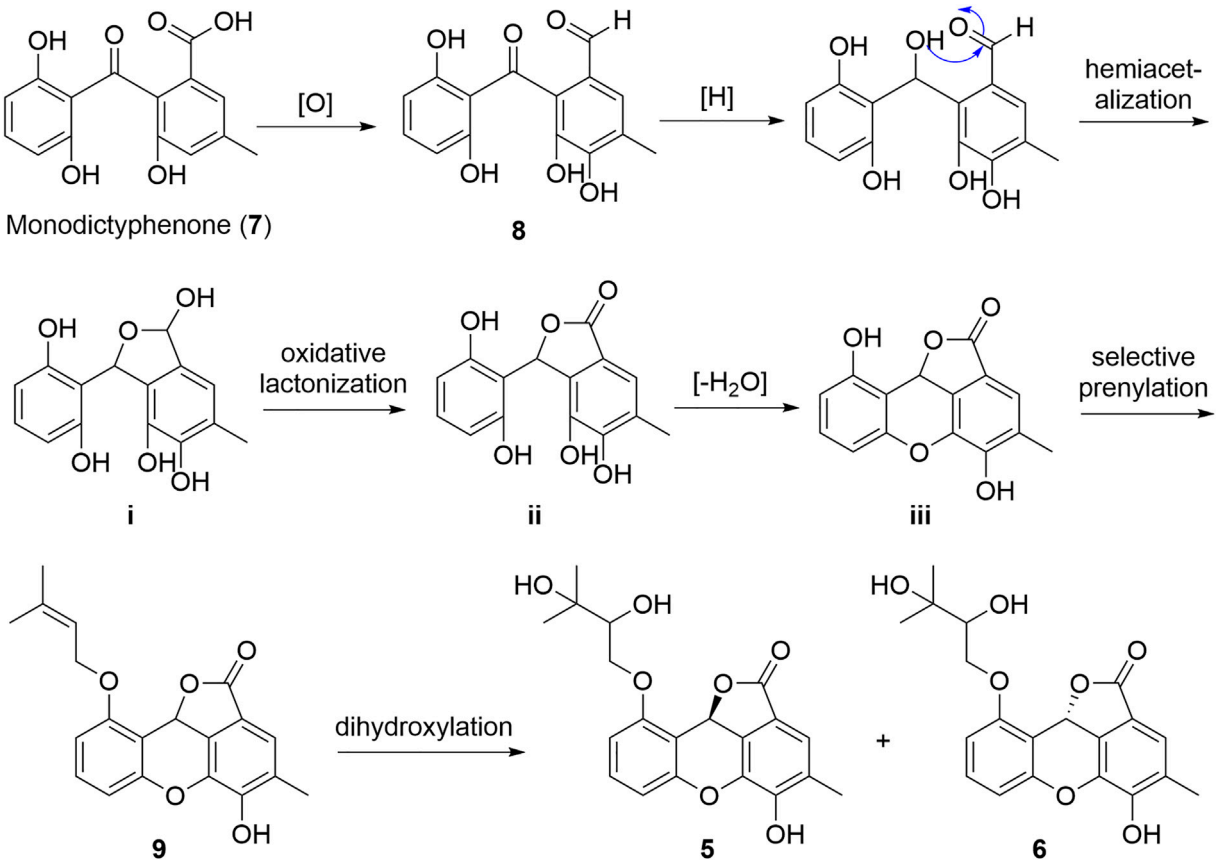

SCHEME 1 | Plausible Biosynthetic Pathways of **5** and **6**.

TABLE 4 | Antioxidant activities of compounds **1**-**6**.

Compounds	EC_{50} (μM)[a]
	DPPH radical scavenging
1	17.39 ± 0.94
2	26.80 ± 0.62
3	5.86 ± 0.71
4	7.72 ± 0.36
5	>100
6	>100
Ascorbic acid	25.53 ± 0.21

[a]*EC_{50} is defined as the concentration sufficient to obtain 50% of a maximum effect estimate in 100%, Values are expressed as the mean ± SD.*

theoretical ECD plots of 7*S* and 7*R* matched with the experimental spectra of **5** and **6**, respectively, which allowed to establish the absolute configurations of 7*S* for **5** and 7*R* for **6** (**Figure 6**). Unsatisfactorily, the absolute configuration for C-2′ was failed to be assigned by the little amount and the lack of CD contribution.

Due to the structural novelty cytorhizophins H-I (**5**-**6**) with fascinating 6/6/6/5 tetracyclic furo [4,3,2-kl]xanthen-2 (10bH)-one skeletons, their biogenetic pathways were proposed as shown in **Scheme 1**. Cytorhizophins H-I (**5**-**6**) were bio-originated from the monodictyphenone (**7**), the following selective oxidation, reduction, and hemiacetalization transformations would result the critical intermediate **i**, which underwent selective oxidative lactonization and dehydrated to generate the key precursors **ii** and **iii**, respectively. Then, the selective prenylation of **iii** further gave rise to cytorhizophins H-I (**5**-**6**).

The characteristic of polyhydroxy groups in these new compounds logically suggested that they might possess antioxidant activity. The further experimental testing confirmed that compounds **1**-**6** indeed showed significant antioxidant activity as evaluated by DPPH (2,2-diphenyl-1-picrylhydrazyl) scavenging assay and described in the Experimental part (Coteele et al., 1996; Mensor et al., 2001). Compounds **1**-**4** showed remarkable DPPH radical scavenging activities with EC_{50} values ranging from 5.86 to 26.80 μM, which are better than that of the positive control ascorbic acid (EC_{50} of 25.53 μM). Compounds **5** and **6** were found to be weak DPPH scavengers at a concentration of 100 μM (**Table 4**). From a comparison of the structures of compounds **1**-**4** with compounds **5** and **6**, it could be readily found that the opening of the middle ring might play the predominant roles in enhancing their DPPH scavenging capacity.

CONCLUSION

The chemical research on the endophytic fungus *Cytospora rhizophorae* has disclosed a new range of antioxidative ingredients, involving six novel phthalan derivatives named as cytorhizophins D-I (**1**-**6**). Among them, cytorhizophins D-E (**1**-**2**) and F-G (**3**-**4**) were two pairs of diastereoisomers, and all of them featuring a 1-phenyl-1,3-dihydroisobenzofuran scaffold with a highly oxygenated *O*-linked isopentenyl unit; whereas cytorhizophins H-I (**5**-**6**) represent the first examples of phthalide family with a fascinating 6/6/6/5 tetracyclic ring system fusing as unprecedented furo [4,3,2-*kl*]xanthen-2 (10b*H*)-one skeleton. Compounds **1**-**4** showed significant DPPH radical scavenging activities with EC_{50} values ranging from 5.86 to 26.80 μM, which are much better than that of the positive control ascorbic acid (EC_{50} of 25.53 μM). Therefore, the preliminary results revealed that cytorhizophins D-G might be served as promising lead compounds for the development of bio-available potent anti-oxidant drugs. The detailed potential mechanisms to explain the antioxidant action of these compounds is now underway and will be reported in due course.

DATA AVAILABILITY STATEMENT

The datasets presented in this study can be found in online repositories. The names of the repository/repositories and accession number(s) can be found below: https://www.ncbi.nlm.nih.gov/genbank/, KU529867.

AUTHOR CONTRIBUTIONS

HL, YZ, and HW conducted and collected the experiment data. HL performed the experiments of compound isolation. ZL carried out the ECD calculations. HL and HT finished the structure identification of the isolated compounds. YC evaluated activities of all the isolates. HL and HT interpreted the data, and wrote the paper. HL, HT, and WZ revised the manuscript. HT and WZ conceived and designed the experiments. All authors read and approved the final manuscript.

FUNDING

Financial support for this research was provided by the Guangdong Special Support Program (2019TQ05Y375), Guangdong Provincial Project for Science and Technology (No. 2021A1515011549), GDAS' Project of Science and Technology Development (2020GDASYL-20200104012), and Youth Innovation Promotion Association of CAS (2020342). We sincerely thank. Can Li of central laboratory of Southern Medical University for NMR measurements.

SUPPLEMENTARY MATERIAL

The Supplementary Material for this article can be found online at: https://www.frontiersin.org/articles/10.3389/fchem.2022.826615/full#supplementary-material

REFERENCES

Aitken, R., De Iuliis, G., Gibb, Z., and Baker, M. (2012). The Simmet Lecture: New Horizons on an Old Landscape - Oxidative Stress, DNA Damage and Apoptosis in the Male Germ Line. *Reprod. Domest. Anim.* 47, 7–14. doi:10.1111/j.1439-0531.2012.02049.x

Bodoira, R., and Maestri, D. (2020). Phenolic Compounds from Nuts: Extraction, Chemical Profiles, and Bioactivity. *J. Agric. Food Chem.* 68, 927–942. doi:10.1021/acs.jafc.9b07160

Breimer, L. H. (1990). Molecular Mechanisms of Oxygen Radical Carcinogenesis and Mutagenesis: the Role of DNA Base Damage. *Mol. Carcinog.* 3, 188–197. doi:10.1002/mc.2940030405

Cerutti, P. A. (1985). Prooxidant States and Tumor Promotion. *Science* 227, 375–381. doi:10.1126/science.2981433

Chen, S., Li, H., Chen, Y., Li, S., Xu, J., Guo, H., et al. (2019). Three New Diterpenes and Two New Sesquiterpenoids from the Endophytic Fungus *Trichoderma Koningiopsis* A729. *Bioorg. Chem.* 86, 368–374. doi:10.1016/j.bioorg.2019.02.005

Cotelle, N., Bernier, J. L., Catteau, J. P., Pommery, J., Wallet, J. C., and Gaydou, E. M. (1996). Antioxidant Properties of Hydroxy-Flavones. *Free Radic. Biol. Med.* 20, 35–43. doi:10.1016/0891-5849(95)02014-4

Dao, D. Q., Phan, T. T. T., Nguyen, T. L. A., Trinh, P. T. H., Tran, T. T. V., Lee, J. S., et al. (2020). Insight into Antioxidant and Photoprotective Properties of Natural Compounds from marine Fungus. *J. Chem. Inf. Model.* 60, 1329–1351. doi:10.1021/acs.jcim.9b00964

Ding, M., Li, J.-J., Leonard, S. S., Ye, J.-P., Shi, X., Colburn, N. H., et al. (1999). Vanadate-induced Activation of Activator Protein-1: Role of Reactive Oxygen Species. *Carcinogenesis* 20, 663–668. doi:10.1093/carcin/20.4.663

El-Hawary, S. S. E.-D., El Zalabani, S. M., Selim, N. M., Ibrahim, M. A., Wahba, F. A., El Badawy, S. A., et al. (2019). Phenolic Constituents of Chrysophyllum Oliviforme L. Leaf Down-Regulate TGF-β Expression and Ameliorate CCl4-Induced Liver Fibrosis: Evidence from *In Vivo* and In Silico Studies. *Antioxidants* 8, 646. doi:10.3390/antiox8120646

Fotso, S., Mahmud, T., Zabriskie, T. M., Santosa, D. A., SulastriProteau, P. J., and Protea, P. J. (2008). Rearranged and Unrearranged Angucyclinones from Indonesian *Streptomyces* Spp. *J. Antibiot.* 61, 449–456. doi:10.1038/ja.2008.61

Grisham, M. B., Jourd'Heuil, D., and Wink, D. A. (2000). Review Article: Chronic Inflammation and Reactive Oxygen and Nitrogen Metabolism - Implications in DNA Damage and Mutagenesis. *Aliment. Pharmacol. Ther. Suppl.* 14, 3–9. doi:10.1046/j.1365-2036.2000.014s1003.x

Halliwell, B. (1987). Oxidants and Human Disease: Some New Concepts 1. *FASEB j.* 1, 358–364. doi:10.1096/fasebj.1.5.2824268

Harper, J. K., Arif, A. M., Ford, E. J., Strobel, G. A., Porco, J. A., Jr., Tomer, D. P., et al. (2003). Pestacin: a 1,3-dihydro Isobenzofuran from *Pestalotiopsis Microspora* Possessing Antioxidant and Antimycotic Activities. *Tetrahedron* 59, 2471–2476. doi:10.1016/s0040-4020(03)00255-2

Kang, H.-S., Jun, E.-M., Park, S.-H., Heo, S.-J., Lee, T.-S., Yoo, I.-D., et al. (2007). Cyathusals A, B, and C, Antioxidants from the Fermented Mushroom Cyathus Stercoreus. *Cyathus Stercoreusj. Nat. Prod.* 70, 1043–1045. doi:10.1021/np060637h

Kapoor, M., Dhawan, S. N., Mor, S., Bhatia, S. C., Gupta, S. C., and Hundal, M. S. (2003). Stereoselective Synthesis of Z-3-Alkoxy-2-[(4′-Methoxyphenyl) methylidene]-1(3h)-Isobenzofuranones. *Tetrahedron* 59, 5027–5031. doi:10.1016/s0040-4020(03)00757-9

Koppenol, W. H., Moreno, J. J., Pryor, W. A., Ischiropoulos, H., and Beckman, J. S. (1992). Peroxynitrite, a Cloaked Oxidant Formed by Nitric Oxide and Superoxide. *Chem. Res. Toxicol.* 5, 834–842. doi:10.1021/tx00030a017

Kusio, J., Sitkowska, K., Konopko, A., and Litwinienko, G. (2020). Hydroxycinnamyl Derived BODIPY as a Lipophilic Fluorescence Probe for Peroxyl Radicals. *Antioxidants* 9, 88. doi:10.3390/antiox9010088

Liu, H.-X., Tan, H.-B., Chen, K., Zhao, L.-Y., Chen, Y.-C., Li, S.-N., et al. (2019b). Cytosporins A-D, Novel Benzophenone Derivatives from the Endophytic Fungus *Cytospora Rhizophorae* A761. *Org. Biomol. Chem.* 17, 2346–2350. doi:10.1039/c8ob03223h

Liu, H.-X., Tan, H.-B., Liu, Y., Chen, Y.-C., Li, S.-N., Sun, Z.-H., et al. (2017). Three New Highly-Oxygenated Metabolites from the Endophytic Fungus *Cytospora Rhizophorae* A761. *Fitoterapia* 117, 1–5. doi:10.1016/j.fitote.2016.12.005

Liu, H., Tan, H., Chen, Y., Guo, X., Wang, W., Guo, H., et al. (2019a). Cytorhizins A-D, Four Highly Structure-Combined Benzophenones from the Endophytic Fungus *Cytospora Rhizophorae*. *Org. Lett.* 21, 1063–1067. doi:10.1021/acs.orglett.8b04107

Liu, H., Tan, H., Wang, W., Zhang, W., Chen, Y., Li, S., et al. (2019c). Cytorhizophins A and B, Benzophenone-Hemiterpene Adducts from the Endophytic Fungus *Cytospora Rhizophorae*. *Org. Chem. Front.* 6, 591–596. doi:10.1039/c8qo01306c

Liu, Z., Tan, H., Chen, K., Chen, Y., Zhang, W., Chen, S., et al. (2019d). Rhizophols A and B, Antioxidant and Axially Chiral Benzophenones from the Endophytic Fungus *Cytospora Rhizophorae*. *Org. Biomol. Chem.* 17, 10009–10012. doi:10.1039/c9ob02282a

López-Alarcón, C., and Denicola, A. (2013). Evaluating the Antioxidant Capacity of Natural Products: A Review on Chemical and Cellular-Based Assays. *Anal. Chim. Acta* 763, 1–10. doi:10.1016/j.aca.2012.11.051

Mensor, L. L., Menezes, F. S., Leitão, G. G., Reis, A. S., Santos, T. C. d., Coube, C. S., et al. (2001). Screening of Brazilian Plant Extracts for Antioxidant Activity by the Use of DPPH Free Radical Method. *Phytother. Res.* 15, 127–130. doi:10.1002/ptr.687

Mussard, E., Cesaro, A., Lespessailles, E., Legrain, B., Berteina-Raboin, S., and Toumi, H. (2019). Andrographolide, a Natural Antioxidant: An Update. *Antioxidants* 8, 571. doi:10.3390/antiox8120571

Naito, S., and Kaneko, Y. (1969). Two New Phenolic Reductones from. *Tetrahedron Lett.* 10, 4675–4678. doi:10.1016/s0040-4039(01)88780-3

Quiñones, M., Miguel, M., and Aleixandre, A. (2012). The Ployphenols, Naturally Occurring Compounds with Beneficial Effects on Cardiovascular Disease. *Nutr. Hosp.* 27, 76–89.

Russell, E. G., and Cotter, T. G. (2015). "New Insight into the Role of Reactive Oxygen Species (ROS) in Cellular Signal-Transduction Processes," in *International Review of Cell and Molecular Biology* (Cambridge, MA, USA: Academic Press), Vol. 319, 221–254. doi:10.1016/bs.ircmb.2015.07.004

Strobel, G., Ford, E., Worapong, J., Harper, J. K., Arif, A. M., Grant, D. M., et al. (2002). Isopestacin, an Isobenzofuranone from *Pestalotiopsis Microspora*, Possessing Antifungal and Antioxidant Activities. *Phytochemistry* 60, 179–183. doi:10.1016/s0031-9422(02)00062-6

Taniguchi, N., Pickett, C. B., and Griffith, O. W. (1993). Oxy Radicals and Antioxidative Responses in Cancer: 12th Sapporo Cancer Seminar. *Cancer Res.* 53, 3207–3210.

Wen, L., Zhao, Y., Jiang, Y., Yu, L., Zeng, X., Yang, J., et al. (2017). Identification of a Flavonoid C -glycoside as Potent Antioxidant. *Free Radic. Biol. Med.* 110, 92–101. doi:10.1016/j.freeradbiomed.2017.05.027

Zhong, W., Chen, Y., Mai, Z., WeiWang, X. J., Wang, J., Zeng, Q., et al. (2020). Euroticins A and B, Two Pairs of Highly Constructed Salicylaldehyde Derivative Enantiomers from a marine-derived Fungus *Eurotium* Sp. SCSIO F452. *J. Org. Chem.* 85, 12754–12759. doi:10.1021/acs.joc.0c01407

Conflict of Interest: The authors declare that the research was conducted in the absence of any commercial or financial relationships that could be construed as a potential conflict of interest.

Publisher's Note: All claims expressed in this article are solely those of the authors and do not necessarily represent those of their affiliated organizations, or those of the publisher, the editors and the reviewers. Any product that may be evaluated in this article, or claim that may be made by its manufacturer, is not guaranteed or endorsed by the publisher.

frontiers in Chemistry

ORIGINAL RESEARCH
published: 14 February 2022
doi: 10.3389/fchem.2021.807508

Huoshanmycins A–C, New Polyketide Dimers Produced by Endophytic *Streptomyces* sp. HS-3-L-1 From *Dendrobium huoshanense*

Youjuan Zhu[1†], Yichao Kong[2†], Yu Hong[1], Ling Zhang[1], Simin Li[1], Shurong Hou[2], Xiabin Chen[2], Tian Xie[2], Yang Hu[1] and Xiachang Wang[1]**

[1]*Jiangsu Key Laboratory for Functional Substances of Chinese Medicine, Nanjing University of Chinese Medicine, Nanjing, China,* [2]*Key Laboratory of Element Class Anti-Cancer Chinese Medicines, Engineering Laboratory of Development and Application of Traditional Chinese Medicines, Collaborative Innovation Center of Traditional Chinese Medicines of Zhejiang Province, School of Pharmacy, Hangzhou Normal University, Hangzhou, China*

Three new polyketide dimers named huoshanmycins A–C (**1**–**3**) were isolated from a plant endophytic *Streptomyces* sp. HS-3-L-1 in the leaf of *Dendrobium huoshanense*, which was collected from the Cultivation base in Jiuxianzun Huoshanshihu Co., Ltd. The dimeric structures of huoshanmycins were composed of unusual polyketides SEK43, SEK15, or UWM4, with a unique methylene linkage. Their structures were elucidated through comprehensive 1D-/2D-NMR and HRESIMS spectroscopic data analysis. The cytotoxicity against MV4-11 human leukemia cell by the Cell Counting Kit-8 (CCK8) method was evaluated using isolated compounds with triptolide as positive control (IC_{50}: 1.1 ± 0.4 μM). Huoshanmycins A and B (**1**, **2**) displayed moderate cytotoxicity with IC_{50} values of 32.9 ± 7.2 and 33.2 ± 6.1 μM, respectively.

Keywords: huoshanmycin, polyketide, *Streptomyces*, *Dendrobium huoshanense*, endophyte

OPEN ACCESS

Edited by:
Bruno Botta,
Sapienza University of Rome, Italy

Reviewed by:
Sabrin R. M. Ibrahim,
Batterjee Medical College, Saudi Arabia
Daniele Passarella,
University of Milan, Italy

****Correspondence:***
Yang Hu
huyang@njucm.edu.cn
Xiachang Wang
xiachangwang@njucm.edu.cn

[†]These authors have contributed equally to this work

Specialty section:
This article was submitted to Organic Chemistry, a section of the journal Frontiers in Chemistry

Received: *02 November 2021*
Accepted: *24 December 2021*
Published: *14 February 2022*

Citation:
Zhu Y, Kong Y, Hong Y, Zhang L, Li S, Hou S, Chen X, Xie T, Hu Y and Wang X (2022) Huoshanmycins A–C, New Polyketide Dimers Produced by Endophytic Streptomyces *sp. HS-3-L-1 From* Dendrobium huoshanense. *Front. Chem. 9:807508. doi: 10.3389/fchem.2021.807508*

INTRODUCTION

Dendrobium huoshanense is a perennial epiphytic Orchidaceae herb with important medicinal and ornamental value. The leaves of *D. huoshanense* have long been utilized for dermatologic disorders, metabolic syndromes, nervous system disorders, and musculoskeletal system disorders (Wang, 2021). Modern pharmacological research has revealed that *D. huoshanense* has anti-inflammatory (Ge et al., 2018; Li et al., 2020), cytotoxic (Chen et al., 2022), hypoglycemic (Wang et al., 2019), anti-atherosclerosis (Fan et al., 2020), and antioxidant (Tian et al., 2013) activity. *Dendrobium* plant is well-known for its rich and diverse endophytic bacterial and fungal community (Chen et al., 2019; Chen et al., 2020). Previous studies have revealed the close relationship between *Dendrobium* and its endophytes, such as improving the seed germination rate (Tsavkelova et al., 2007) and supply of nutrients (Li et al., 2017). At present, research on *D. huoshanense* endophytes mainly focuses on the diversity and functions, while not much is known about their secondary metabolites, especially for bacteria. The main species of bacterial microorganisms of *D. huoshanense* are *Sphingomonas, Acinetobacter, Enterococcus, Bacillus*, and *Methylobacterium* (Chen et al., 2020). *Streptomyces* is the largest genus of Actinobacteria and characterized by producing complex secondary metabolites. They produce over two-thirds of the clinically useful antibiotics of natural origin (e.g., chloramphenicol, streptomycin, tetracycline, erythromycin, ivermectin, and rifamycin) (Raja and Prabakarana, 2011). The last four compounds all belong to polyketides, which are derived from a

precursor molecule consisting of a chain of alternating ketone (or reduced forms of a ketone) and methylene groups.

Since the discovery of taxol and taxane produced by an endophytic fungus from the phloem (inner bark) of Pacific yew in 1993 (Stierle et al., 1993), endophytes have become an important resource in the field of bioactive natural products discovery (Newman and Cragg, 2015; Gómez and Luiz, 2018), as they can produce analogs or bioactivity-related compounds as their hosts did (Cui et al., 2012; Zhao et al., 2020c). As part of an effort to characterize novel natural products from medicinal plants (Wang et al., 2009; Ding et al., 2021; Hu et al., 2021) and their endophytes (Zhao et al., 2020b; Zhao et al., 2020a; Zhu et al., 2021), herein we report the isolation and characterization of three new polyketide dimers from an endophyte *Streptomyces* sp. HS-3-L-1 of the *D. huoshanense* leaf. The dimeric structures of new huoshanmycins A–C (**1**–**3**) were composed of SEK43, SEK15, or UWM4 (Meurer et al., 1997), with a unique methylene linkage. Herein, we report the fermentation, extraction, isolation, structural elucidation, and cytotoxic activity of these secondary metabolites.

MATERIALS AND METHODS

General Experimental Procedures

UV data were acquired on a Persee TU-1810 spectrophotometer (Persee analytics, Beijing, China). IR spectra were measured on a Thermo Scientific Nicolet iS5 FT-IR spectrometer (Thermo, United States). NMR spectra were obtained on a Bruker Advance AV500 spectrometer (Bruker, Germany). HRESIMS spectra were recorded on an Orbitrap Elite mass spectrometer (Thermo Scientific, United States). Liquid chromatography–mass spectrometry (LC-MS) was conducted with an Agilent 1290 system equipped with 6120 Quadrupole MSD mass spectrometer (Agilent Technologies, United States). HPLC analysis was performed on a Waters 2695 system equipped with 2998 PDA detector. Total component analysis was performed on an Agilent 1290 UHPLC-6520 Q-TOF/MS. Preparative HPLC separation was performed on a Waters 1525 EF LC system (Waters Company, United States). MCI GEL high-porous polymer (75–150 μm) was purchased from Mitsubishi Chemical Corporation (Japan). Sephadex LH-20 resin (25–100 μm) was purchased from GE Healthcare Company (Sweden). XAD16N resin (20–60 mesh) was obtained from Yuanye Company (Nanjing, Jiangsu, China). Chemicals were purchased from Juyou Company or Aldrich and used without further purification unless otherwise noted.

Strain Isolation

Plant samples of *D. huoshanense* were provided by Jiuxianzun Huoshanshihu Co., Ltd. (Liu-An City, Anhui Province, China) and identified by co-author Dr. Yang Hu. A voucher specimen (no. 20190309) was deposited at Jiangsu Key Laboratory for Functional Substances of Chinese Medicine, China. The roots, leaves, and stems of *D. huoshanense* were separated and cleaned with water and then rinsed in 0.1% Tween-20 for 30 s, sequentially immersed in 75% ethanol for 5 min and in 2% sodium hypochlorite for 5 min and rinsed with 10% $NaHCO_3$ for 10 min to inhibit fungal growth. After each treatment, samples were rinsed three times in sterile water. The surface sterilized samples were aseptically dissected into small pieces; 0.5 g of each sample was suspended in 1.0 ml of sterile H_2O, and heated at 75°C for 1 min to eliminate nonsporulating bacteria (Zhao et al., 2020a). A 100-μl aliquot of supernatant was streaked on oatmeal agar and on ISP4 agar plates supplemented with nalidixic acid (25 μg/ml) and amphotericin B (25 μg/ml). A number of sporulating bacterial colonies were observed after 1–2 months of incubation at 28°C, and each colony was subsequently purified on a M2 agar plate (Wang et al., 2013). Overall, 54 endophytic strains were isolated from plant samples. The endophytic strain HS-3-L-1 was isolated from the leaf of *D. huoshanense*.

Phylogenetic Analysis

Strain HS-3-L-1 was inoculated in a 20-ml test tube with 4 ml of TSB broth. After 3 days culture at 28°C with 160 rpm agitation, the partial 16S rRNA gene fragment was amplified using universal primers (27F 5′-AGAGTTTGATCMTGGCTCAG-3'; 1492R 5′-GGTTACCTTGTTACGACTT-3′). The amplified fragment (1,367 bp) was sent for sequencing analysis (Shanghai Sangong Company, China), which displayed 99.85% identity (BlastN, https://blast.ncbi.nlm.nih.gov/Blast.cgi) to *Streptomyces polaris* (MW164959.1). The sequence of 16S rRNA has been deposited in the NCBI nucleotide database with the accession number OK161010.

Fermentation, Extraction, and Isolation

Streptomyces sp. HS-3-L-1 was grown on M2 agar plate (glucose 4 g/L, malt extract 10 g/L, yeast extract 4 g/L, and agar 15 g/L) at 28°C for a week. Small pieces of agar with bacterial growth were added to eleven 250-ml Erlenmeyer flasks, each containing 50 ml of medium Bran [corn flour, 40.0 g/L; gluten powder, 5.0 g/L; $K_2HPO_4{\bullet}3H_2O$, 0.5 g/L; glucose, 10.0 g/L; bran, 10.0 g/L; $CaCO_3$, 2.0 g/L; and $(NH_4)_2SO_4$, 1.0 g/L]. After 3 days of incubation at 28°C with 200 rpm agitation, the seed cultures were used to inoculate 100 Erlenmeyer flasks (250 ml), each containing 100 ml of medium Bran (total 10 L). The fermentation was carried out on a rotary shaker (200 rpm) at 28°C for a week. All obtained culture broth was combined and centrifuged at 5,000 ×*g* for 30 min to separate the mycelium and supernatant. Mycelium was extracted with MeOH (3 × 2 L), and the organic phase was evaporated to afford 50.2 g of crude extract A. The supernatant was mixed with 4% (w/v) XAD-16 resin and stirred for 6 h, followed by filtration. The resin was washed with water (3 × 500 ml) and then eluted with MeOH until the eluant was colorless. The MeOH extract was subsequently evaporated to afford 13.3 g of crude extract B.

Crude extract A (50.2 g) was subjected to an MCI column (500 g, 10 × 80 cm) and eluted with a gradient of aqueous MeOH (20, 40, 60, 80, and 100%) to yield 16 fractions (Fr. 1-1 to Fr. 1-16). Fr. 1-9 (0.5 g) was subjected to a Sephadex LH-20 column (4 × 100 cm, 2 ml/min) eluted with 80% aqueous MeOH to obtain 11 subfractions (Fr. 1-9-1 to Fr. 1-9-11). Compound **5** (13.6 mg) was obtained from Fr. 1-9-4. Fr. 1-9-9 was further purified by

TABLE 1 | ^{1}H (500 MHz) and ^{13}C (125 MHz) NMR data of compounds **1–3** in DMSO-d_6.

No	1		2		3	
	δ_C, type	δ_H, *J* in Hz	δ_C, type	δ_H, *J* in Hz	δ_C, type	δ_H, *J* in Hz
1	165.2, C	—	165.2, C	—	165.2, C	—
2	100.0, C	—	100.1, C	—	100.1, C	—
3	166.1, C	—	166.1, C	—	166.3, C	—
4	101.8, CH	5.76, s	101.8, CH	5.75, s	101.6, CH	5.74, s
5	160.9, C	—	160.9, C	—	160.8, C	—
6	36.5, CH_2	3.54, s	36.6, CH_2	3.55, s	36.5, CH_2	3.53, s
7	133.2, C	—	133.2, C	—	133.2, C	—
8	121.3, CH	6.74, dd (7.6, 2.1)	121.3, CH	6.75, d (7.6)	121.2, CH	6.75, d (7.7)
9	130.5, CH	7.22, t (7.7)	130.5, CH	7.22, t (7.9)	130.5, CH	7.21, t (7.9)
10	115.0, CH	6.80, t (8.7)	115.0, CH	6.80, d (8.2)	114.9, CH	6.80, d (8.2)
11	154.2, C	—	154.2, C	—	154.2, C	—
12	131.2, C	—	131.3, C	—	131.2, C	—
13	200.4, C	—	200.4, C	—	200.6, C	—
14	116.0, C	—	116.0, C	—	116.0, C	—
15	165.5, C	—	165.5, C	—	165.5, C	—
16	101.1, CH	6.13, d (2.3)	101.8, CH	6.14, s	101.1, CH	6.13, d (2.1)
17	163.7, C	—	163.6, C	—	163.6, C	—
18	112.0, CH	6.09, d (2.0)	112.0, CH	6.09, s	112.0, CH	6.09, d (1.7)
19	143.4, C		143.4, C		143.4, C	
20	21.9, CH_3	1.83, s	21.9, CH_3	1.84, s	21.9, CH_3	1.84, s
1′	161.9, C	—	165.2, C	—	165.1, C	—
2′	100.1, C	—	100.1, C	—	100.0, C	—
3′	166.3, C	—	166.1, C	—	166.2, C	—
4′	101.7, CH	5.70, s	101.8, CH	5.75, s	101.5, CH	5.74, s
5′	161.4, C	—	160.9, C	—	161.2, C	—
6′	37.0, CH_2	3.47, s	36.6, CH_2	3.55, s	36.7, CH_2	3.48, s
7′	134.8, C	—	133.2, C	—	135.8, C	—
8′	120.9, CH	6.74, dd (7.6, 2.1)	121.3, CH	6.75, d (7.6)	109.5, CH	6.16, d (1.9)
9′	129.1, CH	7.17, t (7.9)	130.5, CH	7.22, t (7.9)	160.1, C	
10′	114.4, CH	6.80, t (8.7)	115.0, CH	6.80, d (8.2)	101.9, CH	6.23, d (1.9)
11′	154.7, C	—	154.2, C	—	157.8, C	—
12′	129.6, C	—	131.3, C	—	121.5, C	—
13′	141.1, C	—	200.4, C	—	200.3, C	—
14′	111.3, CH	5.95, d (2.4)	116.0, C	—	117.6, C	—
15′	162.4, C	—	165.5, C	—	163.2, C	—
16′	102.3, CH	6.27, d (2.4)	101.8, CH	6.14, s	100.9, CH	6.11, s
17′	163.6, C	—	163.6, C	—	162.4, C	—
18′	115.9, C	—	112.0, CH	6.09, s	111.3, CH	6.06, s
19′	203.6, C	—	143.4, C	—	142.1, C	—
20′	30.3, CH_3	1.87, s	21.9, CH_3	1.84, s	21.4, CH_3	1.83, s
1″	17.8, CH_2	3.25, s	17.8, CH_2	3.24, s	17.7, CH_2	3.24, s
11-OH	—	9.81, s	—	9.82, s	—	9.83, s
15-OH	—	12.66, s	—	12.68, s	—	12.68, s
17-OH	—	10.44, s	—	10.45, s	—	10.45, s
9′-OH	—	—	—	—	—	9.88, s
11′-OH	—	9.48, s	—	9.82, s	—	10.26, s
15′-OH	—	10.36, s	—	12.68, s	—	12.05, s
17′-OH	—	12.50, s	—	10.45, s	—	10.21, s

semi-preparative HPLC (38% aqueous MeOH) to yield compound **3** (5.8 mg). Crude extract B (13.3 g) was subjected to an MCI column (200 g, 6 × 30 cm), using gradient elution from 20% to 100% aqueous MeOH to provide 11 fractions (Fr. 2-1 to Fr. 2–11). Fractions Fr. 2-5 (0.7 g) was subjected to a Sephadex LH-20 column (4 × 100 cm, 2 ml/min, 80% aqueous MeOH) to obtain 12 subfractions (Fr. 2-5-1 to Fr. 2-5-12). Fr. 2-5-6 (0.3 g) was further purified by semi-preparative HPLC (45% aqueous MeOH) to yield compounds **4** (7.6 mg) and **7** (9.4 mg). Fr. 2-10 (0.5 g) was also purified by a Sephadex LH-20 column (4 × 100 cm, 2 ml/min, 80% aqueous MeOH) to obtain seven subfractions (Fr. 2-10-1 to Fr. 2-10-7). Fr. 2-10-6 (0.2 g) was further purified by semi-preparative HPLC (63% aqueous MeOH) to yield compounds **1** (8.6 mg), **2** (16.8 mg), and **6** (12.3 mg).

Huoshanmycin A (**1**): Yellow amorphous powder; UV (MeOH) λ_{max} (log ε) 294 nm (4.17); IR (KBr) ν_{max} 3,164, 2,927, 1,680, 1,617, 1,437, 1,401, 1,384, 1,284, 1,207, 1,138, 1,027, 829, 803, and 724 cm^{-1}; ^{13}C and ^{1}H NMR data, see **Table 1**; (+)-ESI-MS: *m/z* 749.0 $[M + H]^+$; (−)-ESI-MS: *m/z*

TABLE 2 | Antiproliferative activity of compounds **1–4** against MV4-11 cell line.

Compounds	IC_{50} ± SD, μM
1	32.9 ± 7.2
2	33.2 ± 6.1
3	>50
4	>50
Triptolide	1.1 ± 0.4

747.2 $[M - H]^-$; (−)-HR-ESI-MS *m/z* 747.17096 $[M - H]^-$ (calcd. for $C_{41}H_{31}O_{14}$ 747.1714).

Huoshanmycin B (**2**): Yellow amorphous powder; UV (MeOH) λ_{max} (log ε) 294 nm (4.44); IR (KBr) ν_{max} 3,184, 2,260, 2,129, 1,675, 1,587, 1,464, 1,284, 1,167, 1,158, 1,024, 995, 926, 826, 769, 722, 699, 656, 633, 611, 576, and 523 cm^{-1}; ^{13}C and ^{1}H NMR data, see **Table 1**; (+)-ESI-MS: *m/z* 749.0 $[M + H]^+$; (−)-ESI-MS: *m/z* 747.2 $[M - H]^-$; (+)-HR-ESI-MS *m/z* 749.18768 $[M + H]^+$ (calcd. for $C_{41}H_{33}O_{14}$ 749.1970).

Huoshanmycin C (**3**): Yellow amorphous powder; UV (MeOH) λ_{max} (log ε) 294 nm (4.41); IR (KBr) ν_{max} 3,172, 2,259, 2,129, 1,677, 1,616, 1,587, 1,464, 1,384, 1,271, 1,204, 1,169, 1,142, 1,024, 999, 926, 844, 800, 766, 722, 600, and 524 cm^{-1}; ^{13}C and ^{1}H NMR data, see **Table 1**; (+)-ESI-MS: *m/z* 765.2 $[M + H]^+$; (−)-ESI-MS: *m/z* 763.2 $[M - H]^-$; (+)-HR-ESI-MS *m/z* 765.1819 $[M + H]^+$ (calcd. for $C_{41}H_{33}O_{15}$, 765.1819), 787.1640 $[M + Na]^+$ (calcd. for $C_{41}H_{32}O_{15}Na$, 787.1639).

Cell Culture and Proliferation Inhibition Assay

The human AML cell line MV4-11 (CRL-9591) was purchased from ATCC and cultured in IMDM (Gibco) supplemented with 10% FBS (Gibco) and 1% penicillin–streptomycin (Gibco). To conduct cell proliferation assay, cells (1.5×10^6 cells/well) in the logarithmic phase were seeded into 96-well plates simultaneously with various concentrations of different compounds (5 μl, final concentration of 50–0.023 μM for IC_{50} determination) or vehicle (0.5% DMSO) for 48 h. Cell viability of compounds **1–4** was measured using Cell Counting Kit-8 (DoJINDO) according to the manufacturer's instructions with triptolide as positive control (**Table 2**). The absorbance was measured at 450 nm using a microplate reader (Epoch, Bio-Tek, United States). The value of half maximal inhibitory concentration (IC_{50}) was calculated using GraphPad Prism 7.

Antimicrobial Assay

Standard strains of *Staphylococcus aureus* (ATCC 29213), *Escherichia coli* (ATCC 25922), *Bacillus subtilis* (A186), *Pseudomonas aeruginosa* (ATCC 27853), and *Acinetobacter baumannii* (ATCC 19606) were obtained from CICC (China Center of Industrial Culture Collection, China). Bacteria were inoculated in LB Broth media and incubated overnight at 37°C. The cultures were quantified *via* a spectrophotometer, and then diluted to A = 0.02 (OD_{600}) and dispensed to 96-well black, clear-bottom assay plates (100 μl/well). Test compounds (final concentration 50 μM) and controls (positive control of 50 μM polymyxin and placebo control of DMSO) were then added. The plates were incubated for 16 h at 37°C, and then measured the absorbance at 600 nm using a microplate reader. Compound activity was calculated on a per-plate basis (Zhao et al., 2020a).

RESULTS AND DISCUSSION

Preliminary HPLC-HRMS metabolic profiling of endophytic actinomycete strains isolated from *D. huoshanense* plant samples revealed that *Streptomyces* sp. HS-3-L-1 is capable of

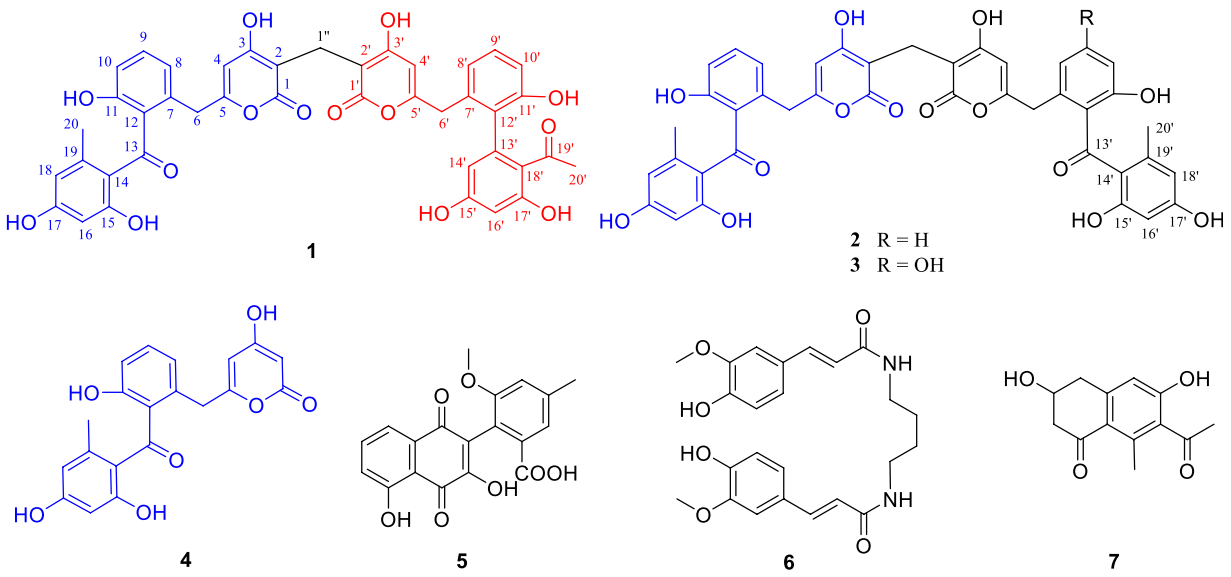

FIGURE 1 | Chemical structures of compounds isolated from *Streptomyces* sp. HS-3-L-1.

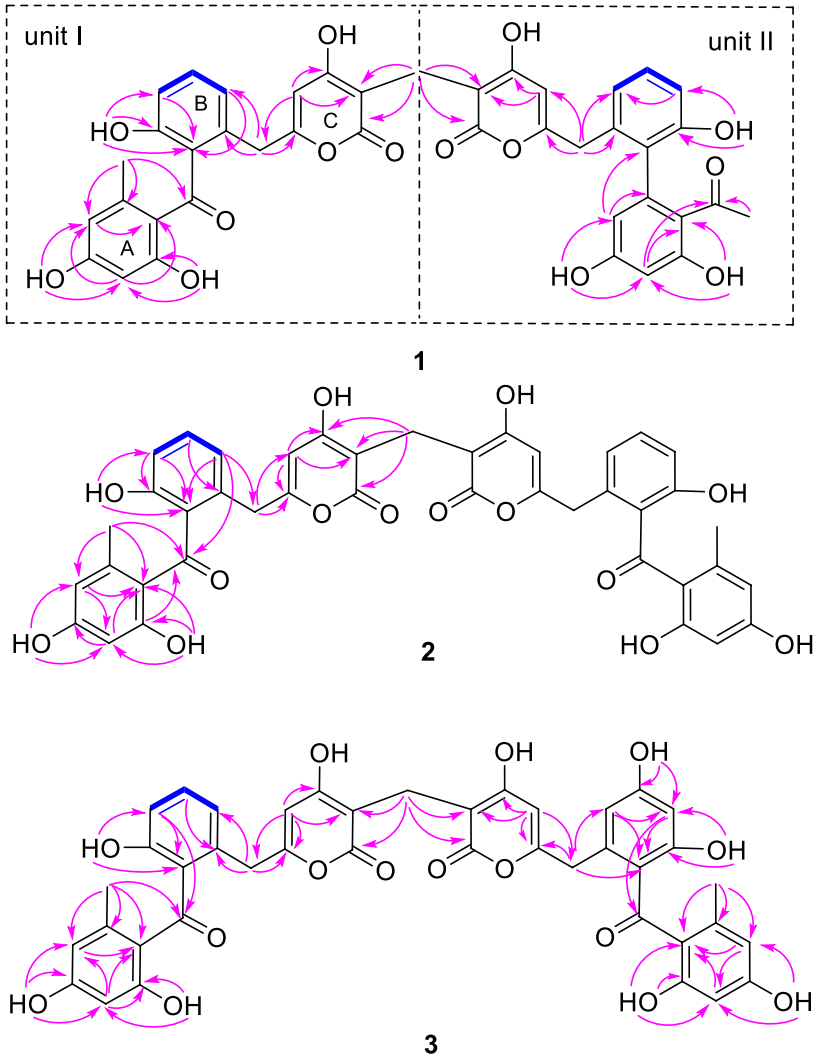

FIGURE 2 | Key COSY (bolds, blue), HMBC (arrows, pink) correlations of 1–3.

novel secondary metabolite production (**Supplementary Figure S1**). After scale-up fermentation (10 L) of *Streptomyces* sp. HS-3-L-1, and further extraction, fractionation, and standard chromatography, three new polyketide dimers were isolated and identified [huoshanmycins A (**1**, yield: 1.68 mg/L), B (**2**, yield: 0.86 mg/L), and C (**3**, yield: 0.58 mg/L)], together with four previously reported metabolites, SEK43 (**4**, yield: 0.76 mg/L), WS-5995 C (**5**, yield: 1.36 mg/L), JBIR-94 (**6**, yield: 12.3 mg/L), and GTRI-02 (**7**, yield: 0.94 mg/L)] (**Figure 1**).

Compound **1** was obtained as a yellow amorphous powder. Its molecular formula was established as $C_{41}H_{32}O_{14}$ based on HRESIMS data, which indicated 26 degrees of unsaturation. The ^{13}C NMR of compound **1** showed 41 carbons, which can be sorted into two methyls, three methylenes, twelve aromatic methines, twenty sp^2 quarternary carbons, and four carbonyls/carboxylic acids, with the aid of HSQC spectrum. The ^{1}H-NMR and HSQC spectra of **1** indicated twelve aromatic protons [δ_H 5.70 (1H, s), 5.76 (1H, s), 5.95 (1H, d, J = 2.4 Hz), 6.09 (1H, d, J = 2.0 Hz), 6.13 (1H, d, J = 2.3 Hz), 6.27 (1H, d, J = 2.4 Hz), 6.74 (2H, dd, J = 2.1, 7.6 Hz), 6.80 (2H, t, J = 8.7 Hz), 7.17 (1H, t, J = 7.9 Hz), and 7.22 (1H, t, J = 7.7 Hz)], two methyls [δ_H 1.83 and 1.87 (each 3H, s)], three methylenes [δ_H 3.25, 3.47, and 3.54 (each 2H, s)], and six hydroxyls showed at low field: δ_H 9.48, 9.81, 10.36, 10.44, 12.50, and 12.66 (each 1H, s). Two spin systems of H-8 (δ_H 6.74)/H-9 (δ_H 7.22)/H-10 (δ_H 6.80) and H-8′ (δ_H 6.74)/H-9′ (δ_H 7.17)/H-10′ (δ_H 6.80) observed in COSY spectrum suggested the presence of two 1,2,3-trisubstiuted benzene rings. Two aromatic protons δ_H 6.13 (H-16) and 6.09 (H-18), together with the HMBC correlations from H_3-20 (δ_H 1.83) to C-13 (δ_C 200.4), C-18 (δ_C 112.0), and C-19 (δ_C 143.4), and from H-16 to C-14 (δ_C 116.0) and C-18, and from H-18 to C-14, C-16 (δ_C 101.1), and C-20 (δ_C 21.9) suggested the presence of a 2,4-dihydroxy-6-methyl-1-keto-phenyl moiety (ring A in **Figure 2**). The two active hydrogens showed key HMBC correlations from 15-OH (δ_H 12.66, s) to C-14/C-15/C-16, and from 17-OH (δ_H 10.44, s) to C-16/C-17/C-18, indicating two

hydroxyl groups located at C-15 and C-17. An unsaturated six-member lactone ring (ring C in **Figure 2**) was constructed by HMBC cross peaks from H-4 (δ_H 5.76) to C-2 (δ_C 100.0), C-3 (δ_C 166.1), and C-6 (δ_C 36.5), and from H-1″ to C-1 (δ_C 165.2) and C-2. The obvious HMBC correlations from H_2 -6 (δ_H 3.54) to C-4 (δ_C 101.8), C-5 (δ_C 160.9), C-7 (δ_C 133.2) and C-8 (δ_C 121.3) permitted the assembly of ring B and ring C through a CH_2 linkage. Analysis of the remaining NMR data revealed that unit I of **1** (**Figure 2**) as C2-substitued SEK43 (**4**) (Meurer et al., 1997). SEK43 was reported as an engineered biosynthesis product, which was isolated and identified likewise from this endophytic strain. In a similar manner, the other decaketide-related subunit II was elucidated as C2′-substitued UMW4 (Meurer et al., 1997) mainly through HMBC correlations (**Figure 2**), e.g., from H-4′ (δ_H 5.70, s) to C-2′ (δ_C 100.1) and C-3′ (δ_C 166.3), from H_2-6′ (δ_H 3.47, s) to C-4′, C-5′ (δ_C 161.4), C-7′ (δ_C 134.8), and C-8′ (δ_C 120.9), from H-14′ (δ_H 5.95, d) to C-12′ (δ_C 129.6) and C-13′ (δ_C 141.1), and from H-16′ (δ_H 6.27, d) to C-14′ (δ_C 111.3), C-18′ (δ_C 115.9), and C-19′ (δ_C 203.6). The strong HMBC correlations from H_2-1″ (δ_H 3.25) to C-1 (δ_C 165.2), C-2 (δ_C 100.0), C-1′ (δ_C 161.9), and C-2′ (δ_C 100.1) unambiguously connected SEK43 and UMW4 with a unique methylene bridge, to form the final dimeric structure of **1**. Thus, compound **1** was identified as a novel polyketide dimer and named huoshanmycin A, to reflect the producing strain's point of origin.

Compound **2** was also obtained as a white amorphous powder and shared the same molecular formula ($C_{41}H_{32}O_{14}$) with huoshanmycin A (**1**). Compound **2** was clearly recognized as a polyketide dimer from its NMR data (**Table 1**), which showed only 21 carbons in ^{13}C NMR spectrum. Analysis of NMR data of compound **2** revealed that it was highly similar to SEK43 (**4**) and shared a same methylene linkage between C-2 and C-2′. This was confirmed by HMBC correlations from H_2-1" (δ_H 3.24) to C-1/C-1′ (δ_C 165.2), C-2/C-2′ (δ_C 100.1), and C-3/C-3′ (δ_C 166.1). The remaining HMBC correlations (**Figure 2**) and NMR data (**Table 1**) were in full agreement with the new structure of compound **2**, and it was named huoshanmycin B.

Compound **3** was obtained as a yellow amorphous powder and its molecular formula was determined as $C_{41}H_{32}O_{15}$ from HRESIMS results. A detailed comparison of the NMR data of **3** and **2** indicated that their structures were highly similar. The significant differences observed in NMR spectra was that one of the 1,2,3-trisubstiuted benzene ring protons in **2** (δ_H 6.75, 7.22, 6.80) was replaced with two olefinic methines (δ_H 6.16, 6.23) and one hydroxyl (δ_H 9.88) in compound **3**. This tetra-substituted benzene moiety was confirmed by the HMBC correlations from H-6′ (δ_H 3.48) to C-7, C-8′, and C-12′, from H-8′ (δ_H 6.16) to C-6′, C-9′, C-10′, and C-12′, and from H-10′ (δ_H 6.23) to C-8′, C-9′, C-11′, and C-12′, as well as the correlation signals from 9′-OH (δ_H 9.88) to C-8′, C-9′, and C-10′. Therefore, the structure of huoshanmycin C (**3**) was elucidated as shown in **Figure 1**.

The other five known compounds were identified as SEK43 (**4**) (McDaniel et al., 1995), WS-5995 C (**5**) (Ikushima et al., 1983), JBIR-94 (**6**) (Taj and Sorensen, 2015), and GTRI-02 (**7**) (Yeo et al., 1998), through comparison with reported data. Although compounds **1**–**7** were inactive at or below 50 μM in a standard antimicrobial assay, huoshanmycins A and B (**1**, **2**), the two isomers, showed antiproliferative activity against the MV4-11 cell line with IC_{50} values of 32.9 ± 7.2 and 33.2 ± 6.1 μM, respectively (**Table 2**).

In summary, the discovery of compounds **1**–**7** as metabolites of the *D. huoshanense* isolate *Streptomyces* sp. HS-3-L-1 further highlights the potential for novel microbial natural product discovery from medicinal plants. Among them, compounds **1**–**3** were unique dimers of SEK43 (**4**), SEK15, or UWM4, three decaketide-related shunt products discovered from minimal *jad*PKS constructs (Meurer et al., 1997). So far, only two similar natural products, strepolyketides B and C, were recently reported from a marine-derived *Streptomyces* (Jiang et al., 2020). Moreover, huoshanmycins A and B showed moderate cytotoxicity against MV4-11 human leukemia cell. The newly isolated **1**–**3** enriched the structural diversity of microbial source. Future investigation to explore the biosynthetic logic of these structurally unique dimers is ongoing.

DATA AVAILABILITY STATEMENT

The datasets presented in this study can be found in online repositories. The names of the repository/repositories and accession number(s) can be found below: https://www.ncbi.nlm.nih.gov/, OK161010.

AUTHOR CONTRIBUTIONS

YZ contributed to the chemical experiments and prepared the manuscript draft. YK performed the identification of strain and the cytotoxicity assay. YuH, LZ, and SL participated in the endophytic strain isolation and antimicrobial assay. SH and XC undertook the MS analysis. TX contributed to collection of plant samples and financial support. YaH and XW contributed to the design of experiment, financial support, and manuscript revision. All authors have approved the submission of this manuscript for publication.

FUNDING

This research was financially supported by the Jiangsu Provincial Innovation and Entrepreneurship Talent Plan (202010528), the Nature Science Foundation of Jiangsu Higher Education Institutions of China (No. 19KJA180008), the National Natural Science Foundation (81803391), and the Natural Science Foundation Youth Program of Nanjing University of Chinese Medicine (NZY81803391).

SUPPLEMENTARY MATERIAL

The Supplementary Material for this article can be found online at: https://www.frontiersin.org/articles/10.3389/fchem.2021.807508/full#supplementary-material

REFERENCES

Chen, S., Dai, J., Song, X., Jiang, X., Zhao, Q., Sun, C., et al. (2020). Endophytic Microbiota Comparison of *Dendrobium huoshanense* Root and Stem in Different Growth Years. *Planta Med.* 86, 967–975. doi:10.1055/a-1046-1022

Chen, S. T., Dai, J., Jiang, X. P., Song, X. W., Chen, C. W., Chen, N. F., et al. (2019). Diversity and Difference of Endophytes in *Dendrobium huoshanense* with Different Growth Years. *Zhongguo Zhong Yao Za Zhi* 44, 1145–1150. doi:10.19540/j.cnki.cjcmm.2019.0022

Chen, X., Hu, J., Wu, S., Zhao, H., Peng, D., Wu, D., et al. (2022). Cytotoxic picrotoxane-type sesquiterpenoid lactones from Dendrobium huoshanense. *Rec. Nat. Prod.* 16, 144–149. doi:10.25135/rnp.260.21.04.2048

Cui, Y., Yi, D., Bai, X., Sun, B., Zhao, Y., and Zhang, Y. (2012). Ginkgolide B Produced Endophytic Fungus (*Fusarium oxysporum*) Isolated from *Ginkgo Biloba*. *Fitoterapia* 83, 913–920. doi:10.1016/j.fitote.2012.04.009

Ding, N., Wang, J., Liu, J., Zhu, Y., Hou, S., Zhao, H., et al. (2021). Cytotoxic Guaianolide Sesquiterpenoids from *Ainsliaea fragrans*. *J. Nat. Prod.* 84, 2568–2574. doi:10.1021/acs.jnatprod.1c00587

Fan, X., Han, J., Zhu, L., Chen, Z., Li, J., Gu, Y., et al. (2020). Protective activities of *Dendrobium huoshanense* C. Z. Tang et S. J. Cheng polysaccharide against high-cholesterol diet-induced atherosclerosis in zebrafish. *Oxidative Med. Cell Longevity* 2020, 1–10. doi:10.1155/2020/8365056

Ge, J.-C., Zha, X.-Q., Nie, C.-Y., Yu, N.-J., Li, Q.-M., Peng, D.-Y., et al. (2018). Polysaccharides from *Dendrobium huoshanense* Stems Alleviates Lung Inflammation in Cigarette Smoke-Induced Mice. *Carbohydr. Polym.* 189, 289–295. doi:10.1016/j.carbpol.2018.02.054

Gómez, O. C., and Luiz, J. H. H. (2018). Endophytic Fungi Isolated from Medicinal Plants: Future Prospects of Bioactive Natural Products from Tabebuia/Handroanthus Endophytes. *Appl. Microbiol. Biotechnol.* 102, 9105–9119. doi:10.1007/s00253-018-9344-3

Hu, Y., Zhao, H., Yang, A., Lv, Q., Ding, N., Lu, T.-L., et al. (2021). Jatrophacine, a 4,5-seco-Rhamnofolane Diterpenoid with Potent Anti-inflammatory Activity from *Jatropha curcas*. *Nat. Product. Res.* 35, 2748–2752. doi:10.1080/14786419.2019.1660656

Ikushima, H., Takase, S., Kawai, Y., Itoh, Y., Okamoto, M., and Tanaka, H. (1983). Structure and Synthesis of New Anticoccidial Antibiotics Isolated from *Streptomyces auranticolor*. *Agric. Biol. Chem.* 47, 2231–2235. doi:10.1080/00021369.1983.10865932

Jiang, Y., Huang, Y., Chen, S., Ji, Y., Ding, W., and Ma, Z. (2020). Strepolyketides A-C, Three Novel SEK15-Derived Polyketides from *Streptomyces* sp. HN2A53. *Tetrahedron Lett.* 61, 151996. doi:10.1016/j.tetlet.2020.151996

Li, O., Xiao, R., Sun, L., Guan, C., Kong, D., and Hu, X. (2017). Bacterial and Diazotrophic Diversities of Endophytes in *Dendrobium catenatum* Determined through Barcoded Pyrosequencing. *PLoS One* 12, e0184717. doi:10.1371/journal.pone.0184717

Li, Q.-M., Jiang, H., Zha, X.-Q., Wu, D.-L., Pan, L.-H., Duan, J., et al. (2020). Anti-inflammatory Bibenzyls from the Stems of *Dendrobium huoshanense* via Bioassay Guided Isolation. *Nat. Product. Res.* 34, 563–566. doi:10.1080/14786419.2018.1489394

McDaniel, R., Ebert-Khosla, S., Hopwood, D. A., and Khosla, C. (1995). Rational Design of Aromatic Polyketide Natural Products by Recombinant Assembly of Enzymatic Subunits. *Nature* 375, 549–554. doi:10.1038/375549a0

Meurer, G., Gerlitz, M., Wendt-Pienkowski, E., Vining, L. C., Rohr, J., and Richard Hutchinson, C. (1997). Iterative Type II Polyketide Synthases, Cyclases and Ketoreductases Exhibit Context-dependent Behavior in the Biosynthesis of Linear and Angular Decapolyketides. *Chem. Biol.* 4, 433–443. doi:10.1016/s1074-5521(97)90195-2

Newman, D. J., and Cragg, G. M. (2015). Endophytic and Epiphytic Microbes as sources of Bioactive Agents. *Front. Chem.* 3, 34. doi:10.3389/fchem.2015.00034

Raja, A., and Prabakaran, P. (2011). Actinomycetes and Drug-An Overview. *Am. J. Drug Discov. Develop.* 1, 75–84. doi:10.3923/ajdd.2011.75.84

Stierle, A., Strobel, G., and Stierle, D. (1993). Taxol and Taxane Production by Taxomyces Andreanae, an Endophytic Fungus of Pacific Yew. *Science* 260, 214–216. doi:10.1126/science.8097061

Taj, R., and Sorensen, J. L. (2015). Synthesis of Actinomycetes Natural Products JBIR-94, JBIR-125, and Related Analogues. *Tetrahedron Lett.* 56, 7108–7111. doi:10.1016/j.tetlet.2015.11.020

Tian, C.-C., Zha, X.-Q., Pan, L.-H., and Luo, J.-P. (2013). Structural Characterization and Antioxidant Activity of a Low-Molecular Polysaccharide from *Dendrobium huoshanense*. *Fitoterapia* 91, 247–255. doi:10.1016/j.fitote.2013.09.018

Tsavkelova, E. A., Cherdyntseva, T. A., Klimova, S. Y., Shestakov, A. I., Botina, S. G., and Netrusov, A. I. (2007). Orchid-associated Bacteria Produce Indole-3-Acetic Acid, Promote Seed Germination, and Increase Their Microbial Yield in Response to Exogenous Auxin. *Arch. Microbiol.* 188, 655–664. doi:10.1007/s00203-007-0286-x

Wang, H.-Y., Li, Q.-M., Yu, N.-J., Chen, W.-D., Zha, X.-Q., Wu, D.-L., et al. (2019). *Dendrobium huoshanense* Polysaccharide Regulates Hepatic Glucose Homeostasis and Pancreatic β-cell Function in Type 2 Diabetic Mice. *Carbohydr. Polym.* 211, 39–48. doi:10.1016/j.carbpol.2019.01.101

Wang, X.-C., Zheng, Z.-P., Gan, X.-W., and Hu, L.-H. (2009). Jatrophalactam, a Novel Diterpenoid Lactam Isolated from *Jatropha curcas*. *Org. Lett.* 11, 5522–5524. doi:10.1021/ol902349f

Wang, X., Shaaban, K. A., Elshahawi, S. I., Ponomareva, L. V., Sunkara, M., Zhang, Y., et al. (2013). Frenolicins C-G, Pyranonaphthoquinones from streptomyces sp. RM-4-15. *J. Nat. Prod.* 76, 1441–1447. doi:10.1021/np400231r

Wang, Y.-H. (2021). Traditional Uses, Chemical Constituents, Pharmacological Activities, and Toxicological Effects of *Dendrobium* Leaves: A Review. *J. Ethnopharmacology* 270, 113851. doi:10.1016/j.jep.2021.113851

Xu, F., Chen, X., Hu, J., Zhao, H., Peng, D., Wu, D., et al. (2022). Cytotoxic Picrotoxane-type Sesquiterpenoid Lactones from *Dendrobium huoshanense*. *Rec. Nat. Prod.* 16, 144–149. doi:10.25135/rnp.260.21.04.2048

Yeo, W.-H., Yun, B.-S., Kim, S.-S., Park, E.-K., Kim, Y.-H., Yoo, I.-D., et al. (1998). GTRI-02, a New Lipid Peroxidation Inhibitor from *Micromonospora* sp. SA246. *J. Antibiot.* 51, 952–953. doi:10.7164/antibiotics.51.952

Zhao, H., Chen, X., Chen, X., Zhu, Y., Kong, Y., Zhang, S., et al. (2020c). New Peptidendrocins and Anticancer Chartreusin from an Endophytic Bacterium of *Dendrobium officinale*. *Ann. Transl. Med.* 8, 455. doi:10.21037/atm.2020.03.227

Zhao, H., Yang, A., Liu, J., Bao, S., Peng, R., Hu, Y., et al. (2020b). Chartspiroton, a Tetracyclic spiro-naphthoquinone Derivative from a Medicinal Plant Endophytic *Streptomyces*. *Org. Lett.* 22, 3739–3743. doi:10.1021/acs.orglett.0c00696

Zhao, H., Yang, A., Zhang, N., Li, S., Yuan, T., Ding, N., et al. (2020a). Insecticidal Endostemonines A-J Produced by Endophytic *Streptomyces* from *Stemona sessilifolia*. *J. Agric. Food Chem.* 68, 1588–1595. doi:10.1021/acs.jafc.9b06755

Zhu, Y., Li, S., Kong, Y., Zhao, H., Hu, Y., Meng, J., et al. (2021). Terragines F-G Produced by *Endophytic bacillus* sp. SH-1.2-ROOT-18 from *Dendrobium officinale*. *Nat. Product. Res.* doi:10.1080/14786419.2021.1914614

Conflict of Interest: The authors declare that the research was conducted in the absence of any commercial or financial relationships that could be construed as a potential conflict of interest.

Publisher's Note: All claims expressed in this article are solely those of the authors and do not necessarily represent those of their affiliated organizations, or those of the publisher, the editors, and the reviewers. Any product that may be evaluated in this article, or claim that may be made by its manufacturer, is not guaranteed or endorsed by the publisher.

frontiers in Chemistry

ORIGINAL RESEARCH
published: 15 February 2022
doi: 10.3389/fchem.2022.842405

Metabolites With Cytotoxic Activities From the Mangrove Endophytic Fungus *Fusarium* sp. 2ST2

Yan Chen[1,2], *Guisheng Wang*[1], *Yilin Yuan*[1], *Ge Zou*[2], *Wencong Yang*[2], *Qi Tan*[2], *Wenyi Kang*[1]* *and Zhigang She*[2]*

[1]National R & D Center for Edible Fungus Processing Technology, Henan University, Kaifeng, China, [2]School of Chemistry, Sun Yat-sen University, Guangzhou, China

Two new 3-decalinoyltetramic acid derivatives with peroxide bridge fusarisetins E (**1**) and F (**2**), one new chromone fusarimone A (**5**), two new benzofurans fusarifurans A (**9**) and B (**10**), three new isocoumarins fusarimarins A–C (**11–13**), as well as five known analogues **3**, **4**, **6–8** and **14** were isolated from mangrove endophytic fungus *Fusarium* sp. 2ST2. Their structures and absolute configurations were established by spectroscopic analysis, density functional theory-gauge invariant atomic orbital NMR calculation with DP4+ statistical analysis, and electronic circular dichroism calculation. Compounds **1** and **2** showed significant cytotoxicity against human A549 cell lines with IC_{50} values of 8.7 and 4.3 μM, respectively.

Keywords: mangrove, endophytic fungus, *Fusarium* sp., cytotoxicity, benzofuran, chromone

OPEN ACCESS

Edited by:
Xiachang Wang,
Nanjing University of Chinese Medicine, China

Reviewed by:
Wei Xu,
State Oceanic Administration, China
ChunLan Xie,
Xiamen University, China

***Correspondence:**
Wenyi Kang
kangwenyi@henu.edu.cn
Zhigang She
cesshzhg@mail.sysu.edu.cn

Specialty section:
This article was submitted to Organic Chemistry, a section of the journal Frontiers in Chemistry

Received: *23 December 2021*
Accepted: *12 January 2022*
Published: *15 February 2022*

Citation:
Chen Y, Wang G, Yuan Y, Zou G, Yang W, Tan Q, Kang W and She Z (2022) Metabolites With Cytotoxic Activities From the Mangrove Endophytic Fungus Fusarium sp. 2ST2. Front. Chem. 10:842405. doi: 10.3389/fchem.2022.842405

INTRODUCTION

Endophytic fungi, inhabiting plants without any negative effects for the host, have been proven to be a promising source of novel structures and unique bioactivities (Liu et al., 2021; Viridiana et al., 2021). *Fusarium* spp. are endophytic fungi widely distributed in association with plants. It has attracted much attention due to their diverse bioactive secondary metabolites, including alkaloids, terpenes, cyclopeptide, anthraquinone, and lactones (Chen et al., 2019)—for example, indole alkaloids fusaindoterpenes A and B from *Fusarium* sp. showed antiviral activity (Guo et al., 2020), and fusarithioamide A from *Fusarium chlamydosporium* exhibited cytotoxic activity (Ibrahim et al., 2018).

Mangrove endophytic fungi, the second largest ecological group of marine fungi, have been reported to produce thousands of new metabolites until now (Chen et al., 2021; Chen et al., 2022). Over the past 2 decades, our group continues to explore bioactive novel structures from mangrove endophytic fungi (Huang et al., 2013; Xiao et al., 2013; Liu et al., 2016; Cui et al., 2017; Cai et al., 2019). In the course of our ongoing search for new antitumor active compounds from mangrove endophytic fungi, the strain *Fusarium* sp. 2ST2 attracted our attention because of the cytotoxicity of the crude extract. Then, eight new metabolites, including two alkaloids fusarisetin E (**1**) and F (**2**), one chromone fusarimone A (**5**), two benzofurans fusarifurans A (**9**) and B (**10**), three isocoumarins fusarimarins A–C (**11–13**), were obtained together with five analogues equisetin (**3**), epi-equisetin (**4**), takanechromone B (**6**), altechromone A (**7**), 4H-1-benzopyran-4-one-2,3-dihydro-5-hydroxy-8-(hydroxylmethyl)-2-methyl (**8**), and aspergisocoumrin A (**14**) (**Figure 1**). As expected, compounds **1** and **2** exhibited significant cytotoxicity against human A549 cell line, and compounds **8** and **14** showed potent cytotoxicity against A549 and MDA-MB-435 cell lines. The isolation, structure elucidation, and biological evaluation of these compounds were reported herein.

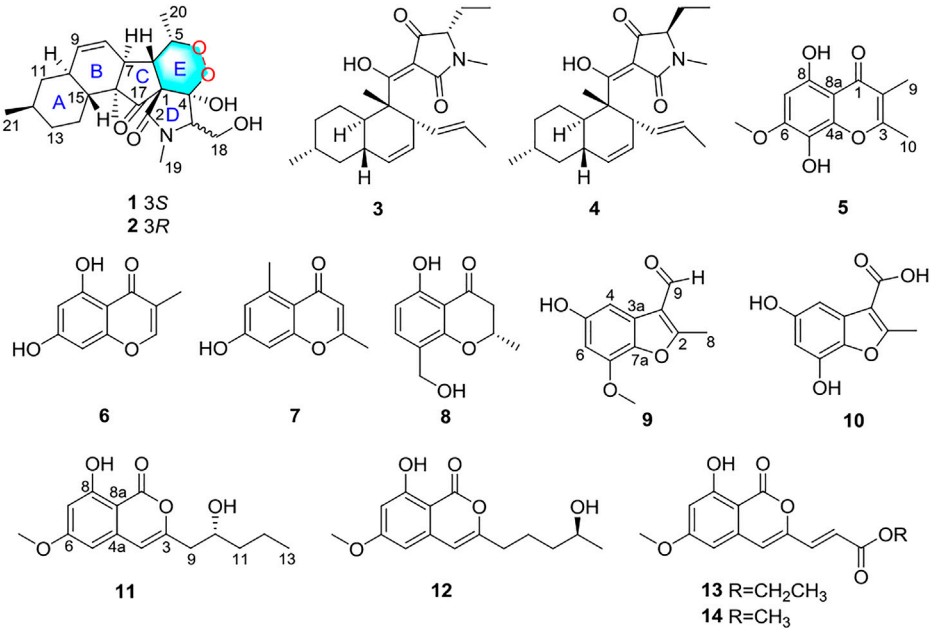

FIGURE 1 | Structures of compounds **1**–**14**.

MATERIALS AND METHODS

General Experimental Procedures

Optical rotations were measured on a PerkinElmer 341 instrument at 25°C. Melting points were recorded on a Fisher-Johns hot-stage apparatus. UV spectra were measured in MeOH using a Shimadzu UV-2700 spectrophotometer. Electronic circular dichroism (ECD) data were obtained on a Chirascan CD spectrometer (Applied Photophysics). A Bruker Avance 500 spectrometer (^{1}H 500 MHz, ^{13}C 125 MHz) was used for the 1D and 2D NMR data collection. All high-resolution electrospray ionization mass spectrometry (HRESIMS) data were obtained on an Agilent G6230 Q-TOF mass spectrometer. Silica gel (200–300 mesh, Qingdao Marine Chemical Factory) and Sephadex LH-20 (Amersham Pharmacia) were used in the column chromatography (CC). Silica gel plates (Qingdao Huang Hai Chemical Group Co., G60, F-254) were used for the thin-layer chromatography.

Fungal Material

The fungus *Fusarium* sp. 2ST2 was isolated from healthy leaves of *Kandelia candel*, which was collected in June 2015 from the South China Sea, Dong Zhai Harbor Mangrove Nature Reserve Area, Hainan Province, China. The strain was identified as *Fusarium* sp. (GenBank no. MZ801734) by a BLAST search which showed it to be 100% identical with the sequence of *Fusarium* sp. (GenBank no. KU296944.1).

Fermentation, Extraction, and Isolation

The fungus *Fusarium* sp. 2ST2 was cultivated on potato dextrose agar for 5 days. The mycelia of the strain were inoculated into 500 ml potato dextrose broth for 3 days to prepare the seed culture and then inoculated into the solid rice medium (70 g of rice, 3 g peptone, and 50 ml of distilled water, 60 flasks). It was incubated for 30 days at room temperature.

The medium was extracted with MeOH for three times, and the total residue of the strain (65.0 g) was obtained. The EtOAc extract was chromatographed by silica gel CC (200–300 mesh silica) and eluted with an increasing gradient of petroleum ether/EtOAc (9:1 to 1:9) to afford six fractions (Fr. A–F). Fraction B was applied to Sephadex LH-20 CC (CH_2Cl_2/MeOH v/v, 1:1) to give three fractions (Fr. B1–B3). Fraction B1 was subjected to silica gel CC (CH_2Cl_2/MeOH v/v, 98:2) to yield compounds **3** (5.8 mg) and **14** (2.5 mg). Fraction B2 was subjected to silica gel CC (CH_2Cl_2/MeOH v/v, 96:4) to yield compounds **9** (8.6 mg) and **13** (4.3 mg). Fraction C was eluted on Sephadex LH-20 CC (100% MeOH) to obtain compound **10** (7.5 mg) and two other fractions (Fr. C1–C2). Fraction C2 was separated using silica gel CC (CH_2Cl_2/MeOH v/v, 95:5) to yield compounds **11** (3.1 mg) and **12** (3.5 mg). Fraction D was eluted on Sephadex LH-20 CC (100% MeOH) to afford three fractions (Fr. D1–D3). Fraction D1 was purified by semipreparative UPLC (MeOH-H_2O, 7:3) to give compounds **1** (3.6 mg) and **2** (4.0 mg). Fraction D2 was subjected to silica gel CC (CH_2Cl_2/MeOH v/v, 9:1) to give compounds **4** (2.5 mg) and **7** (6.5 mg). Fraction E was subjected to Sephadex LH-20 CC (CH_2Cl_2/MeOH v/v, 1:1) to give compound **6** (3.8 mg) and another fraction E1. Compounds **5** (3.0 mg) and **8** (2.8 mg) were obtained from fraction E1, which was subjected to UPLC (MeOH-H_2O, 6:4).

"Fusarisetin E (**1**): Colorless oil, [α] + 10.0 (*c* = 0.16, MeOH). UV (MeOH) λ_{max} (log ε): 206 (3.02), 280 (2.16) nm. HRESIMS *m/*

TABLE 1 | ^{1}H and ^{13}C NMR data of compounds **1** and **2**.

No.	1			2		
	δ_C[a]	δ_H[a]	δ_H[b]	δ_C[a]	δ_H[a]	δ_Hb
1	65.1			65.3		
2	171.2			172.1		
3	68.9	3.16, dd (5.3, 6.8)	3.0, dd (4.2, 7.8)	68.6	4.0, dd (2.7, 7.4)	3.82, brd (8.5)
4	103.2			103.2		
5	76.8	4.37, qd (3.1, 6.9)	4.26, m	76.7	4.36, qd (3.2, 6.9)	4.23, m
6	46.2	2.59, dd (3.1, 11.9)	2.73, dd (3.6, 11.7)	45.1	2.59, dd (3.1, 11.9)	2.76, brd (9.5)
7	44.6	2.85, dd (4.7, 11.9)	2.44, dd (2.2, 11.9)	44.4	2.86, dd (4.6, 11.8)	2.44, dd (2.2, 12.0)
8	127.7	5.89, ddd (2.4, 4.8, 10.1)	5.84, brd (8.8)	127.7	5.88, ddd (2.4, 4.8, 10.1)	5.83, brd (8.8)
9	133.8	5.56, brd (10.1)	5.52, brd (10.1)	133.7	5.56, brd (10.1)	5.52, brd (9.8)
10	38.4	1.89, m	1.84, m	38.3	1.88, m	1.84, m
11	43.0	1.87, m	1.81, m	43.1	1.86, m	1.81, m
		0.82, q (12.7)	0.73, q (12.7)		0.82, q (12.7)	0.73, q (12.7)
12	34.1	1.49, m	1.41, m	34.1	1.49, m	1.41, m
13	36.5	1.75, m	1.70, m	36.4	1.75, m	1.70, m
		0.91, m	0.85, m		0.90, m	0.85, m
14	26.3	1.56, m	1.45, m	26.3	1.55, m	1.45, m
		1.0, m	1.04, m		1.0, m	1.04, m
15	40.0	1.37, m	1.18, m	39.8	1.37, m	1.18, m
16	53.2			53.1		
17	214.3			213.5		
18	62.6	4.07, dd (6.9, 11.7)	3.88, m	58.5	3.95, dd (2.8, 12.3)	3.87, brd (12.1)
		3.96, dd (5.3, 11.7)	3.78, dd (3.1, 11.0)		3.66, dd (7.4, 12.3)	3.38, m
19	30.5	3.03, s	2.92, s	28.6	3.02, s	2.88, s
20	17.7	1.34, d (7.0)	1.26, d (6.9)	17.4	1.33, d (7.0)	1.24, d (6.1)
21	22.7	0.93, d (6.5)	0.86, d (6.5)	22.7	0.93, d (6.5)	0.87, d (6.3)
22	15.0	1.0, s	0.89, s	14.7	1.0, s	0.91, s
OH-4				4.88, s		4.9, s
OH-18				7.3, s		7.5, s

[a]*Measured in CD_3OD.*
[b]*Measured in DMSO-d_6.*

TABLE 2 | ^{1}H and ^{13}C NMR data of compound **5** in $CDCl_3$.

No.	5		No.	5	
	δ_C	δ_H		δ_C	δ_H
1	182.2		8	154.3	
2	114.7		8a	104.2	
3	162.9		9	9.2	2.02, s
4a	143.3		10	18.6	2.44, s
5	125.2		OCH_3-6	56.5	3.96, s
6	151.4		OH-5		5.14, s
7	94.5	6.41, s	OH-8		12.51, s

TABLE 3 | ^{1}H and ^{13}C NMR data of **9** and **10** in CD_3OD.

No.	9		10	
	δ_C	δ_H (*J* in Hz)	δ_C	δ_H (*J* in Hz)
2	169.4		163.5	
3	119.1		128.4	
3a	127.6		109.0	
4	98.9	7.02, d (2.2)	99.6	6.84, d (2.3)
5	139.1		137.2	
6	98.6	6.44, d (2.2)	97.3	6.27, d (2.3)
7	146.5		141.8	
7a	156.9		154.3	
8	12.7	2.75, s	13.1	2.70, s
9	187.4	10.14, s	166.3	
10	56.5	3.95, s		

z 406.22293 $[M + H]^+$ (calculated for $C_{22}H_{32}NO_6$ 406.22241). ^{1}H and ^{13}C NMR (CD_3OD-d_4) data, see **Table 1**.

Fusarisetin E (**2**): Colorless oil, [α] + 11.2 (*c* = 0.19, MeOH). UV (MeOH) λ_{max} (log ε): 204 (3.0), 282 (2.56) nm. HRESIMS *m/z* 406.22274 $[M + H]^+$ (calculated for $C_{22}H_{32}NO_6$ 406.22241). ^{1}H and ^{13}C NMR (CD_3OD-d_4) data, see **Table 1**.

Fusarimone A (**5**): Yellow solid. HRESIMS *m/z* 237.07583 $[M + H]^+$ (calculated for $C_{12}H_{13}O_5$ 237.07575). ^{1}H and ^{13}C NMR ($CDCl_3$) data, see **Table 2**.

Fusarifuran A (**9**): White solid, HRESIMS *m/z* 205.05090 [M-H]- (calculated for $C_{11}H_9O_4$ 205.05063). ^{1}H and ^{13}C NMR (CD_3OD-d_4) data, see **Table 3**.

Fusarifuran B (**10**): White solid, HRESIMS *m/z* 207.03026 $[M-H]^-$ (calculated for $C_{10}H_7O_5$ 207.02990). ^{1}H and ^{13}C NMR (CD_3OD-d_4) data, see **Table 3**.

Fusarimarin A (**11**): Colorless oil, [α] −21.5 (c 0.06, MeOH). UV (MeOH) λ_{max} (log ε): 219 (3.2), 238 (2.4), 318 (3.5) nm. HRESIMS *m/z* 279.12288 $[M + H]^+$ (calculated for $C_{15}H_{19}O_5$ 279.12270). ^{1}H and ^{13}C NMR ($CDCl_3$) data, see **Table 4**.

Fusarimarin B (**12**): Colorless oil, [α] +18.6 (c 0.07, MeOH). UV (MeOH) λ_{max} (log ε): 220 (3.3), 252 (3.0), 316 (3.4) nm.

TABLE 4 | ^{1}H and ^{13}C NMR data of **11–13** in $CDCl_3$.

No.	11		12		13	
	δ_C	δ_H (*J* in Hz)	δ_C	δ_H (*J* in Hz)	δ_C	δ_H (*J* in Hz)
1	166.2		166.6		164.8	
3	155.0		157.7		149.8	
4	106.1	6.29, s	104.3	6.19, s	111.8	6.60, s
4a	139.1		139.5		134.3	
5	101.4	6.33, d (2.2)	100.4	6.46, d (2.2)	103.6	6.49, brs
6	166.9		166.9		166.8	
7	100.5	6.48, d (2.2)	101.3	6.31, d (2.2)	102.1	6.58, brs
8	163.6		163.8		163.9	
8a	100.0		100.1		102.1	
9	41.6	2.69, dd (3.7, 14.6) 2.55, dd (8.6, 14.6)	33.3	2.53, t (2.5)	134.3	7.22, d (15.5)
10	68.9	4.07, m	23.2	1.83, m 1.73, m	122.5	6.68, d (15.5)
11	39.3	1.53, m	38.5	1.52, m	166.1	
12	18.7	1.51, m	67.9	3.84, m	61.0	4.29, dd (7.1, 14.1)
13	14.0	0.96, t (6.9)	23.9	1.22, d (6.2)	14.2	1.36, t (7.0)
OH-8		11.10, s		11.10, s		11.0, s
OCH_3-6	55.7	3.87, s	55.8	3.86, s	55.9	3.91, s

HRESIMS *m/z* 279.12290 $[M + H]^+$ (calculated for $C_{15}H_{19}O_5$ 279.12270). ^{1}H and ^{13}C NMR ($CDCl_3$) data, see **Table 4**.

Fusarimarin C (**13**): Colorless oil, HRESIMS *m/z* 291.08639 $[M + H]^+$ (calculated for $C_{15}H_{15}O_6$ 291.08631). ^{1}H and ^{13}C NMR ($CDCl_3$) data, see **Table 4**.

NMR Calculations

In general, conformational analysis was carried out using Merck Molecular Field by Spartan's 10 software. Conformers above 1% Boltzmann populations were optimized at the B3LYP/6-311+G (d, p) level in polarizable continuum model (PCM) methanol (Gaussian 09). Subsequently, NMR calculations were computed using the gauge invariant atomic orbital (GIAO) method at the mPWLPW91-SCRF/6-311+G (d, p) level using the PCM in methanol (Gaussian 09). Finally, the shielding constants were averaged by Boltzmann distribution theory for each stereoisomer, and their experimental and calculation data were analyzed by DP4+ probability.

ECD Calculations

The ECD calculations were performed as described previously (Chen et al., 2020). Geometric optimization of compounds **1** and **2** was carried out at the B3LYP/6-31+G(d) level in the liquid phase. Then, ECD calculations were performed using the TDDFT methodology at the WB97XD/CC-PVDZ and WB97XD/6-31G levels, respectively.

Cytotoxicity Assay

The cytotoxicity of all compounds against tumor cell lines was tested by the MTT assay as previously reported (Chen et al., 2019).

RESULTS AND DISCUSSION

Compound **1** was isolated as a colorless oil. The molecular formula was determined as $C_{22}H_{32}NO_6$ based on the HRESIMS data (*m/z* 406.22293 $[M + H]^+$). The ^{1}H NMR data of **1** (**Table 1**) showed three methyl signals at δ_H 0.93 (d, *J* = 6.5 Hz), 1.0 (s), and 1.34 (d, *J* = 7.0 Hz), one N-methyl proton at δ_H 3.03 (s), and two olefinic protons at δ_H 5.56 (brd, *J* = 10.1 Hz) and 5.89 (ddd, *J* = 2.4, 4.8, 10.1 Hz). The ^{13}C NMR data of **1** (**Table 1**) displayed 22 carbon signals, including four methyls, four methylenes (one oxygenated), seven methines (two olefinic), and four quaternary carbons (one ketone carbonyl and one ester carbonyl carbon). The planar structure of **1** was a detailed analysis of the 1D and 2D NMR data. The spin system of H_3-20/H-5/H-6/H-7/H-8/H-9/H-10/H_2-11/H-12(/H_3-21)/H_2-13/H_2-14/H-15(/H-10) from ^{1}H-^{1}H COSY data (**Figure 2**), together with the heteronuclear multiple-bond correlations (HMBC) (**Figure 2**) from H_3-22 to C-7, C-15, C-16 and C-17 and from H-6 to C-1, established the partial ring system of A/B/C, while the HMBC correlations from H-6 to C-2 and C-4, from H-3 to C-1 and C-4, and from H_3-19 to C-2 and C-3 indicated the presence of a γ-lactam moiety (ring D). In addition, a peroxide bridge between C-4 and C-5 was proposed according to two additional oxygen atoms in the molecular formula of **1**, which constitute the ring E. Thus, the planar structure of **1** was deduced (**Figure 1**), which was similar to fusarisetin A (Jang et al., 2011), by comparing their NMR data.

Compound **2**, with a molecular formula of $C_{22}H_{32}NO_6$, the same as **1**, was isolated as a colorless oil. The results of comparing the NMR data of **1** and **2** indicated that they shared a planar structure, and this was further confirmed by an extensive analysis of ^{1}H-^{1}H COSY and HMBC correlations (**Figure 2**), while the major difference of NMR shifts at H-3 ($\Delta\delta_H$ +0.84), C-18 ($\Delta\delta_C$ −4.1), and C-19 ($\Delta\delta_C$ −1.9) suggested **1** and **2** to be 3-epimers.

The relative configurations of **1** and **2** were determined by the NOESY correlations (**Figure 3**). The cross-peaks of H-12/H-10/H_3-22/H-7/H_3-20 suggested that these protons were co-facial, while the correlations of H_3-21/H-15/H-6 showed that these protons were on the other face. Considering the absence of

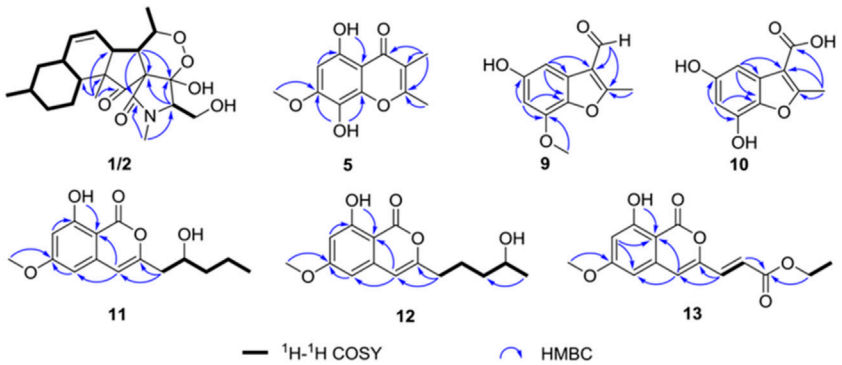

FIGURE 2 | Key heteronuclear multiple-bond correlations and correlation spectroscopy of compounds **1**, **2**, **5** and **9–13**.

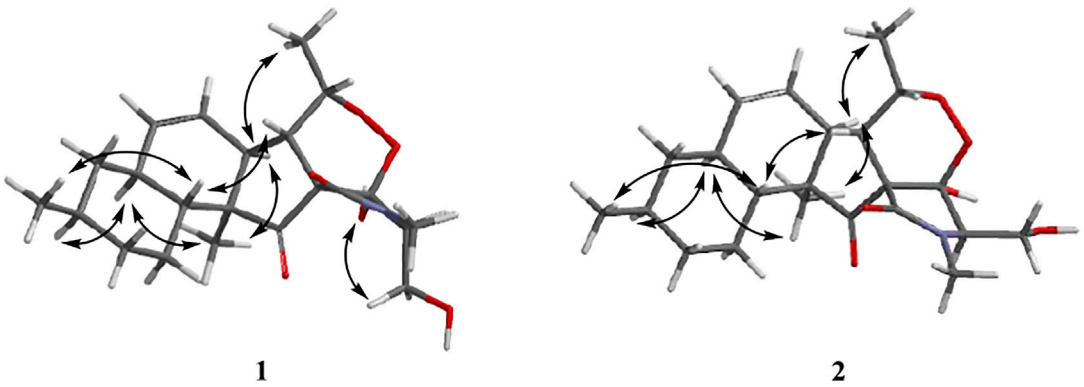

FIGURE 3 | Key nuclear Overhauser effect correlations of compounds **1** and **2**.

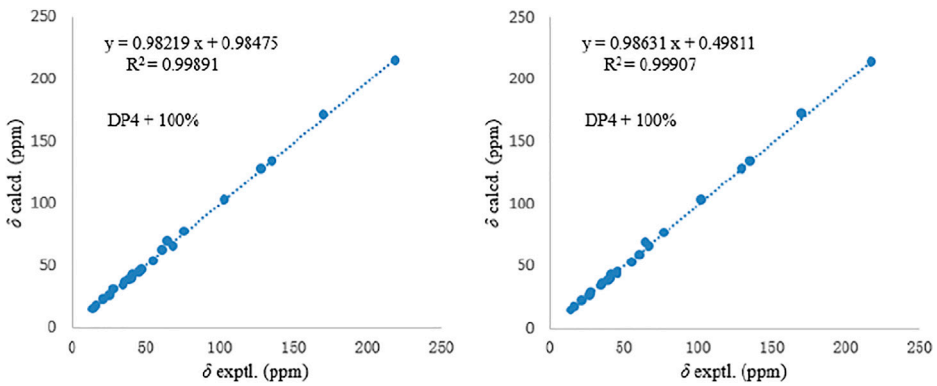

FIGURE 4 | Comparisons of calculated and experimental ^{13}C NMR data of **1** and **2**.

correlation from H_2-18 and 4-OH to other protons, the NOESY spectrum of **1** and **2** were retested in DMSO-d_6 reagent. Then, the correlation of 4-OH/H_2-18 was only detected in **1**, indicating that the protons of OH-4 and H_2-18 were positioned on the same face in **1** and were opposite in **2**. Thus, **1** and **2** were an epimer at C-3. Subsequently, the ^{13}C NMR calculations of (1*R**, 3*S**, 4*R**, 5*S**, 6*S**, 7*S**, 10*S**, 21*R**, 15*R**, 16*S**)-**1a** and (1*R**, 3*R**, 4*S**, 5*S**, 6*S**, 7*S**, 10*S**, 21*R**, 15*R**, 16*S**)-**1b** were carried out using the GIAO method at mPW1PW91-SCRF/6–311+G (d, p)/PCM (MeOH). The results of the DP4+ probability analysis (Smith and Goodman, 2010; Kawazoe et al., 2020; Xu et al., 2021) showed that **1a** was the most likely candidate structure, with a better correlation coefficient (R^2 = 0.99891) and a high DP4+ probability of 100% (all data) probability (**Figure 4**). Similarly,

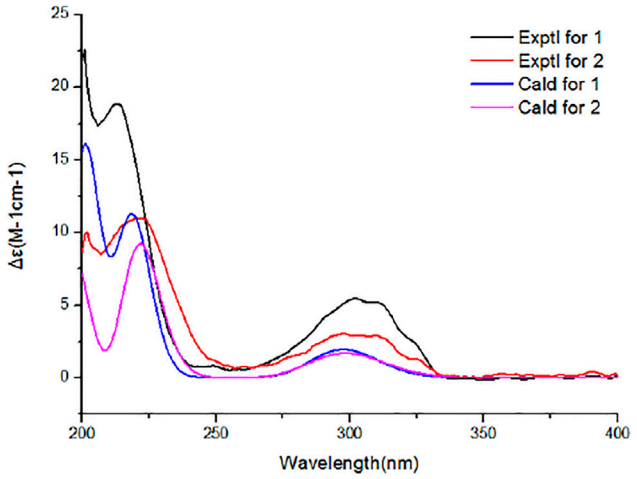

FIGURE 5 | Calculated and experimental electronic circular dichroism spectra of **1** and **2**.

^{13}C NMR calculations with the DP4+ probability analysis of the two isomers [(1*R**, 3*S**, 4*S**, 5*S**, 6*S**, 7*S**, 10*S**, 21*R**, 15*R**, 16S*)-**2a** and (1*R**, 3*R**, 4*R**, 5*S**, 6*S**, 7*S**, 10*S**, 21*R**, 15*R**, 16*S**)-**2b**] of **2** were performed. The results showed that **2** gave the best match of 100% (all data) with the **2b** isomer.

Aiming at determining the absolute configuration of **1**, the ECD calculation was performed at the WB97XD/CC-PVDZ level. The results showed that the calculated ECD curve was in good agreement with the experimental one (**Figure 5**). Therefore, the absolute configuration of **1** was assigned as 1*R*, 3*S*, 4*R*, 5*S*, 6*S*, 7*S*, 10*S*, 21*R*, 15*R*, 16*S*. The absolute configuration of **2** was determined to be 1*R*, 3*R*, 4*R*, 5*S*, 6*S*, 7*S*, 10*S*, 21*R*, 15*R*, 16*S* by the identical experimental and calculated curves (**Figure 5**).

Compound **5** was obtained as a yellow solid. The molecular formula was determined to be $C_{12}H_{13}O_5$ based on HRESIMS data (*m/z* 237.07583 $[M + H]^+$). The ^{1}H NMR spectrum (**Table 2**) of **5** showed two methyl groups at δ_H 2.02 (s), 2.44 (s), one methoxyl group at δ_H 3.96 (s), one olefinic proton at δ_H 6.41 (s), and one chelated hydroxyl group at δ_H 12.51 (s). The ^{13}C NMR data (**Table 2**) of **5** highlighted the presence of 12 carbon resonances, including three methyls (one oxygenated), one olefinic carbon, and eight quaternary carbons (one carbonyl carbon and seven olefinic carbons). The ^{1}H and ^{13}C NMR data of **5** were similar to those of **6**, indicating that **5** was one chromone. The structure of **5** was further established by the HMBC correlations (**Figure 2**) from H_3-9 to C-1, C-2, and C-3 and from H_3-10 to C-3.

Compound **9** was obtained as a white solid. The molecular formula was determined to be $C_{11}H_9O_4$ based on HRESIMS data. The ^{1}H NMR spectrum (**Table 3**) of **9** showed one methyl group at δ_H 2.75 (s), one methoxyl group at δ_H 3.95 (s), and two aromatic protons at δ_H 7.02 (d, J = 2.2 Hz),6.44 (d, J = 2.2 Hz). The ^{13}C NMR data (**Table 3**) of **9** highlighted the presence of 11 carbon resonances, including two methyls, two sp^2 methines, and seven quaternary carbons. These data suggest **9** to be a benzofuran derivate. The NMR data of **9** were closely similar to penicifuran C (Qi et al., 2013), except for the presence of a methoxyl group, The HMBC correlations (**Figure 2**) from H_3-10 to C-7 indicated that the methoxyl group was located at C-7. Thus, the structure of **9** was determined as shown in **Figure 1**.

Compound **10** was obtained as a white solid. The molecular formula was determined to be $C_{10}H_{13}O_5$ based on HRESIMS data. The ^{1}H and ^{13}C NMR data (**Table 3**) of **10** were similar to those of **9**, except that the aldehyde group in **9** was oxidized to the carboxyl group, and there was an absence of the methoxyl group. The deduction was further confirmed by the HMBC correlations (**Figure 2**) from H_3-8 to C-2, C-3, and C-9. Therefore, the structure of **10** was established as shown.

Compound **11** had the molecular formula of $C_{15}H_{18}O_5$ by the HRESIMS data. The ^{1}H NMR spectrum (**Table 4**) of **11** showed one chelated hydroxyl group at δ_H 11.10 (s), one methyl group at δ_H 0.96 (t, J = 6.9 Hz), one methoxyl group at δ_H 3.87 (s), and three olefinic protons at δ_H 6.29 (s), 6.33 (d, J = 2.2 Hz), and 6.48 (d, J = 2.2 Hz). The ^{13}C NMR data (**Table 4**) of **11** revealed the presence of 15 carbon resonances, including two methyls, three methylenes, one sp^3 and three sp^2 methines, and six quaternary carbons. These data suggest **11** to be an isocoumarin class. The spin system of H_2-9/H-10/H_2-11/H_2-12/H_3-13 in the ^{1}H-^{1}H COSY spectrum (**Figure 2**) as well as the HMBC correlations (**Figure 2**) from H_2-9 to C-3 and C-4 showed that the side chain was substituted at C-3. By comparing the specific rotation of **11** [[α]−21.5 (c 0.06, MeOH)] with (−)-citreoisocoumarin [[α] −29.8 (c 0.34, MeOH)] (Mallampudi et al., 2020), the 10*R* configuration at C-10 in **11** was indicated. Thus, the gross structure of **11** was defined as shown.

Compound **12** was isolated as a colorless oil. The molecular formula was determined to be $C_{15}H_{18}O_5$ based on HRESIMS data. The comparison of the ^{1}H and ^{13}C NMR data (**Table 4**) with those of **11** revealed that they share the same isocoumarin structure, except that the hydroxyl group was substituted at C-12 in 12. The spin system of H_2-9/H_2-10/H_2-11/H-12/H_2-13 in the ^{1}H-^{1}H COSY spectrum (**Figure 2**), together with the HMBC correlations (**Figure 2**) from H_2-9 to C-3 and C-4, further supported this possibility. The 12*S* configuration was confirmed by the positive specific rotation value of **12** [[α] +18.6 (c 0.07, MeOH)] when compared with peneciraistin D [[α] +21.1 (c 0.14, MeOH)] (Ma et al., 2012).

Compound **13** was isolated as a colorless oil with the molecular formula of $C_{15}H_{14}O_6$ based on HRESIMS data. Upon comparing the ^{1}H and ^{13}C NMR data (**Table 4**) between **11** and **13**, it was suggested that **13** also possessed the isocoumarin framework. The spin system of H-9/H-10 observed in the ^{1}H-^{1}H COSY spectrum (**Figure 2**) and the HMBC correlations (**Figure 2**) from H-9 to C-3 and C-4 from H-10 to C-11 made it possible to obtain the gross structure. Additionally, an ethyl group was linked with C-11 by the HMBC correlations from H-12 to C-11. The 9*E* configuration of the double bond was determined by the large coupling constant $J_{H\text{-}9,\,H\text{-}10}$ = 15.5 Hz. Thus, the structure of **13** was confirmed as shown in **Figure 1**.

Five known analogues were characterized as equisetin (**3**) (Zhao et al., 2019), epi-equisetin (**4**) (Zhao et al., 2019), takanechromone B (**6**) (Qader et al., 2021), altechromone A (**7**) (Tanaka et al., 2009), 4H-1-benzopyran-4-one- 2,3-dihydro-5-hydroxy-8-(hydroxylmethyl)-2-methyl (**8**) (Sousa et al., 2016), and aspergisocoumrin A (**14**) (Wu

TABLE 5 | Cytotoxicity of compounds **1–4**, **8** and **13** (IC_{50} ± SD, μM).

Compound	A549	HELA	KYSE150	PC-3	MDA-MB-435
1	8.7 ± 0.6	39.2 ± 0.7	36.3 ± 0.5	>50	>50
2	4.3 ± 0.2	>50	>50	>50	>50
4	15.3 ± 0.6	>50	>50	>50	>50
8	5.6 ± 1.3	>50	>50	>50	3.8 ± 0.3
13	>50	>50	>50	>50	30.5 ± 0.1
14	6.2 ± 0.2	—	—	—	2.8 ± 0.8
DDP[a]	25.9 ± 0.8	10.0 ± 0.1	72.6 ± 4.3	41.6 ± 0.9	9.6 ± 0.9

[a]*Positive control. "—" not tested.The IC_{50} values were expressed as means ± SD (n = 3) from three independent experiments.*

et al., 2019) through a comparison of the spectroscopic data with the literature.

All compounds were evaluated for their cytotoxicity against the A549 (lung carcinoma), HELA (cervical carcinoma), KYSE150 (esophageal squamous carcinoma), PC-3 (pancreatic carcinoma), and MDA-MB-435 (breast carcinoma) human cancer cell lines (**Table 5**). As a result, compounds **1** and **2** showed selective cytotoxicity against A549 cell line with IC_{50} values of 8.7 and 4.3 μM, respectively. Compound **8** showed potent cytotoxicity against A549 and MDA-MB-435 cell lines with IC_{50} values of 5.6 and 3.8 μM, respectively. Compound **14** exhibited significant cytotoxicity against A549 and MDA-MB-435 cell lines with IC_{50} values of 6.2 and 2.8 μM, respectively, while the other compounds exhibited non-significant activity against the five cancer cell lines at the concentration of 50 μM.

CONCLUSION

In summary, two new 3-decalinoyltetramic acid (3DTA) derivatives, fusarisetins E (**1**) and F (**2**), with a peroxide bridge, were isolated from mangrove endophytic fungus *Fusarium* sp. 2ST2. The 3DTA derivatives showed various bioactivities, such as antimicrobial, anticancer, larvicidal, cytotoxic, and antiviral (Fan et al., 2020). The structure of fusarisetins E (**1**) and F (**2**) was similar to that of fusarisetin A, which was first isolated from the soil fungus *Fusarium* sp. FN080326 with inhibitory activity to acinar morphogenesis (Jang et al., 2011), while fusarisetin E (**1**) was identified as peroxyfusarisetin (Yin et al., 2012), a synthetic intermediate by mixture. Here fusarisetin E (**1**) was reported first as an optically pure new natural product with 1D and 2D NMR data (**Supplementary Figures S1–S8**). Moreover, natural peroxide compounds that usually have unique pharmacological activities, such as artemisinin with antimalarial activity (Zhao et al., 2018; Pandey et al., 1999), talaperoxides A-D with cytotoxicity (Li et al., 2011), phaeocaulisin M with anti-inflammatory activity (Ma et al., 2015), 1α,8α-epidioxy-4α-hydroxy-5αH-guai-7(11),9-dien-12,8-olide with antiviral activity (Dong et al., 2013), and plakinic acid M with antifungal activity (Matthew et al., 2016), were reported. Compounds **1** and **2** had selective cytotoxicity against A549 cell line with IC_{50} values of 8.7 and 4.38 μM, respectively. The cytotoxicity of fusarisetins was reported for the first time.

DATA AVAILABILITY STATEMENT

The original contributions presented in the study are included in the article/**Supplementary Material**, further inquiries can be directed to the corresponding authors.

AUTHOR CONTRIBUTIONS

YC performed the experiments, analyzed the data, and wrote the paper. GW and YY completed the biological activity test. GZ, WY, and QT participated in the experiments (fermentation and extraction of the strain). WK and ZS reviewed the manuscript. ZS designed and supervised the experiments. All authors have read and agreed to the published version of the manuscript.

FUNDING

This research received generous support and was funded by the National Natural Science Foundation of China (U20A2001, 21877133), Development Program of Guangdong Province (2020B1111030005), Key Project in Science and Technology Agency of Henan Province (212102311029), and Key Scientific Research Project in Colleges and Universities of Henan Province (22B350001).

SUPPLEMENTARY MATERIAL

The Supplementary Material for this article can be found online at: https://www.frontiersin.org/articles/10.3389/fchem.2022.842405/full#supplementary-material

REFERENCES

Cai, R., Jiang, H., Xiao, Z., Cao, W., Yan, T., Liu, Z., et al. (2019). (−)- and (+)-Asperginulin A, a Pair of Indole Diketopiperazine Alkaloid Dimers with a 6/5/4/5/6 Pentacyclic Skeleton from the Mangrove Endophytic Fungus Aspergillus Sp. SK-28. *Org. Lett.* 21, 9633–9636. doi:10.1021/acs.orglett.9b03796

Chen, J., Bai, X., Hua, Y., Zhang, H., and Wang, H. (2019a). Fusariumins C and D, Two Novel Antimicrobial Agents from *Fusarium Oxysporum* ZZP-R1

Symbiotic on Rumex Madaio Makino. *Fitoterapia* 134, 1–4. doi:10.1016/j.fitote.2019.01.016

Chen, S., Cai, R., Liu, Z., Cui, H., and She, Z. (2022). Secondary Metabolites from Mangrove-Associated Fungi: Source, Chemistry and Bioactivities. *Nat. Prod. Rep*. doi:10.1039/D1NP00041A

Chen, Y., Liu, Z., Huang, Y., Liu, L., He, J., Wang, L., et al. (2019b). Ascomylactams A-C, Cytotoxic 12- or 13-Membered-Ring Macrocyclic Alkaloids Isolated from the Mangrove Endophytic Fungus *Didymella* Sp. CYSK-4, and Structure Revisions of Phomapyrrolidones A and C. *J. Nat. Prod.* 82, 1752–1758. doi:10.1021/acs.jnatprod.8b00918

Chen, Y., Zhang, L., Zou, G., Li, C., Yang, W., Liu, H., et al. (2020). Anti-inflammatory Activities of Alkaloids from the Mangrove Endophytic Fungus *Phomopsis* Sp. SYSUQYP-23. *Bioorg. Chem.* 97, 103712. doi:10.1016/j.bioorg.2020.103712

Chen, Y., Zou, G., Yang, W., Zhao, Y., Tan, Q., Chen, L., et al. (2021). Metabolites with Anti-inflammatory Activity from the Mangrove Endophytic Fungus Diaporthe Sp. QYM12. *Mar. Drugs* 19, 56. doi:10.3390/md19020056

Cui, H., Lin, Y., Luo, M., Lu, Y., Huang, X., and She, Z. (2017). Diaporisoindoles A-C: Three Isoprenylisoindole Alkaloid Derivatives from the Mangrove Endophytic Fungus Diaporthe Sp. SYSU-HQ3. *Org. Lett.* 19, 5621–5624. doi:10.1021/acs.orglett.7b02748

Dong, J.-Y., Ma, X.-Y., Cai, X.-Q., Yan, P.-C., Yue, L., Lin, C., et al. (2013). Sesquiterpenoids from *Curcuma Wenyujin* with Anti-influenza Viral Activities. *Phytochemistry* 85, 122–128. doi:10.1016/j.phytochem.2012.09.008

Fan, B., Dewapriya, P., Li, F., Grauso, L., Blümel, M., Mangoni, A., et al. (2020). Pyrenosetin D, a New Pentacyclic Decalinoyltetramic Acid Derivative from the Algicolous Fungus Pyrenochaetopsis Sp. FVE-087. *Mar. Drugs* 18, 281. doi:10.3390/md18060281

Guo, Y.-W., Liu, X.-J., Yuan, J., Li, H.-J., Mahmud, T., Hong, M.-J., et al. (2020). l-Tryptophan Induces a Marine-Derived *Fusarium* Sp. To Produce Indole Alkaloids with Activity against the Zika Virus. *J. Nat. Prod.* 83, 3372–3380. doi:10.1021/acs.jnatprod.0c00717

Huang, X., Huang, H., Li, H., Sun, X., Huang, H., Lu, Y., et al. (2013). Asperterpenoid A, a New Sesterterpenoid as an Inhibitor of Mycobacterium tuberculosis Protein Tyrosine Phosphatase B from the Culture of Aspergillus Sp. 16-5c. *Org. Lett.* 15, 721–723. doi:10.1021/ol303549c

Ibrahim, S. R. M., Mohamed, G. A., Al Haidari, R. A., Zayed, M. F., El-Kholy, A. A., Elkhayat, E. S., et al. (2018). Fusarithioamide B, a New Benzamide Derivative from the Endophytic Fungus *Fusarium Chlamydosporium* with Potent Cytotoxic and Antimicrobial Activities. *Bioorg. Med. Chem.* 26, 786–790. doi:10.1016/j.bmc.2017.12.049

Jang, J.-H., Asami, Y., Jang, J.-P., Kim, S.-O., Moon, D. O., Shin, K.-S., et al. (2011). Fusarisetin A, an Acinar Morphogenesis Inhibitor from a Soil Fungus, Fusarium Sp. FN080326. *J. Am. Chem. Soc.* 133, 6865–6867. doi:10.1021/ja1110688

Kawazoe, R., Matsuo, Y., Saito, Y., and Tanaka, T. (2020). Computationally Assisted Structural Revision of Flavoalkaloids with a Seven-Membered Ring: Aquiledine, Isoaquiledine, and Cheliensisine. *J. Nat. Prod.* 83, 3347–3353. doi:10.1021/acs.jnatprod.0c00691

Li, H., Huang, H., Shao, C., Huang, H., Jiang, J., Zhu, X., et al. (2011). Cytotoxic Norsesquiterpene Peroxides from the Endophytic Fungus *Talaromyces flavus* Isolated from the Mangrove Plant *Sonneratia Apetala*. *J. Nat. Prod.* 74, 1230–1235. doi:10.1021/np200164k

Liu, G., Huo, R., Zhai, Y., and Liu, L. (2021). New Bioactive Sesquiterpeniods from the Plant Endophytic Fungus Pestalotiopsis theae. *Front. Microbiol.* 12, 641504. doi:10.3389/fmicb.2021.641504

Liu, Z., Chen, Y., Chen, S., Liu, Y., Lu, Y., Chen, D., et al. (2016). Aspterpenacids A and B, Two Sesterterpenoids from a Mangrove Endophytic Fungus *Aspergillus terreus* H010. *Org. Lett.* 18, 1406–1409. doi:10.1021/acs.orglett.6b00336

Ma, J.-H., Wang, Y., Liu, Y., Gao, S.-Y., Ding, L.-Q., Zhao, F., et al. (2015). Four New Sesquiterpenes from the Rhizomes ofCurcuma Phaeocaulisand Their iNOS Inhibitory Activities. *J. Asian Nat. Prod. Res.* 17, 532–540. doi:10.1080/10286020.2015.1046449

Ma, L.-Y., Liu, W.-Z., Shen, L., Huang, Y.-L., Rong, X.-G., Xu, Y.-Y., et al. (2012). Spiroketals, Isocoumarin, and Indoleformic Acid Derivatives from saline Soil Derived Fungus *Penicillium raistrickii*. *Tetrahedron* 68, 2276–2282. doi:10.1016/j.tet.2012.01.054

Mallampudi, N. A., Choudhury, U. M., and Mohapatra, D. K. (2020). Total Synthesis of (−)-Citreoisocoumarin, (−)-Citreoisocoumarinol, (−)-12-Epi-Citreoisocoumarinol, and (−)-Mucorisocoumarins A and B Using a Gold(I)-Catalyzed Cyclization Strategy. *J. Org. Chem.* 85, 4122–4129. doi:10.1021/acs.joc.9b03278

Matthew, T. J., Doralyn, S. D., and Tadeusz, F. M. (2016). Peroxide Natural Products from *Plakortis Zyggompha* and the Sponge Association *Plakortis Halichondrioides-Xestospongia Deweerdtae*: Antifungal Activity against *Cryptococcus Gattii*. *J. Nat. Prod.* 79, 555. doi:10.1021/acs.jnatprod.5b00951

Pandey, A. V., Tekwani, B. L., Singh, R. L., and Chauhan, V. S. (1999). Artemisinin, an Endoperoxide Antimalarial, Disrupts the Hemoglobin Catabolism and Heme Detoxification Systems in Malarial Parasite. *J. Biol. Chem.* 274, 19383–19388. doi:10.1074/jbc.274.27.19383

Qader, M. M., Hamed, A. A., Soldatou, S., Abdelraof, M., Elawady, M. E., Hassane, A. S. I., et al. (2021). Antimicrobial and Antibiofilm Activities of the Fungal Metabolites Isolated from the Marine Endophytes *Epicoccum Nigrum* M13 and *Alternaria alternata* 13A. *Mar. Drugs* 19, 232. doi:10.3390/md19040232

Qi, J., Shao, C.-L., Li, Z.-Y., Gan, L.-S., Fu, X.-M., Bian, W.-T., et al. (2013). Isocoumarin Derivatives and Benzofurans from a Sponge-Derived *Penicillium* Sp. Fungus. *J. Nat. Prod.* 76, 571–579. doi:10.1021/np3007556

Smith, S. G., and Goodman, J. M. (2010). Assigning Stereochemistry to Single Diastereoisomers by GIAO NMR Calculation: the DP4 Probability. *J. Am. Chem. Soc.* 132, 12946–12959. doi:10.1021/ja105035r

Sousa, J. P. B., Aguilar-Pérez, M. M., Arnold, A. E., Rios, N., Coley, P. D., Kursar, T. A., et al. (2016). Chemical Constituents and Their Antibacterial Activity from the Tropical Endophytic Fungus *Diaporthe* Sp. F2934. *J. Appl. Microbiol.* 120, 1501–1508. doi:10.1111/jam.13132

Tanaka, N., Kashiwada, Y., Nakano, T., Shibata, H., Higuchi, T., Sekiya, M., et al. (2009). Chromone and Chromanone Glucosides from *Hypericum Sikokumontanum* and Their Anti-Helicobacter pylori Activities. *Phytochemistry* 70, 141–146. doi:10.1016/j.phytochem.2008.11.006

Viridiana, M. S., Carmen, E. D., Olmeda, SA, Valcarcel, F, Elena, T., Azucena, G. C., et al. (2021). Bioactive Metabolites from the Endophytic Fungus *Aspergillus* Sp. SPH2. *J. Fungi* 7, 109. doi:10.3390/md13053091

Wu, Y., Chen, S., Liu, H., Huang, X., Liu, Y., Tao, Y., et al. (2019). Cytotoxic Isocoumarin Derivatives from the Mangrove Endophytic Fungus *Aspergillus* Sp. HN15-5D. *Arch. Pharm. Res.* 42, 326–331. doi:10.1007/s12272-018-1019-1

Xiao, Z. e., Huang, H., Shao, C., Xia, X., Ma, L., Huang, X., et al. (2013). Asperterpenols A and B, New Sesterterpenoids Isolated from a Mangrove Endophytic Fungus Aspergillus Sp. 085242. *Org. Lett.* 15, 2522–2525. doi:10.1021/ol401005j

Xu, M.-M., Zhou, J., Zeng, L., Xu, J., Onakpa, M. M., Duan, J.-A., et al. (2021). Pimarane-derived Diterpenoids with Anti-Helicobacter pylori Activity from the Tuber of Icacina Trichantha. *Org. Chem. Front.* 8, 3014–3022. doi:10.1039/d1qo00374g

Yin, J., Wang, C., Kong, L., Cai, S., and Gao, S. (2012). Asymmetric Synthesis and Biosynthetic Implications of (+)-Fusarisetin A. *Angew. Chem. Int. Ed.* 51, 7786–7789. doi:10.1002/anie.201202455

Zhao, D., Han, X., Wang, D., Liu, M., Gou, J., Peng, Y., et al. (2019). Bioactive 3-Decalinoyltetramic Acids Derivatives from a Marine-Derived Strain of the Fungus *Fusarium Equiseti* D39. *Front. Microbiol.* 10, 1285. doi:10.3389/fmicb.2019.01285

Zhao, Q., Gao, J.-J., Qin, X.-J., Hao, X.-J., He, H.-P., and Liu, H.-Y. (2018). Hedychins A and B, 6,7-Dinorlabdane Diterpenoids with a Peroxide Bridge from Hedychium Forrestii. *Org. Lett.* 20, 704–707. doi:10.1021/acs.orglett.7b03836

Conflict of Interest: The authors declare that the research was conducted in the absence of any commercial or financial relationships that could be construed as a potential conflict of interest.

Publisher's Note: All claims expressed in this article are solely those of the authors and do not necessarily represent those of their affiliated organizations or those of the publisher, the editors, and the reviewers. Any product that may be evaluated in this article or claim that may be made by its manufacturer is not guaranteed or endorsed by the publisher.

Advantages of publishing in Frontiers

OPEN ACCESS
Articles are free to read for greatest visibility and readership

FAST PUBLICATION
Around 90 days from submission to decision

HIGH QUALITY PEER-REVIEW
Rigorous, collaborative, and constructive peer-review

TRANSPARENT PEER-REVIEW
Editors and reviewers acknowledged by name on published articles

Frontiers
Avenue du Tribunal-Fédéral 34
1005 Lausanne | Switzerland

Visit us: www.frontiersin.org
Contact us: frontiersin.org/about/contact

REPRODUCIBILITY OF RESEARCH
Support open data and methods to enhance research reproducibility

DIGITAL PUBLISHING
Articles designed for optimal readership across devices

FOLLOW US
@frontiersin

IMPACT METRICS
Advanced article metrics track visibility across digital media

EXTENSIVE PROMOTION
Marketing and promotion of impactful research

LOOP RESEARCH NETWORK
Our network increases your article's readership